THE ROLE OF CALCIUM IN MATURE OSTEOBLASTS VITAMIN D RECEPTOR (VDR)-MEDIATED ACTIVITIES TO MODULATE SKELETAL STRUCTURES AND MINERAL CONTENT

RAHMA TRILIANA

The Role of Calcium in Mature Osteoblasts Vitamin D Receptor (VDR)-Mediated Activities to Modulate Skeletal Structures and Mineral Content

---

Rahma Triliana MD, M.Health

Discipline of Medicine

School of Medicine

Faculty of Health Science

A thesis submitted in fulfilment for the degree of

Doctor of Philosophy

To

The University of Adelaide

South Australia, Australia

July, 2016

Table of Contents

Thesis Abstract

Vitamin D plays a role in the prevention of rickets in children and osteomalacia in adults. However, direct activity of vitamin D and Vitamin D Receptor (VDR) in bone cells has not been fully understood. Vitamin D receptor activities in bone cells are modulated by the dietary calcium in endocrine and bone paracrine/autocrine pathways in various studies. However, confirmation of direct VDR activities in bone cells in conjunction with calcium interactions on genetically modified animals has not been previously evaluated. Studies in these settings will assist our understanding of Vitamin D activities and VDR physiology in bone cells to modulate bone structures.

In chapter 3, a study on the generation and characterisation of transgenic over-expression of VDR in mature osteoblast using the osteocalcin promoter in *C57bl6/J* background (ObVDR-B6) was conducted. Results of this chapter confirm the anabolic action of this transgene and demonstrate that the VDR activity in mature osteoblasts exerts gender-specific and anatomical specific activities.

In chapter 4, the ObVDR-B6 mouse line was subjected to normal dietary calcium and phosphate intakes and extremely low dietary calcium (0.03 %) and phosphate (0.08 %) levels (LowCaP diet) over short term (3w) and long term (17w) periods to investigate its effects on bone mineral and skeletal structure. The study provides evidence that VDR activities in mature osteoblasts are anti-catabolic for skeletal structures with normal dietary calcium/phosphate, but catabolic with extremely low calcium/phosphate diets.

Whether deletion of VDR in mature osteoblasts using the *Cre/lox*-P system and osteocalcin promoter (ObVDR-KO) can rescue the skeletal structure of the mice when fed LowCaP diet is addressed in chapter 5. Results from this study confirmed that the activities of VDR in mature osteoblasts are modulated by the levels of dietary calcium and phosphate. Under normal calcium/phosphate levels, ObVDR-KO bone structures were not different from control mice. However, when fed LowCaP diet, the ObVDR-KO has anomalous bone structure with very high cortical porosity and high serum PTH and 1α,25 dihydroxyvitamin D_3 (1,25D) levels.

Although these studies and the mouse models have several limitations, overall data have contributed to elucidating the role of VDR activities in mature osteoblasts in skeletal biology and physiology in regards to dietary calcium/phosphate and further strengthen the evidence of the direct activities of VDR in skeletal health and mineral homeostasis. However, skeletal sites, region examined, sex, and age of the animals significantly influenced the results. Therefore, careful adjustment and further studies are needed to reveal the activities of mature osteoblast VDR in both genders, various skeletal sites, age related bone properties and its interaction with dietary calcium/phosphate.

Declaration

"I certify that this work contains no material which has been accepted for the award of any other degree or diploma in my name, in any university or other tertiary institution and, to the best of my knowledge and belief, contains no material previously published or written by another person, except where due reference has been made in the text. In addition, I certify that no part of this work will, in the future, be used in a submission in my name, for any other degree or diploma in any university or other tertiary institution without the prior approval of the University of Adelaide and where applicable, any partner institution responsible for the joint-award of this degree."

"I give consent to this copy of my thesis when deposited in the University Library, being made available for loan and photocopying, subject to the provisions of the Copyright Act 1968."

"I acknowledge that copyright of published works contained within this thesis resides with the copyright holder(s) of those works. "

"I also give permission for the digital version of my thesis to be made available on the web, via the University's digital research repository, the Library Search and also through web search engines, unless permission has been granted by the University to restrict access for a period of time "

Signature: Date: 26 JULY 2016

Rahma Triliana, MD

Acknowledgements

Firstly, I want to thank my supervisors Prof. Howard A. Morris and A/Prof. Paul H. Anderson. It was a privilege to be offered a PhD position in the Musculoskeletal Biology Research Laboratory under the supervision of these outstanding supervisors. They've made available amount of effort and time for my project, indulged my curiosity, and step by step teaching me the scientific thinking of research and improved my academic writing skill. Only with their continuous encouragement, guidance and supports, I could deal with the difficulties and problems I encountered during research and enabled me to complete my PhD.

Secondly, I thank Dr Andrew Turner, for teaching most of the molecular techniques in bone research along with the tips and tricks to achieve the best outcomes and the "I hate you" thing. I thank Ms Rebecca Sawyer and Mrs Helen Tsangari for assisting the bone histology and staining matters and to Ms Kate Barratt for being such a great friend and my 'mouse lady'. Without her friendship and companion, in and out of the lab, I'll go crazy. To Mrs Yolandi Starczak and Mr Jackson Ryan, thank you for the peer-feeling of being PhD student, the occasional discussion, banters, jokes, or the April mop. Thank you to members of Bone Cell Biology Group, "the Lab Next Door", Prof. Gerald Atkins, Dr. Asiri Wijenayaka, Ms Renee Ormsby, Dr. Masakazu Kogawa, Dr. Nobuaki Ito, Dr. Matt Prideaux and Mr Daniel Reinke during our lab collaborations, conference experiences, and Friday drinks. To Prof. David Callen, the PGC of Discipline of Medicine, thank you for introducing me to my supervisor and being the start and finish point of my PhD. I also acknowledged Prof. Edith Gardiner, Prof. John Eisman, and A/Prof. Paul Baldock for the providence of OSVDR mouse

line, A/Prof. Peter O'Loughlin and Dr. Nga Ngoc Lam for previous works of the OSVDR mouse model and A/Prof. Rachel Davey, Prof. S. Kato, Prof. T.L. Clemens for providence of ObVDR-KO mouse line.

Thirdly, I extend my gratitude to Directorate General of Higher Education (DGHE/ DIKTI), Ministry of Education, and Government of Indonesia for the International PhD Scholarship and to my home-base university, The Islamic University of Malang (UNISMA), for financial and institutional supports. To all the staffs, members and students of the Faculty of Medicine in UNISMA, thank you for supporting my study and bridging the connection with all involving parties in Indonesia while I was away.

My biggest gratitude and acknowledgement goes to my beloved husband Pungky Prasetyo MD, for his constant encouragement, understanding, love and support. To my beautiful, astonishing, and amazing daughter, Miss Rasyida Asha Nagari, thank you for being such an exceptional little girl where-ever you are. Big love and thanks to my Dad, Gatot Triyatno, my Mom, Rochajanah, my Sis, Riva Yunia Restriana and my Bro, Reindi Trisetyo Nugroho, for everything in my life. To my personal assistant, Katemi, and all my in-laws, thank you for taking care of my daughter when I'm not around. To all my extended families, friends and co-workers in Indonesia or anywhere around the globe, who cheered, supported, and prayed for my wellbeing and success, THANK YOU. May ALLAH bless you and your family just as ALLAH has blessed mine. Most of all, Thank YOU ALLAH, GOD almighty for allowing me to take this great, extraordinary, marvellous and complete life.

ALHAMDULILLAH.

Presentation, Awards and Publication Arising From This Thesis

PUBLICATION

Published Paper: **Triliana R**, Lam NN, Sawyer RK, Atkins GJ, Morris HA, Anderson, PH. Skeletal characterization of an osteoblast-specific vitamin D receptor transgenic (ObVDR-B6) mouse model. Journal of Steroid Biochemistry & Molecular Biology 2016; 164: 331-336, doi: 10.1016/j.jsbmb.2015.08.009. Epub 2015, Sep 4

PRESENTATIONS

International

Oral: **Triliana R**, Sawyer RK, Barratt K, Atkins G, Morris HA, Anderson PH. Transgenic Over-Expression of Vitamin D Receptor in Mature Osteoblasts Enhances Catabolic Activities under Dietary Calcium and Phosphorus Restriction. *International Bone & Mineral Society (IBMS) combined with European Calcified Tissue Society (ECTS-IBMS)*, Rotterdam, The Netherlands, April, 2015

Poster: **Triliana R**, Sawyer RK, Barratt K, Atkins G, Morris HA, Anderson PH. Transgenic Over-Expression of Vitamin D Receptor in Mature Osteoblasts Enhances Catabolic Activities under Dietary Calcium and Phosphorus Restriction. *18th Vitamin D Workshop*, Delft, the Netherlands, April 2015

Poster: **Triliana R**, Turner AG, Chan KK, Sawyer RK, Morris HA, Anderson PH. Over-expression of Vitamin D Receptor in Mature Osteoblasts/Osteocytes Promotes High Bone Turnover and Bone Loss under Dietary Calcium/Phosphate Restriction. *American Society of Bone Mineral Research (ASBMR)*, Houston, Texas, September 2014

National/Local Meeting

Poster: **Triliana R**, Sawyer RK, Barratt K, Atkins G, Morris HA, Anderson PH. Transgenic Over-Expression of Vitamin D Receptor in Mature Osteoblasts Enhances Catabolic Activities under Dietary Calcium and Phosphorus Restriction. *Australian Society of Medical Research (ASMR), Institute of Wine Centre, Adelaide*, June 2015

Poster: **Triliana R**, Turner AG, Chan KK, Sawyer RK, Morris HA, Anderson PH. Over-expression of Vitamin D Receptor in Mature Osteoblasts/Osteocytes Promotes High Bone Turnover and Bone Loss under Dietary Calcium/Phosphate Restriction. *Faculty of Health Science, Post Graduate Conference, Institute of Wine Centre, Adelaide*, September 2014

Poster: **Triliana R**, **Turner AG**, Chan KK, Sawyer RK, Morris HA, Anderson PH. Over-expression of Vitamin D Receptor in Mature Osteoblasts/Osteocytes Promotes High Bone Turnover and Bone Loss under Dietary Calcium/Phosphate Restriction. *Australian New Zealand Bone Mineral Society (ANZBMS),* Queenstown, New Zealand, September 2014

Poster: **Triliana R**, Sawyer RK, Morris HA, Anderson PH. Vitamin D Receptor in Mature Osteoblasts mediates both Anabolic and Catabolic and Catabolic Activities: Evidence from The OSVDR Mouse Model. *Australian Society of Medical Research (ASMR), Adelaide Convention Centre, Adelaide*, June 2014

Poster: **Triliana R**, Sawyer RK, Morris HA, Anderson PH. Vitamin D Receptor in Mature Osteoblasts mediates both Anabolic and Catabolic and Catabolic Activities: Evidence from The OSVDR Mouse Model. The 6th *Clare Valley Bone Meeting*, McLaren Vale, March 2014

Poster: **Triliana R,** Yang DQ, Atkins G, Anderson PH, Morris HA Clinical Manifestation of Rickets Is Enhanced In Low Calcium/Phosphate Fed Osteoblast-

Specific VDR (OSVDR) Transgenic Mice: Evidence for Direct Negative Effects of Vitamin D on Mineralisation. *Australian & New Zealand Bone and Mineral Society Conference (ANZBMS)*, Melbourne, Australia, September 2013

Poster: **Triliana R,** Lam NN, O'Loughlin PD, Morris HA, Anderson PH. Osteoblastic VDR over-expression Mediates both Anabolic and Anti Anabolic Activities Depending on Dietary Calcium and Serum 1,25D levels. *Australian & New Zealand Bone and Mineral Society Conference (ANZBMS)*, Perth, Australia, September 2012

AWARDS

- Best poster submission and presentation on 22 April 2015, Vitamin D workshop, Delft, April 2015
- Discipline of Medicine, School of Medicine, Faculty of Health Science, the University of Adelaide. Travel Awards, 2015
- SA Pathology Medical Specialist Staff Fund. Travel Grant, 2014
- Australian & New Zealand Bone and Medical Society. Travel Awards 2013
- Australian & New Zealand Bone and Medical Society. Travel Awards 2012

List of Figures

List of Tables

List of Abbreviation

1,25D	1α, 25 Dihydroxyvitamin D_3
1,24,25D	1α, 24,25 Dihydroxyvitamin D_3
25D	25 Hydroxyvitamin D_3
24,25D	24,25 Dihydroxyvitamin D_3
7-DHC	7-Dehydrocholesterol
AcP	Acid-phosphatase
ADHR	Autosomal Dominant Hypophosphatemic Rickets/ Osteomalacia
AF-1	Activation Function-1
AI	Adequate Intake
ALP	Alkaline Phosphatase
AP-1	Activator Protein-1
ATF-4	Activating Transcription Factor-4
AveOc.Ar	Average Osteoclast Area/Size
BFR/BV	Bone Formation Rate/Bone Volume.
BMP	Bone Morphogenic Protein
BMD	Bone Mineral Density
BGLAP	Bone γ-Carboxyglutamic Acid Protein
B.Pm	Bone Perimeter
BSP-1	Bone Sialoprotein-1
BV	Bone Volume
BV/TV	Bone Volume per Total Volume
CAL	Cortical Ascending Loop

Calbindin D_{9k}	Calcium Binding Protein D_{9k}
CatK	Cathepsin K
cDNA	Complementary DNA
CRS	Clinical Record Sheets
CSF-1	Colony Stimulating Factor-1
C-Term	Carboxyl-Terminal
Conn.D	Connectivity Density
Cor.BV	Cortical Bone Volume
Cort.Th	Cortical Thickness
CNT	Connecting Tubule
CYP27B1	25-Hydroxyvitamin D 1α-Hydroxylase
CYP2R1	Vitamin D-25-Hydroxylase
CYP24	25-Hydroxyvitamin D 24-Hydroxylase
DAP12	DNAX-Activating Protein of 12 kDa
DBD	DNA-Binding Domain
DBP	Vitamin D Binding Protein
DCT	Distal Convoluted Tubule
DC-STAMP	Dendritic Cells-Specific Trans Membrane Protein
DMP-1	Dentin Matrix Protein-1
DMF	Dimethlyformamide
DNA	Deoxyribonucleic Acid
DRIP/TRAP	Vitamin D Receptor Interacting Protein/Thyroid Hormone Receptor-Associated Proteins
ECM	Extracellular Matrix
ECaC	Epithelial Calcium Channel

EDTA	Ethylenediamine-Tetra Acetic Acid
EIA	Enzyme Immunoassay
ELISA	Enzyme-Linked ImmunoSorbent Assay
EGF	Epidermal Growth Factor
ENPP-1	Endonucleotide Pyrophosphate/Phosphodiesterase-1
ER	Estrogen Receptor
ERK	Extracellular Signal-Regulated Kinase
Es.Pm	Endosteal Perimeter
FGF-7	Fibroblast Growth Factor-7
FGF-23	Fibroblast Growth Factor-23
GM-CSF	Granulocyte-Macrophage Colony Stimulating Factor
HA	Hydroxyapatite [$Ca_{10}(PO_4)_6(OH)_2$]
HomC	Homozygous *Lox-P* Mice
HRP	Horseradish Peroxidase
HSC	Hematopoietic Stem Cells
ICAM-1	Intercellular Adhesion Molecule-1
IGF-1	Insulin-Like Growth Factor-1
IL-1	Interleukin 1
KO	Knockout
kgBW	Kilogram Body Weight
LAS	Laboratory Animal Services of the University Of Adelaide
LBD	Ligand Binding Domain
LFA	Leucocyte Function-associated Antigen
LowCaP	Low Dietary Calcium (0.03 %) And Phosphate (0.08 %)
L.Pm	Label Perimeter

LSD	Least Significant Difference
MAL	Medullary Ascending Loop
MAR	Mineral Apposition Rate
MAP Kinases	Mitogen-Activated Protein Kinases
MARRS	1α,25-Dihydroxy-Membrane Associated Rapid Response Steroid Binding
M-CSF	Macrophage Colony-Stimulating Factor
MEPE	Matrix Extracellular Phosphoglycoprotein
Micro-CT	Micro-Computed Tomography
MITF	Microphthalmia-associated Transcription Factor
MMP-9	Matrix Metalloproteinase-9
MMA	Methylmethacrylate
mRNA	Messenger RNA
MSC	Mesenchymal Stem Cells
MS/BS	Mineralising Surface/Bone Surface
mTOR	Mammalian Target of Rapamycin
MyoD	Myoblast Determination Protein 1
$NaHCO_3$	Natrium (Sodium) Bicarbonate
NCX1	Na^{2+}/Ca^{2+}-Exchanger
NFATc1	Nuclear Factor of Activated T-Cells Cytoplasmic 1
NF-κB	Nuclear Transcription Factors Nuclear Factor κB
NormCaP	Normal Dietary Calcium (1 %) And Phosphate (0.625 %)
N.Oc	Number of Osteoclasts
N.Ot	Number of Osteocytes
N.Ot/BV	Osteocyte Density

N.Oc/B.Pm	Number of Osteoclast/Bone Perimeter
NaPi2a	Natrium (sodium)/Phosphate Co-transporter-2a
NaPi2c	Natrium (sodium)/Phosphate Co-transporter-2c
OC	Osteocalcin
OB	Osteoblast
Oc.Ar	Osteoclast Size (Total)
OC	Osteoclast
OCy	Osteocytes
OcnCre	Osteocalcin-Promoter Driven-*Cre* Recombinase
OCN	Osteocalcin
Oc.Pm	Osteoclast Perimeter
OPG	Osteoprotegerin
Os.S/BS	Osteoclast Attachment Surface
OSCAR	Osteoclast-Associated Receptor
OSVDR	Over-Expression of VDR in Mature Osteoblasts on *FVB/N* Background
ObVDR-B6	Osteoblast Specific Vitamin D Receptor-Transgenic Mice on *C57bl6 Background*
ObVDR-KO	Osteoblast Specific Vitamin D Receptor Knock-Out Mice on *C57bl6 Background*
PBS	Phosphate Buffer Solution
PBM	Peak Bone Mass
PCMA	Plasma Membrane Ca^{2+}-ATP-ase
PCT	Proximal Convoluted Tubule
PCR	Polymerase Chain Reaction

PEG 400	Polyethylene Glycol
PGE-2	Prostaglandin E-2
PHEX	Phosphate Regulating Endopeptidase Homolog, X-Linked (Endopeptidases on the X-Chromosome)
PMC	Peripheral Mononuclear Cells
PPAR-γ	Peroxisome Proliferator Activator Receptor-γ
Ps.Pm	Periosteal Perimeter
PST	Proximal Straight Tubule
Pre-D3	Pre-Vitamin D3
PTH	Parathyroid Hormone
PTHR	Parathyroid Hormone Receptor
qRT-PCR	qualitative Reverse Transcriptase Polymerase Chain Reaction
Raf	Rapidly Growing Fibrosarcoma
RAF	Reid Animal Facility of University Of South Australia
RANK	Receptor Activator of Nuclear Factor Kb
RANKL	Receptor Activator of Nuclear Factor Kb Ligand
RCTs	Randomized Controlled Trials
RDI	Recommended Daily Intakes
RIN	RNA (Ribonucleic Acid) Integrity Number
RNA	Ribonucleic Acid
ROI	Region of Interest
Runx2	Runt-Related Transcription Factor 2
RXR	Retinoid X Receptors
SA Pathology	South Australia Pathology Animal Facility
Sfrp-4	Secreted Frizzled-Related Protein-4

SMI	Structural Model Index
SOST	Sclerostin
SOX-9	Sry-related HMG-Box
Tb.N	Trabecular Number
Tb.Sp	Trabecular Separation
Tb.Th	Trabecular Thickness
TE Buffer	Tris-EDTA-Buffer
TG	Transgenic
TghuRANKL	Transgenic Mice with human RANKL
TGF-B	Transforming Growth Factor B
TNF-A	Tumour Necrosis Factor A
TolB	Toluidine Blue
TRAP	Tartrate-Resistant Acid Phosphatase
TRAP-5b	Tartrate-Resistant Acid Phosphatase-5b
TIO	Tumour-Induced Rickets/Osteomalacia
TRPV5	Transient Receptor Potential Cation Channel, Subfamily Vanilloid, Member 5
TRPV6	Transient Receptor Potential Cation Channel, Subfamily Vanilloid, Member 6
TRPV	Transient Receptor Potential Vanilloid
UBV	Ultraviolet B
$VDR^{fl/fl}$ Mice	Mice with Homozygous Lox-P Sites Inserted Into Intronic Sequence of Exon-2 of the *Vdr* Gene
VDR	Vitamin D Receptor
hVDR	Human Vitamin D Receptor

mVDR	Mouse Vitamin D Receptor
VDREs	Vitamin D-Responsive Elements
VOI	Volume of Interest
Waf1/Cip1	Cyclin-Dependent Kinase Inhibitors P21
WHO	World Health Organization
Wnt	Wingless
WT	Wild Type
XLH	X-Linked Hypophosphatemic Rickets/Osteomalacia

List of Appendices

CHAPTER 1: LITERATURE REVIEW

THE ROLE OF DIETARY CALCIUM/PHOSPHATE IN VITAMIN D RECEPTOR MEDIATED ACTIVITIES IN BONE CELLS TO MODULATE BONE STRUCTURE AND MINERAL HOMEOSTASIS

This literature review provides a summary of the interaction between vitamin D, vitamin D receptor (VDR), dietary calcium and phosphate in bone cells to maintain bone mineral homeostasis. VDR and calcium play multiple important roles in the modulation of skeletal structure as indicated in *in-vitro* and *in vivo* studies. However, the controversy of a direct action of vitamin D in mature osteoblasts to modulate skeletal structure persists. This controversy is, arises, in part, from insufficient data on the role of dietary calcium on bone structure derived from *in-vivo* studies utilising specific mouse models in which the genes for VDR and vitamin D metabolising enzymes have been altered. Dietary calcium *in vivo* and extracellular calcium *in vitro* can enhance osteoblast maturation and improve skeletal structures. However, the interaction with bone cell vitamin D activity *in-vivo* and the possible mechanisms are not fully understood. This literature review briefly summarises the current research progress in vitamin D, dietary calcium, phosphate, and calcium/phosphate regulation of bone cell activities in both *in-vitro* and *in-vivo* studies as a guide towards the research activities conducted for this PhD project.

CHAPTER 1: LITERATURE REVIEW

1.1. INTRODUCTION

Osteoporosis is a metabolic bone disorder that is a worldwide health problem (1). The World Health Organization (WHO) has defined osteoporosis as "*a disease characterized by low bone mass and micro-architectural deterioration of bone tissue leading to enhanced bone fragility and a consequent increase in fracture risk*" (2) due to imbalance of bone remodelling especially in elderly people. In developing countries such as Indonesia, some 22.3 % of men & 32 % of women were reported to have osteoporosis in 2006 (3), while in a developed country such as Australia, 1 in 2 women and 1 in 4 men age over 60 years old have been diagnosed with osteoporosis (4). Several risk factors for the development of osteoporosis are well known including poor nutrition, decreased physical activity, smoking, alcohol consumption, and drugs (5). Geographical location also plays a role in the pathogenesis of osteoporosis due to the seasonal variations and degree of sunlight exposure which are determinants of vitamin D status (6).

Vitamin D deficiency is significantly associated with osteoporosis (7) and increased incidence of fracture (8). The bone loss that occurs in osteoporosis is often undetected until a significant fracture occurs (5). The wrist, spine, and hip are the most common regions for osteoporotic fracture which can lead to disability, increased dependency and financial burden (9). Therefore, effective strategies to prevent the onset of osteoporosis are imperative to reduce the health and financial burdens to individuals and the community.

Dietary intervention is a recognized method for treating mild osteoporosis (10) and calcium supplementation is known to be a useful treatment to improve bone health (11). Bone density in elderly females with osteoporosis (12), menopausal women (13) and adolescent girls (14) was increased while the risk of fractures was decreased with dietary calcium and/or calcium-rich foods (15,16). Calcium is an essential nutrient because plasma calcium levels affect various important cellular activities due to intracellular signalling pathways and other actions (17). Plasma calcium homeostasis is tightly regulated by the processes of renal tubular reabsorption of calcium, intestinal calcium absorption, and bone remodelling as sources of calcium for the plasma compartment (18). The calciotropic hormones, parathyroid hormone (PTH), calcitonin and vitamin D (19), play a key role in regulating plasma calcium homeostasis in a concerted manner.

Vitamin D has been known as the *bone vitamin* since the beginning of the 20th century and plays a role in preventing the onset of rickets or osteomalacia which has re-emerged in the 21st century (20). Osteomalacia is a bone disease characterised by the marked under-mineralization of bone which occurs due to the failure of maintaining plasma calcium and/or phosphate homeostasis (21). The role for vitamin D activity to prevent osteomalacia by maintaining plasma calcium and phosphate level was clearly demonstrated by studies with vitamin D receptor (VDR) knockout mice as described by Li et.al in 1998 (22) and Amling et.al in 1999 (23). They showed that hypo-mineralized skeletal phenotype of VDR knockout mice was normalized by providing a high dietary calcium and phosphate regimen that restored plasma calcium and phosphate levels.

In addition to the role of vitamin D in preventing osteomalacia, there is a large body of data implicating vitamin D deficiency in the aetiology of the bone disease osteoporosis (7) and increased risk of fracture (24). However, results from the randomized controlled trials (RCTs) of vitamin D supplementations and fracture risk have been controversial (25-27). Meta-analyses of data from large RCTs indicate combination of vitamin D with calcium (28) are best to reduce osteoporosis and the risk of fractures. Although vitamin D activity is important to prevent bone loss and osteoporosis, the mechanism by which this occurs is not entirely clear. In osteoporotic hip fracture patients with low vitamin D status, there is no evidence of a calcium and phosphate malabsorption or disturbed calcium and/or phosphate homeostasis (29,30). Therefore, in addition to the role of vitamin D activity to maintain plasma calcium and phosphate homeostasis, it has been proposed that vitamin D can act directly on bone cells, particularly bone forming cell, osteoblasts, to promote bone mineralisation and to improve bone health (31)

The discovery that bone cells are capable of synthesising 1α, 25 dihydroxyvitamin D_3 (1,25D) and respond to 1,25D to elicit autocrine and paracrine actions (32) has brought a new perspective on vitamin D metabolism and VDR-mediated activities in bone. Osteoblasts express the 25-hydroxyvitamin D 1α-hydroxylase (CYP27B1) enzyme which metabolizes the prohormone 25-hydroxyvitamin D (25D) to the biologically active 1,25D (33). *In-vitro* studies have demonstrated the importance of vitamin D in bone cells. Incubation of osteoblasts with 25D modulates osteoblasts activity, induces alkaline phosphatase (ALP) activity, osteocalcin (OC) and 25-hydroxyvitamin D 24-hydroxylase (CYP24) mRNA expression, and enhances mineralization (34) for which the expression of CYP27B1 was essential. The CYP27B1 enzyme is also present in

precursor and mature osteoclasts such that incubation of 25D with human peripheral mononuclear cells (PMC) or mouse RAW264.7 cells up-regulate the expression of osteoclast transcription factor (nuclear factor of activated T cells-cytoplasmic 1 / NFATc1) and other osteoclast marker genes to generate osteoclasts with reduced resorptive capacity in both models (35). Various animal models have been used for *in-vivo* studies of vitamin D metabolism and/or VDR activities. One mouse model overexpresses the human VDR gene under the control of the osteoblast-specific promoter of the gene for osteocalcin. This transgene increased VDR protein levels 2 to 3-fold in the bone of this mouse model (36). This mouse line, known as the OSVDR mouse, exhibited increased cortical and trabecular bone volumes due to increased periosteal mineral apposition rate (MAR) and reduced trabecular resorption surfaces (36) suggesting distinct and diverse vitamin D regulatory pathways in bone forming cells with the conclusion that increased VDR in mature osteoblasts is anabolic for bone.

Baldock et al. in 2006 (37) demonstrated that the anabolic effect of the osteoblast specific VDR overexpression is dependent on dietary calcium intake. A comprehensive study to determine the role of dietary calcium in vitamin D and/or VDR activities on bone cell will provide further insights on bone physiology and remodelling. Therefore, the main idea of this thesis is to evaluate the role of calcium in the direct activity of vitamin D and VDR in mature osteoblasts to maintain skeletal health using various mouse models.

1.2. BONE STRUCTURE, PHYSIOLOGY & BIOLOGY

The human skeleton serves as a unique organ in providing structures to protect vital organs but light enough to permit easy movement and locomotion (38). As cited by Clarke, 2008 (38), the adult human skeleton consist of 213 bones which are composed of two main structures, trabecular (cancellous) and cortical (compact) bone and collectively comprises the bone mass. The structure of compact bone which comprises 80 % of whole bone mass based on their size scale is depicted in **figure 1.1** to illustrate macroscopic and microscopic structure of the bone. Trabecular bone (or spongy bone) is less dense, highly vascular, has a higher ratio of surface area to mass, and is in close contact with bone marrow (39). Therefore it is softer, weaker and has flexible characteristics suitable for metabolic activity such as ion exchange while the cortical (compact) bone will determine bone mass and bone strength.

Bone mass is the result of bone formation and bone resorption through periods of growth, maturity and senescence (40) with or without adequate calcium intake as depicted in **figure 1.2**. Osteopenia and osteoporosis are characterized by low bone mass or $\leq$ -1 SD of average peak of young adult Bone Mineral Density (BMD) (9)

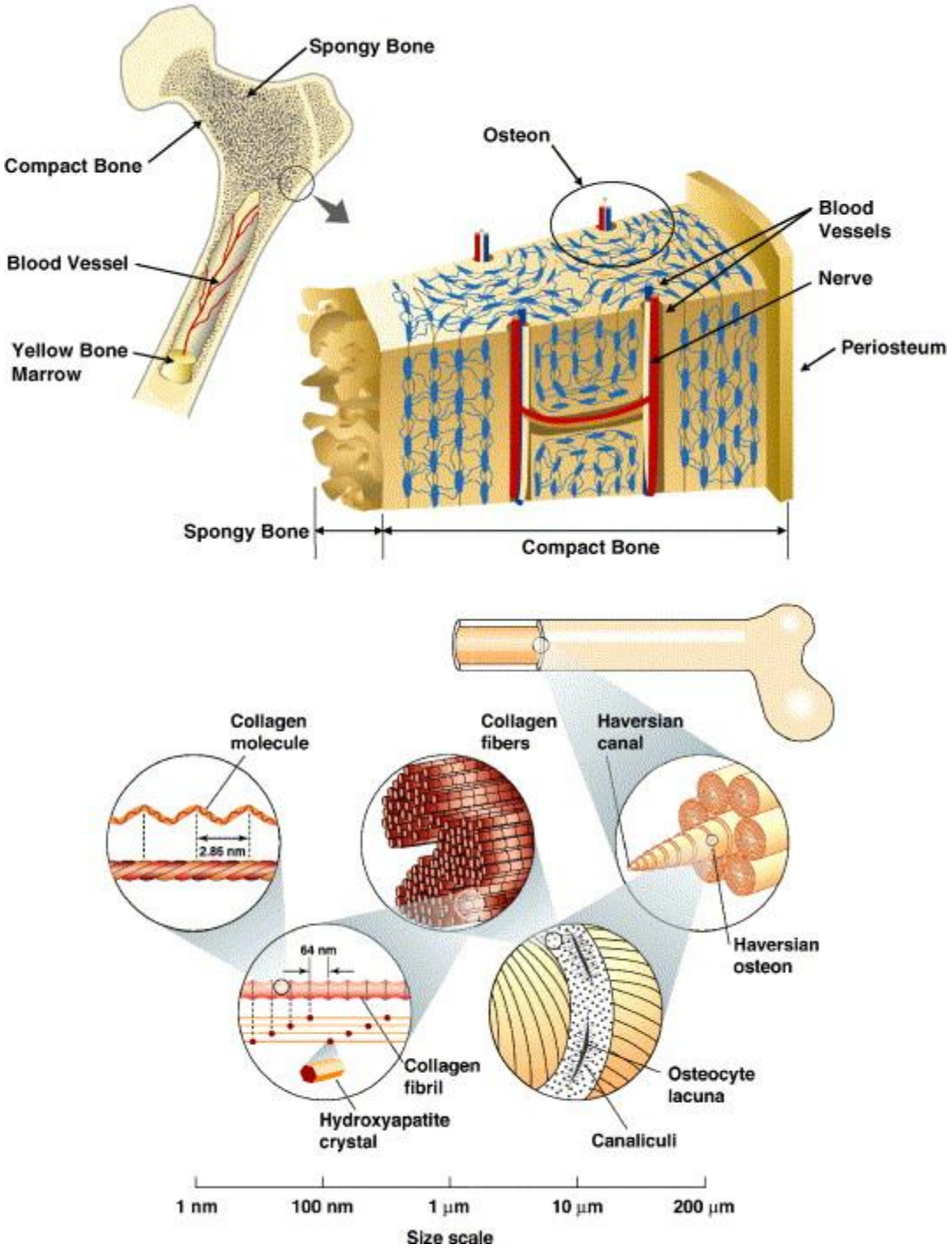

Figure 1.1. Hierarchical Structure of Human Cortical Bone

Human cortical bone consists of Harversian osteons with canaliculi, collagen fibres, and hydroxyapatite crystals providing a denser composition than trabecular bone. Therefore, cortical bone is harder, stronger, and stiffer. Any changes in macroscopic structures can be linked to changes of the hierarchical structure of bone at the microscopic scales. Adapted from Nalla et al. 2006. (41)

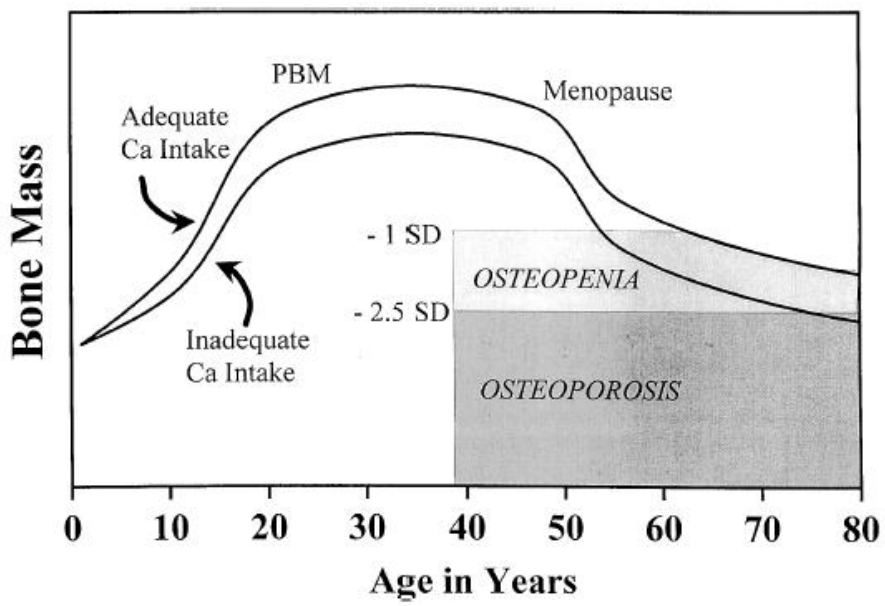

Figure 1.2. Bone Mass Alteration in Women (Arbitrary Units) With Age

Peak Bone Mass (PBM) is determined by various factors including calcium intake throughout life. Bone mass accrual still occurs with an inadequate calcium intake. However, PBM achieved with inadequate calcium intake is lower which determines susceptibility to osteopenia, osteoporosis and fracture later in life. Adapted from Ilich and Kerstetter 2000 (40).

During growth and development in childhood and adolescence, the rate of bone formation exceeds the rate of bone resorption and a net gain of bone mass is achieved (38). This process is termed bone modelling by which bones change shape and structure leading to gradual adjustment of the skeleton and is affected by endogenous (genetic, hormonal) and exogenous (nutritional, mechanical or physical activity) factors (42). When peak bone mass is achieved at maturity or after the age of 25 years (43), bone formation and bone resorption come into equilibrium and bone mass remains stable until mid-life (40). At this age, bone remodelling predominates to renew, replace, and maintain bone strength and mineral homeostasis to meet metabolic demands in a tightly coupled manner (38). Cortical bone is remodelled at a lower rate than trabecular bone which suggests that the role of cortical bone remodelling is to maintain bone biomechanical strength while trabecular bone remodelling is mostly for mineral homeostasis (39). In contrast to bone modelling, bone remodelling occurs at the same location with cyclical timing beginning with the activation process, followed by bone resorption and ending with formation of new bone (42) as depicted in **figure 1.3**. During senescence, beginning at the menopause in women and at about the age of 55 in men, the bone remodelling equilibrium is disturbed (38). This results in a progressive decline of bone mass which continues to the end of life and increases the incidence of fractures in both sexes (44,45).

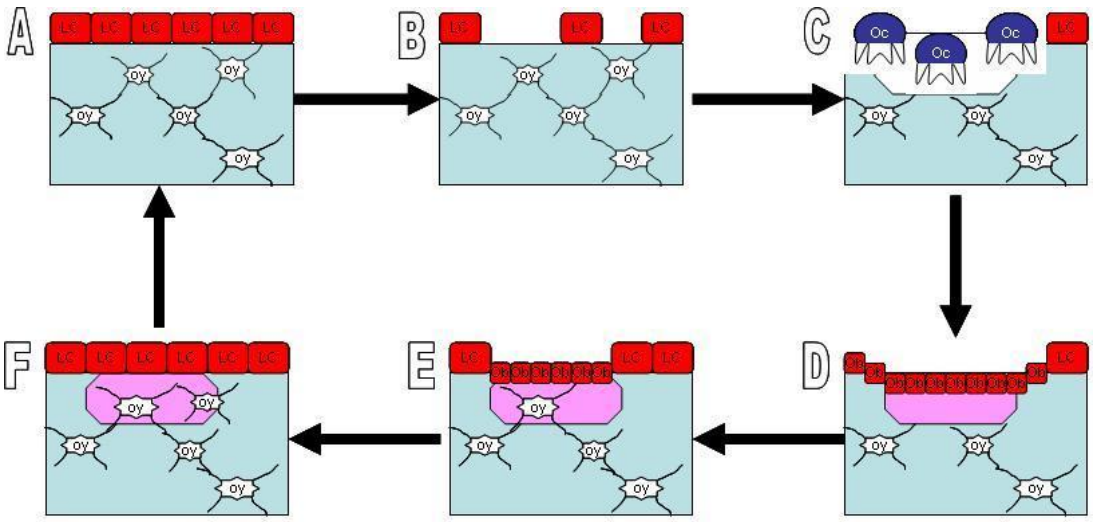

Figure 1.3. Phases of Bone Remodelling

Bone remodelling starts from the quiescent phase (A) with flat bone lining cells (LC) covering the endosteal membrane. Activation of bone resorption produces the activation phase (B) characterised by lining cell retraction and recruitment of osteoclasts (OC) to start the resorption phase (C). When the resorption phase is ended, osteoblasts (OB) are recruited along the resorption pit to begin the formation phase (D). Osteoblasts synthesise extracellular matrix and begin to form new osteoid (pink) which is later mineralised to form bone (E). Some osteoblasts differentiate into lining cells while osteoblasts trapped within the osteoid become osteocytes (Oy/Ocy) and formation of the new bone is completed (F) or termination phase and progress towards the quiescent phase for the cycle to begin again. Modified from Kini et al 2012 (39)

Changes in the relationship between bone formation and bone resorption throughout stages of life are dependent on the activities of the three major types of bone cells; osteoblasts and osteocytes derived from mesenchymal stem cells (MSC) (46), and osteoclasts which arise from haematopoietic stem cells (HSC) (47). The osteoblasts and osteoclasts exist on the bone surfaces while the osteocytes are embedded in the mineralised collagenous matrix (38). The proliferation and activities of these cells are coordinated by mechanisms yet to be fully elucidated.

1.2.1. Osteoblasts and Osteocytes

Osteoblasts (48) and osteocytes (49) regulate bone formation and are derived from MSC which function to maintain the number of osteoblasts within bone throughout life. The exact locations of skeletal MSC are unknown, although it is suggested that they came from pericytes on the sinusoidal wall (50) and from the bone marrow MSC that differentiate into osteoblasts as a response to various hormonal, mechanical, or cytokine signals (46). Osteoblasts have at least four major functions; 1) secretion of bone extracellular matrix (ECM) which includes collagen, osteocalcin and alkaline phosphatase (51); 2) expression of genes for mineralization of ECM; (52) 3) controlling osteoclast differentiation thereby influencing bone resorption; (53) and 4) differentiation into osteocytes (54) as depicted in **figure 1.4**. Bone ECM consists of organic materials (85-90 % collagenous proteins, predominantly type I collagen, 10-15 % of non-collagenous proteins (e.g. osteocalcin/osteonectin, proteoglycan) derived exogenously (55)) and inorganic materials (calcium hydroxyapatite/HA or $Ca_{10}(PO_4)_6(OH)_2$) (56) which made up to 50 % by volume of bone (38,39).

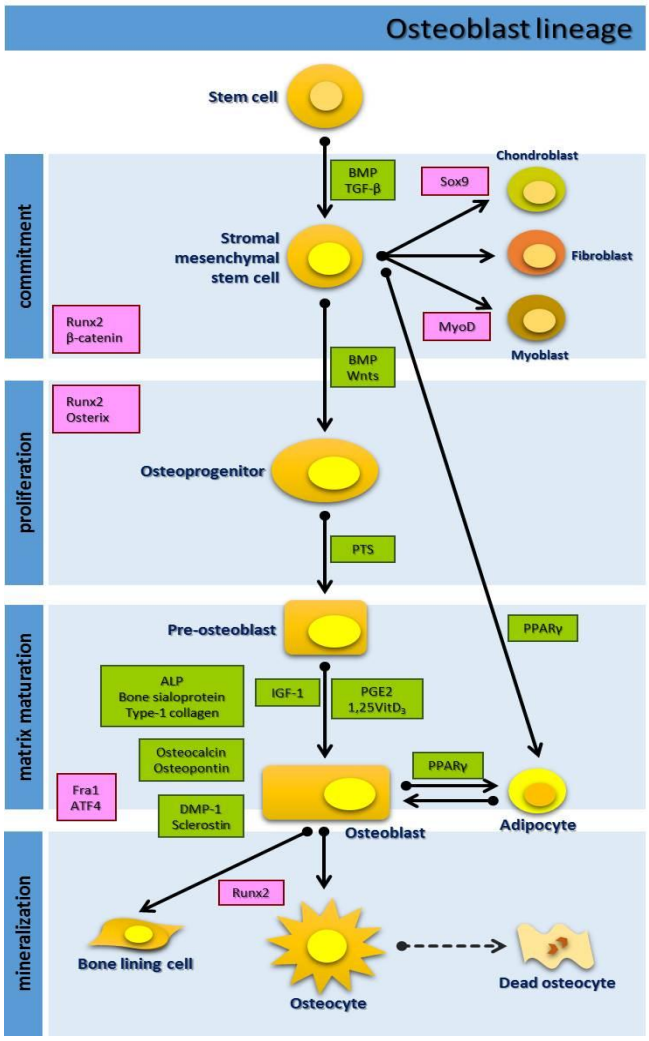

Figure 1.4. Osteoblast Lineage during Osteoblastogenesis

MSC undergo commitment to osteoprogenitor cells proliferating and maturing to become pre-osteoblasts, mature osteoblasts and lastly osteocytes depicted according to their differentiation steps (blue box). These processes are regulated by concerted expression of several transcription factors such as Runx2, β-catenin, and ATF-4 (pink colour box). Bone formation by osteoblasts is regulated by local and systemic signalling factors such as BMP, TGF-β, and PPAR-γ (green colour box) during bone modelling in development and throughout life. Mature osteoblasts can also differentiate into bone lining cells or undergo apoptosis. During certain physiological or pathological condition, osteocyte death can occur and dead osteocytes leave empty lacunae in bone. Adapted from Crockett et al. 2011 (57)

Osteocytes embedded within mineralized bone are terminally differentiated osteoblasts and they function to support bone structure and mineral metabolism (58). Osteocytes connect to each other and the bone surface *via* multiple filipodial processes which support intercellular adhesion and mineral exchange within the lacunae and canalicular networks (59). The connection between the filipodial processes of each osteocyte are known as gap junctions, which are also required for maturation, activity, and survival of osteocytes during bone turnover (60)**.** Therefore, under normal condition, osteocytes can live for up to decades in the absence of bone turnover.

The primary known function of osteocytes is mechanosensation (54)**.** Osteocytes act as the transducer of stress signals for bone biological activity when subject to bending or stretching via the flow of fluid through the canalicular networks (61). The flow is believed to be a signal between osteocytes within the bone and osteoblasts on the bone surface to induce their cellular activities. Disruption of intercellular signalling at the gap junctions or cell–matrix interactions may cause osteocytes to become active or undergo apoptosis (54). Activated osteocytes became phagocytic cells due to their lysosomal enzymes and apoptotic osteocytes will produce empty lacunae within the bone resulting in a decrease of bone density and osteoporosis (38,60).

Osteocytes also regulate bone turnover and assist in mineral metabolism due to their enormous surface area and location to easily dissolve bone mineral matrix (62). Osteocytes remodel their perilacunar/canalicular structures through an osteocyte-mediated demineralization process in response to various stimuli such as parathyroid hormone and calcium restriction (63). This process is known as osteocytic osteolysis.

However, the exact mechanism by which this process occurs and is regulated is unclear and warrants further investigations.

1.2.2. Osteoclasts

Osteoclasts are bone surface cells that are able to resorb bone (47). They are multinucleated giant cells derived from mononuclear precursor cells of the monocyte macrophage lineage from the HSC (64) in a process called osteoclastogenesis (depicted in **figure 1.5**). Osteoclastogenesis requires the presence of stromal cells including osteoblasts because they secrete receptor activator of nuclear factor-κB ligand (RANKL) and macrophage colony stimulating factor (M-CSF) (65). These cytokines are critical for osteoclast formation, proliferation, survival, and differentiation as well as cytoskeletal rearrangement required for osteoclastic bone resorption (38).

Osteoclastic bone resorption consists of several processes including 1) osteoclastogenesis, 2) activation phase, 3) bone resorption and 4) osteoclast apoptosis when the bone resorption process is completed (66). These processes are highly complex and regulated by various factors and conditions. During the activation phase, pre-osteoclasts will fuse to produce multinucleated giant cells, attach to calcified tissue and develop a ruffled border at the mineral interface to create a resorption compartment with an acidic microenvironment (67). In this compartment, hydroxy-apatite crystals are solubilised and bone matrix proteins are degraded by the proteolytic enzymes secreted by the active osteoclasts to release calcium into the blood stream (67,68). Increased osteoclast activity and decreased osteoclast apoptotic rate have been proposed as a cause of osteoporosis with low dietary calcium intakes and/or in vitamin

D insufficiency particularly in elderly people (69). Therefore maintaining sufficient dietary calcium and vitamin D is crucial for bone health especially at older age (> 55 years).

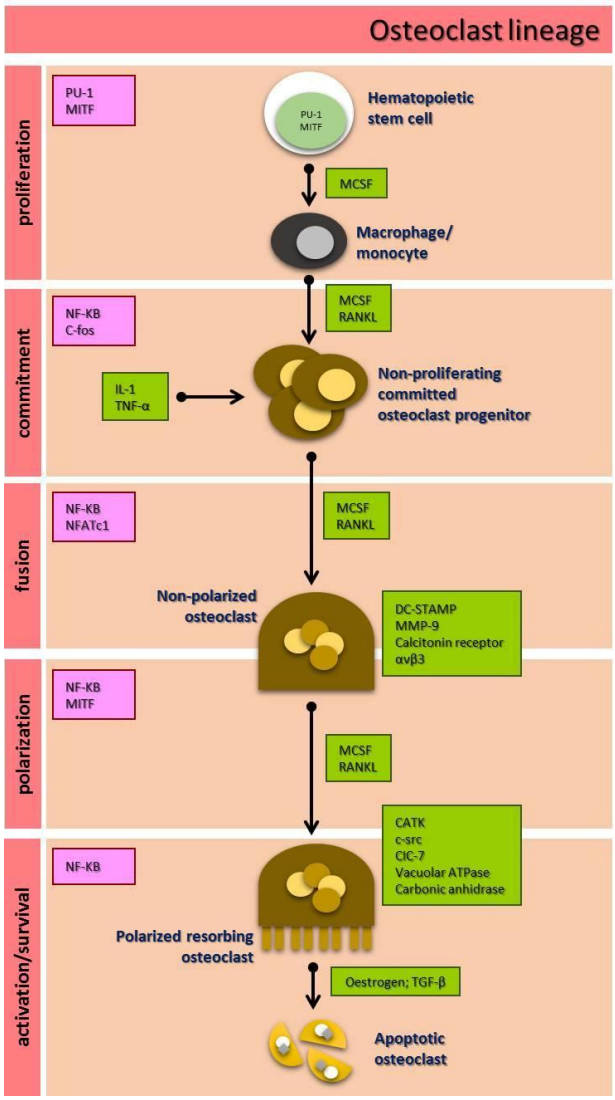

Figure 1.5. Osteoclast Lineage during Osteoclastogenesis

Osteoclast development and stages of differentiation from HSC to become active osteoclasts are depicted in red coloured boxed. Transcription factors such as NK-κB, NFATc-1 and MITF (pink box) regulating these differentiation stages and the bone resorption process are regulated by local and systemic signalling factors such as M-CSF, RANKL, and MMP-9 (green colour box). Osteoclasts death is normally by apoptosis which serves as the termination signal of the bone resorption process. Adapted from Crockett et al. 2011 (57)

1.3. CALCIUM

Calcium is an essential mineral and physiologically indispensable ion in the human body. It is an important cation in both the extracellular and intracellular spaces. Intracellular calcium acts as a second messenger controlling various cellular functions including exocytosis and secretion of cellular products, chemotaxis, intercellular adhesion, enzymatic activities, fertilization, proliferation, differentiation, and apoptosis (70). Extracellular calcium is crucial for a broad range of physiological function such as blood coagulation, release of neurotransmitters, nerve impulse transmission, heart and muscle contraction, and maintaining skeletal integrity (17). Thus, maintaining extracellular calcium homeostasis is essential for appropriate whole body functions.

The total calcium is around 1 kg in an adult with 99 % of which is within the skeleton while the 1 % resides in plasma compartment which is the most regulated calcium compartment (71). Plasma calcium levels are approximately 2.2–2.5mmol/L which consist of 47.5 % calcium ion, 46 % protein-(such as albumin and globulins)-bound calcium, and 6.5 % in complexed fractions which bind to phosphate and citrate anions (72). The exchange of calcium across the various compartments is common but regulation of calcium concentration is based on the plasma ionised calcium level.

The plasma calcium level is held in a very narrow range although calcium can move across cellular compartments due to physiological changes such as pH or hormonal effects (72). Various physiological conditions such as pregnancy, lactation, growth, aging, changes of calciotropic hormone level and activity, changes in other minerals (such as magnesium and phosphate), or pathological conditions such as cancer can

effect plasma calcium levels (18). Thus, several regulatory mechanisms are coordinated to maintain plasma calcium homeostasis in the context of large variations of calcium input and output of the body.

The regulatory system of calcium homeostasis is mainly conducted by the intestine via intestinal calcium absorption, the kidney via renal tubular reabsorption, and the bone tissues through the bone remodelling process as sources of plasma calcium (19). Although it is tightly controlled, calcium loss is occurring all the time through urinary excretion because kidney can only reabsorb 97 – 99 % of filtered calcium (73). Therefore, adequate dietary calcium is essential to meet the obligatory calcium loss to maintain skeletal health.

1.3.1. Recommended Daily Allowance of Calcium and Source of dietary calcium

Calcium requirement is estimated from the dietary calcium intake needed for desirable calcium retention necessary for sufficient absorption to meet the obligatory calcium losses through skin (via sweating), bowel and urinary excretion (74). The requirement is calculated based on individual need within certain age, gender groups, physiologic conditions and presence of pathologic conditions. The Commonwealth Government of Australia, in 2006 has published guidelines for calcium recommended daily intakes (RDI) based on age, sex and physiological groups (i.e. pregnancy and lactation) (75) to meet the need of calcium and maintain health. To achieve the desirable calcium intake, a number of dietary calcium sources should be taken. Major calcium food sources are milk and milk-based foods, low-oxalate vegetables, bony fish, legumes, nuts, and soy (76) in fresh or fortified products (75).

Meeting the RDI of calcium is essential to maintain calcium balance, normal body functions and minimize bone resorption. However, many adults, menopausal woman, and children do not meet this RDI of calcium through diet alone or supplemental calcium due to low compliance (77). These findings have highlighted the need for research on calcium metabolism and factors regulating calcium metabolism as important issues to maintain skeletal structure.

1.3.2. Calcium Metabolism

1.3.2.1. Intestinal Calcium Absorption

Intestinal absorption of dietary calcium occurs by either an active transcellular transport or a passive non-saturable paracellular route (78). The active transport system occurs primarily within the duodenum of the small intestine while the passive absorption occurs via tight junctions between enterocytes or a direct exchange of calcium between two compartments (79). Calcium movement in the paracellular pathway is dependent on; 1) the concentration and electric gradients across epithelia, 2) solubility of the calcium in the diet, and 3) diffusion rate between intestinal lumen and lymph or blood (80). During high dietary calcium, the passive absorption of calcium increases because of the short transit time in the intestine as well as the down regulation of proteins involved in the transcellular route (78).

The active transcellular transport of calcium occurs across two plasma membrane barriers. Calcium entry into epithelial cells occurs via the calcium channels, transient receptor potential vanilloid (TRPV) 5 and TRPV6 (81). The cytosolic diffusion of calcium is mediated by calbindin-D 9k (CaBP-9k) (82) and extrusion of calcium across the basal membrane is facilitated by the calcium transporter, plasma membrane Ca^{2+}-

ATP-ase (PCMA), and Na^{2+}/Ca^{2+}-exchanger (NCX1)) (79). Therefore, absorption of calcium is the main instrument to maintain sufficient calcium absorption during low availability of dietary calcium, and/or during increased physiological demand. Active intestinal calcium absorption is mainly stimulated by vitamin D by influencing each step of active intestinal calcium transport (80).Vitamin D enhances the expression of TRPV5, TRPV6, CaBP-D9k, as well as the co-transporter such as Na^{2+}/Pi co-transport proteins, thereby promoting the net absorption of calcium as well as phosphate in the intestine (78,79,83).

1.3.2.2. Renal Tubular Reabsorption of Calcium

The kidney plays a role to maintain calcium balance by regulating calcium excretion. On a daily basis, approximately 8g of calcium is filtered by the glomerulus but less than 2 % are excreted into the urine (84) in a process known as renal tubular reabsorption. Calcium enters the renal tubules through plasma ultrafiltration by the glomerulus, followed by calcium reabsorption across the renal tubule before being excreted through the urine (73). Within the proximal convoluted tubule (PCT) and the proximal straight tubule (PST), calcium is osmotically reabsorbed via passive paracellular route up to 80 % of the filtered calcium (85). This paracellular calcium transport route occurs due to differences in trans-epithelial electrochemical gradient generated by sodium and water reabsorption (73). Therefore, changes in water and sodium balance can affect calcium reabsorption by the kidney and hormones that control water and sodium reabsorption, such as alpha-adrenergic, angiotensin II, and dopamine, can also indirectly affects calcium reabsorption (86).

Calcium is not reabsorbed along the thin segment of the loop of Henle. However, along the medullary ascending loop (MAL) and cortical ascending loop (CAL) of Henle, calcium is actively reabsorbed by active trans-cellular transport mechanism (73). Distal convoluted tubule (DCT) reabsorb around 10 % of the filtered Calcium, and 3% to 10 % are reabsorbed in the connecting tubule (CNT) (18). In these regions, fine regulation of calcium excretion in the kidney occurs. In contrast to the passive paracellular pathway, the transcellular pathway allows the kidney to regulate calcium reabsorption independent of sodium and water balance, or electrochemical gradient (86). Therefore, the human body can respond to fluctuations in dietary calcium and adapt to the demand of physiological changes such as growth, pregnancy, lactation, and aging (18). As such, disturbances in transcellular calcium reabsorption are usually accompanied by significant changes in calcium homeostasis.

Transcellular calcium reabsorption occurs in a sequence of events similar to the intestinal calcium absorption process except for the calcium entry from lumen which is conducted by the epithelial calcium channel (ECaC) (87) which serves as a gatekeeper in transcellular calcium reabsorption. The transcellular calcium transport is a rate-limiting step and tightly controlled by the calciotropic hormones (Vitamin D, PTH, and calcitonin) (88). Vitamin D and PTH stimulate transcellular calcium transport in the CAL and DCT and increase calcium reabsorption while calcitonin controls calcium reabsorption in MAL where it acts to decrease it (85). Vitamin D increases calcium reabsorption via increasing expression of calbindin, and PTH-dependent calcium transport in DCT (87). Vitamin D also modulates renal absorption of phosphate, and improves podocytes function and longevity, thus, maintaining renal function (89,90). Under steady-state conditions, urinary calcium excretion depends on

plasma calcium levels and therefore can correspond to calcium intake by the gastrointestinal tract. However, under other circumstances, the skeleton is called upon to act as a calcium source to maintain blood calcium levels (91)

1.3.2.3. Bone Remodelling as Source of Calcium

Total calcium content in a person weighing 70 kg is approximately 1250 g and almost 99 % of it is predominantly incorporated into mineralized bone (30). During bone modelling, as the skeleton grows and bone mineral accumulates, the mass of human bone increases 7-fold from birth to puberty and a further 3-fold during adolescence (92). The skeleton acts as calcium reserve capable of releasing calcium into the blood stream during increased calcium demand or calcium depletion. About 1 % of total bone calcium is available as an exchangeable pool. When bone exchangeable pool cannot meet requirements, the non-exchangeable pool may be affected which causes bone loss and increasing the risk of fracture over the long term (44).

Bone remodelling is modulated by various factors. Vitamin D and PTH maintain calcium balance induced by changes of dietary calcium which can affect bone health as depicted in **figure 1.6** (93). The mechanism by which dietary calcium is involved in altering bone health during physiologic adaptation to environmental changes has not been fully elucidated. Therefore, studies in vitamin D metabolism and/or VDR activities in relation to dietary calcium on bone cell activities are required especially in adults or elderly people.

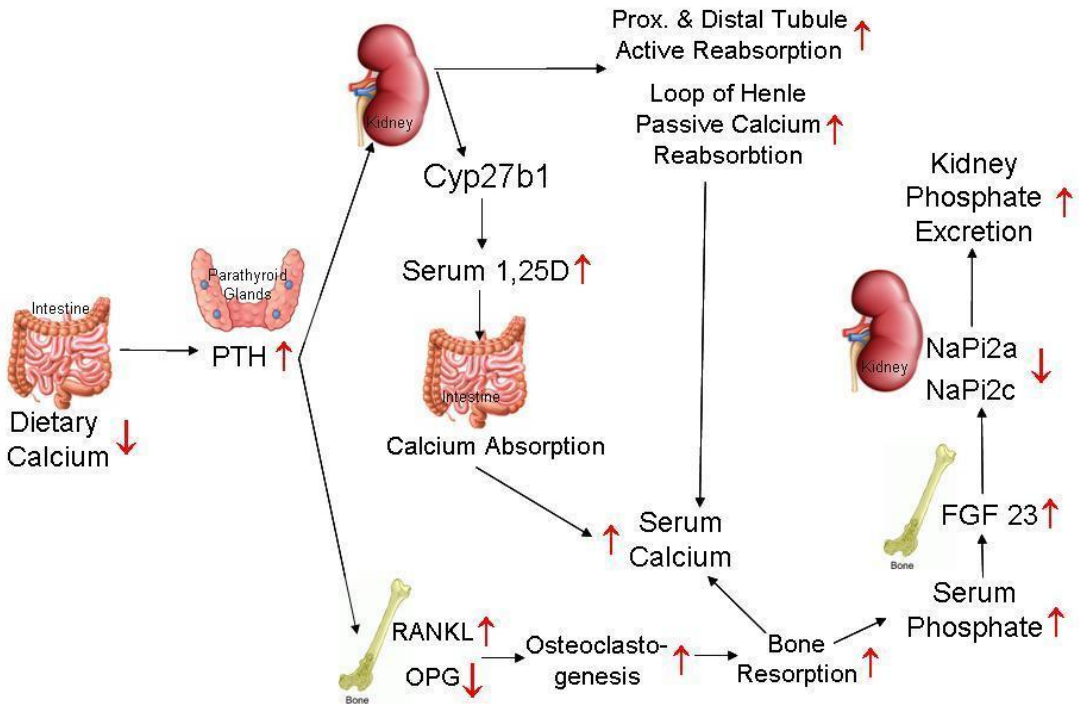

Figure 1.6. Calcium Metabolism during Low Dietary Calcium Intake

Schematic flow of the effects of low dietary calcium on calcium metabolism modified from Allgrove 2003 and Blaine 2014. (19,73)

1.3.3. The Interaction between Calcium and Phosphate Metabolism

As depicted in **figure 1.6**, calcium metabolism is tightly related to phosphate metabolism. Therefore, understanding phosphate metabolism is just as important as calcium metabolism in any dietary study, especially on bone metabolism. Phosphate is the most abundant anion and plays an important role in various biological functions, including bone mineralization, cell signalling via protein phosphorylation, nucleotide and energy metabolism, and maintaining acid-base homeostasis (94). Therefore, disorders in phosphorus homeostasis will affect various physiological processes.

Phosphorus homeostasis is regulated by interplay of the intestine, kidney, bone, parathyroid gland, as well as the vitamin D system and phosphatonins (**Figure 1.7**) (95). The kidney modulates regulation of phosphate changes during short term condition while effects on intestinal phosphate absorption adapts to long term phosphate changes by hormonal mechanisms (96). Several phosphaturic peptides such as fibroblast growth factor 23 (FGF-23), FGF-7, matrix extracellular phosphoglyco-protein (MEPE) and secreted frizzled-related protein-4 (sFRP-4) (97) have been shown to play a role in phosphate metabolism in genetic hypophosphatemic disorders by inducing phosphaturia and hypophosphatemia (98). Interestingly, despite the induction of hypophosphatemia by the FGF-23 *in-vi*vo, serum 1, 25D is decreased or remains normal indicating an inhibitory effect of this hormone on renal Cyp27B1 activity (99). Therefore, understanding vitamin D metabolism and its relation to bone remodelling, mineralisation, calcium and phosphate homeostasis is needed to further understand the role of dietary calcium/phosphate in bone cells activity and biology.

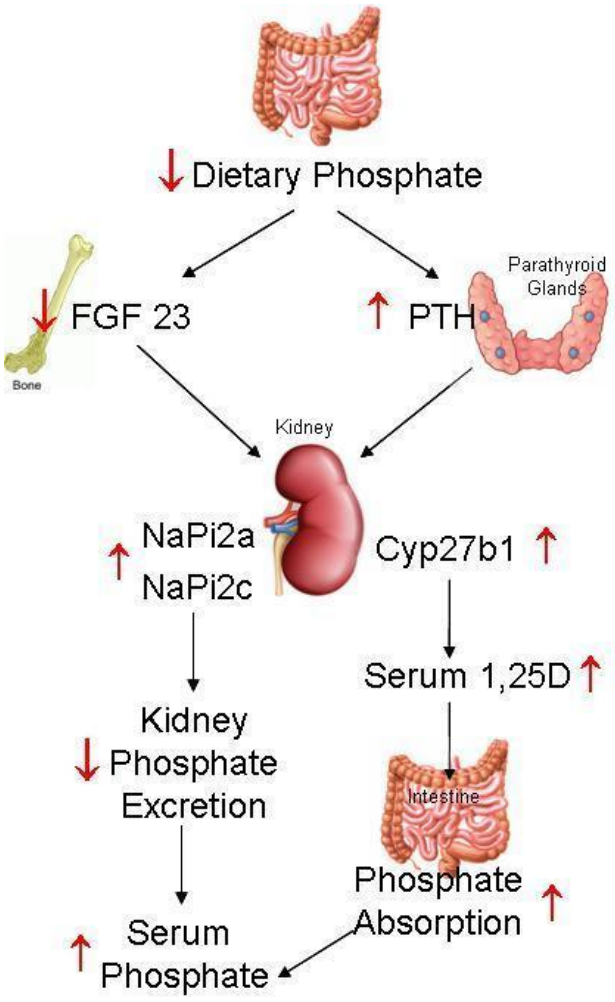

Figure 1.7. Regulation of Phosphate Balance with Low Dietary Phosphate Intake

When serum phosphate is low, FGF-23 production in bone is reduced and PTH synthesis by the parathyroid glands is induced resulting in increased synthesis of 1,25D by the kidney Cyp27B1 enzyme, and increased expression of sodium-phosphate co-transporter (NaPi2a, NaPi2c). These changes increase phosphate reabsorption by the kidney and phosphate absorption in the intestine to restore phosphate balance. Modified from Lien AJ 2013 (95)

1.4. VITAMIN D AND VITAMIN D METABOLISM

Vitamin D was discovered in the beginning of 20th century as a nutrient to prevent rickets, a disease in children characterized by defect in the growth plate and mineralization (21). Under normal physiological conditions, Vitamin D is mainly supplied by the skin through the conversion of 7-dehydrocholesterol (7-DHC) to pre-vitamin D3 (pre-D3) by ultraviolet radiation and from dietary sources such as fatty fish, vegetable or fish oil, eggs and fortified vitamin D products (75).

The Commonwealth Government of Australia, in 2006, made a recommendation of vitamin D adequate intake (AI) which is an estimated vitamin D intake observed or experimentally-determined in healthy individuals based on serum 25D level (75). The serum 25D is suitable for assessing vitamin D status because it accounts for vitamin D production from the skin and dietary intakes, and serves as a suitable biomarker for vitamin D status (100).

However, there is a disagreement in the literature and clinical practice over the critical level for serum 25D required for optimal health function especially in the skeleton (101). A Working Group of the Australian and New Zealand Bone and Mineral Society, the Endocrine Society of Australia and Osteoporosis Australia in 2005 (102) has defined vitamin D deficiency as mild (25–50 nmol/L), moderate (12.5–25 nmol/L) and severe (<12.5 nmol/L) based on the serum 25D level. However, another recommendation suggests increasing the serum 25D levels above 75 nmol/L in elderly people to support optimal bone health (8). This recommendation was also supported by the evidence of vitamin D role in prevention (103) and treatment (104) of other chronic health diseases such as diabetes (105), cancer (106) and immune disorders

(107). Although vitamin D is an important nutrient, a large proportion of the population do not achieve an adequate vitamin D status with increased evidence of vitamin D deficiency and/or insufficiency in newborn (108), adolescent (109), pregnant (110) or non-pregnant women (111) and across various sections of the population in Australia (112) and around the world (113). A clear understanding of vitamin D metabolism is needed to meet the required vitamin D status in the community (114) and to recognise the role of vitamin D in bone cells.

1.4.3. Vitamin D metabolism

Vitamin D undergoes an extensive metabolic pathway to generate the biologically active metabolite, 1,25D (**Figure 1.8**). Vitamin D from skin production and dietary sources are transported by lipoproteins, albumin, or vitamin D binding protein (DBP) to the liver where it is converted by the Vitamin D-25-hydroxylase (CYP2R1) to 25D (115). The 25D then undergoes the next hydroxylation step into 1,25D in the kidneys by the activity of 25-hydroxyvitamin-D-1α-hydroxylase (CYP27B1) and serves as the major source of plasma 1,25D. The renal production of 1,25D is tightly regulated by factors such as serum calcium and phosphorus levels, and by its own feedback mechanism (116). Increased 1,25D levels act as a negative inhibitor to CYP27B1 expression and up regulate 25-hydroxyvitamin-D-24-hydroxylase (CYP24) expression, an enzyme responsible for catabolism of 25D to 24,25 dihydroxyvitamin-D (24,25D) and 1,25D to 1,24,25 trihydroxyvitamin D (1,24,25D). This is the first step of the C-24 oxidation pathway which catabolises vitamin D to calcitroic acid which then excreted in the bile or kidney (100,116,117).

The kidney is not the sole organ which expresses the CYP27B1 gene. Extra-renal production of 1,25D has been widely described in the last few decades. The existence of the mRNA encoding CYP27B1, presence of CYP27B1 protein and/or its enzymatic activity have been demonstrated in normal and or pathologic human tissues (118). Such a wide spread distribution of enzyme expression and the fact that plasma 1,25D level largely arises from the renal synthesis, have led some to suggest that the expression of CYP27B1 in non-renal cells is responsible for autocrine and paracrine actions of vitamin D. These activities are achieved through interaction between its synthesis and its local actions in a manner which has not been clearly explained (119). The vitamin D receptor (VDR) is also widely expressed amongst tissues to elicit the actions of vitamin D (120). Local biological activity of vitamin D is apparently a combination of expression and activities of the synthesizing enzyme, CYP27B1, its metabolising enzyme, CYP24 and its receptor, the VDR.

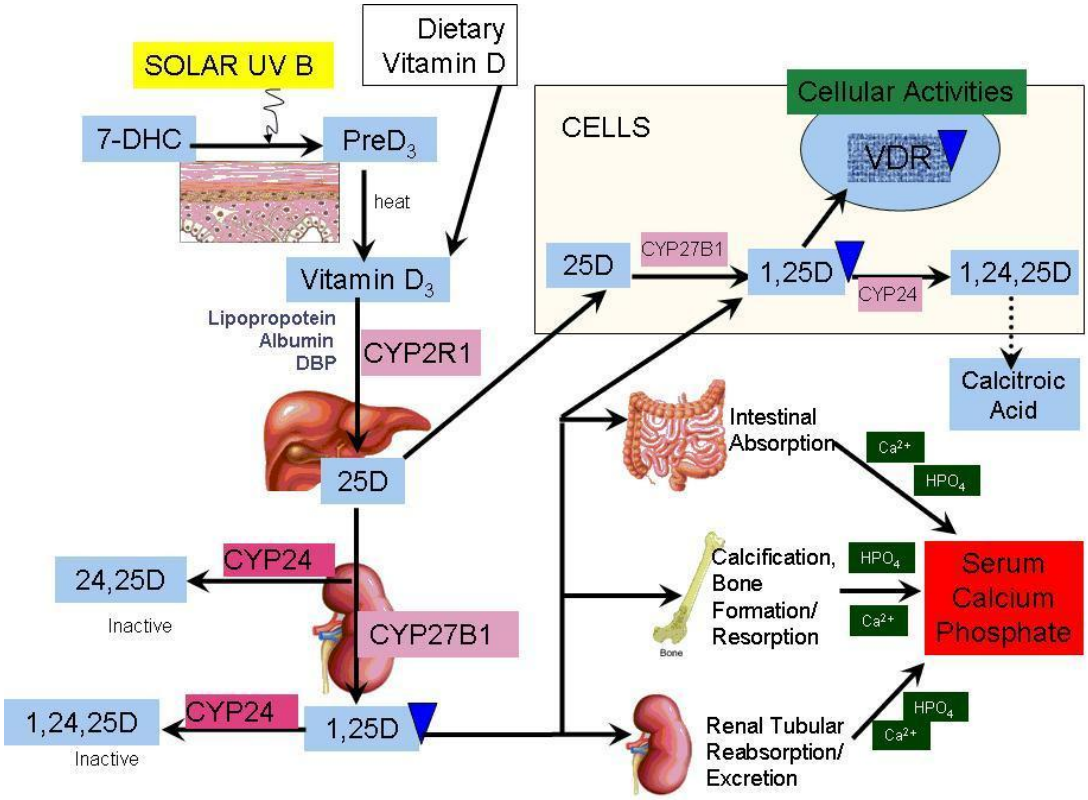

Figure 1.8. Vitamin D Metabolism

7-Dehydrocholesterol (7DHC) is converted to Pre-D3 and vitamin D3 by solar Ultraviolet B (UBV) light. Together with vitamin D3 from dietary intakes, vitamin D3 is transported to the liver by lipoproteins, albumin, or vitamin D binding protein (DBP) to be converted to 25D by CYP2R1. 25D is transported to the kidney for the next hydroxylation by CYP27B1 to produce 1,25D or to be converted to 24,25D by CYP24. Extra-renal cell can utilise serum 25D or 1,25D to elicit its cellular activities by a similar mechanism. Active 1,25D will modulate serum calcium and phosphate levels by modulating intestinal absorption, bone calcification via bone formation or resorption and renal tubular reabsorption or excretion of calcium/phosphate. Serum 1,25D can be converted to 1,24,25D by CYP24 in the kidney or within cells to produce calcitroic acid and excreted in the bile or urine. Modified from Holick and Chen, 2008 and Anderson et al. 2008 (31,113)

1.4.4. Vitamin D Receptor (VDR)

VDR was first discovered in around 1969 as a high-affinity nuclear receptor which acts as a ligand-activated transcription factor to modulate genes and affect diverse cellular processes (121). The VDR consist of 3 major domains, 1) ligand-independent transactivation function (activation function-1/AF-1) which is necessary for VDR-mediated gene transactivation, 2) DNA-binding domain (DBD) which responsible for high-affinity interaction with specific DNA sequences called the Vitamin D-Responsive Elements (VDREs) and 3) ligand binding domain (LBD), the retinoid X receptors (RXR) heterodimerization motif, and a ligand-dependent transactivation function, AF-2 (122).

There are three major steps in VDR activation, 1) ligand binding followed by hetero-dimerization with RXRs, 2) binding of the heterodimer to VDREs in the promoter region of vitamin D-responsive genes, and 3) recruitment of VDR-interacting nuclear proteins (coregulators) into the transcriptional pre-initiation complex via AF-1 region (123). Corepressors, such as Hairless, modify histone deacetylase activities resulting in chromatin compaction and gene silencing while coactivators, such as DRIP-TRAP, change the conformation and phosphorylation of the VDR heterodimer, promote histone acetylation, chromatin modification, and interaction with RNA polymerase machinery to stimulate gene transcription (122,124). Some coregulators can either be corepressors or coactivators, therefore, gene expression regulation by vitamin D-VDR complex is dependent on the ability to recruit co-regulatory protein complexes including coactivators and the interacting protein to activate or repress mRNA synthesis (125).

To elicit vitamin D biological activities, VDR can modulate the expression of vitamin D-responsive genes in three different ways; 1) regulate certain gene expression by binding to the VDREs of the gene's promoter regions, 2) regulate transcription through changes in the recruitment of coregulatory complexes, 3) inhibit the expression of some genes by suppression of certain transcription factors (125). Other than genomic or the DNA binding-dependent actions, vitamin D can induce rapid non-genomic actions via activation of second messenger systems and cytoplasmic membrane-associated events such as activation of mitogen-activated protein kinases (MAP kinases), 1α,25-dihydroxy-membrane associated rapid response steroid binding (MARRS), and rapidly-growing fibrosarcoma (Raf) kinase pathways (100). VDR is also able to influence calcium influx and release of calcium from intracellular stores via voltage-gated calcium opening, modulation of adenylate cyclase, protein kinases C and D, phospholipase C, or generation of other second messengers which also play a role in genomic actions (124). The non-genomic vitamin D effects are elicited by the nuclear VDR at the cytoplasmic membrane or by a plasma membrane VDR (126) which has been proposed to be located in caveolae of various cells such as keratinocytes, enterocytes, osteoblasts, or kidney. However the nature of the receptor remains controversial and the model has not been fully validated yet.

The vast array of vitamin D-VDR-VDRE activities needs to be regulated to maintain normal body function. This process is thought to be conducted via 1) control of ligand accessibility to VDR; 2) control on VDR cellular content through cell-specific VDR regulation; 3) genetic and post-translational VDR modifications, and 4) availability and activation state of the nuclear co-regulators which effect vitamin D-VDR-VDRE activities (122,123). Therefore, VDR research is vast and challenging to identify and

recognize the mechanism and activities of Vitamin D VDR-VDRE in various cells including bone.

1.4.5. Direct Vitamin D and VDR Activities in Bone Cells (Autocrine/Paracrine Actions of Vitamin D and VDR)

Traditionally vitamin D has been thought to exert its beneficial anabolic effects by enhancing intestinal calcium absorption, reabsorption in the kidney, and create an endocrine loop to maintain calcium and phosphate balance. However, recent findings have shown that vitamin D is important for skeletal development and mineralization by contributing to the growth plate development (127) and optimal maintenance of osteoblastic bone formation and osteoclastic bone resorption through regulation and control of osteogenesis, osteoclastogenesis, osteoblastogenesis and mineralization (31) as depicted in **figure 1.9**. A discussion of current knowledge of the roles of vitamin D and VDR in each of the bone cells is elaborated in the following sections.

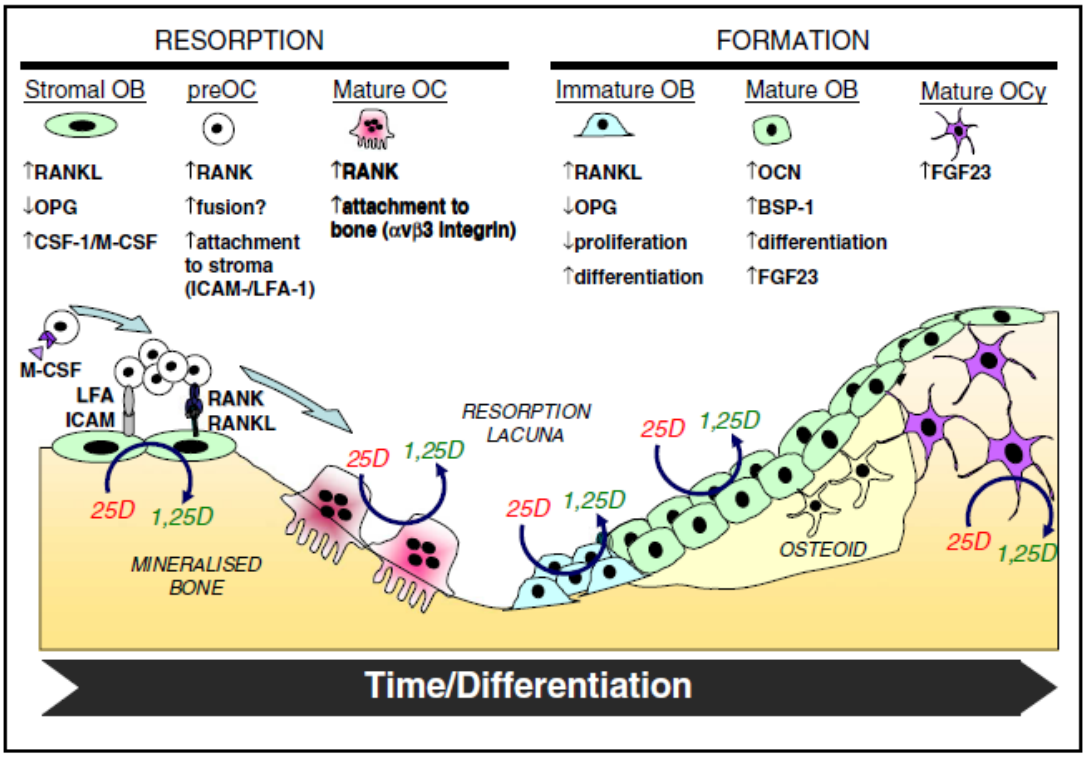

Figure 1.9. The Role of Vitamin D and VDR Activities in Bone Remodelling

This image depicts cellular events during bone remodelling and the role of 25D metabolism and VDR in osteoblast (OB), osteoclast (OC) and Osteocytes (OCy). Conversion of 25D to 1,25D supports osteoclast differentiation and maturation in bone resorption process. New bone is laid down on the resorbed site by immature OB, which proliferate and differentiate into mature OB that lay down osteoid, some of which are entrapped within the osteoid to become mature OCy. The role of 1,25D conversion and VDR in the corresponding cells are inferred from the known effect of vitamin D and VDR in each bone cells as stated in this literature review. Adapted from Anderson and Atkins 2008

1.4.5.1. Vitamin D and VDR-mediated Activities in Osteoclasts

Osteoclast differentiation, activation, and survival is regulated by several factors including macrophage colony-stimulating factor (M-CSF), interleukin 1 (IL-1), receptor activator of nuclear factor (NF)-κB ligand (RANKL), and tumour necrosis factor-α (TNF-α) (66). The role of vitamin D in osteoclasts is one of the first established direct effects of 1,25D in which the generation of osteoclasts from bone marrow and spleen cells requires 1,25D (47) via its binding to VDR in osteoblasts (128). Vitamin D-VDR activities in osteoblasts stimulate osteoclast activation via expression of RANKL (65) while expression of osteoprotegerin (OPG), a decoy receptor, inhibits RANKL activity, thereby modulating osteoclastogenesis (129). 1,25D also facilitates osteoclast precursor adhesion to stromal osteoblasts via increased expression of intercellular adhesion molecule-1 (ICAM-1) to direct the site for bone resorption (130). *In-vivo* studies using RANKL transgenic mice (TghuRANKL) demonstrated that the levels of huRANKL expression were correlated with bone resorption, disease severity and induced early-onset bone loss (131) similar to the findings in OPG knock-out mice (132). These findings are in contrast to transgenic mice in which the genes coding for OPG and RANKL were knocked out in mice which exhibited severe osteopetrosis and the complete absence of osteoclasts (133). These findings suggest that modulation of RANKL and OPG is essential for osteoclastic bone resorption.

Osteoclasts express CYP27B1 and metabolize 25D into active 1,25D resulting in up-regulation of osteoclast transcription factor, NFATc1, and a number of key osteoclast marker genes which associated with osteoclastogenesis (35). This suggests that 25D metabolism in osteoclasts can play an important role in osteoclast differentiation,

activity, and promoting the coupling of bone resorption to formation *in-vitro*. However, little is known regarding the *in-vivo* effects of osteoclast specific CYP27B1 modulation which warrant further investigations.

The presence of VDR in osteoclasts is still under debate due to difficulties in obtaining sections of undecalcified adult bone and lack of antibodies with the required specificity. One study shows mRNA expression of VDR was detected in osteoclast-like cells (osteoclastoma) (134) suggesting that osteoclasts are able to modulate responses to 1,25D. However, another study using a specific immunohistochemistry method failed to demonstrate the presence of VDR in multinucleated osteoclasts, and chondroclasts (135). This latter finding suggests that osteoclasts and chondroclasts are minor targets of 1,25D and that osteoblasts are the main driver of vitamin D signalling in bone. Further study is needed to solve this controversy and to elucidate the role of VDR in osteoclasts during bone remodelling.

1.4.5.2. Vitamin D and VDR-mediated Activities in Osteoblasts and Osteocytes

The role of vitamin D and VDR in osteoblasts and osteocytes has been extensively studied in the last few decades. VDR is highly expressed in primary osteoblasts and various osteoblasts cell lines where it is co-expressed with the CYP27B1 to elicit autocrine/paracrine actions of vitamin D-VDR in these cells (33). The VDR expression can be regulated by 1,25D, PTH, glucocorticoids, transforming growth factor-β (TGF-β), and epidermal growth factor (EGF) (136). VDR regulation of gene transcription in osteoblasts via interaction of various transcription factors, DNA and histone-modifying proteins has been established (137). However, the regulation of VDR expression in osteoblasts by other factors than those mentioned above which influence

VDR expression, and its activities is still one of the most interesting areas of research in this field.

CYP27B1 expression in osteoblasts is modulated by TGF-β (138), 1,25D, Interferon-β, IL-1, and insulin-like growth factor-1 (IGF-1) (139). However, functional consequences of CYP27B1 activity for osteoblast biology were unclear due to limited data on the regulation of CYP27B1 in osteoblasts. Regulation of CYP27B1 expression in osteoblasts is more complex than in the kidney which involves local regulators and may differ depending on the differentiation stage of the osteoblasts (139). Therefore, further *in-vitro* and *in-vivo* studies on the activity of CYP27B1 in osteoblasts is needed to elucidate the role of CYP27B1 expression in osteoblast activity.

Vitamin D-VDR activities in osteoblasts or osteoblast-like cells include; 1) increase expression and/or protein levels of osteocalcin and osteopontin, thus supporting bone matrix formation and improved bone mineralization (140), 2) increase expression of RANKL which is involved in the activation of osteoclasts for bone remodelling (141), 3) shifting the expression of predominantly L-type to T-type voltage-sensitive calcium channels which alters calcium permeability to support differentiated functions of osteoblasts (142), 4) alter membrane lipid turn-over, prostaglandin production, protease activity or other second messengers which leads to modification of bone matrix, calcification or other cellular function (143), 5) repress phosphate regulating gene with homology to endopeptidases on the X-chromosome (PHEX) expression and FGF-23 to sustain phosphaturic activities for bone remodelling (144), and 6) up-regulate cyclin-dependent kinase inhibitors p21 (waf1/cip1), p27, cyclin C and blocks

the cell cycle transition to control cell function, proliferation and differentiation during bone remodelling (145).

Osteocytes produce FGF-23, an important regulator of serum phosphate and 1,25D levels (146). Elevated FGF-23 levels increase phosphate excretion, reduce serum phosphate levels, CYP27B1 activity and increasing PTH secretion (147). Thus, FGF-23 plays an adaptive role in regulating serum phosphate in responses to changes of serum calcium (148) as a secondary endocrine loop with vitamin D/FGF-23/Phosphate axis superimposed physiologically on vitamin D/PTH/Calcium axis (149). This mechanism is thought to facilitate the integration of ion homeostasis and prevent bone over-mineralization and ectopic calcification in other soft tissues and kidney (150). Therefore, the vitamin D-VDR actions on bone are not limited to calcium metabolism and homeostasis but also phosphate metabolism and homeostasis to balance the effect of bone remodelling process.

Studies of vitamin D-VDR-VDRE in the skin have shown a vitamin D-calcium paradox where vitamin D inhibits keratinocyte proliferation in psoriatic skin but induces epidermal proliferation in normal skin (126). Therefore, vitamin D-VDR-VDRE activities in osteoblasts might have the similar properties during differences in calcium, phosphate and/or vitamin D status. This is an important notion for further understanding of the role of dietary calcium intake in vitamin D-VDR activities during physiological and/or pathological condition and during acute or chronic hypocalcemic settings.

Dietary calcium is considered to affect VDR gene responsiveness, bone size, and bone mass via insulin or insulin-like growth factor pathways (151) or by other pathways which need to be elucidated. *In-vitro* study using the mature osteoblast cell line MLO-A5, suggested that extracellular calcium promotes mineral deposition via activity of nucleotide pyrophosphate phosphodiesterase (NPP1) (152) and in primary OSVDR calvarial bone culture, increased extracellular calcium enhanced mineral deposition (153). Interaction between dietary calcium and VDR activities in bone forming cells has not been established in *in-vivo* studies. Research is needed to shed more light on this relationship if we are to optimize calcium and vitamin D status in the population. This goal can be achieved through studies in animal models to explain the *in-vivo* phenomenon of dietary calcium and vitamin D-VDR-VDRE activities on bone forming cells.

1.5. IN VIVO STUDIES ON THE ROLE OF CALCIUM, VITAMIN D AND VDR ALTERATIONS IN BONE CELLS

1.5.3. Dietary modification of vitamin D and calcium

Rat and mice are the most commonly used animals for dietary alteration in calcium, and or phosphate and/or vitamin D due to their similarities with human metabolism and ease of use. One dietary study which investigated the role of vitamin D in bone and bone cells activities was conducted by Anderson et al. in 2008 (154) using a rodent model of vitamin D depletion over a range of serum 25D levels (10 - 115 nM). In their study, the 7 months old rats demonstrated a positive association between bone volume and circulating 25D levels, osteoclast surface levels and RANKL to OPG mRNA ratio which were independent of serum 1,25D levels. This study also demonstrated that

osteopenia arises at serum 25D levels below 80 nM due to increased osteoclastogenesis. Another model of vitamin D deficiency status in rats was conducted by Mailhot et al. 2007 (155) using an *in-vivo* depletion, repletion followed by redepletion of vitamin D to assess bone consequences with cyclic nutritional changes. This study showed the importance of dietary calcium/phosphate ratio to maintain optimum concentration of serum calcium/phosphate for bone health in growing animals during the cyclic changes of vitamin D levels.

Calcium supplementation increases bone density in female adolescent (156) or elderly (12), ambulatory subjects or post fracture patients (157). In animal models, increased dietary calcium also demonstrates beneficial effects on bone mineral status (158,159). Therefore, calcium supplementation has been used as a nutritional treatment for osteoporosis and other low bone density diseases (11).

Dietary phosphate's role on bone health is still currently under debate. In a human study, variation in dietary phosphate induced changes in FGF-23 and serum 1,25D levels as well as urinary phosphate excretion (160). Recent studies of inherited and acquired hypophosphatemia (X-linked hypophosphatemic rickets/osteomalacia (XLH), autosomal dominant hypophosphatemic rickets/osteomalacia (ADHR) and tumour-induced rickets/osteomalacia (TIO)), have identified novel genes (PHEX, FGF-23) in the regulation of phosphate homeostasis which are mainly controlled by bone cells (146,147). However, the detailed mechanism by which dietary phosphate directly modulates bone cells activities is still unknown.

1.5.4. Genetically-modified mice

Genetically modified mice have been used to elucidate the role of a specific gene/s in various studies of physiological activities including vitamin D by modulating the genes encoding the VDR, or the enzymes controlling vitamin D metabolism (161). These genes can be completely ablated to create a global deletion mouse model or using specific promoters to delete the gene in specific cells and create conditional knock-out mouse models. These genes can also be inserted into the genome using specific promoters to produce overexpression of the genes in specific cells (the transgenic mouse models). Generation of these mouse models can be useful for generating data of direct activities of vitamin D in bone cells modulating bone turnover and mineral status.

The first genetically modified mouse model to investigate VDR activities in bone cells was the global VDR-knock out (VDR-KO) mice (which was reported by Li et al. in 1998 (22) and Amling et al. in 1999 (23)). They observed phenotypic abnormalities of the global VDR ablated mice and its relation to dietary calcium. Dietary regimens which normalized serum calcium and phosphate levels have prevented the development of osteomalacia or rickets but did not correct the alopecia occurring in these mice. The global VDR-KO mice revealed growth plate disorganization, matrix and bone fragility when fed a normal diet due to impaired intestinal calcium absorption and/or effects of secondary hyperparathyroidism due to hypocalcaemia. Thus, the apparent normalization of the bone phenotype when serum calcium and phosphate were normalized suggested that VDR activities on bone cells are not essential when calcium intake is adequate.

The above conclusions were challenged by a study in aged global VDR-KO mice (17 weeks old) by Panda et al. in 2004 (162). This study demonstrated that by feeding a rescue diet containing high calcium (2 %) and phosphorus (1.25 %), the normalization of plasma calcium and PTH levels was able to normalize cartilage and skeletal mineralization. However, the rescue diet was unable to overcome the bone loss that occurred in the global VDR-KO mouse line as they aged. Importantly, the bone loss that occurred in the VDR-KO mice was not due to increased bone resorption but was associated with a marked reduction of bone formation. This suggested that vitamin D activity in osteoblasts might be important for bone formation in aged mice and that calcium and vitamin D/VDR system may exert effects on bone co-ordinately or independently by mechanisms which have not been fully understood.

Since the above study uses global knock-out model, it is difficult to distinguish the role of VDR in bone cells as endocrine or as an autocrine/paracrine effect in the physiology of bone. Therefore, direct effects of VDR on bone cells activities remains poorly understood due to the systemic defects on calcium metabolism in the global VDR-KO mice. The technology to design and make conditional knock out mouse lines using various promoters have been developed in the last few years (163,164). The most commonly used method to generate a conditional mouse model is the *Cre/LoxP* system which act as “genetic switches” to spliced the gene flanked with homozygous LoxP sites in the presence of Cre-recombinase (165). Therefore, this system provides a relatively straight-forward method to delete a gene within a specific type of cell creating a useful mouse models to study specific activity of the gene within the specific cell type.

The VDR conditional knock out in chondrocytes using *Cre-loxP* system and Collagen 2a1 promoter model demonstrated normal growth-plate chondrocyte development with impaired vascular invasion and a reduction of osteoclast number in 15 day old mice resulting in increased trabecular bone mass (166). Increase serum 1,25D levels, together with reduction of RANKL in their *in-vitro* study suggest VDR in chondrocytes is required for osteoclast formation during bone development.

Conditional knock out of the VDR gene in osteoblasts using a similar system with the osteoblast-specific 2.3 kb collagen1a1 promoter also shows increased bone mass in radiological assessments without disturbance of mineral metabolism (167). Bone histomorphometry analyses in this study indicates that the phenotype occurs due to the reduction of bone resorption with decreased expression of RANKL suggesting VDR in osteoblasts is a negative regulator of bone mass. Interestingly, osteocyte specific knock out of VDR using *Dmp1-cre* mouse model shows no phenotype and no changes to RANKL expression (168). These data suggest that VDR in chondrocytes and immature osteoblasts is important for regulating RANKL expression under normal dietary calcium/phosphate intakes.

Studies on the conditional knock out of VDR in the intestine using Villin-$Cre^{+/-}Vdr^{fl/fl}$ (Vdr^{int-}) mouse model showed decrease of TRPV5, TRPV6, and Calbindin D_{9K} expression with a decrease of calcium absorption without a change in serum calcium (168). This mouse model also shows changes in the bone structure and inhibition of mineralisation suggesting that with normal VDR levels in bone, the endocrine effect from inhibition of calcium absorption is stronger than the local effect of VDR under normal dietary regiment.

Another model that had emerged in the study of VDR in osteoblasts cells is the overexpression of VDR solely in mature osteoblasts (OSVDR mice) which was generated to test the potential value of increasing VDR activity in osteoblasts. This mouse model demonstrated increased mineral content (169), decreased bone resorption, and increased cortical periosteal bone formation without changes to the calciotropic hormones (36). More recently, the OSVDR mouse model was used by Baldock et al. 2006 (37) and Lam et al. 2014 ((170) to show that increased bone volume in OSVDR mice was dependent on the levels dietary calcium but not on vitamin D status. OSVDR mice demonstrated an increased in bone volume when fed a normal level of dietary calcium (1 %) but lost this phenotype when fed moderately low calcium diet due to increased RANKL/OPG ratio. This finding signifies the importance of direct vitamin D anabolic activity in osteoblasts in the pathways of maturation and mineralisation of osteoblastic cells as well as to indirectly inhibit osteoclastogenesis and osteoclastic bone resorption.

All ligand-inducible nuclear transcription factors such as the VDR recognizes the hormone responsive elements in the promoter of its target genes such as osteocalcin (171). Osteocalcin or also known as bone γ-carboxyglutamic acid protein (BGLAP) is expressed to supports bone matrix formation and improved bone mineralization (140) which are the characteristics of mature osteoblasts. Osteocalcin expression is induced by the VDR which acts on the osteocalcin promoter to drive its osteoblast-specific expression (172).

A thorough investigation of the role of dietary calcium/phosphate on vitamin D-mediated activities in bone cells have yet to be conducted. Similar setting, background, treatment and conditions must be made for a comparable and comprehensive study in VDR-mediated activities of the bone forming cells. Thus, studies which utilised over-expression/transgenic and conditional knock out mouse models of the VDR in mature osteoblasts using osteocalcin promoter during dietary restriction of calcium/phosphate are needed to elucidate the bone physiology with regard to VDR activities on mature osteoblasts.

1.6. RESEARCH QUESTION

In order to investigate the interaction between dietary calcium and VDR-mediated activities in bone cells, this research aims to answer the following question:

- What are the effects of dietary calcium/phosphate intakes on VDR activities within mature osteoblasts to modulate plasma calcium and phosphate levels, calciotropic and phosphate regulating hormone levels, skeletal structure and bone mineral status?

1.7. HYPOTHESIS AND AIMS

1.7.1. Hypothesis

Dietary calcium intake sufficient to maintain calcium balance will modulate direct and indirect activities of VDR to alter gene expression and protein production in bone forming cells to enhance skeletal structure, mineral content and bone strength.

1.7.2. Aims

Objectives

In order to answer the questions above, the studies in this theses has the following objectives;

a. To characterize mouse models with regard to bone structure and plasma calcium homeostasis in which the expression of *Vdr* gene is modified in bone forming cells.
b. To describe VDR actions in bone forming cells activities that modulate bone structure.
c. To explore the interaction between dietary calcium/phosphate intakes and vitamin D activities in osteoblasts to modulate bone remodelling and skeletal structure.

Specific

The studies described in this thesis addresses the following specific aims;

a. Establishing the physiological role of VDR in mature osteoblasts in bone structure and mineral homeostasis
b. Determining the effects of dietary calcium/phosphate on the bone structure, biochemical parameters, and gene expression of the genetically modified mouse models in which the VDR is either a) overexpressed in mature osteoblasts (ObVDR-B6) or b) specifically deleted in the mature osteoblasts (ObVDR-KO).
c. Characterise the structural, biochemical, cellular and molecular mechanisms which underpin the influence of low dietary calcium stress in determining the bone phenotype

1.8. SIGNIFICANCE OF PROJECT

Current knowledge of the role of VDR in skeletal health is ONLY to regulate serum calcium and phosphate homeostasis via the modulation of intestinal calcium/ phosphate absorption. Recent findings have proposed a direct role of vitamin D in skeletal health. However, few have disputed this hypothesis due to little *in-vivo* evidences to support the direct role of vitamin D and VDR within osteoblasts to change bone structure and or modulate mineral homeostasis. Therefore, the proposed studies within this thesis are required to elucidate and further strengthen the evidence of the direct involvement of VDR in skeletal health and mineral homeostasis.

CHAPTER 2: MATERIALS AND METHODS

2.1. MATERIALS

Consumables and chemicals used in these experiments were purchased from Sigma Chemical Company (Sigma-Aldirch, New South Wales, Australia), unless stated otherwise.

2.2. ANIMALS

Animals used in the experiments were male and female mice on *C57Bl6/J* genetic background obtained from breeding programmes either within the South Australia Pathology Animal Facility (SA Pathology, Adelaide), the University of South Australia Reid Animal Facility, (RAF) or the University of Adelaide, Laboratory Animal Services (LAS). Records on birth, date of tissue specimen (tail) collection for genotyping, day of injection, and culling date were maintained on clinical record sheets (CRS) in accordance to requirements of the University of Adelaide Animal Ethics Committee for each project. All studies were approved by the University of Adelaide Animal Ethics Committee Medical project number M-2012-092, RM No. 0000013478. Ethics approval is attached in the appendix section. Concurrent ethical clearance was obtained from the University of South Australia and SA Pathology Animal Ethics committees.

2.2.1. Wild Type (WT)

The wild-type (WT) mouse from *C57Bl6/J* genetic background were used as control animals for the transgenic mouse model ObVDR-B6. WT mice used in the studies

were either purchased and or litter-matched depending on the experiment as indicated in each corresponding experiment.

2.2.2. Overexpression of Vitamin D Receptor in Mature Osteoblasts Transgenic Mice (ObVDR-B6)

The transgenic mouse model in which the gene for the human vitamin D receptor is over-expressed in mature osteoblasts on the *FVB/N* genetic background (OSVDR) was provided by the Garvan Institute (Darlinghurst, Sydney, NSW, Australia). The OSVDR were backcrossed onto the *C57bl6/J* genetic background for more than 6 generations resulting in 98.4 % *C57Bl6* congenicity. This new mouse line was labelled as *ObVDR-B6*.

2.2.3. Mature Osteoblasts Specific Vitamin D Receptor Knockout Mice (ObVDR-KO)

The osteoblast-specific vitamin D-receptor knock out mouse model (*ObVDR-KO*) was generated using *Cre-LoxP* methods under the supervision of A/Prof. Rachel Davey, University of Melbourne at the Austin Animal Facility, Melbourne, Victoria. Mice homozygous for the floxed VDR gene, in which exon 2 of the VDR is flanked by *lox-P* sites or the $VDR^{fl/fl}$ mice, supplied by Professor S. Kato (University of Tokyo, Japan), were mated with osteocalcin promoter driven-*cre* recombinase ($OcnCre^{+/-}$) transgenic mice, supplied by Professor T.L. Clemens (University of Cincinnati, USA) to produce $ObVDR^{fl/flCre+}$ (ObVDR-KO). Control animals used in the study were littermates of the ObVDR-KO or the $ObVDR^{fl/flCre-}$ ($VDR^{fl/fl}$) mice,

2.3. HOUSING

All mice were housed in 22 – 24ºC room with a 12h light/dark cycle and exposed to standard lighting. All mice were weaned at 20 to 21 days of age and housed in 2 – 5 mice/cage. Cage conditions were kept constant throughout the projects (e.g. bedding, boxes, toys, cage cleaning, etc.). Mice were provided *ad-libitum* diet in accordance to the study conducted and free access of water. Diets were modified for each project as described in the corresponding chapter.

2.4. TISSUE COLLECTIONS AND STORAGE

All animals were humanely killed in accordance to the procedures and ethics requirements. In brief, mice were anaesthetised using isoflurane prior to cardiac puncture and cervical dislocation. The tissue collection and storage of tissue were performed immediately after death. Right femora and vertebrae were stored immediately in 10 % formalin for 4 – 6 days prior to micro-CT analyses and histological sectioning. For RNA analyses, the right tibia, left radius, heart, lung, liver, spleen, kidney, proximal intestine, muscle, and skin tissues were immersed in RNALater® (Ambion ®, Life technologies, Austin, Texas, USA) overnight at 4ºC and then stored at -80 ºC. Other tissues such as scapulae were wrapped in gauze, and immediately stored at -80 ºC.

2.5. BLOOD BIOCHEMISTRY

2.5.1. Serum Collections

Cardiac blood specimens were immediately placed on ice. Serum was collected by centrifugation for 15 to 20 minutes at 4500 rpm and stored in -80 ^{o}C until required for analyses.

2.5.2. Serum Calcium, Phosphate and Alkaline Phosphatase

Serum calcium and phosphate were measured on chemical analyser Konelab® 20/20XT using reagents manufactured by Thermo Fisher Scientific (Vantaa, Finland).

2.5.3. Serum 1,25-dihydroxyvitamin D_3

Serum 1,25-dihydroxyvitamin D_3 was measured using ImmunoDiagnostic Systems chemiluminescent immunoassay according to the manufacturer's instructions**.**

2.5.4. Serum Fibroblast Growth Factor-23 (FGF-23)

Serum FGF-23 was measured using Enzyme-Linked ImmunoSorbent Assay (ELISA) kit for quantitative determination of mouse FGF-23 manufactured by Immutopics International (San Clemente, USA). This kit uses goat polyclonal antibodies which bind specifically to epitopes within the carboxyl-terminal (C-term) region of the mouse FGF-23. The assay was performed in accordance to the manufacturer's instructions.

2.5.5. Serum Parathyroid Hormone (PTH)

Serum PTH was quantified using mouse PTH 1-84 enzyme-linked immunosorbent assay (ELISA) kit from Immutopics International (San Clemente, USA). The kit uses two different goat polyclonal antibodies against mouse PTH to detect the biologically

active intact form of PTH. The biotinylated antibody targets the mid-region /c-terminal portion (39-84) and the second antibody conjugated with horseradish peroxidase (HRP) targets the N-terminal region (1-34). Assays were performed in accordance to the manufacturer's instructions.

2.5.6. Serum C-terminal Telopeptides of Type 1 Collagen

The fragments of C-terminal telopeptides of type 1 collagen (CrossLaps) in mouse serum were measured using enzyme immunoassay (EIA) kit from IDS (ImmunoDiagnostic System, USA). The RatLaps^{TM} polyclonal antibodies react against synthetic peptide (sequence EKSQDGGR) specific for C-terminal telopeptide α-1 chain of type 1 collagen in rats. Assays were conducted according to the manufacturer's instructions.

2.5.7. Serum Tartrate-resistant Acid Phosphatase-5b (TRAP5b)

Serum concentrations of TRAP5b were measured using solid phase immuno-fixed enzyme activity assay (IEA) with MouseTRAP^{TM} assay from IDS (ImmunoDiagnostic System, USA). The MouseTRAP^{TM} kit uses polyclonal antibodies which react to recombinant mouse TRAP5b antigen that can be used as confirmation or prediction of osteoclast number. Assays were conducted based on manufacturer's instructions.

2.6. X-RAY IMAGERY AND MICRO-COMPUTED TOMOGRAPHY

2.6.1. Femur

Femoral bone was analysed by micro-CT using a Skyscan 1076 scanner (Kartuizersweg, Belgium). Femora were de-fleshed and placed inside a 5mL polypropylene tube containing 10 % formalin for up to 6 days at 4^{o}C prior to storage

in 70 % ethanol. Prior to micro-CT scanning, femora were X-ray imaged (Faxitron LX-60, Tucson, AZ, USA) with X-ray voltage at 31kV, and an exposure time of 11.5 – 16.5 ms. Each bone was then inserted into a sealed drinking straws containing 70 % ethanol prior to micro-CT scanning. Bones were then scanned at a voxel size of 9 µm with a 0.5 mm aluminium filter, X-ray source current of 110 µA, voltage 50 kV, and camera exposure time of 5890 ms. At the end of each scan, reconstructions of TIF image datasets into Z-stack BMP datasets were conducted using NRecon software (version 1.6.9.18). The settings for NRecon included ring artefact correction at 12, beam hardening correction at 30 % and smoothing set radius of 1. Reconstructed images were realigned using Dataviewer (version 1.5.1.2) to ensure comparable alignment of all bones. Realigned z-stack BMP datasets were than analysed CTAn software (Skyscan/Bruker, version 1.14.4.1) as described in **section 2.6.3** and **2.6.4** below.

2.6.2. Vertebral Bone

For vertebra, micro-CT analyses were performed using Skyscan 1174 scanner (Kartuizersweg, Belgium). Vertebrae were placed in 5mL polypropylene tubes containing 10 % formalin for up to 6 days at 4 ^{o}C prior to storage in 70 % ethanol. Muscle and fasciae surrounding the vertebrae were removed while keeping the lower ribs intact and attached as markers for the position of Vertebra Lumbar-1 (L-1). Bones were tightly packed using gauze soaked with 70 % ethanol.

Image acquisition was obtained with voxel size of 6.5 µm with X-ray source voltage of 50 kV, source current at 800 µA, exposure of 2,600 ms and a 0.25 mm aluminium filter. After image acquisition was complete, reconstructions were performed with

NRecon program (version 1.6.9.18) as described in **Section 2.6.1**. Realignment and image data analyses were conducted in the same manner as described in **Section 2.6.1.**

2.6.3. Anatomical Definitions

To measure specific compartment of bone anatomy, the manually delineation of each anatomical region was done using CTAn software (Skyscan/Bruker, version 1.14.4.1). For metaphyseal trabecular bone, distal femoral secondary spongiosa was investigated. A volume of interest (VOI) for distal femoral secondary spongiosa was defined by a region devoid of primary spongiosa and cortical bone and encapsulating a metaphyseal regions equivalent to either 10 % or 20 % of the full femur length depending on the study. The distal boundary of each VOI was set based on a defined distance from outermost aspect of the epiphyseal cortical bone. For VOI's based on 20 % of full-femur length, the set distance was 1.8mm. For VOI's based on 10 % of full-femur length, 2.3mm was the set distance.

For femoral cortical bone, mid-shaft diaphyseal bone was isolated as being exactly mid-point of the full femur length. Depending on the study, a volume of cortical bone was defined by either 2mm or 10 % of the femur length, evenly spanning the mid-point. The cortical bone was devoid of trabecular bone in this region.

For vertebra, trabecular bone was analysed using a fitted elliptical region of interest (ROI) placed within the vertebral body, which excluded cortical bone. For 6 week old mice, the VOI included 1.2mm or 185 trans-axial slices. For all older mice, the VOI included 1.5mm or 231 trans-axial slices.

2.6.4. Segmentation Methods.

To binarize the grey-scale image stacks for each VOI, a different method was adopted for trabecular and cortical bone segmentation. For trabecular bone analyses, an adaptive threshold technique was used. Adaptive thresholding, using CTAn software, was set with the upper and lower pre-thresholding limits of 255 and 60 respectively. The pre-threshold effectively delineates a region of interest in which adaptive thresholding is applied. All pixels outside the pre-threshold white mask are excluded from adaptive thresholding and set as black (space). The radius was set to 5 pixels. The radius defines the circle/sphere in which the threshold is calculated. To remove any residual artefact signal from the VOI z-stack, black and white bodies with radius less than 10 pixels was removed by a despeckling process.

For cortical analyses, a global thresholding technique was used whereby upper threshold was set to 255 and lower threshold set to at 60 or 80 for full femur length analyses or mid-shaft cortical analyses respectively. To remove any residual artefact signal from the VOI z-stack, black and white bodies with radius less than 10 pixels was removed by a despeckling process.

2.6.5. Calculated Bone Parameters

Trabecular bone was calculated based on 3D methods using a marching-cubes algorithm set by the software and results are reported as follows and according to the guidelines for assessment of bone microstructure in rodents by Bouxsein et al 2010 (173).

- Bone volume per total volume (BV/TV); a ratio of segmented bone volume to total volume of the VOI.

- Trabecular thickness (Tb.Th); Mean thickness of trabeculae based on direct 3D methods.
- Trabecular number (Tb.N); Average number of trabeculae/unit length.
- Trabecular separation (Tb.Sp); Mean distance between trabeculae.
- Connectivity density (Conn.D); a measure of connectivity of the trabeculae normalized by tissue volume indices.
- Structural model index (SMI); indicator for structure of trabeculae in which SMI will be 0 for parallel plates and 3 for cylindrical rods.

For mid-shaft cortical analyses, a shrink wrap ROI in 2D space was applied prior to analysis. Using 2D analysis, the measures reported include periosteal perimeter (Ps.Pm) and bone perimeter (B.Pm) which were used to derive endosteal perimeter (Es.Pm). Using 3D analysis, the measures reported include cortical bone volume (BV) and cortical thickness (Cort.Th).

2.7. BONE HISTOLOGY

2.7.1. Injections of Fluorochrome Labels

Fluorochrome labels used in the studies were calcein and xylenol orange to label active bone forming surfaces. Calcein was prepared by mixing 0.1 g of calcein ($C_3H_{26}N_2O_{13}$) and 0.1 g of sodium bicarbonate ($NaHCO_3$) in 10 mL of 0.9 % sterile saline to produce 10mg/mL stock solution. Xylenol orange was prepared by adding 0.45 g xylenol orange ($C_{31}H_{28}N_2Na_4O_{135}$) and 0.2 g sodium bicarbonate into 10mL of 0.9 % sterile saline to produce 45 mg/mL of stock solution. At 7 and 2 days prior to death (or as

otherwise stated), animals were intra-peritoneally injected with 10 mg/kgBW of calcein and 90 mg/kgBW of xylenol orange respectively as previously described (174).

2.7.2. Bone Preparation for Dynamic Histomorphometry

Bones were cut using slow speed saw from Beuhler Ltd (Lake Bluff, Illinois, USA) equipped with diamond edged blade bathed in 70 % ethanol to expose the metaphyseal and diaphyseal region. For dehydration, bones were submersed in 90 % ethanol for 24 hours and room temperature followed by two 24 hours periods in 100 % ethanol. Bones were then transferred into 2mL softener solution containing 100 % methyl methacrylate/MMA and 10 % v/v polyethylene glycol/PEG 400 and left at room temperature for 10 - 14 days.

To embed bone in resin, solutions of 100 % MMA and 10 % PEG 400 were mixed with 0.4 % Peroxydicarbonate (perkadox-16) in a 5 mL polypropylene container and placed in the oven at 37 °C for 24 hours. Distal femora exposed on the metaphyseal region were placed facing down while the proximal ends were placed flat on the bottom of the tube. The proximal end of the femoral bones was also processed and place flat on the bottom of the tube during embedding process.

Once set, samples were then removed from the tube and fixated to an aluminium stub (Biorad, Gladesville, NSW, Australia) with either Araldite™ glue (Selleys, Padstow, NSW, Australia) or co-extruded epoxy putty (Selleys, Padstow, NSW, Australia), giving care to ensure that the bone specimen was aligned according to the desired section orientation. The distal metaphysis bone samples were place flat on the exposed

sagittal surface, while the proximal end was placed upright to reveal its trans-axial shaft region.

Resin embedded bones, fixed to aluminium stubs were trimmed to expose the bone surface area by removing the plastic excess using a motorized microtome (Leica 2255, Germany). When the bone alignment and shape was satisfactory, 5µm sections were then mounted onto slides and immersed in heated spreading solution for 2-4 minutes. Spreading solution was made by adding 30 %: 70 % ethylene glycol and mono-ethyl-ether in 70 % ethanol solution. Sections were dipped 2-3 times into 65 – 70 ^{o}C spreading solution, covered with plastic film and flattened onto slides prior to clamping with blotting paper and placed into 37 ^{o}C oven for 12 – 24 hours.

2.7.3. Double Label Fluorochrome Measurement

Double label fluorochrome measures were conducted on unstained slides by removing the polyethelene (resin) plastic with acetone for 12 – 15 minutes followed by dipping into xylene (2 x 100 %) before being mounted in xylene-based mounting medium (DePex mounting medium Burr, Prolabo, BDH Laboratory Supplies, England).

Slides were analysed using fluorescence microscope on filter 3 (Olympus DP73 and Olympus BX 53) using OsteoMeasure^{TM} software version 3.3.O.2. In brief, secondary spongiosa from each section was analysed, with 10x objective magnification, starting from the top upper growth plate down to approximately 2cm towards diaphysis (**Figure 2.1**). A total 16 visual fields were analysed by drawing a bone map consisting of double label, single label and bone perimeter which were automatically computed and tabulated by the software. Results reported were histology BV/TV, Label

Perimeter (L.Pm), Mineral Apposition Rate (MAR), Mineralising Surface/Bone Surface (MS/BS), and Bone Formation Rate/Bone Volume (BFR/BV).

2.7.4. Toluidine Blue Bone Staining and Analysis of Osteocyte Density

Toluidine blue (TolB) staining is used to visualise osteoblasts and measure cortical osteocyte density on paraffin or resin sections. TolB stains were made by mixing 0.1g of toluidine blue O (ProSciTech, Kirwan, Qld, Australia) with 0.1 g of sodium tetraborate in 100 mL distilled water, filtered into a bottle wrapped with aluminium foil and stored as 0.1 % stock solution in 2 – 8 ^{o}C.

TolB staining was performed on resin sections (or as otherwise stated) by removal of resin from slides and placing them on a 90 – 95 ^{o}C heating block. A few drops of 0.01% TolB working solution were placed over the bone tissue for 2 minutes and blotted onto filter paper prior bathing in distilled water. Slides were sequentially dipped into 1 x 50 % ethanol, 2 x 100 % ethanol, 2 x 100 % xylene before being cover-slipped with xylene based mounting medium.

To assess osteocyte density, slides were imaged using 4x and 200x magnification (Olympus Microscope, DP73 and BX 53) and analysed using OsteoMeasure^{TM} software (V3.3.0.2). Measurements were performed on 1mm length cortices of distal metaphysis starting from 0.5 – 0.6 mm from the edge of growth plate (**Figure 2.2**) and results reported as Metaphyseal Cortical Bone volume (BV), Number of Osteocytes (N.Ot) and Osteocyte Density (N.Ot/BV).

2.7.5. Tartrate Resistant Acid-phosphatase (TRAP) Staining of Osteoclasts

Sections for TRAP stains were placed in Coplin jar and resin was removed with acetone processing. Tris-HCl buffer pH 9.4 was added and placed in the oven at 37ºC prior to washing with demineralised H_2O. Acid-phosphatase (AcP) stain was prepared using a formula for 1 Coplin jar (8 slides). Briefly; 100 µL of 0.4 g sodium nitrite in 10 ml dH_2O solution was added with 100 µL basic fuchsin until a fetid scent was produced. Tartaric acid (0.035g) in 35 mL sodium acetate buffer (pH 5.2) were added and mixed with 0.04 g napthol ASBI Phosphate in 2 mL dimethlyformamide (DMF). The final solution has pink tinge and was used to incubate the slides for 1 hour at 37ºC in the oven. Demineralised water was used to rinse the slides prior to counter-staining with Haematoxylin for 1 minute followed by few dips in acid carbonate solution. Slides were sequentially dipped into 2 x 100 % ethanol baths followed by xylene, before being cover-slipped using mounting medium.

Using an Olympus microscope with OsteoMeasure^{TM} (V3.3.0.2), maps of tissue area were drawn on 40x magnification which encompassed approximately 1.8 – 2.2 mm region in the trabecular distal metaphysis. To determine osteoclast number, size, perimeter and attachment surface, analyses were conducted on 200x magnification on top of the first maps and the second maps (with bone and osteoclast measures) were created. Result were reported as Number of Osteoclasts (N.Oc), Total Osteoclast Area/Size (Oc.Ar), Average Osteoclast Area/Size (AveOc.Ar), Osteoclast perimeter (Oc.Pm), Number of Osteoclast/Bone Perimeter (N.Oc/B.Pm) and Osteoclast Attachment Surface or Osteoclast Surface per Bone Surface (Os.S/BS)

2.8. THREE POINT BENDING MECHANICAL TESTING

Biomechanical properties were evaluated in the long bones. Left femur wrapped in Phosphate Buffer Solution (PBS) soaked gauze were slowly brought to room temperature and dissected to clean the remaining soft tissue then placed inside room temperature PBS prior to three-point bending tests using Instron 5944 Single Column Table Top Systems (Instron Pty Ltd. Bayswater, Melbourne, Victoria). Femurs were dried using gauze prior to being placed condyles face down on top of 2 x 100 mm anvil with a 6 mm gap. Load was applied, midway between the lower anvils, at a rate of 0.01 mm/s with 0.01 N increments. Time, load, and energy in which the femurs reach yield, maximal load and break point were recorded and analysed.

2.9. GENE EXPRESSION

2.9.1. DNA Extraction and Genotyping

ObVDR-B6 were genotyped by identifying the presence of human-*Vdr* gene within the genome while the $VDR^{fl/fl}$ control and ObVDR-KO mice were determine by the presence of *Cre* gene in the DNA specimen from the tails of 10 days old mice. DNA from a tail specimen was extracted using isopropanol method. Briefly, approximately 0.3 mm of tail specimen was digested overnight with 12.5 μL of proteinase K in 500 μL of tail buffer on 60 °C heating block. Tail buffer was made by adding 2 mL of 10 % SDS, 1 mL of 1 M Tris-HCl, 400 μL of 500 mM EDTA, 500 μL of 4 M NaCl and 16.1 mL MQ water. The digested samples were mixed and spun at 13,000 rpm for 5 minutes at room temperature. Approximately 450 μL of supernatant from each sample was collected and mixed with 1mL of 100 % isopropanol and gently mixed for 2-3 minutes then spun at 8,000 rpm for 5 minutes to precipitate DNA. The supernatant from each sample was then carefully removed so as not to disturb the pellet, and 75

μL of 1x Tris-EDTA-buffer (TE buffer) was added to each tube and heated to 60 ºC heating block for 2-3 minutes. The DNA concentration for each sample was quantified using a nanodrop spectrophotometer (Nanodrop 1000, Thermo Scientific, Wilmington USA). Working DNA samples were made by diluting the DNA to 20 ng/μL for each sample prior to conducting quantitative real time polymerase chain reaction (PCR) analyses, as detailed in section 2.8.2.4.

2.9.2. Gene Expression Analyses

2.9.3. Extraction of Total RNA

Tissues were immediately placed in RNALater® (Ambion ®, Life technologies, Austin, Texas, USA) following collection and placed in 2 - 8ºC for 24h prior to storage at -80 ºC as described earlier. Around 50 mg – 100 mg of tissue were used for RNA extraction by placing it in 1 mL TRIzol® (Invitrogen, Australia) inside a 5 mL polypropylene tube or 1.5 mL Eppendorf tube. Biopulverizer (BioSpec 59013N, Canada) or basic electric homogenizer (IKA T10, IKA, Germany) were used to extract RNA from bone tissue or a micro-pestle was used to homogenise soft tissue samples, which were then centrifuged at 12,000 rpm at 4 ºC for 10 minutes.

Approximately 850-900 μL of supernatant from each sample was collected and 200μL of chloroform added, vortexed and then incubated at room temperature for 4 minutes. Samples were then centrifuged at 12,000 rpm at 4 ºC for 15 minutes before removal of supernatant into a fresh tube with 0.5 mL isopropanol and 2 μL of 5 mg/mL glycogen solution. Solutions were vortexed and then placed on ice for 1h prior to overnight storage at -80 ºC.

To precipitate the RNA, samples were centrifuged at 12,000 rpm at 4 ^{o}C for 15 minutes. The supernatant from each tube was then carefully and completely discarded. The precipitated RNA pellet was then washed with 1 mL 75 % ethanol and spun at 7,500 rpm at 4 ^{o}C for 10 minutes. The supernatant was carefully and completely discarded from each tube and remaining RNA pellet was left to air dry for 5 minutes prior to addition of 35 – 50 µL of TE buffer, which was then heated for 2 minutes at 60 ^{o}C to assist in the complete dissolution of RNA pellet into solution.

2.9.4. Quantification of RNA

RNA quantification and purity were determined using a nanodrop spectrophotometer. A 1.5µL of solution from each RNA sample was measured against TE buffer blank at 260 and 280 nm. RNA was considered of sufficient purity when the absorbance ratio of A_{260}/A_{280} was equal to or greater than 1.9 and with absorbance ratio of A_{260}/A_{230} above 1.4. Assessment of the integrity of RNA was performed using an Agilent 2100 Bioanalyzer on selected samples as per manufacturer's instructions. An RNA Integrity Number (RIN), as determined by 28S:18S ratio, of 5 and above was considered adequate for qRT-PCR analyses.

2.9.5. Removal of DNA Contamination of RNA samples

For hVDR gene expression quantification in bone and other tissues, RNA preparations were treated with DNase to ensure all genomic DNA was destroyed. Briefly, 2 µg RNA was combined with DNA-se mixed solution containing 0.5 µL DNA-se, 1µL DNase buffer, and brought to 11.5 µL total volume with DEPC-treated H_2O, which was then incubated at 37 ^{o}C for 10 minutes. The reaction was then stopped by adding 1 µL of 50 mM EDTA and incubating at 75 ^{o}C for 10 minutes.

2.9.6. Complementary DNA (cDNA) Synthesis

Complementary DNA for each RNA sample was generated using Transcriptor First Strand cDNA Synthesis Kit (Roche Diagnostic, Indianapolis, USA) based on the manufacturer's instructions. 2µg of RNA was combined with 1µL of OligoDT and brought to 12µL with DEPC-treated H_2O. Samples were briefly vortexed and centrifuged prior to incubation at 65 °C for 5 minutes and rapidly chilling at 4°C. A 7µL master mix solution was then added to each sample consisting of 4µL reaction buffer, 0.5 µL RNase inhibitor, 2 µL nucleotide mix and 0.5 µL of transcriptor enzyme. Samples were briefly vortexed and centrifuged prior to incubation at 50 °C for 60 minutes, followed by enzyme denaturing at 70 °C for 5 minutes. Samples were then cooled to 4 °C and then stored at -80 °C prior to qRT-PCR analyses.

2.9.7. Messenger RNA (mRNA) Analysis

Messenger RNA for genes of interest were analysed by quantitative Reverse Transcriptase Polymerase Chain Reaction (qRT-PCR) using SYBR green incorporation technique. Each PCR was conducted using RotorGene 5000 machine (Corbett Research, USA) or otherwise stated. All PCR results were validated by melt curve analyses of product's peak based on the amplicon size constructed from Primer-Blasts programme (http://www.ncbi.nlm.nih.gov/tools/primer-blast/) according to the primer used. Relative expressions of mRNA were quantified using RotorGene software comparative cycle threshold (CT) value and was normalised against the house-keeping gene beta-actin.

PCR were conducted as follows; DNA or cDNA samples were thawed at room temperature and briefly heated at 50 °C to allow complete dissolution. DNA (3 μL) or cDNA (1 μL) was combined with 7 μL or 9 μL of PCR master-mix respectively. PCR master-mix consisted of 5μL iQ-SYBR supermix (Bio-Rad Laboratories, USA), 0.5μL forward primer, and 0.5 μL reversed primer (Gene-works, Adelaide, Australia) and brought to 20 μL with DEPC-treated H_2O. The PCR cycling conditions were 95 °C for 15 minutes, 35 cycles of 95 °C for 30 seconds, 60 °C for 30 seconds, and 70 °C for 30 seconds. These settings were followed by incubation at 72 °C for 4 minutes and a melt curve analysis with an incremental increase from 72 °C to 95 °C over 5 minutes.

All primers were designed in house, except for the hVDR primer which used primers as described by Gardiner et al., 2000. All primers used are listed in **table 2.1.**

2.10. STATISTICAL ANALYSES

All analyses were conducted using Graphpad Prism, version 6.05.

2.10.1. Two tail Independent t-test

Two tail Independent student t-test analyses were used for 2 group studies with the confidence interval (α) set at 95 % and a p-value < 0.05 with Levene's test for equality of variance above 0.05 (equal variances assumed) was considered statistically significant.

2.10.2. Two way analysis of variance (Two Way ANOVA)

Two-way analysis of variance (ANOVA) was applied to analyse the interactions between the effects of dietary calcium and genotype on dietary studies and effect of

age and genotype. The confidence interval (α) was set at 95 %. Statistical significance was set at a p value < 0.05.

2.10.3. Post-hoc Test

A Least Significant Difference (LSD) post-hoc test was used to identify the group/s that were significantly different within the data sets analysed by Two-Way ANOVA and $p < 0.05$ is considered as statistically significant. All analyses were conducted with the assumption of equal variance amongst the group.

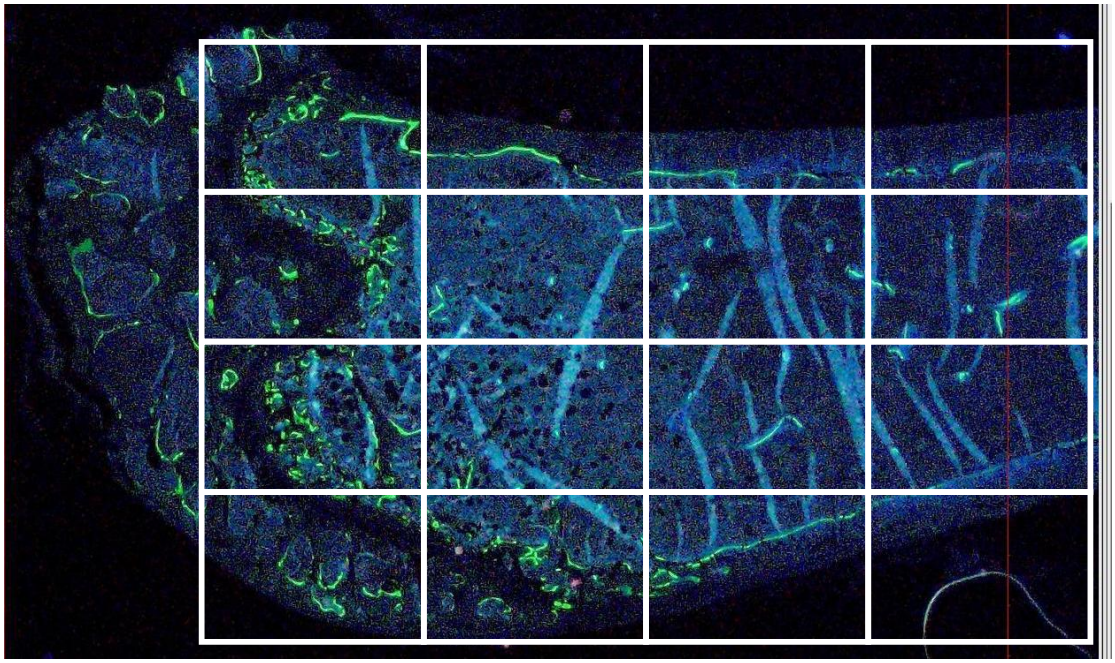

Figure 2.1. Field of View to Measure the Trabecular Double Fluorochrome Labels

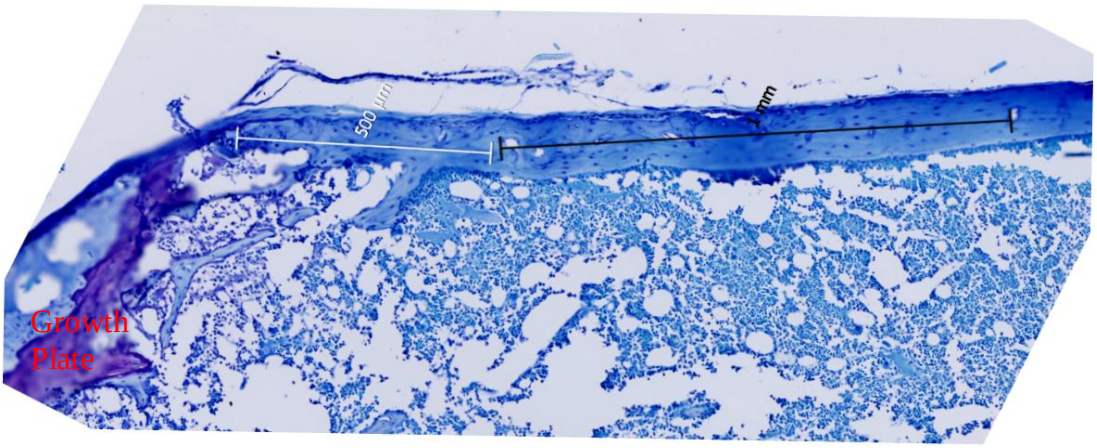

Figure 2.2. Site to Measure Cortical Osteocyte Density in the Distal Metaphysis Area

Table 2. 1 Primer Sequences Used in the Studies

Gene		Sequence (5'to 3') of the oligonucleotide primers	Gene bank accession number	Amplicon size (bp)
β-Actin	Forward	AGG GTG TGA TGG TGG GAA T	NM_007393.3	721
	Reverse	GCT GGG GTG TTG AAG GTC T		
mVdr	Forward	CTG AAT GAA GAA GGC TCC GAT	NM_009504.4	171
	Reverse	AGC AGGACAATCTGGTCATCA		
hVDR	Forward	GGA CGC CCA CCA TAA GAC CTA	KR710973.1	380
	Reverse	CTC CCT CCA CCA TCA TTC ACA		
OSVDR	Forward	TCA TTC TGA CAG ATG AGG AAG TGC	Specific Design	N/A
	Reverse	TCC TGG TAT CAT CTT AGC AAA GCC		
mCyp27b1	Forward	GAC CTT GTG CGA CGA CTA A	NM_010009.2	167
	Reverse	TCT GTG TCA GGA GGG ACT TCA		
mCyp24a1	Forward	TTG AAA GCA TCT GCC TTG TGT	NM_009996.3	130

Gene		Sequence (5'to 3') of the oligonucleotide primers	Gene bank accession number	Amplicon size (bp)
	Reverse	GTC ACC ATC ATC TTC CCA AAT		
mRunx2	Forward	ACA AGG ACA GAG TCA GAT TAC AGA T	NM_001146038.2 (isoform 1) NM_001145920.2 (isoform 2) NM_001271630.1 (isoform 3) NM_001271631.1 (isoform 4)	122
	Reverse	CGT GGT GGA GTG GAT GGA T		
mOpg	Forward	GTC CCT TGC CCT GAC CAC T	NM_008764.3	151
	Reverse	GGT AAC GCC CTT CCT CAC AC		
mRankl	Forward	TGA AGA CAC ACT ACC TGA CTC CTG	NM_011613.3	198
	Reverse	CTG GCA GCA TTG ATG GTG AG		
mOcn	Forward	AGA CCT AGC AGA CAC CAT GA	NM_031368.4	118
	Reverse	GAA GGC TTT GTC AGA CTC AG		
mSost	Forward	CCA CCA TCC CTA TGA CGC CAA	NM_024449.5 73	72
	Reverse	TGT CAG GAA GCG GGT GTA GT		

Gene		Sequence (5'to 3') of the oligonucleotide primers	Gene bank accession number	Amplicon size (bp)
mFgf23	Forward	GGA AGC CTG ACC CAC CTG T	NM_022657.3 133	36
	Reverse	CGG CGT CCT CTG ATG TAA TC		
mPhex	Forward	GAA AAG CTG TTC CCA AAA CAG AG	NM_011077.2	156
	Reverse	TAG CAC CAT AAC TCA GGG ATC G		
mDmp1	Forward	GAA AGC TCT GAA GAG AGG ACG GG	NM_016779.2	121
	Reverse	TGT CCG TGT GGT CAC TAT TTG CCT		
mEnpp1	Forward	AAG CGC TTA CAC TTC GCT AAA AG	NM_008813.3	87
	Reverse	TGA TGG ATT CAA CGC AAG TTG		
rNaPi2a	Forward	GCT GTC CTC TAC CTG CTC GTG TG	BC078876.1	91
	Reverse	GCG TGC CCA CTC CGA CCA TAG		
rNaPi2c	Forward	TTG CTG CCG CTG GAG AGT GC	N/A	N/A
	Reverse	ACT GCT TCC CTG GGG CGT CT		

CHAPTER 3: SKELETAL CHARACTERIZATION OF AN OSTEOBLAST-SPECIFIC VITAMIN D RECEPTOR TRANSGENIC (OBVDR-B6) MOUSE MODEL.

As published in the *Journal of Steroid Biochemistry and Molecular Biology*, 2016 Nov 164:331-336, doi: 10.1016/j.jsbmb.2015.08.009. Epub 2015, Sep 4

The aim of this chapter was to characterize the ObVDR-B6 at 3, 9 and 20 weeks (w) of age to address the backcrossing of OSVDR from *FVB/N* background onto the *C57black6/J* genetic background. The rationale behind this study was to determine whether the human *Vdr* gene is truly present in the backcrossed mice and to assess the bone properties and characteristics of the backcrossed mice considering that the *C57black6/J* is known to have low bone mass and different mouse strain characteristics compared to the FVB/N. Therefore, this study attempted to evaluate serum, bone and histological properties of ObVDR-B6 mice and observed any differences with its predecessor, the OSVDR or OSV3 mouse model.

The serum, skeletal and histomorphometry were analysed at 3w, 9w, and 20w of age male and female ObVDR-B6 Mice and published in *J Steroid Biochem Mol Biol*. 2016 Nov. 164:331-336, doi: 10.1016/j.jsbmb.2015.08.009. Epub *J Steroid Biochem Mol Biol*. 2015 Sep 4. S0960-0760 (15) 30046-7, as attached. In this chapter the supplementary data and the data not shown in the publication are also presented.

Statement of Authorship

Title of Paper	SKELETAL CHARACTERIZATION OF AN OSTEOBLAST-SPECIFIC VITAMIN D RECEPTOR TRANSGENIC (OBVDR-B6) MOUSE MODEL.
Publication Status	◉ Published, ○ Accepted for Publication, ○ Submitted for Publication, ○ Publication style
Publication Details	Journal of Steroid Biochemistry & Molecular Biology (J Steroid Biochem Mol Biol.) 2016 Nov;164:331-336. doi: 10.1016/j.jsbmb.2015.08.009. Epub 2015 Sep 4.

Author Contributions

By signing the Statement of Authorship, each author certifies that their stated contribution to the publication is accurate and that permission is granted for the publication to be included in the candidate's thesis.

Name of Principal Author (Candidate)	RAHMA TRILIANA		
Contribution to the Paper	Conducting the study, generated data and analysed results, reviewed the literatures, preparation of tables and figures, and sections of the manuscript. I hereby certify that the statement of contribution is accurate		
Signature		Date	22/7/2016

Name of Co-Author	Nga Ngoc Lam		
Contribution to the Paper	Generated the backcrossed mice prior to age study, helped with manuscript preparation. I hereby certify that the statement of contribution is accurate		
Signature		Date	25-7-2016

Name of Co-Author	Rebecca K Sawyer		
Contribution to the Paper	Generated some of the images and created the histology preparation and data I hereby certify that the statement of contribution is accurate		
Signature		Date	25-7-2016

Name of Co-Author	Gerald J Atkins		
Contribution to the Paper	Help with data analyses and manuscript preparation I hereby certify that the statement of contribution is accurate		
Signature		Date	25/07/16

Statement of Authorship

Title of Paper	SKELETAL CHARACTERIZATION OF AN OSTEOBLAST-SPECIFIC VITAMIN D RECEPTOR TRANSGENIC (OBVDR-B6) MOUSE MODEL.
Publication Status	◉ Published, ○ Accepted for Publication, ○ Submitted for Publication, ○ Publication style
Publication Details	Journal of Steroid Biochemistry & Molecular Biology (J Steroid Biochem Mol Biol.) 2016 Nov;164:331-336. doi: 10.1016/j.jsbmb.2015.08.009. Epub 2015 Sep 4.

Author Contributions

By signing the Statement of Authorship, each author certifies that their stated contribution to the publication is accurate and that permission is granted for the publication to be included in the candidate's thesis.

Name of Principal Author (Candidate)	RAHMA TRILIANA		
Contribution to the Paper	Conducting the study, generated data and analysed results, reviewed the literatures, preparation of tables and figures, and sections of the manuscript. I hereby certify that the statement of contribution is accurate		
Signature		Date	22/7/2016

Name of Co-Author	Howard A Morris		
Contribution to the Paper	Supervised the research project, helped with data interpretation and manuscript evaluation I hereby certify that the statement of contribution is accurate		
Signature		Date	22.7.2016

Name of Co-Author	Paul H. Anderson		
Contribution to the Paper	Planned and supervised the research project, helped with data interpretation, analyses and manuscript preparation. I hereby certify that the statement of contribution is accurate		
Signature		Date	22-7-2016

Name of Co-Author			
Contribution to the Paper			
Signature		Date	

Journal of Steroid Biochemistry & Molecular Biology 164 (2016) 331–336

Contents lists available at ScienceDirect

Journal of Steroid Biochemistry & Molecular Biology

journal homepage: www.elsevier.com/locate/jsbmb

Review

Skeletal characterization of an osteoblast-specific vitamin D receptor transgenic (ObVDR-B6) mouse model

Rahma Triliana[a,b], Nga N. Lam[b], Rebecca K. Sawyer[d], Gerald J. Atkins[c], Howard A. Morris[b,d,1], Paul H. Anderson[d,*,1]

[a] Faculty of Medicine, Islamic University of Malang, Malang, East Java 65144 Indonesia
[b] School of Medicine, Faculty of Health Science, The University of Adelaide, Adelaide, 5000 SA, Australia
[c] Centre for Orthopaedics and Trauma Research, The University of Adelaide, Adelaide, 5000 SA, Australia
[d] School of Pharmacy and Medical Sciences, University of South Australia, Adelaide, 5001 SA, Australia

ARTICLE INFO

Article history:
Received 15 June 2015
Received in revised form 5 August 2015
Accepted 11 August 2015
Available online 4 September 2015

Keywords:
Vitamin D receptor
Bone mineral
Bone morphology

ABSTRACT

Background: Overexpression of the human vitamin D receptor (hVDR) transgene under control of the human osteocalcin promoter in FVB/N mice (OSVDR) was previously demonstrated to exhibit increased cortical and trabecular bone volume and strength due to decreased bone resorption and increased bone formation. An important question to address is whether the OSVDR bone phenotype persists on an alternative genetic background such as *C57Bl6/J*.

Methods: OSVDR mice (OSV3 line) were backcrossed onto the *C57Bl6/J* genetic background for at least 6 generations to produce OSVDR mice with 98.4% *C57Bl6/J* congenicity (ObVDR-B6 mice). Hemizygous male and female ObVDR-B6 and littermate wild-type (WT) mice were fed a standard laboratory chow diet and killed at 3, 9 and 20 weeks of age for analyses of biochemical and structural variables and dynamic indices of bone histomorphometry.

Results: At 9 weeks of age, both cortical and trabecular femoral bone volumes were increased in both male and female ObVDR-B6 mice, when compared to WT levels ($P < 0.05$), without systemic changes to calciotropic parameters. The increase in femoral trabecular bone volume was associated with increase in MAR ($P < 0.01$) and reduced osteoclast size ($P < 0.05$). However, in female mice trabecular bone volume was unchanged in femoral metaphysis of 20 weeks mice and in vertebra both at 9 and 20 weeks of age. Increased cortical bone in both male and female ObVDR-B6 mice was due largely to increased periosteal expansion and was associated with increased cortical strength at 20 weeks of age.

Conclusion: Overexpression of the human VDR gene in mature osteoblasts of *C57Bl6/J* mice increases cortical and trabecular bone volumes and confirms the previous reports of increased bone in OSVDR mice on the FVB/N background. However, site-specific and gender-related differences in bone volume suggest that the effects of osteoblast-specific VDR overexpression are more complex than hitherto recognised.

Contents

* Corresponding author at: School of Pharmacy and Medical Sciences, University of South Australia, GPO Box 2471, Adelaide, SA 5001, Australia.
E-mail address: paul.anderson@unisa.edu.au (P.H. Anderson).
[1] Co-senior authors.

http://dx.doi.org/10.1016/j.jsbmb.2015.08.009
0960-0760/

1. Introduction

The vitamin D receptor (VDR) is expressed in wide variety of bone cells, including osteoblasts and osteocytes where it mediates vitamin D-stimulated osteoclastic bone resorption and bone loss [1,2] as well as the inhibition of mineralisation when exposed to high 1,25-dihydroxyvitamin D (1,25D) levels [3]. In contrast, VDR-mediated activities have also been shown to enhance osteoblast differentiation and mineralisation [4], and inhibit osteoblast apoptosis [5,6]. Current evidence suggests that the stage of osteoblast differentiation as well as the level of dietary calcium and phosphate may play a role in determining whether VDR mediates anabolic or catabolic activities on bone mineral [7,8].

Previously, the transgenic overexpression of the human gene for VDR under the regulation of human osteocalcin promoter (OSVDR) on the FVB/N mouse genetic background was shown to enhance trabecular bone volume in female caudal vertebrae [9]. This increase in trabecular bone volume was associated with increased trabecular thickness and reduced osteoclast activity. In addition, tibial and femoral cortical bone areas of OSVDR mice were increased associated with increased strength and periosteal mineral apposition rate (MAR) [9,10]. While we previously [11] reported that the bone phenotype of OSVDR was partially preserved during vitamin D deficiency, Baldock et al. [12] reported that the OSVDR bone phenotype was abrogated when fed low dietary calcium.

The FVB/N genetic background is a common inbred mouse strain used for transgenic mouse models due to its high reproductive performance, large litter size and prominent pronuclei which assist microinjection of DNA constructs [13]. However, since bone density, extrinsic femoral strength and cross-sectional geometry vary between mouse genetic backgrounds [14,15], a question remains as to whether the bone phenotype elicited by overexpression of the hVDR transgene is dependent on the genetic background of the mouse line. We now report bone structures on hVDR transgenic mice on the *C57Bl6/J* genetic background using advanced micro-computed tomography methods providing 3D assessment of bone structures.

Table 1
Body weight and blood biochemistry of WT and ObVDR-B6 mice. ALP, alkaline phosphatase; 1,25D, 1,25-dihydroxyvitamin D. Values are mean ± SEM, * $P < 0.05$ vs. WT mice. N/A; not available.

	9 weeks	
	WT	ObVDR-B6
Female (n)	(11)	(10)
Body weight (g)	18.6 ± 0.3	20.3 ± 0.6*
Calcium (mmol/L)	2.35 ± 0.04	2.36 ± 0.08
Phosphate (mmol/L)	1.62 ± 0.21	1.87 ± 0.15
ALP (U/L)	175.0 ± 10.0	181.3 ± 10.0
1,25D (pmol/L)	140.9 ± 18.8	134.9 ± 65.5
Male (n)	(12)	(10)
Body weight (g)	24.3 ± 0.5	24.1 ± 0.7
Calcium (mmol/L)	2.51 ± 0.08	2.62 ± 0.09
Phosphate(mmol/L)	1.70 ± 0.16	2.05 ± 0.11
ALP (U/L)	141.5 ± 11.7	170.7 ± 13.2
1,25D (pmol/L)	N/A	N/A

2. Materials and methods

2.1. Animals

FVB/N transgenic mice overexpressing hVDR transgene under the control of the human osteocalcin promoter (OSVDR) was provided by Dr Edith Gardiner and colleagues (Garvan Institute, Darlinghurst, Sydney, NSW, Australia). The pOSVDR construct was previously generated by inserting a human VDR cDNA 2.1 kb EcoRI fragment from phVDR1/3 [16] into the human osteocalcin-based pGOSCAS vector [17] followed by SV40 small t-antigen splice and polyadenylation signals immediately downstream. OSVDR transgenic mice were then generated by pronuclear injection of FVB/N embryos. The OSV3 line carries a single insertion of 10 copies of the transgene, as previously described [9]. OSVDR mice (OSV3 line) were then backcrossed onto the *C57bl6/J* genetic background for at least 6 generations to produce OSVDR mice with 98.4% *C57Bl6/J* congenicity (ObVDR-B6 mice). Male and female hemizygous ObVDR-B6 and litter-matched wild-type (WT) mice were housed in groups of five in individually ventilated cages maintained at 22–23 °C. All animals received free access to water and chow diet, containing 0.8% calcium and 0.7% phosphate. All animal procedures were approved and performed in accordance to requirements of the animal ethics committees for the University of Adelaide, University of South Australia and SA Pathology/CALHN.

2.2. Biochemistry

Serum calcium, phosphate and alkaline phosphatase were measured by the Konelab® 20/20XT chemical analyser using standard reagents (Thermo Fisher Scientific, Vantaa, Finland). Serum 1,25-dihydroxyvitamin D levels were measured using solid-phase immunoextraction followed by quantitative determination on the IDS-iSYS automated immunoassay system (Immunodiagnostic System, Boldon, UK).

2.3. Micro-CT

Mice were killed at 3, 9 and 20 weeks of age. At death, mice were weighed and the right femora and vertebrae collected and fixed with 10% formalin for 5 days and stored in 70% ethanol at 2–8 °C prior bone scanning. Femoral length was measured using digital callipers. Femora and vertebrae were scanned by micro-CT (Skyscan 1076, Bruker/Skyscan, Belgium) at a pixel size of 8.65 μm. X-ray tube potential of 48 kV and 110 μA, rotation step of 0.8 degrees and in a scan medium of 70% ethanol. Acquired X-ray images were reconstructed using nRecon (v1.6.9, Skyscan) with an isotropic voxel size of 8.65 μm. Volumetric analyses of cortical bone used a 2 mm segment of midshaft femoral cortical bone. A secondary spongiosa volume representing 20% of the femur length, was isolated in the distal femoral metaphysis to quantify trabecular bone volume. The inferior trabecular bone of the L1 vertebrae was isolated to quantify the trabecular bone volume in this region. Cortical parameters (volume, cortical width, periosteal and endosteal circumference) and trabecular bone parameters (volume, thickness, number) were all were calculated

Table 2
Cortical bone measurements at the femoral mid shaft of WT and ObVDR-B6 female and male mice at 3, 9 and 20 weeks of age. Ct.BV, cortical bone volume; Ct.Th, cortical thickness; P.Pm, periosteal perimeter; E.Pm, endosteal perimeter. Values are mean ± SEM. $P < 0.05$ for ANOVA analyses in (a) genotype, (b) age and (c) interaction. *$P < 0.05$ vs. WT mice, ♣ $P < 0.05$ vs. 3 weeks mice, ◆ $P < 0.05$ vs. 9 weeks mice.

	3 weeks		9 weeks		20 weeks	
	WT	ObVDR-B6	WT	ObVDR-B6	WT	ObVDR-B6
Female (*n*)	(7)	(7)	(11)	(10)	(13)	(13)
Femur Length[a,b]	10.7 ± 0.1	11.1 ± 0.1*	14.6 ± 0.1♣	14.9 ± 0.1*♣	16.1 ± 0.1◆	16.1 ± 0.1◆
Ct.BV(mm^3)[a,b]	0.74 ± 0.03	0.68 ± 0.12	1.38 ± 0.03♣	1.52 + 0.05*♣	1.72 ± 0.02◆	1.81 ± 0.02*◆
Ct.Th (μm) [a,b]	113.2 ± 3.5	117.3 ± 3.5	176.6 ± 2.9♣	184.9 + 3.2*♣	209.8 ± 1.9◆	216.3 ± 1.89*◆
P.Pm (mm) [a,b]	4.17 ± 0.08	4.37 ± 0.09*	5.06 ± 0.03♣	5.30 + 0.08*♣	5.31 ± 0.03◆	5.44 ± 0.04*
E.Pm (mm) [a,b]	3.46 ± 0.06	3.64 ± 0.08*	3.88 ± 0.02♣	4.10 + 0.07*♣	3.91 ± 0.02	4.04 ± 0.04*
Peak load (N)	–	–	–	–	16.76 ± 0.41	21.07 ± 0.74*
Modulus (GPa)	–	–	–	–	4.46 ± 1.53	5.58 ± 1.27*
Male (*n*)	(9)	(5)	(12)	(10)	(8)	(8)
Femur length[b]	10.9 ± 0.2	10.9 ± 0.2	15.1 ± 0.1♣	15.2 ± 0.1♣	16.1 ± 0.1◆	15.9 ± 0.1◆
Ct.BV (mm^3)[a,b,c]	0.76 ± 0.03	0.78 ± 0.06	1.57 ± 0.04♣	1.84 + 0.05*♣	1.91 ± 0.02◆	2.09 ± 0.04*◆
Ct.Th (μm) [a,b,c]	117.0 ± 3.2	116.4 ± 5.3	190.4 ± 5.5♣	212.8 + 4.1*♣	213.6 ± 2.1◆	241.3 ± 3.6*◆
P.Pm (mm) [b,c]	4.21 ± 0.09	4.29 ± 0.13	5.43 ± 0.05♣	5.72 + 0.10*♣	5.89 ± 0.05◆	5.79 ± 0.06
E.Pm (mm) [b,c]	3.47 ± 0.08	3.59 ± 0.12	4.17 ± 0.08♣	4.32 + 0.09♣	4.56 ± 0.07◆	4.26 ± 0.04*
Peak load (N)	–	–	–	–	14.01 ± 0.31	18.27 ± 0.26*
Modulus (GPa)	–	–	–	–	3.56 ± 1.79	4.62 ± 1.66*

using direct 3D and 2D approaches using CTan software (v1.7, Skyscan).

2.4. Three point mechanical testing

Biomechanical properties of femora from 20 weeks old mice only were evaluated. The left femur from each mouse was placed centred between anvils with a 6 mm gap. Load was applied at a rate of 0.01 mm/s in 0.01 Newton increments. Load, compression, and break point were recorded for each femur allowing for the calculation of Young's Modulus and Maximum Load (Instron 5944, Instron Pty Ltd., Melbourne, Australia).

2.5. Dynamic histomorphometry

Formalin-fixed femurs were bisected in the sagittal plane with a diamond-tipped cutting blade using a slow speed saw and processed for resin embedding as previously described [18]. Sequential sagittal sections were cut to 5 μm thickness. For bone mineralisation analyses of the distal femoral metaphysis, unstained fluorochrome labelled sections were prepared by placing in acetone for 15 min and protected from light. Measures of mineral apposition rate (MAR, μm/day) and bone formation rate (BFR, $\mu m^3/\mu m^2$/day) were obtained from these sections. For bone resorption analyses, sections were stained for tartrate-resistant acid phosphatase (TRAP) to identify TRAP-positive osteoclasts. Briefly, resin-embedded sections are de-waxed in acetone for 15 min before 60 min incubation in Tris–HCL buffer (pH 9.4) at 37 °C followed by two washes in distilled water. Sections are then incubated at 37 °C for 60 min in an acid phosphatase (AcP) stain prepared by adding (A) 0.035 g of tartaric acid dissolved in 35 ml of sodium acetate (pH 5.2) to (B) 100 μl basic fuchsin in a 100 μl solution containing 0.4 mg of sodium nitrite. This solution is then added to a solution containing 0.04 g Napthol ASBI phosphate in 2 ml dimethylformamide before being counter-stained with haematoxylin. Histomorphometric analyses were performed using OsteoMeasure (v3.3.0.2, Osteometrics Inc GA, USA).

2.6. Statistical analysis

Two-way analysis of variance was used to determine the effect of age and genotype on bone structure. Least significant difference (LSD) *post-hoc* analysis was used to identify groups reaching significant differences. Significance was set at $P < 0.05$ using GraphPad Prism, version 6.05.

3. Results

The human VDR transgene demonstrated high expression in bone samples and was undetected in brain, heart, liver, spleen, intestine, lung, muscle, and kidney similar to that demonstrated for the FVB/N mice [9] (data not shown). The mean body weight of female ObVDR-B6 mice body weight was 9% greater at 9 weeks of age ($P < 0.05$, Table 1). However, the body weight of 3 weeks and 20 weeks female ObVDR-B6 mice and male ObVDR-B6 at all ages and was unchanged (data not shown). Serum calcium, phosphate, ALP and 1,25D level were unchanged in ObVDR-B6 mice when compared to WT mice (Table 1).

At 3 and 9 weeks of age, femur length was increased by 4% and 2% ($P < 0.05$) respectively when compared to WT mice (Table 2). Growth plate width was unchanged in ObVDR-B6 mice (data not shown). Although cortical bone volume (Ct.BV) was unchanged in 3 weeks old ObVDR-B6 mice, a 5% increase in both periosteal perimeter (P.Pm) and endosteal perimeter (E.Pm) were observed in female ObVDR-B6 mice only ($P < 0.05$, Table 2). At 9 weeks and 20 weeks of age, both male and female ObVDR-B6 mice demonstrated increased Ct.BV. In male ObVDR-B6 mice, Ct.BV was increased by 17% at 9 weeks ($P < 0.05$) and 9% at 20 weeks of age ($P < 0.05$). In female ObVDR-B6 mice, Ct.BV at 9 weeks and 20 weeks was increased (10% and 5% respectively) when compared to WT mice ($P < 0.05$) (Fig. 1; Table 2). The sub-regional bone mineral cross-sectional area of ObVDR-B6 femora demonstrated largely uniform increases in bone mineral across the diaphysis in 9 weeks and 20 weeks mice (Supplementary Fig. 1). At 9 weeks of age, in both male and female, the increase in Ct.BV mice was due to a 5% increase in P.Pm ($P < 0.05$) despite an increase in E.Pm which reached significance in female mice only (5%, $P < 0.05$, Table 2). While the more modest increase in Ct.BV in 20 weeks female ObVDR-B6 mice was related to 2.4% increase in P.Pm ($P < 0.05$), the increase in Ct.BV in 20 weeks male ObVDR-B6 mice was due to a 6% reduction in E.Pm ($P < 0.01$) and without change to P.Pm. These 20 weeks male ObVDR-B6 mice demonstrated a 30% increase in peak load and modulus when compared to WT mice ($P < 0.05$, Table 2).

At 9 weeks of age, femoral metaphyseal trabecular bone volumes (BV/TV) were increased in both male and female ObVDR-B6 mice (female 13% $P < 0.05$; male 24% $P < 0.05$) due to increased

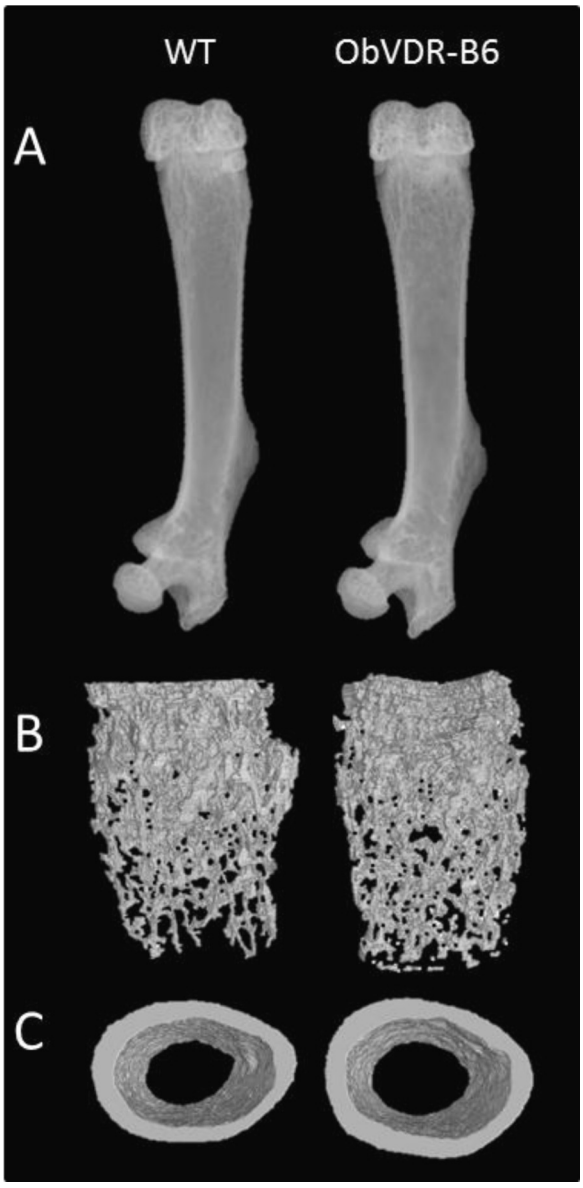

Fig. 1. Fermoral bone from 9 weeks female ObVDR-B6 and WT femora representing (a) coronal X-ray images, (b) 3D reconstructed metaphyseal trabecular bone and (c) mid shaft cortical bone.

trabecular number (Tb.N) and, in male mice only, trabecular thickness (Tb.Th) (Fig. 1 and Table 3). At 20 weeks of age, only male mice exhibited increased BV/TV (28%, $P<0.05$) due to increase Tb.N (14%, $P<0.05$). However, Tb.Th was increased in both 20 weeks male (10%, $P<0.05$) and female (5%, $P<0.05$) ObVDR-B6 mice. With regards to vertebral trabecular bone, only male ObVDR-B6 mice demonstrated an increase in BV/TV%, both at 9 weeks (9%, $P<0.05$) and 20 weeks (16%, $P<0.05$) of age. This increase in BV/TV was due to increased Tb.Th and, at 20 weeks of age only, due to increased Tb.N (Table 4).

The increased femoral trabecular bone volume in 9 weeks female ObVDR-B6 mice was associated with 15% increase in mineral apposition rate (MAR) ($P<0.05$) (Table 5). However, these mice also demonstrated unchanged bone formation rate (BFR/BV) due to a strong trend towards reduced mineralising surface (MS/BS). In addition, the mean osteoclast size (Ocl. Ar) was reduced by 22% ($P<0.05$) in female 9 weeks ObVDR-B6 mice which was associated with a trend to decreased osteoclast attachment surface

Table 3
Trabecular bone measurements at the femoral distal metaphysis of WT and ObVDR-B6 female and male mice at 9 and 20 weeks of age. BV/TV, trabecular bone volume/total volume; Tb.N, trabecular number; Tb.Th, trabecular thickness. Values are mean ± SEM. $P<0.05$ for ANOVA analyses in (a) genotype, (b) age, and (c) interaction. * $P<0.05$ vs. WT mice, ◆ $P<0.05$ vs. 9 weeks mice.

	9 weeks		20 weeks	
	WT	ObVDR-B6	WT	ObVDR-B6
Female (n)	(11)	(10)	(13)	(13)
BV/TV (%)$^{(a,b,c)}$	9.7 ± 0.28	11.0 ± 0.40*	6.4 ± 0.3◆	6.3 ± 0.23◆
Tb.N (#/mm) $^{(b,c)}$	2.47 ± 0.08	2.81 ± 0.09*	1.61 ± 0.07◆	1.52 ± 0.06◆
Tb.Th (μm) $^{(b,c)}$	39.6 ± 0.5	39.16 ± 0.5	39.8 ± 0.6	41.6 ± 0.6*◆
Male (n)	(12)	(10)	(8)	(8)
BV/TV (%)$^{(a,b)}$	12.6 ± 1.0	15.6 ± 0.9*	8.9 ± 0.3◆	11.4 ± 0.8*◆
Tb.N (#/mm) $^{(a,b)}$	3.19 ± 0.22	3.76 ± 0.19*	1.90 ± 0.07◆	2.18 ± 0.14◆
Tb.Th (μm)$^{(a,b)}$	39.2 ± 0.7	41.6 ± 0.5*	47.1 ± 0.3◆	51.9 ± 0.8*◆

(Ocl. S/BS). However, no significant reduction in osteoclast numbers (N.Oc/B.Pm) was determined in the female 9 weeks ObVDR-B6 mice femora when compared to WT mice (Table 5).

4. Discussion

We backcrossed the OSVDR transgenic mouse line (OSV3 line) from the FVB/N genetic background onto the *C57bl6/J* background to generate ObVDR-B6 mice, in order to assess whether the reported increase in bone mineral in OSVDR mice persisted on another genetic background. As was shown for OSVDR mice [9], we demonstrated specific expression of the VDR transgene in the bone of ObVDR-B6 mice under the control of the human osteocalcin promoter. In ObVDR-B6, no apparent perturbations in systemic calciotropic measures were observed and, aside from 9 weeks female mice, body weight was unchanged in the other ObVDR-B6 age groups and in ObVDR-B6 male mice, suggesting that enhanced osteoblastic VDR levels principally regulates local activities of bone remodelling, at least under normal circumstances.

The femoral cortical bone mineral volumes of male and female ObVDR-B6 mice were increased at both 9 weeks and 20 weeks of age due largely to increased periosteal expansion, which is consistent with the bone phenotype of the OSVDR mouse [9]. The sub-regional analyses of femora from ObVDR-B6 mice demonstrated uniform increases in bone mineral occurred across the diaphysis. Interestingly, by 20 weeks of age, male ObVDR-B6 mice demonstrated that despite a cessation in further periosteal expansion, cortical bone volume increased due to reduced endosteal circumference. While reasons for gender-related differences in cortical remodelling are not clear, one possibility may be related to differences in growth and mechanical loading. As previously described, the overexpression of VDR by the human osteocalcin-promoter results in increased VDR expression within osteocytes as well as osteoblasts [9]. Given that osteocytes coordinate the bone remodelling process in response to mechanical changes, elevated VDR in the transgenic mice, may alter the osteocytic-driven cortical remodelling differently in male mice. While it is not possible to draw such a conclusion from the current study, gender-related differences in skeletal acquisition of mature heterozygous global VDR-KO mice [19], suggesting that further investigations in relation to interactions between VDR, gender and mechanical loading are warranted.

With regards to trabecular bone, female ObVDR-B6 mice demonstrated an increase in BV/TV at 9 weeks of age, specifically in the femoral metaphysis. In contrast, in male ObVDR-B6 mice trabecular bone volumes at the femoral distal metaphysis and lumbar vertebra both were increased. Previously, female OSVDR

Table 4
Trabecular bone measurements of vertebral body lumbar-1 in WT and ObVDR-B6 female and male mice at 9 and 20 weeks of age. BV/TV, trabecular bone volume/total volume; Tb.N, trabecular number; Tb.Th, trabecular thickness. Values are mean ± SEM. $P < 0.05$ for ANOVA analyses in (a) genotype, (b) age and (c) interaction. * $P < 0.05$ vs. WT mice, ◆ $P < 0.05$ vs. 9 weeks mice.

	9 Weeks		20 Weeks	
	WT	ObVDR-B6	WT	ObVDR-B6
Female (n)	(11)	(10)	(13)	(13)
BV/TV (%)	19.2 ± 0.4	19.2 ± 0.4	19.2 ± 0.7	18.6 ± 0.7
Tb.Th (μm)[(b)]	39.5 ± 0.3	40.0 ± 0.4	44.08 ± 0.43◆	44.5 ± 0.6◆
Tb.N (#/mm)[(b)]	4.85 ± 0.07	4.79 ± 0.08	4.35 ± 0.15◆	4.18 ± 0.15◆
Male (*n*)	(12)	(10)	(8)	(8)
BV/TV (%)[(a,b)]	20.8 ± 0.7	22.6 ± 0.6*	17.6 ± 0.6◆	20.5 ± 0.5*◆
Tb.Th (μm)[(a)]	39.5 ± 0.6	41.9 ± 0.3*	38.9 ± 0.7	42.0 ± 0.4*
Tb.N (#/mm)[(a)(b)]	5.26 ± 0.12	5.39 ± 0.11	4.52 ± 0.09◆	4.88 ± 0.07*◆

mice were shown to exhibit increased caudal vertebral bone volume [9], which is consistent with the male, but not female, ObVDR-B6 bone phenotype. In 9 weeks female ObVDR-B6 mice, the increase of metaphyseal bone volume was associated with increased MAR, a modest decrease in osteoclast size and no change to osteoclast numbers, which is consistent with findings in the OSVDR mice [9].

Recently, the conditional deletion of VDR in osteoblasts using the Col1a1-Cre founder mouse line was performed to demonstrate that increased bone volume occurred at 16 weeks of age in male osteoblast-specific VDRKO mice [1]. This increase in bone, which did not occur in younger mice, was associated with both reduced tibial cortical RANKL expression and osteoclast numbers, and without change to MAR. Thus, while the deletion and over-expression of VDR in osteoblasts both result in increased bone volume, differences occur with respect to the temporal, spatial development of the bone phenotype as well as the mechanisms by which the increased bone volume develops. Overexpression of VDR in osteoblasts increases periosteal and trabecular bone in young mice associated with increased MAR. Whereas the deletion of VDR in osteoblasts appears to principally impair bone resorption in adult mice [1]. The direct comparison of these two mouse models is limited, however, given that the deletion and over-expression of VDR were performed using different promoters and thus potentially representing different pools of osteoblast-lineage cells. Furthermore, while the overexpression of VDR using the osteocalcin promoter has been shown to increase VDR within osteocytes [9], the deletion of VDR using the Col1a1-Cre curiously does not appear to reduce VDR expression in osteocytes [1]. Thus, further studies with appropriate mouse models would be of value to be able to directly compare and contrast the bone remodelling effects of overexpression and conditional deletion of VDR in osteoblasts.

Table 5
Dynamic histomorphometry of 9 weeks old female WT and ObVDR-B6 mice. Values are mean ± SEM. MS/BS, mineralising surface/bone surface; MAR, mineral apposition rate; BFR/BS, bone formation rate /bone surface; Ocl. Ar, osteoclasts size; Ocl. S/BS, osteoclast surface/bone surface; N.Oc/B.Pm, osteoclast number/bone perimeter.

	WT	ObVDR- B6	*P*-value
(*n*)	(5)	(5)	
MS/BS (%)	34.95 ± 1.44	29.05 ± 3.00	0.053
MAR (μm/d)	2.73 ± 0.09	3.13 ± 0.13	0.018
BFR/BS ($\mu m^3/\mu m^2/d$)	0.96 ± 0.05	0.90 ± 0.08	0.303
Ocl. Ar. (μm^2)	0.0213 ± 0.0018	0.0167 ± 0.0016	0.047
Ocl. S/BS (%)	23.15 ± 1.01	18.40 ± 2.58	0.062
N.Oc/B.Pm (#/μm)	8.54 ± 0.29	7.30 ± 0.85	0.102

5. Conclusion

The over expression of the human VDR gene in mature osteoblasts plays a significant role on bone mineral accrual at cortical and trabecular sites of *C57Bl6/J* transgenic mice similar to the OSVDR mice on the *FVB/N* genetic background. While skeletal structural differences are observed between male and female mice, a consistent increase in cortical bone volume and strength for both female and male ObVDR-B6 mice indicates that VDR plays an importantly role in cortical bone remodelling, possibly through enhancing VDR-mediated activities in osteocytes as well as osteoblasts. Further studies are required, however, to establish the role of osteoblastic VDR under pathological conditions.

Acknowledgments

Funding for this project was provided by National Health and Medical Research Council. Rahma Triliana was supported by a Directorate General of Higher Education (DGHE), Government of Indonesia PhD Scholarship. Paul H. Anderson was supported by a Career Development Fellowship provided by the Australian National Health and Medical Research Council.

Appendix A. Supplementary data

Supplementary data associated with this article can be found, in the online version, at http://dx.doi.org/10.1016/j.jsbmb.2015.08.009.

References

[1] Y. Yamamoto, T. Yoshizawa, T. Fukuda, Y. Shirode-Fukuda, T. Yu, K. Sekine, T. Sato, H. Kawano, K. Aihara, Y. Nakamichi, T. Watanabe, M. Shindo, K. Inoue, E. Inoue, N. Tsuji, M. Hoshino, G. Karsenty, D. Metzger, P. Chambon, S. Kato, Y. Imai, Vitamin D receptor in osteoblasts is a negative regulator of bone mass control, Endocrinology 154 (2013) 1008–1020.
[2] S. Takeda, T. Yoshizawa, Y. Nagai, H. Yamato, S. Fukumoto, K. Sekine, S. Kato, T. Matsumoto, T. Fujita, Stimulation of osteoclast formation by 1,25-dihydroxyvitamin D requires its binding to vitamin D receptor (VDR) in osteoblastic cells studies using VDR knockout mice, Endocrinology 140 (1999) 1005–1008.
[3] L. Lieben, R. Masuyama, S. Torrekens, R. Van Looveren, J. Schrooten, P. Baatsen, M.H. Lafage-Proust, T. Dresselaers, J.Q. Feng, L.F. Bonewald, M.B. Meyer, J.W. Pike, R. Bouillon, G. Carmeliet, Normocalcemia is maintained in mice under conditions of calcium malabsorption by vitamin D-induced inhibition of bone mineralization, J. Clin. Invest. 122 (2012) 1803–1815.
[4] P.H. Anderson, R.K. Sawyer, A.J. Moore, B.K. May, P.D. O'Loughlin, H.A. Morris, Vitamin D depletion induces RANKL-mediated osteoclastogenesis and bone loss in a rodent model, J. Bone Miner. Res. 23 (2008) 1789–1797.
[5] G.J. Atkins, P.H. Anderson, D.M. Findlay, K.J. Welldon, C. Vincent, A.C.W. Zannettino, P.D. O'Loughlin, H.A. Morris, Metabolism of vitamin D3 in human osteoblasts: evidence for autocrine and paracrine activities of 1α,25-dihydroxyvitamin D3, Bone 40 (2007) 1517–1528.
[6] X. Zhang, L.P. Zanello, Vitamin D receptor-dependent 1α,25(OH)2 vitamin D 3-induced anti-apoptotic PI3K/AKT signaling in osteoblasts, J. Bone Miner. Res. 23 (2008) 1238–1248.
[7] G.J. Atkins, P. Kostakis, B. Pan, A. Farrugia, S. Gronthos, A. Evdokiou, K. Harrison, D.M. Findlay, A.C.W. Zannettino, RANKL expression is related to the differentiation state of human osteoblasts, J. Bone Miner. Res. 18 (2003) 1088–1098.
[8] D. Yang, A.G. Turner, A.R. Wijenayaka, P.H. Anderson, H.A. Morris, G.J. Atkins, 1,25-Dihydroxyvitamin D3 and extracellular calcium promote mineral deposition via NPP1 activity in a mature osteoblast cell line MLO-A, Mol. Cell Endocrinol. 412 (2015) 140–147.
[9] E.M. Gardiner, P.A. Baldock, G.P. Thomas, N.A. Sims, N.K. Henderson, B. Hollis, C. P. White, K.L. Sunn, N.A. Morrison, W.R. Walsh, J.A. Eisman, Increased formation and decreased resorption of bone in mice with elevated vitamin D receptor in mature cells of the osteoblastic lineage, FASEB J. 14 (2000) 1908–1916.
[10] B.M. Misof, P. Roschger, W. Tesch, P.A. Baldock, A. Valenta, P. Messmer, J.A. Eisman, A.L. Boskey, E.M. Gardiner, P. Fratzl, K. Klaushofer, Targeted overexpression of vitamin D receptor in osteoblasts increases calcium concentration without affecting structural properties of bone mineral crystals, Calcif. Tissue Int. 73 (2003) 251–257.
[11] N.N. Lam, R. Triliana, R.K. Sawyer, G.J. Atkins, H.A. Morris, P.D. O'Loughlin, P.H. Anderson, Vitamin D receptor overexpression in osteoblasts and osteocytes

prevents bone loss during vitamin D-deficiency, J. Steroid Biochem. Mol. Biol. 144 (2014) 128–131.
[12] P.A. Baldock, G.P. Thomas, J.M. Hodge, S.U.K. Baker, U. Dressel, P.D. O'Loughlin, G.C. Nicholson, K.H. Briffa, J.A. Eisman, E.M. Gardiner, Vitamin D action and regulation of bone remodeling: suppression of osteoclastogenesis by the mature osteoblast, J. Bone Miner. Res. 21 (2006) 1618–1626.
[13] M. Taketo, A.C. Schroeder, L.E. Mobraaten, K.B. Gunnings, G. Hanten, R.R. Fox, T. H. Roderick, C.L. Stewar, F.L. Ii, C.T. Hansen, P.A. Overbeek, FVB/N: an inbred mouse strain preferable for transgenic analyses. (ES ceils/blastocyst chimera/ germ-line tanission), Proc. Natl. Acad. Sci. U. S. A. 88 (1991) 2065–2069.
[14] W.G. Beamer, L.R. Donahue, C.J. Rosen, D.J. Baylink, Genetic variability in adult bone density among inbred strains of mice, Bone 18 (1996) 397–403.
[15] J.E. Wergedal, M.H. Sheng, C.L. Ackert-Bicknell, W.G. Beamer, D.J. Baylink, Genetic variation in femur extrinsic strength in 29 different inbred strains of mice is dependent on variations in femur cross-sectional geometry and bone density, Bone 36 (2005) 111–122.
[16] D.P. McDonnell, R.A. Scott, S.A. Kerner, B.W. O'Malley, J.W. Pike, Functional domains of the human vitamin D3 receptor regulate osteocalcin gene expression, Mol. Endocrinol. 3 (1989) 635–644.
[17] N.A. Sims, C.P. White, K.L. Sunn, G.P. Thomas, M.L. Drummond, N.A. Morrison, J. A. Eisman, E.M. Gardiner, Human and murine osteocalcin gene expression: conserved tissue restricted expression and divergent responses to 1,25-dihydroxyvitamin D3 in vivo, Mol. Endocrinol. 11 (1997) 1695–1708.
[18] P.H. Anderson, R.K. Sawyer, A.J. Moore, B.K. May, P.D. O'Loughlin, H.A. Morris, Vitamin D depletion induces RANKL-mediated osteoclastogenesis and bone loss in a rodent model, J. Bone Miner. Res. 23 (2008) 1789–1797.
[19] F.J. de Paula, I. Dick-de-Paula, S. Bornstein, B. Rostama, P. Le, S. Lotinun, R. Baron, C.J. Rosen, VDR haploinsufficiency impacts body composition and skeletal acquisition in a gender-specific manner, Calcif. Tissue Int. 89 (2011) 179–191.

SUPPLEMENTARY DATA

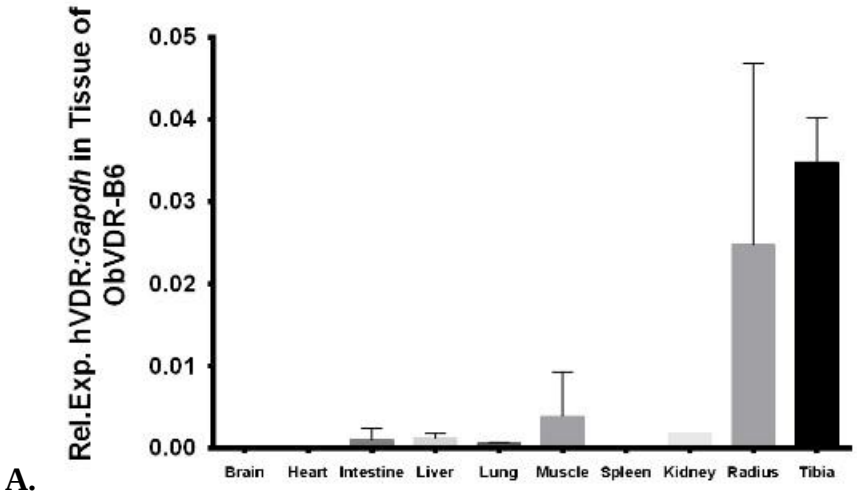

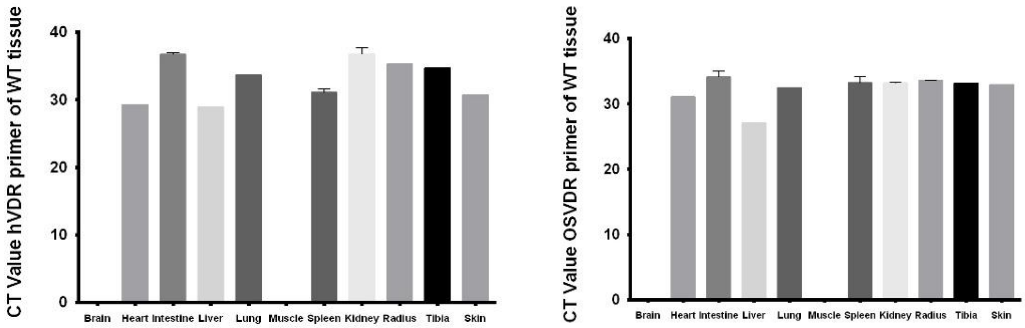

Supplementary Figure 3. 1. Tissue Expression of hVDR (A) and Specificity Testing hVDR and OSVDR Primers on Various Tissue of WT Mice

Gene expression of h*Vdr* (A) on the brain, heart, intestine, liver, lung, muscle, spleen, kidney and bone of the ObVDR-B6 mice. *Vdr* and *OSVDR* primers were tested for specificity in amplifying the h*Vdr* on WT tissues (**Figure 1B and C)** suggesting that the h*Vdr* and OSVDR primer design was not specific and may result in cross reactivity with mouse *Vdr*.

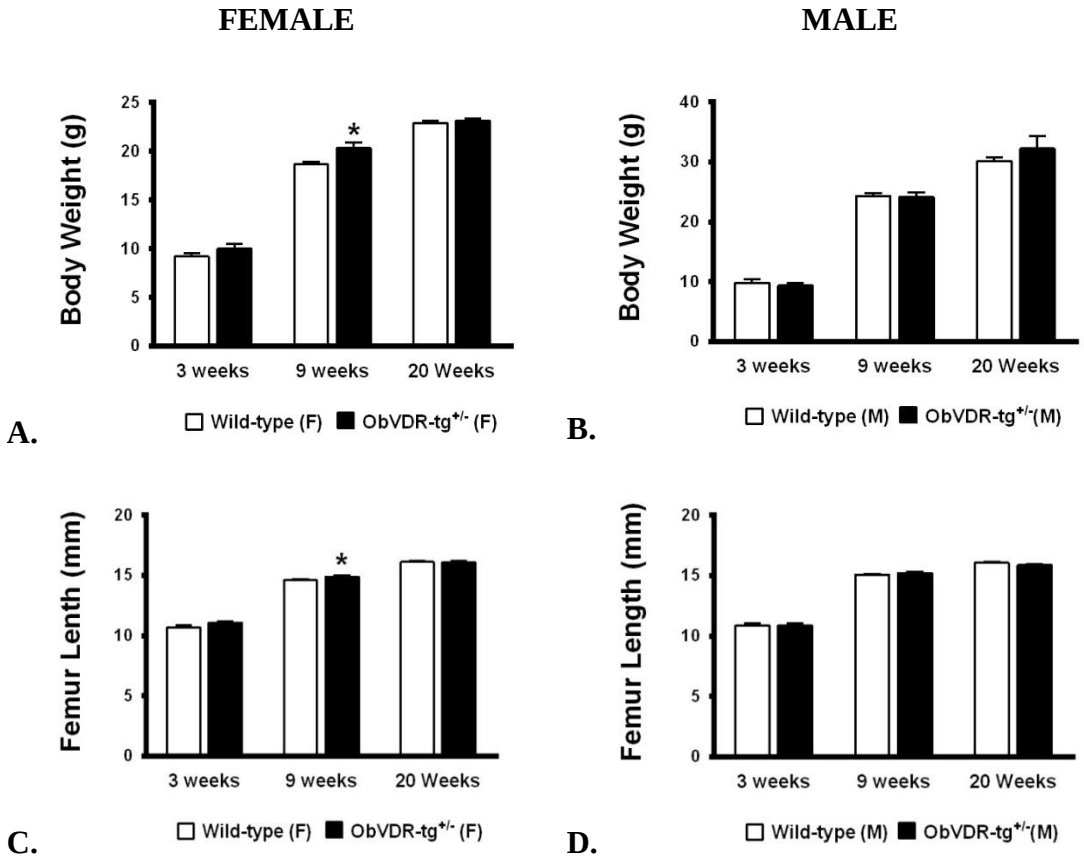

Supplementary Figure 3. 2. Body Weight (A, B) and Femur Length (C, D) of Male and Female 3w, 9w, 20w WT and ObVDR-B6 Mice.

Values are mean $\pm$ SEM, * $P < 0.05$ vs. WT

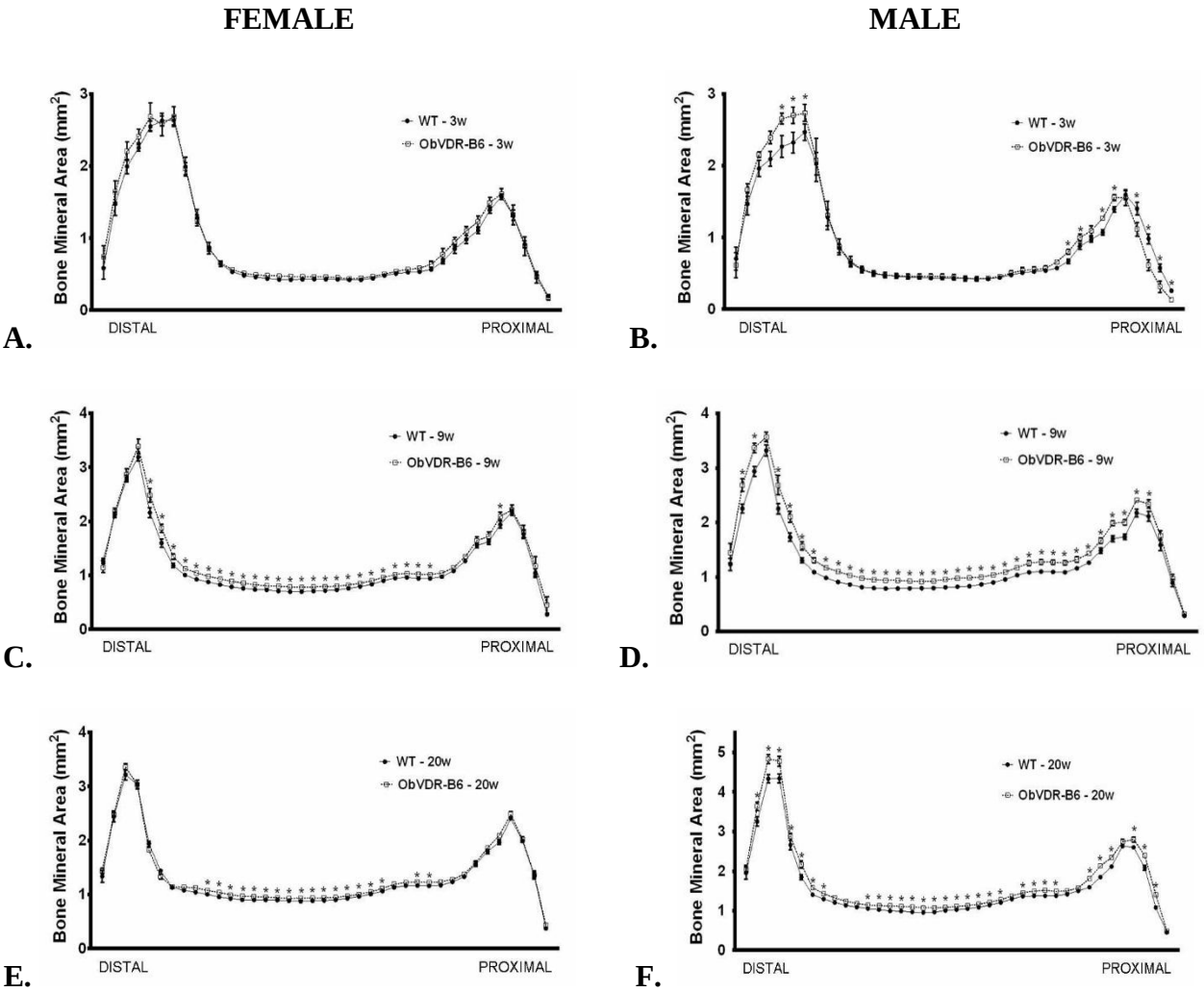

Supplementary Figure 3. 3. Femoral Segmental Bone Mineral Area in 3w (A and B), 9w (C and D), and 20w (E and F) of Female and Male WT and ObVDR-B6 Mice.

Comparison of femoral bone mineral cross-sectional area at every 2.5 % sub-regional area of the femur in WT and ObVDR-B6 at 3w, 9w, 20w in Female and Male Mice.

Values are mean $\pm$ SEM, n =5 - 13/group. * $P < 0.01$ vs. WT

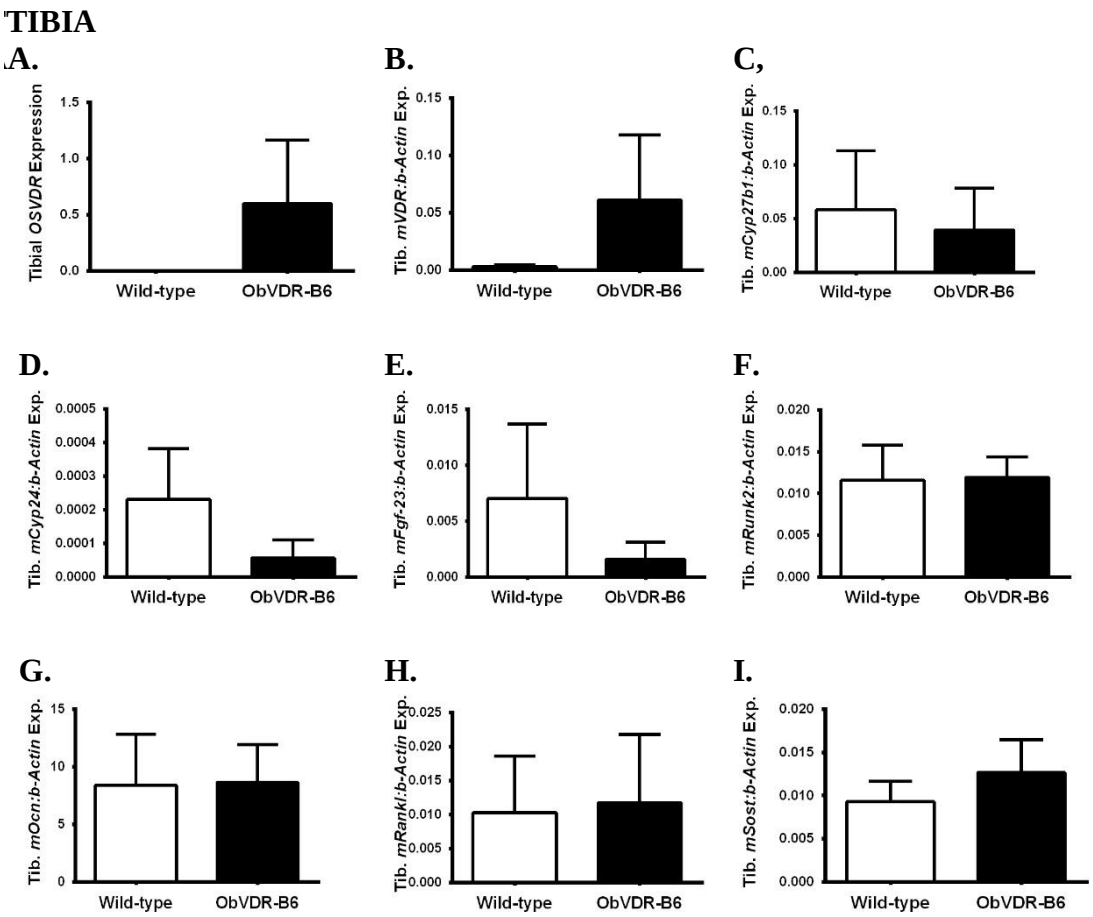

Supplementary Figure 3. 4. Tibial Gene Expression of WT and ObVDR-B6 Mice at 9w.

Tibial gene expression of OSVDR (A), h*Vdr* (B), m*Cyp27B1* (C) m*Cyp24* (D), m*Fgf23* (E), m*Runx2* (F), m*Ocn* (G), m*Rankl* (H), m*Sost* (I) on WT and Ob-VDR-B6.

Supplementary Table 3. 1. Blood biochemistry of WT and ObVDR –B6 mice

	3w		20w	
	WT	***ObVDR-B6***	***WT***	***ObVDR-B6***
Female (n)	*(7)*	*(7)*	*(13)*	*(13)*
Calcium[(b)]	3.00 ± 0.09	3.19 ± 0.13	3.13 ± 0.18♦	3.14 ± 0.15♦
Phosphate[(b)]	2.69 ± 0.17	2.69 ± 0.15	2.29 ± 0.16♦	1.97 ± 0.18
ALP[(b)]	771.97 ± 71.53	704.46 ± 78.41	167.94 ± 10.26	108.87 ± 7.71
1,25D[(b)]	533.52 ± 125.82	385.81 ± 117.23	70.66 ± 8.66	85.04 ± 17.32
Male (n)	*(9)*	*(5)*	*(8)*	*(8)*
Calcium[(a)(b)(c)]	3.21 ± 0.16	3.07 ± 0.18	2.58 ± 0.14♦	3.45 ± 0.21*♦
Phosphorus[(b)(c)]	2.57 ± 0.31	2.72 ± 0.33	1.76 ± 0.09♦	2.33 ± 0.17*♦
ALP[(b)]	902.54 ± 88.93	841.08 ± 65.48	81.30 ± 4.57♦	75.56 ± 7.03♦
1,25D[(b)]	474.32 ± 133.41	635.86 ± 212.66	173.58 ± 46.8	190.70 ± 3.18

Values are mean ± SEM, Two-way Anova significant at $p < 0.05$ for Interaction (a), Age (b), and genotype (c). Least Significant Difference (LSD) of Wild type vs. ObVDR-B6 animals * $p < 0.05$, **$p < 0.001$, ♣$p < 0.05$ for 3 weeks vs. 9 weeks and ♦$p < 0.05$ for 9 Weeks vs. 20 weeks within the same genotype. N/A not available

Supplementary Table 3. 2. Trabecular bone measurements of vertebral body lumbar-1 in WT and ObVDR-B6 mice

	9 Weeks		20 Weeks	
	WT	***ObVDR-B6***	***WT***	***ObVDR-B6***
Female (n)	*(11)*	*(10)*	*(13)*	*(13)*
BV/TV (%)	19.2 ± 0.4	19.2 ± 0.4	19.2 ± 0.7	18.6 ± 0.7
Tb.Th (□m)[(b)]	39.5 ± 0.3	40.0 ± 0.4	44.08 ± 0.43♦	44.5 ± 0.6♦
Tb.N (#/mm)[(b)]	4.85 ± 0.07	4.79 ± 0.08	4.35 ± 0.15♦	4.18 ± 0.15♦
Male (n)	*(12)*	*(10)*	*(8)*	*(8)*
BV/TV (%)[(a)(b)]	20.8 ± 0.7	22.6 ± 0.6*	17.6 ± 0.6♦	20.5 ± 0.5*♦
Tb.Th (□m)[(a)]	39.5 ± 0.6	41.9 ± 0.3*	38.9 ± 0.7	42.0 ± 0.4**
Tb.N (#/mm)[(a)(b)]	5.26 ± 0.12	5.39 ± 0.11	4.52 ± 0.09♦	4.88 ± 0.07*♦

Values are mean ± SEM, $p < 0.05$ for ANOVA analyses in Genotype (a), Age (b), and Interaction (c). * $P < 0.05$ vs. WT mice, ♦ $P < 0.05$ for 9 vs. 20w within the same genotype. Trabecular bone volume (BV/TV), Trabecular thickness. (Tb.Th); Trabecular number (Tb.N).

CHAPTER 4: THE INTERACTION OF VDR IN MATURE OSTEOBLASTS WITH DIETARY CALCIUM/PHOSPHATE ON BONE STRUCTURE

Chapter Summary

The bone phenotype of OSVDR mice is dependent on dietary calcium intake, with increased bone mineral when fed an adequate calcium diet which is lost when fed a low calcium diet. I have investigated the overexpression of VDR in mature osteoblasts on the *C57bl6/J* genetic background (ObVDR-B6) mouse model using an extremely low dietary calcium and phosphate with the aim of exacerbating the effects of the increased VDR activities under conditions of elevated calciotropic hormones.

Three week old female Wild Type (WT) and ObVDR-B6 mice were fed a diet containing calcium (0.03 %) and phosphorus (0.08 %) (LowCaP) for a period of 3w (short term) and 17w (long term) at which time they were compared to mice fed a normal calcium (1 %) and phosphorus (0.625 %) (NormCaP) diet.

At 3w of age, no apparent changes in body weight, femur length, serum biochemistry or bone structure are observed between WT and ObVDR-B6. When fed LowCaP diet for a short term (3w), femur length is decreased with femoral structural changes in ObVDR-B6 mice are evident without visible changes to the growth plate. An increase in femoral mid-shaft cortical porosity is observed in ObVDR-B6 mice suggesting skeletal integrity is compromised at some sites. In contrast, increased trabecular bone volumes at the distal metaphysis and vertebrae are observed in ObVDR-B6 mice fed

short term LowCaP diet compared to WT fed the same diet suggesting that increased osteoblast VDR maintains trabecular bone at particular sites even when calciotropic hormones are elevated by low calcium/phosphate intakes.

With long term treatment (17w), the LowCaP diet induced marked changes in bone structure of the ObVDR-B6 mice with splaying of the metaphysis, disrupted growth plate and increased of cortical porosity compared to WT mice fed similar diet while the NormCaP fed ObVDR-B6 has increased trabecular bone volume in the distal metaphysis and vertebrae and increased cortical bone in mid-shaft. These structural changes of the ObVDR-B6 mice arose from a decrease of bone resorption in the ObVDR-B6 NormCaP fed mice and an increase of bone resorption in the LowCaP fed mice. Most interesting is the evidence that VDR activities in mature osteoblasts can modulate plasma levels of calciotropic hormones. ObVDR-B6 mice fed the LowCaP diet for 17w demonstrated a 50 % decrease in serum FGF-23 and a 100 % increase in serum 1,25D levels compared to WT mice fed the identical diet. These changes suggest that VDR in mature osteoblasts can modulate both anti-catabolic and catabolic activities depending on the level of dietary calcium/phosphate intake.

CHAPTER 4

4.1. INTRODUCTION

A transgenic model in which the human vitamin D receptor (*Vdr)* gene is solely over-expressed in mature osteoblasts under the control of the human osteocalcin promoter in *FVB/N* genetic background (OSVDR mice) was reported by Gardiner and colleagues in 2000 (36). This mouse model demonstrated increased bone mass due to an increase in mineral apposition rate and reduction in bone resorption without changes to calciotropic hormone levels. Using OSVDR mice, Baldock et al. in 2006 (37) reported that the increased bone volume in this mice was dependent on the level and duration of dietary calcium with no differences in bone mineral volumes between wild type (WT) and OSVDR mice when fed a moderately low calcium diet up to 6 months of age.

Backcrossing the OSVDR mice from the *FVB/N* background onto the *C57Bl6/J* background (ObVDR-B6), as reported in chapter 3, confirmed that when fed a standard chow diet (0.8 % calcium / 0.7 % phosphorus), overexpression of human *Vdr* gene in mature osteoblasts results in increased cortical and trabecular bone volumes. However, the findings also illustrated site-specific and gender-related differences suggesting the effects of osteoblast-specific VDR overexpression are more complex than previously recognised.

Dietary calcium affects bone mineral levels through modulation of calciotropic hormones to maintain plasma calcium and phosphate homeostasis (18). A low dietary calcium increases plasma 1α,25 dihydroxyvitamin D_3 (1,25D) and parathyroid

hormone (PTH) to stimulate calcium fluxes across the kidney, intestine and bone (91). Ionised calcium activates the Calcium Sensing Receptor (CaSR) modulating a range of activities in numerous cell types including osteoblasts. Adequate dietary calcium can improve bone volume in rat models while low dietary calcium can decrease bone volume by increasing osteoclastogenesis (37).

The current study examined the effects of over-expression of VDR in mature osteoblasts in female ObVDR-B6 mice fed a very low dietary calcium/phosphate diet compared to WT mice fed the same diet and these mice fed an adequate calcium and phosphate diet. This study aimed to generate further evidence of VDR activities in osteoblasts under conditions when the actions of 1,25D and PTH are markedly up-regulated.

4.2. METHODS

4.2.1. Animals and Dietary Used

WT and ObVDR-B6 mice were housed as described in **Chapter 2, Section 2.3** and fed semi-synthetic diets containing either 1 % calcium / 0.625 % phosphorus (NormCaP/SF12-076, Specialty Feeds, Glen Forrest, Western Australia) or 0.03 % calcium / 0.08 % phosphorus (LowCaP/SF12-077, Specialty Feeds, Glen Forrest, Western Australia) from weaning (3w) until 6w of age (short term treatment) and 20w of age (long term treatment). Given the time constraints of the project, only female mice were studied. The semi-synthetic diet was formulated with whey-based protein to achieve low phosphate levels while maintaining adequate levels of other nutrients such as amino acids, vitamins and fatty acids. The differences between the two diets were calcium and phosphorus levels derived from calcium carbonate, monocalcium phosphate and potassium dihydrogen phosphate. Detailed dietary composition of the diets used in this study is attached in the **Appendix** section.

Calcein and xylenol orange fluorochrome labels were injected intra-peritoneally at 8 and 2 days prior to death as described in **Chapter 2, Section 2.7**. At time of death, blood was drawn using external cardiac punctures techniques while femora and vertebrae were collected for micro-CT analyses and histology. Right tibia, kidney and other tissues were collected in RNA-Later® (Ambion ®, Life technologies, Austin, Texas, USA) for further analyses. All animal details and procedures were recorded on clinical record sheets (CRS) in accordance the University of Adelaide Animal Ethics Committee for project number M-2012-092.

To assess bone structure before commencing the experimental diets, 3w old female WT and ObVDR-B6 were culled and serum biochemistry and femoral skeletal structures were analysed as a baseline.

4.2.2. Serum Biochemistry

Serum calcium, phosphate, ALP, 1,25D, FGF-23, PTH, CrossLaps^{TM} and TRAP5b levels were measured as previously described in **Chapter 2, Section 2.5.**

4.2.3. Micro-Computed Tomography

Right femora were initially imaged using X-ray imaging (Faxitron LX-60, Tucson, AZ, USA) to visualise bone prior to microstructure analyses using micro-CT system at 9um/pixel (1076 Skyscan, Bruker, Germany) as described previously (**Chapter 2, Section 2.6.1**). Vertebrae were scanned on 6.5um/pixel micro-CT system (1174 Skyscan, Bruker, Germany) as described in **Chapter 2, Section 2.6.2**. Total and segmental bone mineral content on full length femora were analysed followed by femoral cortical and trabecular bone analyses. Cortical bone analyses were measured over a region comprising 10 % of the femur length at the mid-shaft while trabecular bone analyses were performed from a region starting 0.6 mm from end of visible growth plate (roughly 2.2 - 2.3 mm from the start of bone) extending 10 % of the femur length at the femoral distal metaphysis. Regional femoral bone assessments were modified due to significant differences in femur length between groups and visible changes of bone structure in some of the groups. Vertebral trabecular analyses were conducted as described in **Chapter 2, Section 2.6.4.**

4.2.4. Histomorphometric Analyses

4.2.4.1. Paraffin Sections

Whole femora were cleaned of surrounding tissue and fixed with 4 % paraformaldehyde for 2 days. Femora were decalcified by immersing bones in 10 % ethylenediamine-tetra acetic acid (EDTA) solution for 7 - 10 days. During the decalcification process, bones were imaged consecutively using Faxitron X-ray imaging to assess the decalcification process. Once bones were decalcified, they were packed inside paraffin cassettes for processing and embedded longitudinally in paraffin. They were left for 24 hours to allow the paraffin to set prior to sectioning. Paraffin sections of 5 µm thickness were prepared using a motorized microtome (Leica 2255, Germany) and stained with Toluidine Blue as described in **Chapter 2, Section 2.7.4**.

4.2.4.2. Resin Sections

After being scanned, the right femora were cut using a slow speed saw to reveal the metaphyseal area followed by graded-ethanol dehydration and embedded in methyl methacrylate as previously described in **Chapter 2.** Sections of 5 µm thickness were stained with Tartrate Resistant Acid- Phosphatase (TRAP) for analysis of osteoclasts as previously described in **Section 2.7.5** while unstained sections were used to measure double fluorochrome labels**.** Results are reported using terminology and units in accordance with the American Society of Bone Mineral Research Histomorphometry Nomenclature Committee (175)

4.2.5. Quantitative Real Time PCR

mRNA was extracted from kidney and left tibia using TRIzol® methods, and cDNA was generated using reverse transcriptase enzyme as described in **Section 2.8.** Tibial cDNA was analysed for genes related to bone formation and bone resorption while kidney cDNA was analysed for gene expression of vitamin D metabolism/activities and FGF-23 responsive genes using PCR primers as listed in **table 2.1** in **chapter 2**.

4.2.6. Statistical Analyses

Two-tail independent student t-test analyses were conducted for studies of 3w and 6w groups. Two-way ANOVA was conducted to analyse the effects of genotype, diet and interactions between genotype and diet on skeletal structure of the 20w groups with a confidence interval (α) set at 95 % and p value < 0.05 was considered as statistically significant. Least Significant Difference (LSD) post-hoc tests were applied to identify the group/s that were significantly different. Variables which were not normally distributed based on Kolmogorov-Smirnov normality test were then analysed using the Mann-Whitney Test as indicated in the results.

4.3. RESULTS

4.3.1. Transgenic Over-Expression of VDR in Mature Osteoblast mice (ObVDR-B6) at 3w-Age and following Short Term LowCaP Feeding

At weaning female and following short term LowCaP feeding WT and ObVDR-B6 have similar body weights (**Figure 4.1**). There are no significant changes in serum calcium and phosphate or bone turnover markers between WT and ObVDR-B6 at 3w of age or following short term LowCaP dietary feeding (**Table 4.1**). Serum 1,25D is increased in the 6w ObVDR-B6 mice with a trend for an increase of PTH ($p = 0.07$) and a decrease of FGF-23 ($p= 0.1$) (Mann Whitney tests).

Femur length, total mineral content and segmental analyses of WT and ObVDR-B6 at 3w are not significantly different (**Figure 4.3. A, B, and C**). However, after short term LowCaP feeding, femur length is decreased in ObVDR-B6 mice together with disruption of the growth plate compared to WT fed this diet without a change in total mineral content **(Figures 4.2. B, 4.3. A and B).** Segmental analyses of the full length femur **(Figure 4.3. D)** demonstrate site specific structural changes in ObVDR-B6 fed short term LowCaP diet apparent in the Faxitron images (**Figure 4.2. A**). Significant differences between WT and ObVDR-B6 are identified in segments 7 – 15 (distal metaphyseal region) and segments 23 – 31 (third trochanter region) (**Figure 4.3. D**). While cortical bone volume is unaltered with short term LowCaP diet, significantly thicker cortices in ObVDR-B6 mice arise from small non-significant variations of periosteal and endosteal perimeters **(Table 4.2).** Most importantly cortical porosity is markedly increased (20-fold) in ObVDR-B6 mice fed the LowCaP diet for 3w compared to WT fed the same diet (Mann-Whitney test) **(Figure 4.2. C and D, Table 4.2)**.

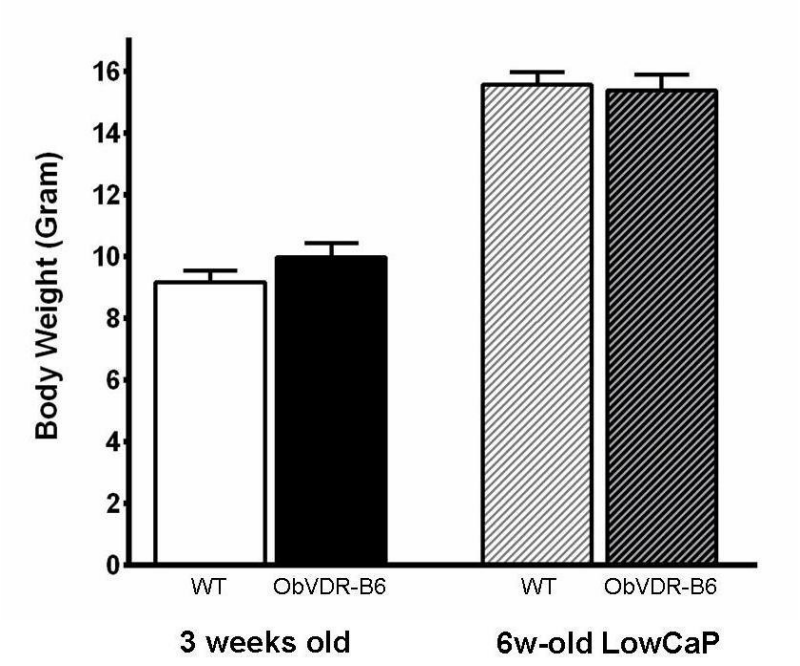

Figure 4.1. Body Weight of WT and ObVDR-B6 mice at Weaning (3w) and at 6w of Age Fed LowCaP.

Values are Mean ± SEM, n = 7/groups (at 3w) and 8/groups of the 6w LowCaP.

Table 4.1. Serum Biochemistry of WT and ObVDR-B6 Mice at 3w and 6w Old Fed LowCaP Diet for 3w

	3w Old		6w Old Fed LowCaP Diet for 3w	
	WT	**ObVDR-B6**	**WT**	**ObVDR-B6**
(n)	***(7)***	***(7)***	***(8)***	***(8)***
Calcium (mmol/L)	3.00 ± 0.09	3.19 ± 0.13	2.29 ± 0.04	2.42 ± 0.09
Phosphate (mmol/L)	2.69 ± 0.17	2.69 ± 0.15	1.93 ± 0.11	2.08 ± 0.20
ALP (mmol/L)	771.97 ± 71.53	704.46 ± 78.41	859.04 ± 100.78	990.35 ± 85.49
1,25(OH)D (pmol/L)	533.52 ± 125.82	385.81 ± 117.23	1351.55 ± 134.17	1870.66 ± 234.26*
CrossLaps (ng/mL)	N/A	N/A	72.29 ± 2.73	79.63 ± 2.30
FGF-23 (pg/mL)	N/A	N/A	92.26 ± 17.42	56.38 ± 8.41
PTH (pg/mL)	N/A	N/A	35.40 ± 14.18	165.26 ± 79.70

Values are mean ± SEM, * P < 0.05 vs. WT mice. Not Available (N/A)

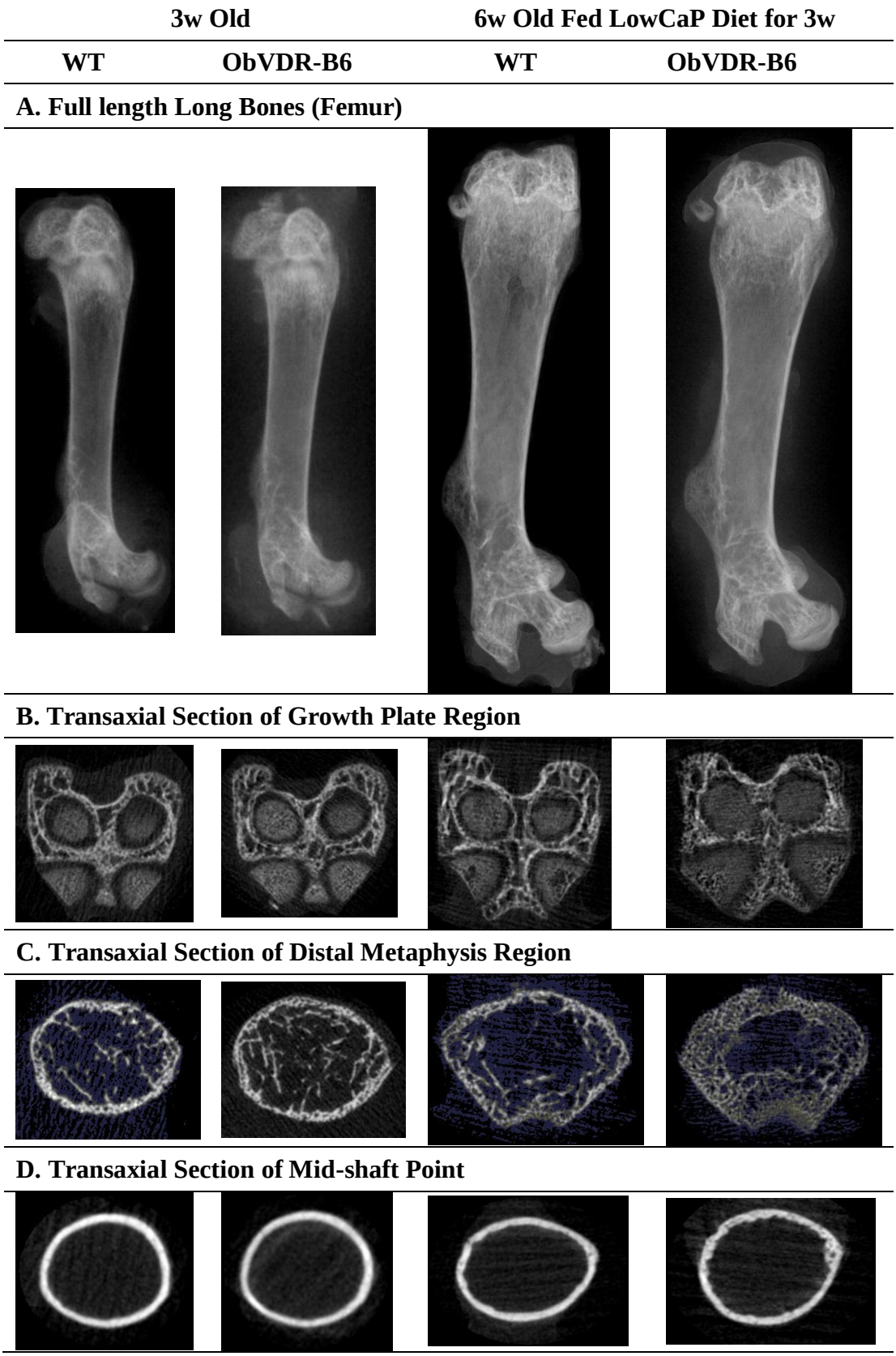

Figure 4.2. X-ray Images of Whole Femora (A) and Micro-CT Transaxial Sections of Growth Plate (B), Distal Metaphysis (C) and Mid-shaft (D) from WT and ObVDR-B6 at 3w and 6w Old Fed LowCaP for 3w.

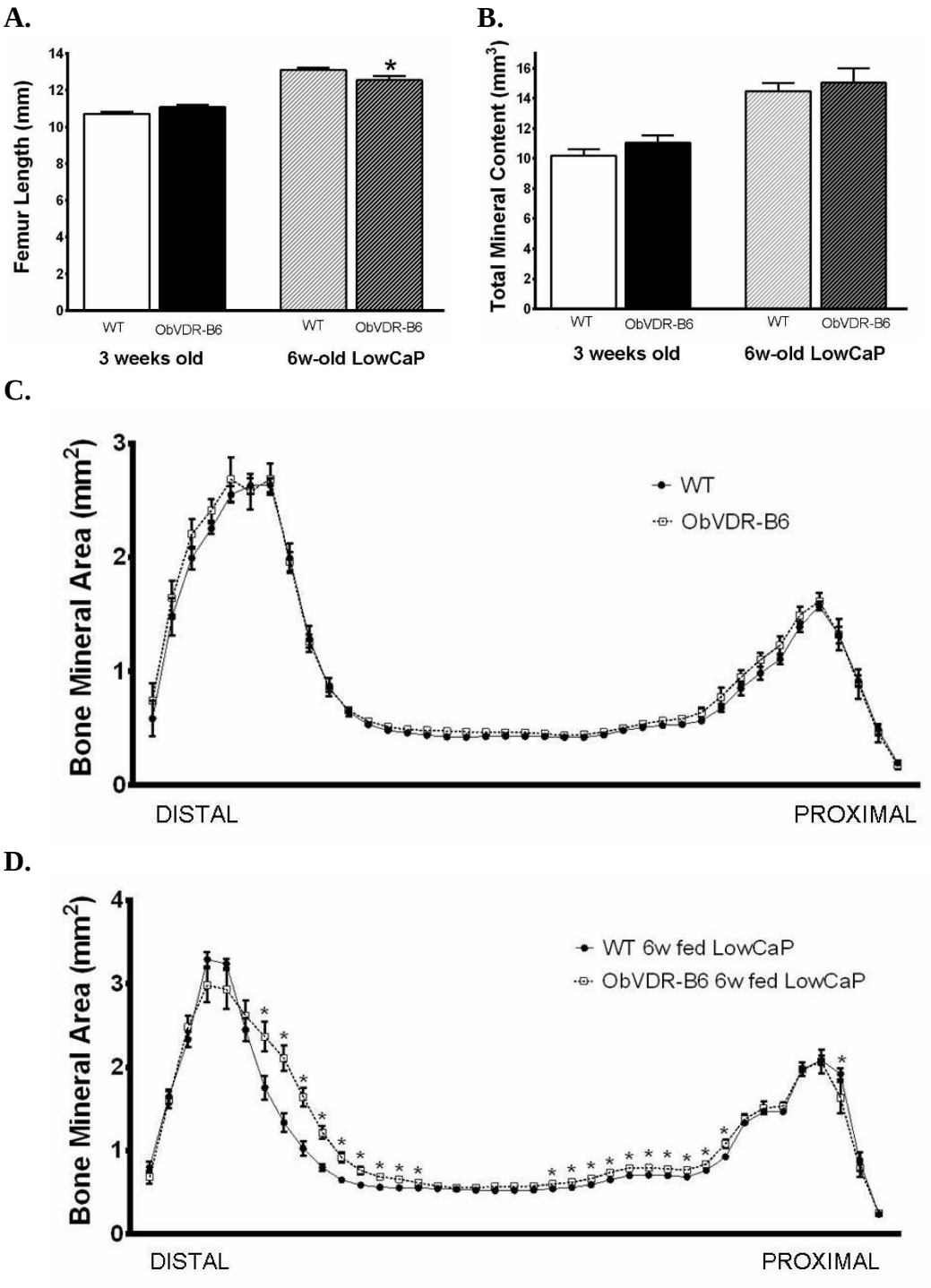

Figure 4.3. Femur Length (A), Full Length Total Mineral Content (B), and Sub-Regional Femoral Analyses of 3w Old (C) and 6w Old (D) Fed LowCaP Diet in WT and ObVDR-B6 Mice

Values are mean + SEM, * $P < 0.05$ vs. WT mice, n = 7/groups for 3w and n = 8/groups for 6 weeks

Table 4.2. Cortical Parameters of Mid-shaft Region of Female 3w Old and 6w Old Fed LowCaP WT and ObVDR-B6 Mice

	3w Old		6w Old Fed LowCaP	
	WT	**ObVDR-B6**	**WT**	**ObVDR-B6**
(n)	***(7)***	***(7)***	***(8)***	***(8)***
Cort. BV (mm^3)	0.74 ± 0.03	0.68 ± 0.12	0.62 ± 0.02	0.66 ± 0.04
Cort.Th (μm)	113.18 ± 3.52	117.29 ± 3.52	126.07 ± 2.88	147.04 ± 4.82*
Ps.Pm (mm)	4.17 ± 0.08	4.37 ± 0.09*	4.79 ± 0.04	4.83 ± 0.07
Es.Pm (mm)	3.46 ± 0.06	3.64 ± 0.08*	4.02 ± 0.03	3.94 ± 0.07
Porosity (%)	N/D	N/D	0.0047 ± 0.0047	0.0952 ± 0.0432*

Values are mean ± SEM, * $P < 0.05$ vs. WT mice within same group. Cortical Bone volume, (Cort.BV); Cortical thickness. (Cort.Th); Periosteal perimeter (Ps.Pm); and Endosteal perimeter, (Es.Pm). N/D (not detected)

Trabecular bone analyses at the femoral distal metaphysis and vertebra-L1 demonstrate significant increases in trabecular bone volume due to increased trabecular number with decrease of trabecular thickness and almost double connectivity density in ObVDR-B6 even when fed the LowCaP diet for 3 weeks (**Table 4.3**). Trabecular separation is unchanged in distal metaphysis but is decreased at vertebral body of L1 without a change in the vertebral height.

Table 4.3. Trabecular Bone Analyses of Femoral Distal Metaphysis and Vertebral Body of L-1 of 6w Old Mice Fed LowCaP Diet for 3w

	Femoral Distal Metaphysis		**Vertebra Body L-1**	
	WT	**ObVDR-B6**	**WT**	**ObVDR-B6**
(n)	***(8)***	***(8)***	***(8)***	***(5)***
L-1 Height (mm)	N/A	N/A	2.34 ± 0.04	2.29 ± 0.03
BV/TV (%)	3.27 ± 0.15	4.37 ± 0.41*	11.01 ± 0.22	12.95 ± 0.71*
Tb.Th (µm)	51.10 ± 0.86	47.57 ± 0.84*	34.53 ± 0.39	32.91 ± 0.60*
Tb.N (1/mm)	0.64 ± 0.03	0.92 ± 0.09*	3.18 ± 0.05	3.95 ± 0.25*
Tb.Sp (µm)	755.4 ± 20.7	736.8 ± 33.2	182.4 ± 3.8	163.3 ± 11.2*
Conn.D (1/mm^3)	14.95 ± 1.02	37.65 ± 4.38*	334.1 ± 25.5	620.8 ± 112.4*
SMI	2.28 ± 0.02	2.18 ± 0.05	2.12 ± 0.04	2.14 ± 0.04

Values are mean ± SEM, * $P < 0.05$ vs. WT mice within same group. Trabecular Bone Volume (BV/TV), Trabecular Thickness (Tb.Th), Trabecular Separation (Tb.Sp), Structural Model Index (SMI), Connectivity density (Conn.D).

4.3.2. Effects of Transgenic Over-expression of VDR in Mature Osteoblasts Fed NormCaP and LowCaP Diets for Long Term (17w)

Body weights of WT and ObVDR-B6 mice fed NormCaP and LowCaP diet for 17w show no significant differences between groups from the start of treatment until 20w of age **(Figure 4.4. A and B)**. When fed NormCaP, there are no significant changes in serum calcium, phosphate, CrossLaps, TRAP5b, or 1,25D levels between WT and ObVDR-B6 but serum FGF-23 levels are significantly lower with decreased CrossLaps/TRAP5b ratio in ObVDR-B6 mice. Long term LowCaP feeding significantly increases the serum ALP, CrossLaps, TRAP5b, 1,25D and FGF-23 levels in WT and/or ObVDR-B6 mice. Between genotype analyses of WT vs ObVDR-B6 mice on LowCaP diet indicated no significant differences in serum levels of calcium, phosphate, ALP, Crosslaps, TRAP5b and CrossLaps/TRAP5b ratio (**Table 4.4**). Serum 1,25D levels are significantly higher in ObVDR-B6 while serum FGF-23 levels are significantly lower than the WT mice. Changes in serum PTH between NormCaP and LowCaP diet or between genotype were not detected, likely due to technical errors during serum storage or PTH analyses (data not presented).

Bone images are depicted in **Figure 4.5** indicating no detectable differences between WT and ObVDR-B6 fed NormCaP. However, flat bones (scapula) and femora show distinct changes in skeletal structures when ObVDR-B6 mice are fed LowCaP diet. The scapula of LowCaP fed ObVDR-B6 mice are smaller, narrower and the structure of the upper curve is changed relative to the other groups (**Figure 4.5. A**). Femur length is obviously decreased with the LowCaP feeding in both groups but the changes are more marked in the distal metaphysis region and marked widening of the femur column diameter is apparent in the ObVDR-B6 mice (**Figure 4.5. B)**. The growth plate

is disrupted in ObVDR-B6 mice fed LowCaP diet with obvious increased cortical porosity in the distal metaphysis (**Figure 4.5. C and D**). Trabecular bone at the femoral distal metaphysis and vertebra is increased in ObVDR-B6 mice compared to the WT mice fed the same diet although more marked at the vertebra than the metaphysis and even when fed LowCaP (**Figure 4.5. E and F).** Cortical bone at the femoral mid-shaft was largely intact although ObVDR-B6 mice fed LowCaP demonstrated increased resorption surfaces compared to LowCaP fed WT mice (**Figure 4.5. G and H).**

Femur length is not significantly different in NormCaP fed mice (**Figure 4.6. A**) but total mineral content is increased in ObVDR-B6 mice (**Figure 4.6. B**) especially in the diaphyseal region of the femur (**Figure 4.6. C**). When fed LowCaP diet, femur length is significantly decreased in ObVDR-B6 compared to WT mice. Interestingly even with LowCaP diet, total mineral content of ObVDR-B6 mice remains higher than WT due to significant increases in almost all segments of the femur (**Figure 4.6. B and D**).

Femoral mid-shaft cortical analyses show similar findings to the segmental analyses of femora (**Table 4.5**). A near significant increase of cortical bone volume (8 %, $p = 0.057$) is observed on NormCaP fed ObVDR-B6 due to increased periosteal and endosteal perimeters suggesting a larger increase in the periosteal perimeter than the endosteal perimeter. Feeding the LowCaP diet reduces cortical volumes and thicknesses and reduces the effect of the VDR transgene on cortical bone volume. LowCaP fed ObVDR-B6 still have increased periosteal and endosteal perimeters. No porosity in the femoral mid-shaft is detectable in WT and ObVDR-B6 on NormCaP diet but cortical porosity is markedly increased in ObVDR-B6 mice fed LowCaP compared to all other groups.

A.

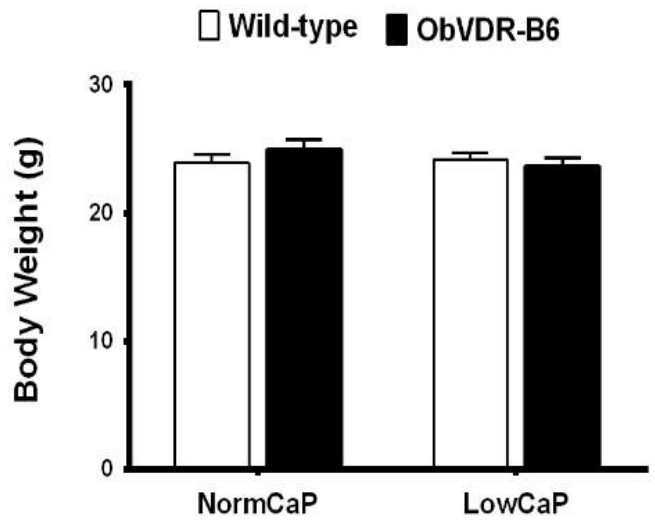

B.

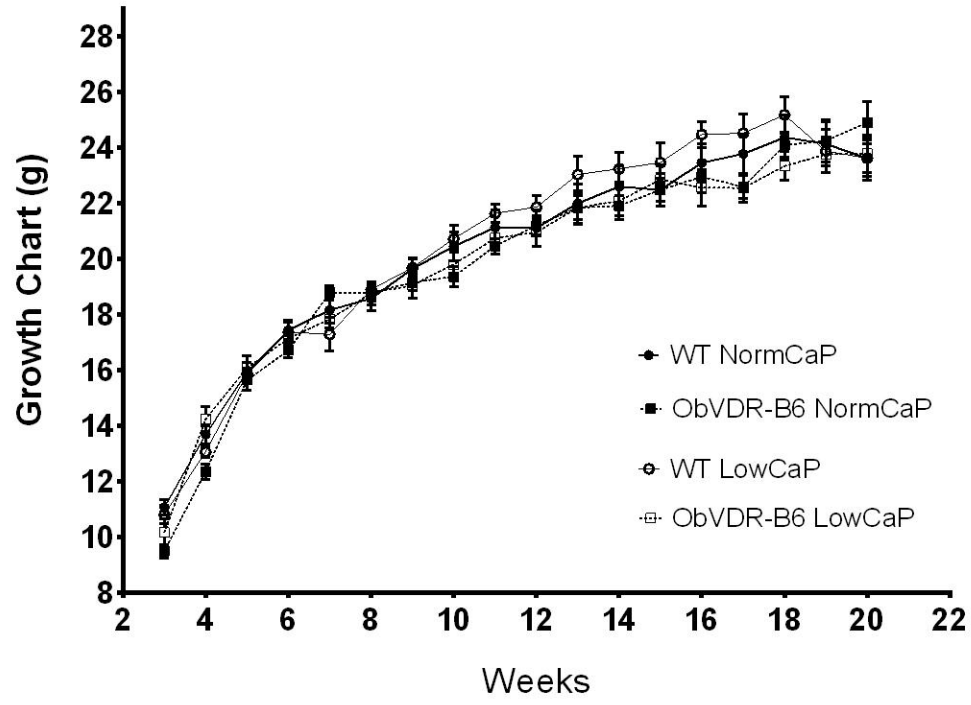

Figure 4.4. Body Weight at 20w (A) and Growth Chart during 17w of Dietary Treatment (B)

Values are mean ± SEM

Table 4.4. Serum Biochemistry of WT and ObVDR-B6 Mice Fed with NormCaP and LowCaP Diet for 17w (20w of age)

	NormCaP		LowCaP	
	WT	**ObVDR-B6**	**WT**	**ObVDR-B6**
(n)	***(7)***	***(7)***	***(7)***	***(9)***
Calcium (mmol/L)	2.31 ± 0.05	2.26 ± 0.12	2.30 ± 0.09	2.24 ± 0.05
Phosphate (mmol/L)	1.16 ± 0.05	1.28 ± 0.05	1.09 ± 0.14	1.01 ± 0.11
ALP (mmol/L)[(b,c)]	124.04 ± 3.01	67.64 ± 12.29	274.03 ± 28.45♣	370.12 ± 57.30♣
CrossLaps (ng/mL)[(b)]	21.69 ± 1.76	26.39 ± 2.77	36.39 ± 5.70♣	42.42 ± 3.34♣
TRAP5b (ng/mL)[(b)]	4.51 ± 0.53	5.82 ± 0.36	7.52 ± 1.14♣	7.41 ± 0.51
CrossLaps/TRAP5b	5.34 ± 0.99	4.53 ± 0.32*	4.91 ± 0.36	5.80 ± 0.42
1,25(OH)D (pmol/L) [(a,b,c)]	182.35 ± 30.50	145.86 ± 8.56	872.82 ± 70.48♣	1345.5 ± 122.9*♣
FGF-23 (pg/mL)[(a,b)]	358.97 ± 33.56	254.78 ± 30.63*	176.17 ± 25.14♣	105.91 ± 14.61*♣
PTH (pg/mL)	189.96 ± 40.52	234.71 ± 54.66	165.85 ± 60.09	241.78 ± 56.98

Values are mean ± SEM, Two-way ANOVA significant at $p < 0.05$ for genotype (a), dietary (b), and interaction (c). * $p < 0.05$ vs. WT mice, ♣ $p < 0.05$ vs. NormCaP within same genotype

NormCaP		LowCaP	
WT	**ObVDR-B6**	**WT**	**ObVDR-B6**
A. X-ray Images of Flat Bone (Scapula)			
	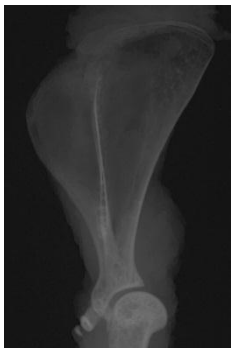		
B. X-Ray Images of Long Bones (Femur)			
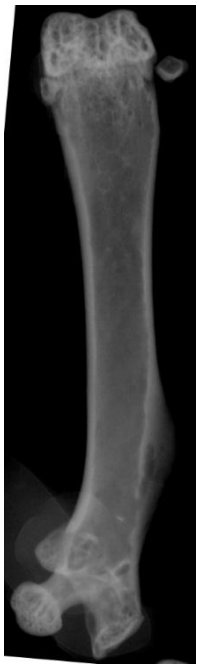			
C. 3D Reconstruction of Growth Plate Region			
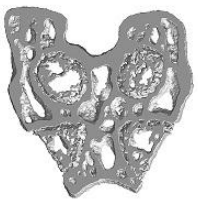			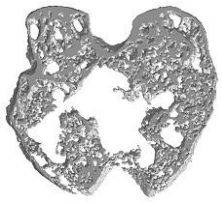
D. 3D Reconstruction of Distal Metaphysis Region			
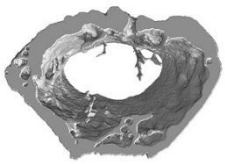	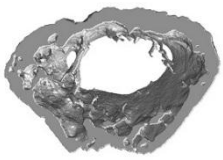	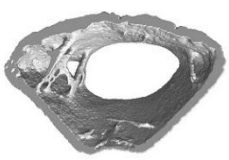	

E. 3D Reconstruction of Trabecular Bone at Distal Metaphysis

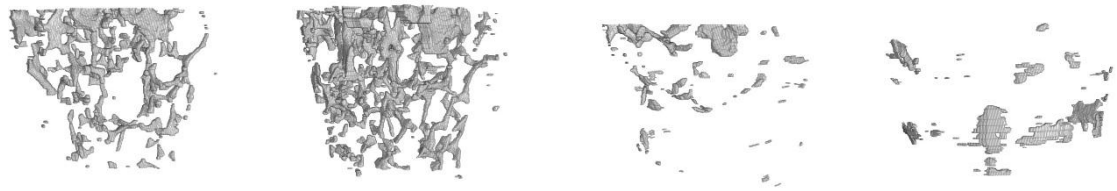

F. 3D Reconstruction of Trabecular Bone at Vertebral Body of Lumbar-1

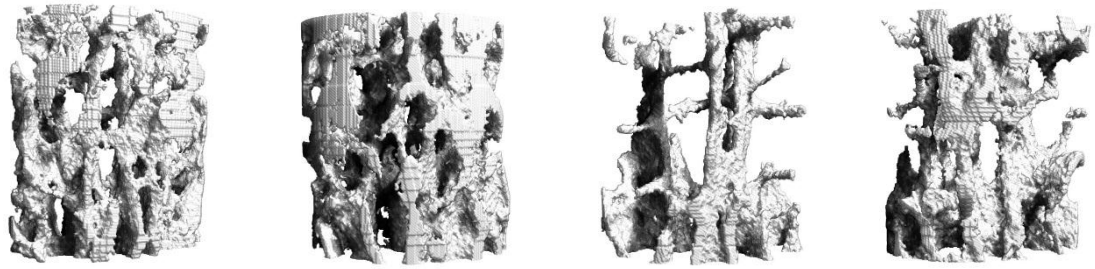

G. 3D Reconstruction of Cortical Bone at Mid-shaft Region

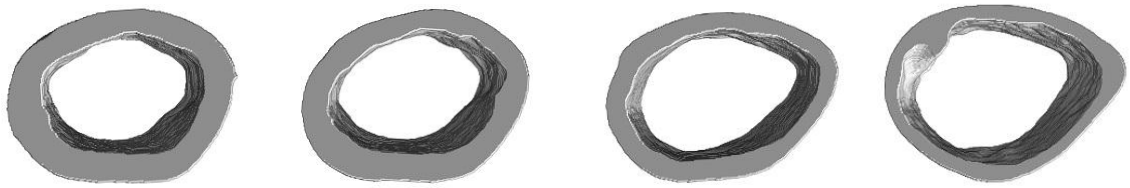

H. Transverse section at Mid-Point

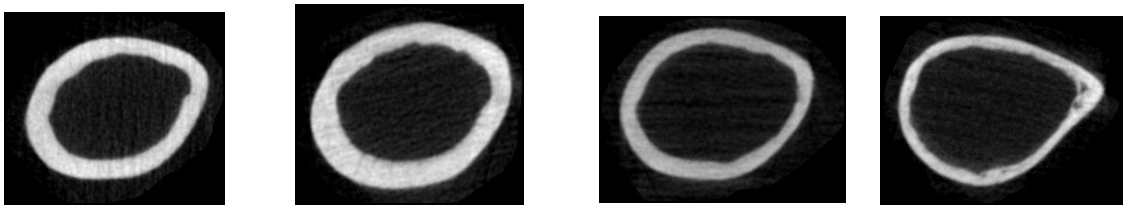

Figure 4.5 X-Ray Images of Flat Bone (Scapula) (A) and Long Bone (Femur) (B), 3D Reconstruction of Growth Plate (C), Distal Metaphysis (D), Trabecular Bone (E and F), Cortical Mid-Shaft (F) and Transaxial Images at Mid-point (H) Following Long Term Dietary Treatment.

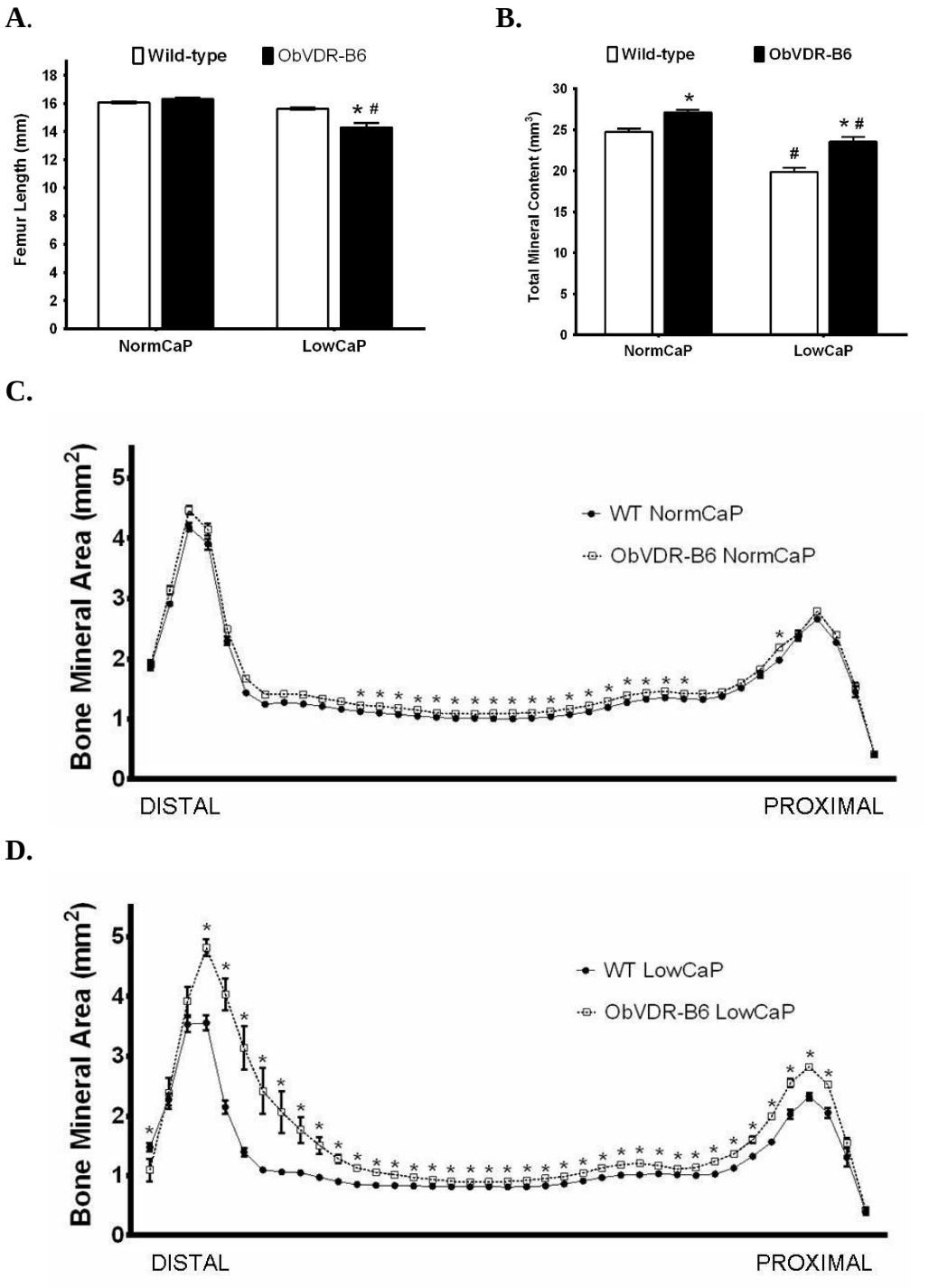

Figure 4.6. Femur Length (A), Full Length Femoral Mineral Content (B), and Femoral Segmental Bone Mineral Area (C) of WT and ObVDR-B6 Mice Fed NormCaP and LowCaP for 17w.

Values are mean ± SEM, * $p < 0.05$ vs. WT mice, # $p < 0.05$ vs. NormCaP within same genotype

Table 4.5. Cortical Variables at Femoral Mid-shaft Region of WT and ObVDR-B6 Mice Fed NormCaP and LowCaP for 17w

	NormCaP		LowCaP	
	WT	**ObVDR-B6**	**WT**	**ObVDR-B6**
(n)	***(7)***	***(7)***	***(7)***	***(9)***
Cor. BV (mm^3) [b, c]	1.57 ± 0.06	1.70 ± 0.02	1.19 ± 0.03♣	1.22 ± 0.05♣
Cor.Th (μm) [b]	237.12 ± 3.06	245.15 ± 2.43	183.77 ± 3.38♣	187.88 ± 4.38♣
Ps.Pm (mm) [a,b,c]	5.34 ± 0.05	5.61 ± 0.03**	5.34 ± 0.08	5.86 ± 0.04*♣
Es.Pm (mm) [a,b,c]	3.85 ± 0.04	4.09 ± 0.04*	4.19 ± 0.07♣	4.69 ± 0.06*♣
Porosity (%)	N/D	N/D	N/D	0.0213 ± 0.0140

Values are mean ± SEM, Two-way ANOVA significant at $p < 0.05$ for genotype (a), dietary (b), and interaction (c). * $p < 0.05$ vs. WT mice, ♣ = $p < 0.05$ vs. NormCaP within same genotype. Cortical Bone Volume (Cor.BV), Cortical Thickness (Cor.Th), Periosteal Circumference (Ps.Pm), Endosteal Perimeter (Es.Pm). Not Detected (N/D)

Trabecular bone analyses at the femoral distal metaphysis of ObVDR-B6 fed NormCaP diet (**Table 4.6**) show a significant increase of trabecular bone volume due to increased trabecular number and improved connectivity density. Increased trabecular bone volume is still maintained by LowCaP fed ObVDR-B6 due to increase trabecular number. Feeding the LowCaP diet decreases trabecular bone volume, trabecular number and connectivity density and increase trabecular separation irrespective of genotype. Interestingly, structural model index (SMI) is decreased in ObVDR-B6 mice but unchanged by dietary treatment indicating that the number of trabecular parallel plates is increased by over-expression of the VDR gene in mature osteoblasts even under the conditions of high bone turnover resulting from the LowCaP diet.

Similar to the finding of NormCaP fed ObVDR-B6 in the femoral distal metaphysis, trabecular bone volume in the vertebral body of L-1 is increased due to an increase in trabecular number and connectivity with a decrease in SMI indicating increased number of trabecular plates (**Table 4.6**). Interestingly, when fed LowCaP, the increased trabecular bone volume observed in distal metaphysis is lost in the vertebra although a decrease of trabecular separation is now apparent and the trabecular plates are preserved as indicated by the preservation of the decreased SMI. The LowCaP treatment decreases trabecular bone volume, trabecular number and connectivity density while increasing trabecular separation irrespective of genotype similar to effects on trabecular bone in the femoral distal metaphysis. The height of the vertebral body of lumbar-1 (VBL-1) was not different between genotypes or dietary treatments.

Table 4.6. Trabecular Bone in Distal Metaphysis and Vertebral Body of L-1 after Long Term Dietary Treatment in WT and ObVDR-B6 Mice

	NormCaP		LowCaP	
	WT	**ObVDR-B6**	**WT**	**ObVDR-B6**
(n)	***(7)***	***(7)***	***(7)***	***(9)***
DISTAL METAPHYSIS				
BV/TV (%)[a,b]	3.15 ± 0.11	5.19 ± 0.42*	0.96 ± 0.15♣	1.98 ± 0.45*♣
Tb.Th (µm)	49.40 ± 1.22	50.30 ± 0.41	53.59 ± 3.03	48.10 ± 4.39
Tb.N (#/um) [a,b]	640.03 ± 24.88	1032.88 ± 83.52*	178.54 ± 23.86♣	377.89 ± 80.91*♣
Tb.Sp (um) [b,c]	363.44 ± 6.38	313.77 ± 8.56	672.66 ± 30.29♣	866.82 ± 91.73*♣
Conn.D (#/mm^3)[a,b,c]	4.85 ± 0.70	20.54 ± 3.69*	1.13 ± 0.19	6.21 ± 1.35♣
SMI[a]	2.75 ± 0.04	2.53 ± 0.05*	2.87 ± 0.06	2.50 ± 0.09*
VERTEBRA				
L-1 Height (mm)	2.78 ± 0.03	2.73 ± 0.04	2.80 ± 0.03	2.74 ± 0.03
BV/TV (%)[a,b]	18.47 ± 0.94	22.12 ± 0.89*	8.92 ± 0.48♣	10.38 ± 0.59♣
Tb.Th (µm)[b]	47.29 ± 0.49	48.86 ± 0.83	39.98 ± 0.48♣	40.80 ± 0.54♣
Tb.N (#/mm)[a,b]	3.90 ± 0.18	4.53 ± 0.16*	2.23 ± 0.10♣	2.54 ± 0.14♣
Tb.Sp (µm)[a,b]	200.48 ± 5.03	180.54 ± 6.27	300.34 ± 10.07♣	275.08 ± 8.97*♣
Conn.D (#/mm^3) [a,b,c]	269.83 ± 24.38	394.34 ± 23.27*	194.00 ± 19.51	236.43 ± 30.39♣
SMI [a]	1.45 ± 0.06	1.28 ± 0.06*	1.58 ± 0.06	1.53 ± 0.08*

Values are mean ± SEM, Two-way ANOVA significant at $p < 0.05$ for genotype (a), dietary (b), and interaction (c). * $p < 0.05$ vs. WT mice, ♣ = $p < 0.05$ vs. NormCaP within same genotype. Trabecular Bone Volume (BV/TV), Trabecular Thickness (Tb.Th), Trabecular Separation (Tb.Sp), Structural Model Index (SMI), Connectivity density (Conn.D).

Histology of the distal femora confirmed the disruption of growth plate in the ObVDR-B6 mice fed LowCaP as indicated by changes in growth plate width and growth plate area compared to WT fed the same diet or ObVDR-B6 fed NormCaP (**Figure 4.7**). Masson trichrome stain indicates growth plate (in green) in m-shape feature which was clearly disrupted in the ObVDR-B6 mice fed LowCaP diet.

Dynamic histomorphometry at this site shows distinct double fluorochrome labels in trabecular and cortical bone indicating normal mineralisation and no evidence of osteomalacia. No significant changes in bone formation rate between WT and ObVDR-B6 fed NormCaP is detected (**Table 4.7, Figure 4.8)**. MS/BS and MAR are not significantly different between WT and ObVDR-B6 fed NormCaP. TRAP stain analyses demonstrate a significant decrease of osteoclast number per bone perimeter and a trend toward decrease ($p = 0.0612$) in osteoclast attachment surface (Oc.S/BS) between WT and ObVDR-B6 fed NormCaP diet (**Table 4.7, Figure 4.9)**. The distal metaphyseal region was not suitable for dynamic histomorphometry in mice fed LowCaP because there was too little trabecular bone available for meaningful measurements. Osteocyte density in the cortical region of distal metaphysis shows no significant changes between WT and ObVDR-B6 fed NormCaP or LowCaP (**Figure 4.10**).

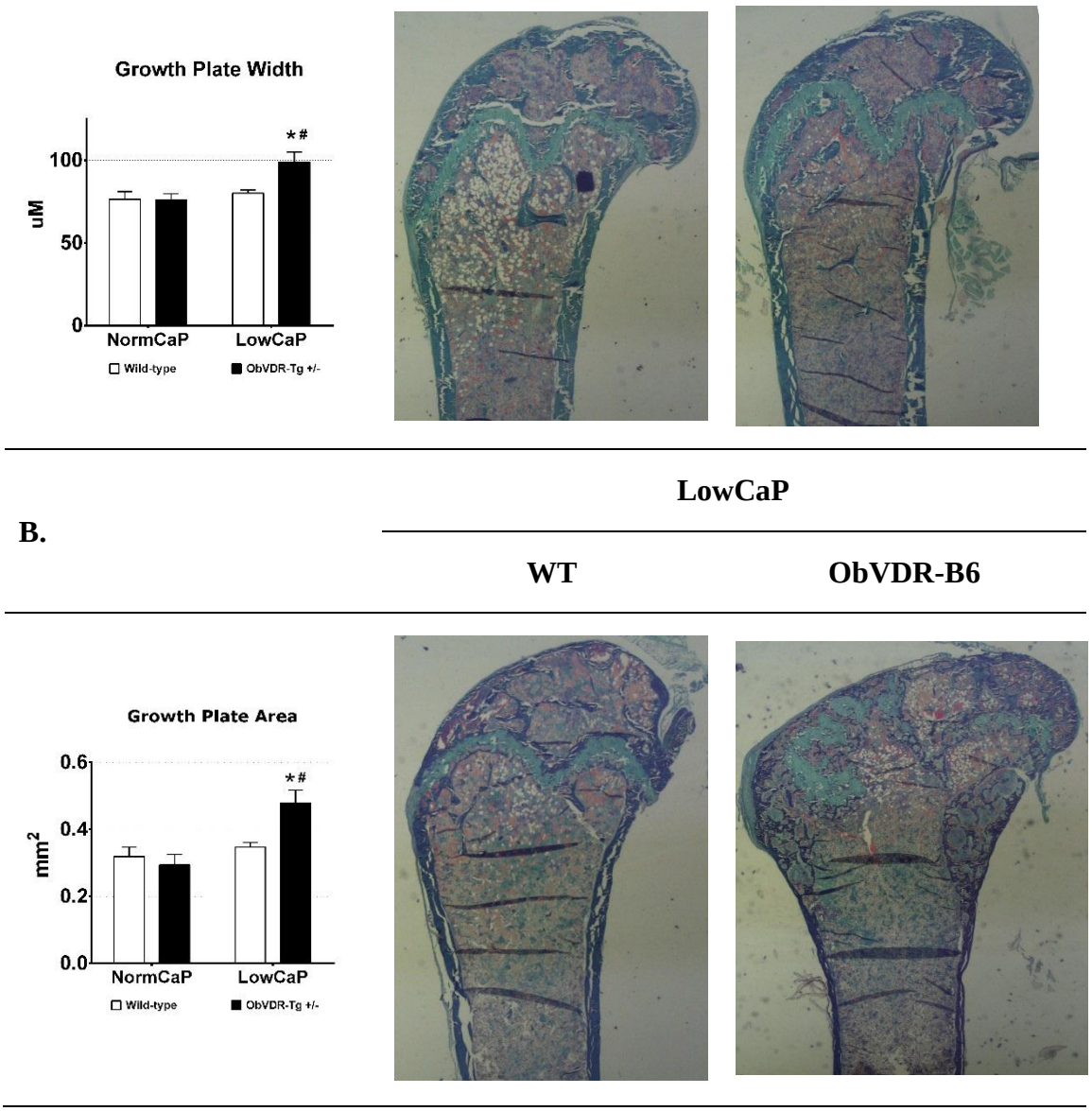

Figure 4.7. Histological Assessment of Growth Plate Width (A), Area (B) and Images of Masson Trichrome Stains of WT and ObVDR-B6 Mice after Long Term Dietary Treatment

M shape in green illustrates the growth plate, at 20x magnification. The ObVDR-B6 growth plate is visually disrupted. Values are mean $\pm$ SEM, * $p < 0.05$ vs. WT, # $p < 0.05$ vs. NormCaP within the same genotype

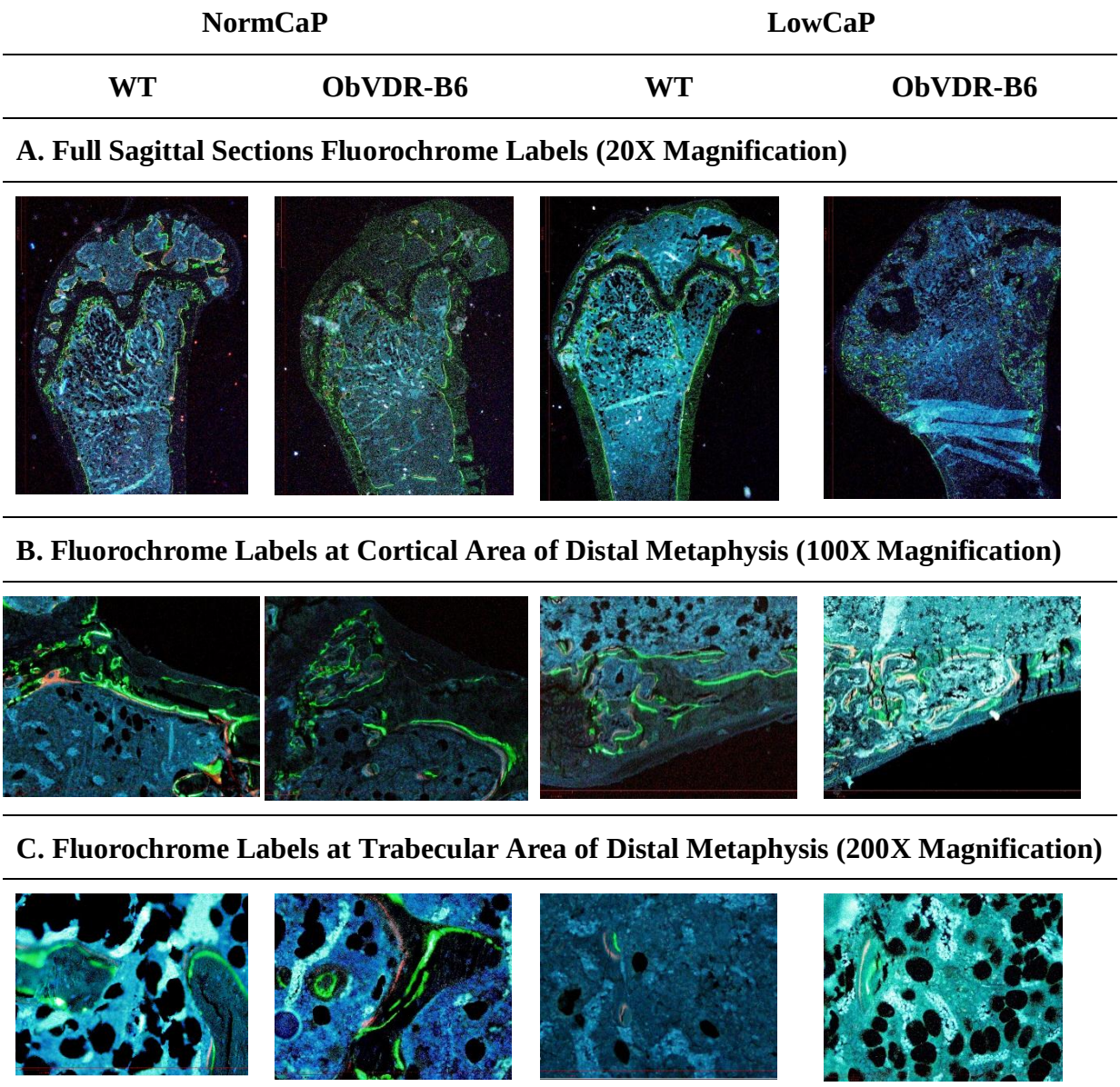

Figure 4.8. Images of Double Fluorochrome Labels at Full Section (A), Cortical Region (B) and Trabecular Region (C) of WT and ObVDR-B6 Mice Fed NormCaP and LowCaP for 17w.

At 20x magnification, growth plate disruption is evident in ObVDR-B6 fed LowCaP. Distinct double labels are evident in all bones indicating normal mineralisation even when fed LowCaP and irrespective of genotype. In the cortices at 100x magnification, increased cortical porosity in distal metaphysis region near growth plate is evident in ObVDR-B6 fed LowCaP. Although trabecular bone is scarce in the LowCaP fed ObVDR-B6, double labels are still clear and distinct (C).

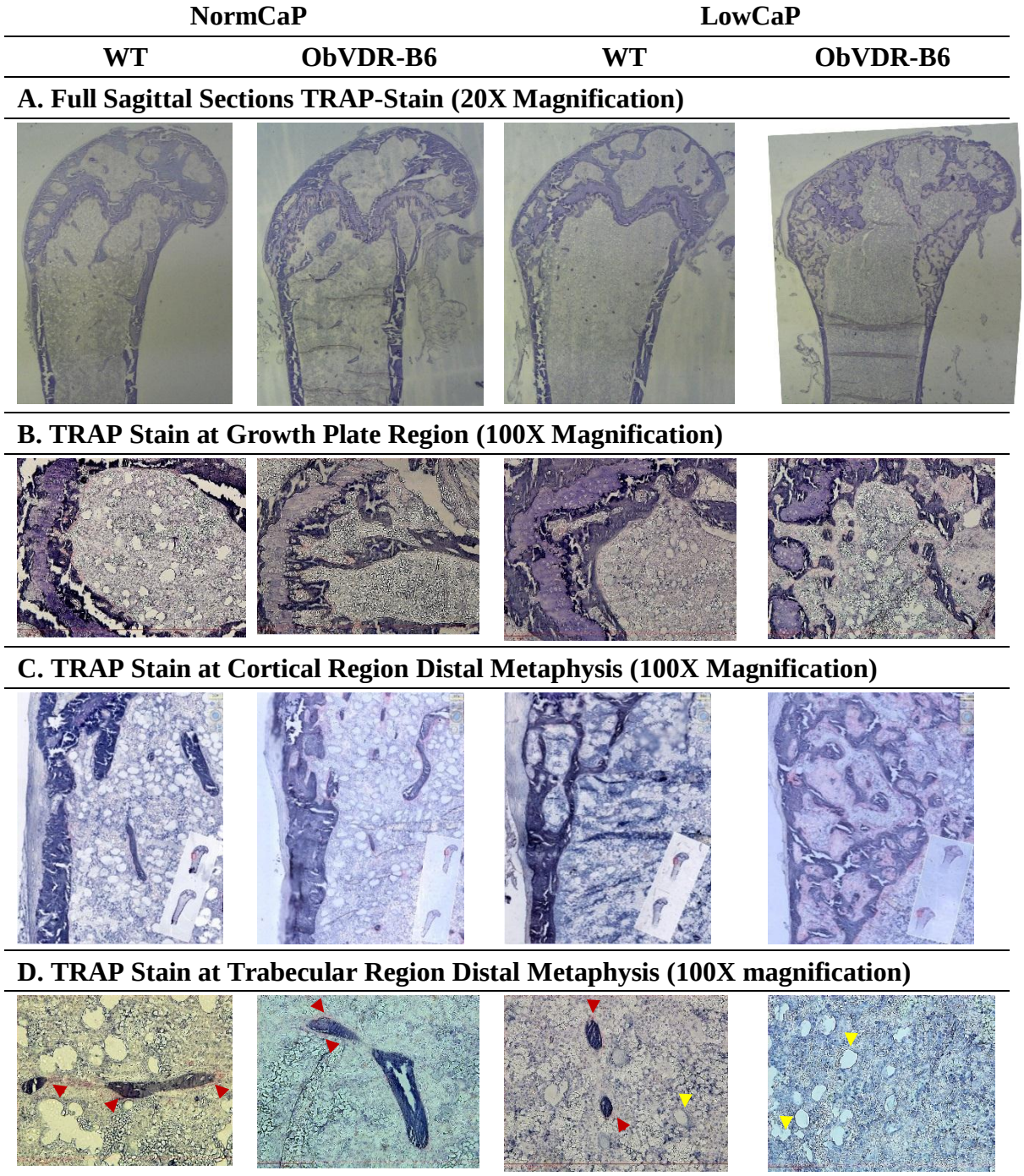

Figure 4.9. Images of Tartrate-Resistant Acid Phosphatase (TRAP) Stain at Full Sagittal Sections (A), Growth Plate Region (B), Cortical Region (C), and Trabecular Region of Distal Metaphysis (D) of WT and ObVDR-B6 Mice Fed NormCaP and LowCaP for 17w

Growth plate disruption is evident in ObVDR-B6 fed LowCaP. Cortices at 100X magnification indicate increased cortical porosity in the distal metaphysis region near the growth plate in ObVDR-B6 fed LowCaP with TRAP *+ve* cells evident.

Table 4.7. Trabecular Dynamic Histomorphometry at the Femoral Distal Metaphysis of WT and ObVDR-B6 Mice Fed NormCaP for 17w.

	NormCaP		LowCaP	
	WT	**ObVDR-B6**	**WT**	**ObVDR-B6**
Double Label (n)	***(7)***	***(7)***		
MS/BS (%)	43.09 ± 1.94	41.51 ± 1.24	N/A	N/A
MAR (µm/day)	2.21 ± 0.12	2.28 ± 0.10	N/A	N/A
BFR/BS (µm^2/µm/d)	0.94 ± 0.05	0.94 ± 0.05	N/A	N/A
TRAP +ve cells (n)	***(7)***	***(7)***		
Oc.Ar (mm^2)	0.0105 ± 0.0014	0.0107 ± 0.0017	N/A	N/A
Oc.S/BS (%)	26.00 ± 1.07	20.40 ± 1.88	N/A	N/A
N.Oc/B.Pm (#/mm)[(a)]	9.27 ± 0.55	7.07 ± 0.50*	N/A	N/A

Values are mean ± SEM, * $p < 0.05$ vs. WT mice. Mineralising Surface/Bone Surface (MS/BS), Mineral Apposition Rate (MAR), Bone Formation Rate (BFR), Total Osteoclasts Area (Oc.Ar), Osteoclasts attachment surface or Osteoclasts Surface/Bone Surface (Oc.S/BS), Number of Osteoclasts per Bone Perimeter (N.Oc/B.Pm)

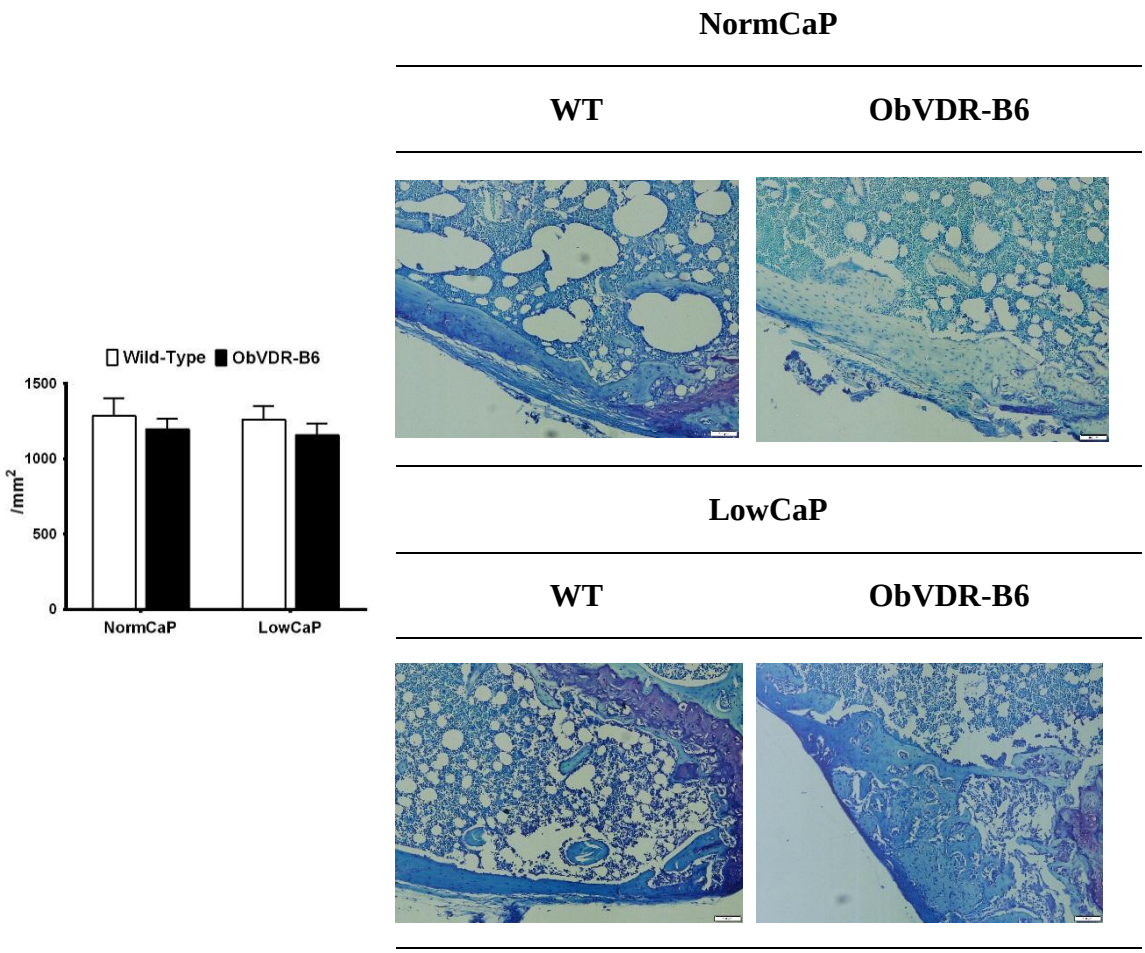

Figure 4.10. Osteocytes Density of WT and ObVDR-B6 Mice Fed after Long Dietary Treatment and Images of Toluidine Blue Staining on Cortical Regions.

Images of the distal metaphyseal cortices for osteocyte density measurements at 100x Magnification. Values are mean ± SEM

Messenger RNA levels of a range of target genes show significant reduction of *Rankl* mRNA in ObVDR-B6 fed NormCaP in comparison to WT with no significant differences detectable for the other genes (**Figure 4.11. A to J**). The LowCaP diet decreased *Sost*, and *Dmp-1* mRNA levels in WT compared to NormCaP levels while in ObVDR-B6, the LowCaP significantly increased *Rankl*, *Rankl*/*Opg* mRNA ratio and *Dmp-1* mRNA levels compared to WT on this diet.

No significant changes of mRNA levels were detected for genes coding for vitamin D metabolising enzymes or FGF-23-responsive genes in the kidneys of WT and ObVDR-B6 fed NormCaP (**Figure 4.12. A to D**). However, when fed LowCaP, a significant increase in *Cyp27B1* mRNA levels in both WT and ObVDR-B6 mice with a trend towards a greater increase in ObVDR-B6 mice compared with WT were observed. WT mice increased *Cyp24* mRNA levels increased with LowCaP but there was no increase in ObVDR-B6 mice fed LowCaP. The *NaPi2* gene mRNA levels were unaffected by genotype or diet.

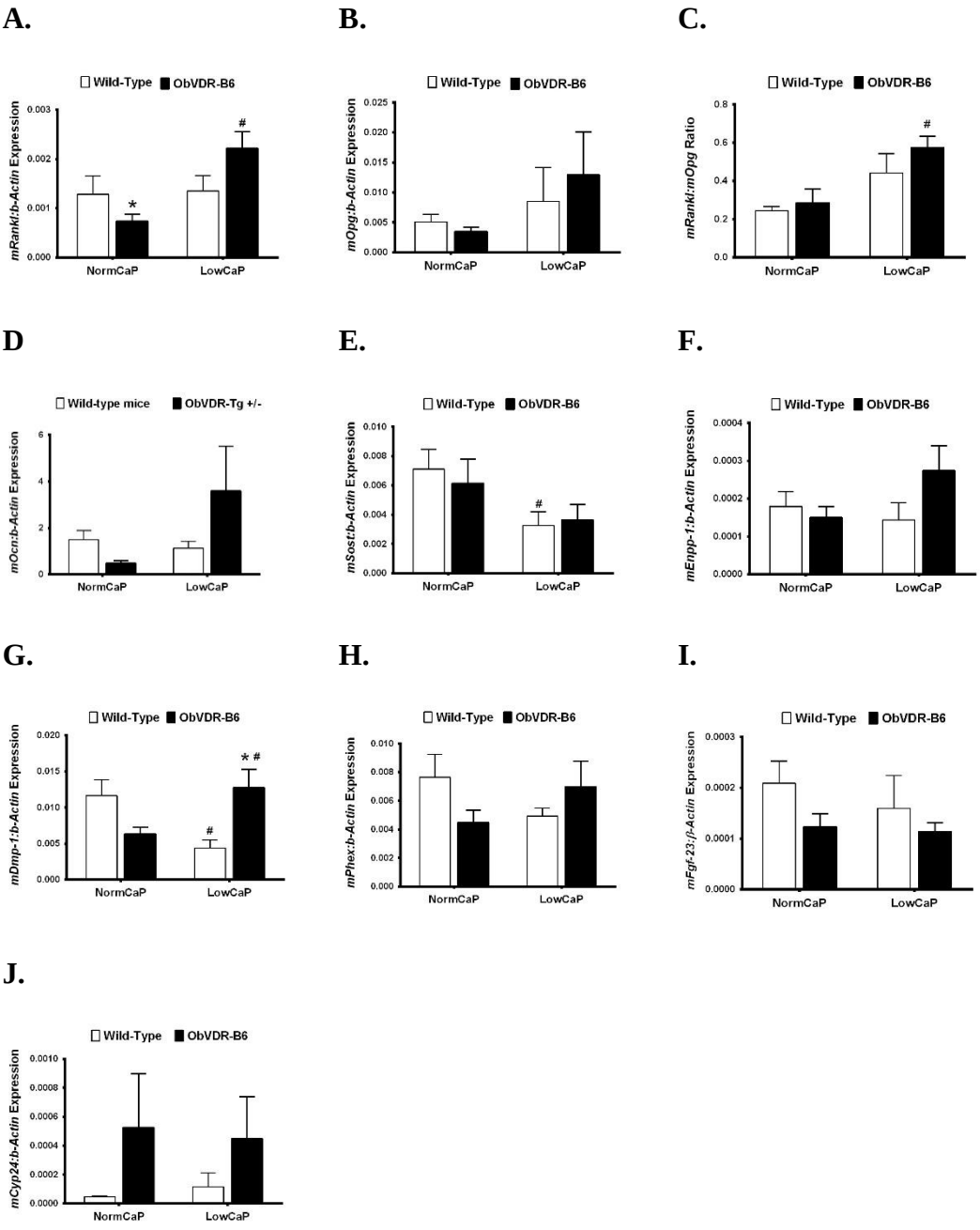

Figure 4.11. Tibial Gene Expression of WT and ObVDR-B6 Mice Fed NormCaP and LowCaP for 17w (20w old mice)

Values are mean ± SEM, * $p < 0.05$ vs. WT, # $p < 0.05$ vs. NormCaP within the same genotype

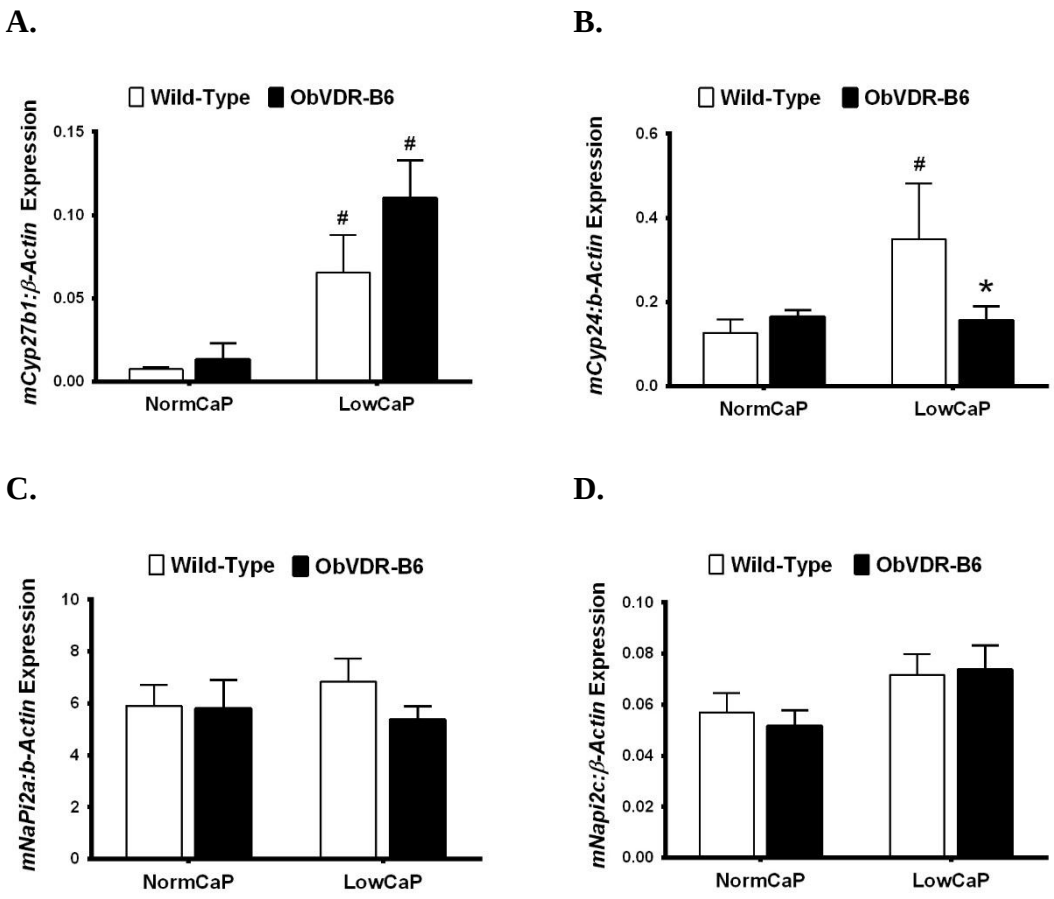

Figure 4.12. Kidney Gene Expression of WT and ObVDR-B6 Mice after Long Term Dietary Treatment.

Values are mean ± SEM, * $p < 0.05$ vs. WT, # $p < 0.05$ vs. NormCaP within the same genotype

4.4. DISCUSSION

4.4.1. Effect of Short Term Dietary LowCaP Treatment

Tailing at 10 days of age showed the expression of human *Vdr* transgene, however, at weaning (3w of age), no significant differences between WT and ObVDR-B6 were found for most of the measured variables suggesting that mature osteoblast VDR had only minor activities during foetal and neonatal growth. However, these ObVDR-B6 weanling mice did have increased mid-shaft cortical size arising from increased cortical perimeters compared to WT suggesting some role for VDR in mature osteoblasts to modulate bone size even at this very early age. Further analyses of gene expressions at foetal, neonatal and weaning are needed to confirm the exact period during the development that the *Vdr* transgene has been over-expressed and started elicit its effect on bone.

Foetal and neonatal bone health is largely determined by the mother's nutritional status including calcium and vitamin D intakes (176). The role of VDR in mature osteoblasts during pregnancy and lactation in maintaining mother's and infant's skeletal health is poorly understood. Current knowledge emphasises the role of vitamin D to stimulate osteoclastic-bone resorption through modulation of the RANKL/RANK/OPG system contributing to the regulation of bone modeling and remodeling (177). Increased periosteal and endosteal perimeters observed in ObVDR-B6 mice at 3w of age suggested a role of osteoblast VDR in increasing bone resorption at the endosteal surface as well as increasing bone formation at the periosteal surface although direct measurements of the osteoclasts using histomorphometry analyses were not conducted on these surfaces. During bone modelling, increased mineral accrual and expansion of the periosteal and endosteal perimeters changes bone size, shape (178) and increasing

bone strength (179). Transgenic expression of human *Vdr* gene in osteoblasts consistently demonstrated increased cortical bone in male and female during growth and adulthood as reported and discussed in chapter 3. These data indicated that such activities commenced at the earliest stages of growth since the expression of transgenic h*Vdr* gene was shown at 10 days of age.

Very young, actively growing mice, irrespective of genotype, maintained normal serum calcium and phosphate levels when fed LowCaP for 3 weeks indicating that plasma mineral homeostasis was adequate irrespective of osteoblast VDR status. However in ObVDR-B6 mice, this homeostasis increased the serum 1,25D levels with a trend towards increased serum PTH levels and decreased serum FGF-23 levels. These data suggest that osteoblast VDR contributed to the endocrine feedback loop regulating serum PTH, 1,25D and FGF-23 contributing to mineral homeostasis and skeletal structure particularly when stressed by low dietary calcium and phosphate intakes even during pre-pubertal growth over the short-term period.

At the end of short term LowCaP treatment, femur length was decreased in ObVDR-B6 mice compared to WT mice fed the same diet although the full length femoral mineral content was similar suggesting a VDR transgene effects to reduce bone growth but not overall mineral accrual. Reduced bone growth was associated with the disrupted growth plate. The osteocalcin promoter used to drive the expression of the VDR transgene was expressed in the growth plate, especially in young mice, as well as in mature bone (180). Segmental analyses adjusted for femur length revealed that the bones from LowCaP fed WT mice had similar shape and mineral distribution to that of the adult mice at 9w of age as depicted in chapter 3 or at 20w of age as depicted

in **figure 4.6. C** and **D** unlike ObVDR-B6 femora. Thus, prepubertal WT mice were capable of maintaining femoral bone structure during short term LowCaP diet in contrast to ObVDR-B6 femora in which the structure was disrupted. This outcome was possibly due to the effects of high serum 1,25D and increased VDR expression on the growth plate, affecting the development and formation of cortical and trabecular bone in the femoral distal metaphysis. Idelevich et al. in 2011 (127) demonstrated the negative effects of 1,25D on growth plate and bone development using short term consecutive and long term intermittent injections of 1,25D in rats. Treatment with 1,25D increased chondrocyte proliferation, altered chondrocyte maturation, and induced apoptosis of the terminal hypertrophic cells with reduced cortical thickness and increased cortical porosity as indicated by micro-CT structural analyses. Thus the LowCaP diet had similar effects to 1,25D injection with WT mice demonstrating mild cortical porosity. The transgenic overexpression of VDR in mature osteoblasts further enhanced the effects of LowCaP diet on cortical porosity.

Interestingly, even when fed the LowCaP diet, the transgenic VDR expression in mature osteoblasts had increased cortical thickness and maintained increased femoral trabecular bone volumes compared to WT mice as observed in ObVDR-B6 mice during growth (see female 9w group in chapter 3). The increased trabecular bone volume in the ObVDR-B6 mice was due to increased trabecular number and thickness suggesting both effects to increase bone formation and reduce resorption. Further dynamic histomorphometry analyses would complement the study and confirm this hypothesis.

4.4.2. Effect of Long Term Dietary NormCaP and LowCaP Treatments

ObVDR B6 mice fed either the NormCaP or chow diet until 20w of age confirmed the improved cortical structural changes as described in Chapter 3. Femoral total mineral content, periosteal perimeter and endosteal perimeter were increased consistent with the increased strength of bones from these mice as reported in Chapter 3. Feeding the slightly higher calcium/phosphate diet than chow (NormCaP had 1 % Calcium and 0.625 % Phosphorus) demonstrated increased trabecular BV/TV in distal femoral metaphysis and vertebrae compared to the WT mice which were not detected in the chow diet (see female 20w group in chapter 3). Trabecular bone volumes were increased with marked increased trabecular number and conectivity and decreased trabecular separation. Interestingly the SMI also decreased which indicated a larger ratio of trabecular plates to rods, a change likely to increase bone strength. These data suggest that VDR in mature osteoblast interacted with adequate dietary calcium and phosphate levels to preserve and improve cortical and trabecular bone compartments. Improvement of bone mineral content, increased bone mineral density (BMD) and vertebral calcium content in aging rats (181) and trabecular bone volume in mice (182) had been reported with increased dietary calcium intake and adequate vitamin D diet. Therefore, overall data on NormCaP groups were consistent with previous findings.

The major question here is the mechanism by which increased osteoblast VDR can elicit this increase in bone mineral accrual. The structural changes to trabecular bone were consistent with a reduction in bone resorption. No major effects on serum calcium, phosphate, CrossLaps, Trap5B, 1,25D or PTH levels were observed in ObVDR B6 mice, although a significant decrease in serum CrossLaps/Trap5B ratio was identified suggesting that mature osteoblast VDR activities may reduce overall

osteoclast activity. Histological analyses for osteoclasts with TRAP staining demonstrated a significant decrease of the number of osteoclasts per bone surface (N.Oc/B.Pm) and a trend towards a decrease in osteoclast attachment surface (Oc.S/BS). These changes were associated with lower *Rankl* mRNA levels in bone. Collectively, these data indicated that increased VDR in mature osteoblasts may reduce bone resorption in trabecular bone confirming previous *in vitro* data (37) which may contribute to the increased bone mineral volume and strength. These data also confirmed that an adequate vitamin D status combined with adequate dietary calcium can reduce bone *Rankl* mRNA levels and osteoclast surface while increasing trabecular bone volumes in rats (154).

Bone formation parameters assessed as double fluorochrome labels at the femoral metaphyseal trabecular bone region showed no significant differences between WT and ObVDR-B6 mice. A previous study on OSVDR mice demonstrated an increase in periosteal bone MAR with increase of tibial and femoral diameters (36). The structural changes to cortical bone, particularly the increase in periosteal perimeter at the femoral mid-shaft of the ObVDR-B6 mice, were consistent with an increase in bone formation suggesting similar process to that of the previous study.

A further factor which can modulate bone mineralization is the FGF-23/FGFR system which links the bone-kidney axis through regulation of the renal handling of phosphate and renal synthesis of 1,25D (144). Serum FGF-23 was significantly reduced and lower bone *Fgf-23* mRNA expression was observed in the NormCaP fed ObVDR-B6 compared to WT. These data suggested that VDR activities in mature osteoblasts may inhibit FGF-23 production by a mechanism which is not fully understood. Phosphate

is a key component of hydroxyapatite (HA) and is essential for calcium deposition within mineralised tissue (183). Seeding of hydroxyapatite (HA) within the collagen fibrils is regulated by propagators and inhibitors of calcification including inorganic phosphate (Pi) and inorganic pyrophosphate (PPi). Therefore, Pi/PPi homeostasis plays a critical role in biomineralisation (184).

Long term LowCaP treatment exerted a considerable stress on mineral homeostasis in WT and ObVDR-B6 mice as indicated by significantly increased serum CrossLaps, TRAP5b, ALP and 1,25D levels although the high bone turnover was able to maintain normal serum calcium and phosphate levels. Serum FGF-23 levels were decreased with the LowCaP diet presumably as a result of the very low phosphate content since dietary phosphate regulates serum FGF-23 level (160,185). Changes to PTH levels with LowCaP diet were unable to be detected unlike the the short term LowCaP diet study, possibly due to technical errors with multiple freeze thawing of the serum specimen during storage. Serum PTH is known to be influenced by storage temperature, repeat freeze-thaw and is relatively unstable compared to the EDTA-plasma samples (186) which may play a role in the unchanged PTH levels on the long term LowCaP fed study.

Significant structural changes to cortical and trabecular bone compartments were elicited with LowCaP diet. The high bone turnover state reduced cortical bone volume and cortical thickness and increased endosteal perimeter. Trabecular bone volumes were markedly reduced at the femoral distal metaphysis and vertebral body of L-1 with a greater than 50 % reduction in BV/TV as a result of 3-fold reduction of trabecular number and connectivity in the femoral diaphysis with increased trabecular spacing.

The changes in the vertebra were not as marked as in the femoral metaphysis although they achieved statistical significance.

The ObVDR-B6 mice fed long term LowCaP diet demonstrated remarkable structural changes throughout the skeleton with marked changes to both long and flat bones indicating the effects of over-expression of VDR in osteoblasts on intramembranous and endochondral bone formation during growth. As an example, scapula are illustrated in **figure 4.5**. The ObVDR-B6 scapula was smaller than the WT with an abnormal edge suggesting a defect in bone modelling under these conditions. Decreased femur length, disorganised growth plate, cortical splaying and pronounced intra-cortical porosity were all observed in ObVDR-B6 mice fed LowCaP diet compared to WT fed the same diet. Interestingly, these bone changes occurred without hypocalcaemia, or hypophosphatemia which indicated maintenance of serum calcium/ phosphate through high bone turnover. Most importantly, the clearly defined double fluorochrome labels illustrated in **figure 4.8** demonstrated that mineralization was unimpaired under these conditions in both WT and ObVDR-B6 mice. Therefore, the structural changes did not appear to be the result of a mineralization defect and warrant further investigations.

A major question arising from these findings is why do increased osteoblast VDR activities, arising from increased VDR levels, disrupt bone structure during growth? As stated above, markers of bone turnover including serum ALP and CrossLaps were increased similarly in WT mice. Interestingly, the increase in serum 1,25D levels in ObVDR-B6 mice on the LowCaP diet was some 50 % greater than WT mice on this diet reaching some 1.8 nM, almost 10-fold greater than with the NormCaP diet. While

serum FGF-23 levels was decreased in both genotypes on the LowCaP diet, the significant decrease in the OBVDR-B6 mice compared to the WT was maintained. These data confirmed the endocrine impact of mature osteoblast VDR on serum FGF-23 levels and suggested that on the LowCaP diet, the difference in serum FGF-23 levels was sufficient to elicit a significant difference in serum 1,25D levels and markedly increased the endocrine activities of 1,25D in the ObVDR-B6 mice compared to WT mice.

One likely consequence of this increased level of 1,25D and osteoblast VDR was the increased *Rankl* mRNA levels in ObVDR-B6 bone compared to WT on LowCaP diet and compared to the NormCaP diet, unlike WT for which there was no detectable change. There was also an increased ratio of *Rankl/Opg* mRNA levels in the ObVDR-B6 bones. It is likely that these changes were responsible for increased osteoclast surface and the number of osteoclasts per bone perimeter compared with the ObVDR-B6 fed NormCaP diet. The actual change that occurred with the ObVDR-B6 mice was that on the NormCaP diet these osteoclast variables were reduced compared to WT while on the LowCaP diet ObVDR-B6 they were increased. Therefore, with adequate dietary calcium and phosphate, VDR in mature osteoblasts reduces osteoclastogenesis through reducing expression of bone *Rankl* mRNA while under low dietary calcium/phosphate intakes, VDR in mature osteoblasts increases *Rankl* mRNA to enhance bone resorption thus maintaining serum calcium/phosphate levels. These data support the concept that the mature osteoblast VDR contributes to plasma calcium and phosphate homeostasis with effects on bone mineral homeostasis and that over-expression of the human *Vdr* gene under the control of the human osteocalcin promoter in mice amplified these normal activities of osteoblast VDR.

Osteocytes are major targets for hormonal control of bone remodelling. The osteocyte specific deletion of the mouse *Rankl* gene using the *Dmp1-Cre* model demonstrated a blunted response in bone *Rankl* expression and failure to increase osteoclasts number during short term low dietary calcium (187). These data indicated that mature osteoblasts/osteocytes were the main source of *Rankl* expression and regulation of bone resorption with low dietary calcium. Our data demonstrated increased cortical porosity in the distal metaphysis and in mid-shaft regions of the ObVDR-B6 mice fed LowCaP diet suggesting that increased mature osteoblast/osteocyte VDR initiated the increased bone resorption by osteocytes. Since osteocyte density in this cortical region was unaffected by dietary calcium/phosphate or genotype, it can be inferred that increased bone resorption was the major cause of cortical porosity and not osteocyte death or apoptosis. Assessment of the osteocyte lacunae structure and size would be beneficial to evaluate the possibility of osteocytic osteolyses in the formation of cortical porosity of the ObVDR-B6 mice fed LowCaP diet.

Higher serum 1,25D levels in LowCaP fed mice on both genotypes were associated with increased kidney *Cyp27B1* mRNA in ObVDR-B6 mice suggesting increased renal synthesis of 1,25D and providing a source for their higher serum 1,25D levels. Furthermore, ObVDR-B6 mice fed LowCaP diet had significantly lower kidney *Cyp24* mRNA expression compared to the WT indicating reduced catabolism of 1,25D contributed to the increased serum 1,25D levels.

These data are consistent with the lower serum FGF-23 in ObVDR-B6 mice as this hormone decreases renal *Cyp27B1* and increases renal *Cyp24* expressions. Lower

expression of bone *Fgf23* mRNA level strengthened the evidence of decreased serum FGF-23 in ObVDR-B6 mice. The significantly increased *Dmp-1* mRNA levels in the ObVDR-B6 mouse bone was a possible contributor to the reduced *Fgf23* mRNA since the DMP-1 protein inhibits the production of bone FGF-23. DMP-1 is critical for mineralization of bone mineral. In undifferentiated osteoblasts, DMP-1 regulated the expression of osteoblast-specific genes while in mature osteoblasts, it is phosphorylated and exported to extra-cellular matrix and orchestrates mineralized matrix formation (188). Endocytosis of DMP-1 has been shown to increase intracellular free calcium, induces *Runx2* expression and regulates osteoblast differentiation (189). However, an *in-vitro* study on murine cementoblasts (OCCM-30) and osteocyte-like cells (MLO-Y4 and MLO-A5) on the effects of 1,25D on *Dmp1* expression demonstrated a decrease in *Dmp*1 mRNA levels via VDR dependent mechanism (190). The mechanisms by which DMP-1 regulates FGF-23 expression is poorly understood and several mechanisms have been proposed including modulation of FGF Receptor-1 signaling (144), DMP-1 as a transcription factor (188,191), changes in local extra-cellular matrix to stimulate FGF-23 production or interactions between PHEX/DMP-1 with unknown genes and proteins (190). The mechanism of this process and its interaction with dietary calcium intakes or extracellular calcium level is unknown and warrant further studies.

This study has provided strong evidence on the delicate relationship between plasma calcium homeostasis, plasma phosphate homeostasis, bone mineral homeostasis and vitamin D activities involving both endocrine and bone autocrine/paracrine activities. Therefore, the ObVDR-B6 is a suitable mouse model for further studies on the anabolic and catabolic effects of vitamin D and its relation to bone health.

4.5. CONCLUSION

This study demonstrated the effects of VDR activities in mature osteoblasts in mice as modulated by dietary calcium/phosphate. On a normal dietary calcium and phosphate intake, VDR in mature osteoblasts reduces bone resorption by direct effects on osteoclastogenesis combined with some indication of enhancement of periosteal bone formation, increasing cortical and trabecular bone volumes. With prolonged low dietary calcium/phosphate intakes, VDR in mature osteoblasts disrupted bone growth and stimulated bone turnover with increased cortical porosity, decreased trabecular number and increased trabecular separation and endosteal circumference.

CHAPTER 5: *Vdr* GENE ABLATION IN MATURE OSTEOBLASTS EXACERBATES SECONDARY HYPERPARATHYROIDISM AND RICKETS DURING DIETARY CALCIUM/PHOSPHATE RESTRICTION

Chapter Summary

Overexpression of VDR in mature osteoblasts increased bone resorption when ObVDR-B6 mice are fed very low dietary calcium/phosphate. Whether ablation of VDR in mature osteoblast has a protective effect during LowCaP treatment is unknown. To address this question, 3w old female $VDR^{fl/fl}$ as control mice and ObVDR-KO were fed 1 % Calcium / 0.625 % Phosphorus (NormCaP) or 0.03 % Calcium / 0.08 % Phosphorus (LowCaP) for 17 weeks (17w) whereupon they were culled and tissues were collected for analyses. In contrast to the ObVDR-B6 mice which gain trabecular bone with NormCaP diet, ObVDR-KO mice on this diet demonstrate no significant skeletal changes at 20w of age compared to the $VDR^{fl/fl}$ control. When fed LowCaP diet, ObVDR-KO mice have shorter femora, obvious splaying of metaphysis and very disturbed growth plate as a major clinical sign of rickets which also affects flat bones. Interestingly, the $VDR^{fl/fl}$ mice which are the control animals for this model are not identical to WT on LowCaP diet described in chapter 4. Overall, these data support a critical role of osteoblastic VDR activities in contributing to plasma calcium and phosphate homeostasis under conditions of extremely low dietary calcium/phosphate intakes in mice.

5.1. INTRODUCTION

VDR activities in osteoblasts contribute to bone mineral accrual and bone health which is dependent on the stage of maturation of the osteoblast (36,37,136,192). Mice in which the gene for VDR is over-expressed in mature osteoblasts (ObVDR-B6) have increased bone volumes when fed chow or NormCaP diet (Chapters 3 and 4) at 20w of age due to decreased bone resorption and possibly parameters indicating increased bone formation such as increased in periosteal circumference. However, when these mice are fed LowCaP diet, ObVDR-B6 exhibit increased bone turnover resulting in bone catabolism suggesting that the VDR in mature osteoblasts is contributing to the maintenance of plasma mineral homeostasis during periods of severe dietary calcium and phosphate restriction.

The osteoblast-specific VDR knock out mouse model (ObVDR-KO) is a conditional knockout created using *Cre-lox*P system driven by the human osteocalcin promoter. This mouse model is the opposite of ObVDR-B6 mice. The ObVDR-KO mice were shown to have deletion of the VDR in calvarial and femoral bone but not in the liver, intestine and kidney (193) and shown to have increased trabecular BV/TV at 6w of age due to increased trabecular number (194). However, at 12w and 26w of age, there were no significant differences in the trabecular BV/TV between $VDR^{fl/fl}$ (control) and the ObVDR-KO mice suggesting an age specific activities of the VDR in mature osteoblast. The cortical bone phenotypes of the ObVDR-KO were not as pronounced as their trabecular bone phenotype. Female ObVDR-KO mice had increased cortical bone due significant expansion of periosteal perimeter at 6w but not at 12w or 26w of age (193). Gene analyses suggested that the absence of VDR in mature osteoblasts

contributed to the regulation of mRNA expression for genes regulating both bone formation and bone resorption to maintain bone volume (193,194).

Since osteoblastic VDR contributes to maintain plasma calcium and phosphate homeostasis under conditions of severe dietary restriction, it was important to assess the effects of this condition on mice in which the VDR gene in mature osteoblasts is ablated and to test whether such ablation will interfere with the mobilization of calcium and phosphate from bone and changes in their skeletal structure or bone mineral content.

5.2. METHODS

5.2.1. Animal Models, Housing, and Care

The osteoblast-specific vitamin D-receptor knock out mouse model (ObVDR-KO) was generated using *Cre-LoxP* methods as described in **Chapter 2, Section 2.3**. Littermate $VDR^{fl/fl}$ control ($ObVDR^{fl/flCre-}$) and ObVDR-KO ($ObVDR^{fl/flCre+}$) mice were produced by mating the homozygous *LoxP* mice with osteocalcin-promoter driven-*cre* recombinase ($OcnCre^{+/-}$) transgenic mice. Homozygous LoxP mice were determined by PCR and gel analyses of PCR product using VDRloxP forward primer 5'-CCT TGG TGA GCT GAG TTT ACT CTT-3' and reversed primer 5'-CAG GAG TGG GAT TAC TGA TAT-3'. Products were 491kb of WT band and 575bp of VDR-lox band which splits into 145bp and 429bp products with EcoR1 digestion. Genotype were determined by the presence of universal *Cre* gene assessed using PCR analyses with a forward primer 5'-GCG GCA TGG TGC AAG TTG ATT-3' and a reverse primer 5'-ACC CCC AGG CTA AGT GCC TT-3' on tail DNA at 10 days of age.

Mice were housed and maintained as described in **Chapter 2, Section 2.3** and received free access to water and synthetic diets containing either 1 % calcium / 0.625 % phosphorus (NormCaP) (SF12-076, Specialty feeds, Glen Forrest, Western Australia) or 0.03 % calcium / 0.08 % phosphorus (LowCaP) (SF12-077, Specialty feeds, Glen Forrest, Western Australia) from weaning (3w) for 17w. Diets were formulated and designed as described in appendix section. At 8 and 2 days prior to death, calcein and xylenol orange fluorochrome labels were administered as described previously.

At 20w of age, serum, right femur, and vertebrae were collected and stored as described in **Chapter 2, Section 2.4** for micro-CT and histology analyses. Animal details and treatments were recorded in the clinical record sheets (CRS) in accordance the University of Adelaide Animal Ethics Committee for project number M-2012-092.

5.2.2. Serum Biochemistry

Serum calcium, phosphate, alkaline phosphatase, 1,25D, FGF-23, PTH, and CrossLaps levels were analysed as described in **Chapter 2, Section 2.5**.

5.2.3. Micro-computed Tomography

Microstructures of right femora were assessed using micro-CT system at 9 um/pixel (1076 Skyscan, Bruker, Germany) as described in **Chapter 2, Section 2.6.1**. The vertebrae were scanned on 6.5 um/pixel micro-CT system (1174 Skyscan, Bruker, Germany). Total mineral content and segmental slice analysis were measured on full length femora as described in **Chapter 2, Section 2.6.4**. Cortical bone volume and size analyses were conducted on the mid-shaft region constituting 10 % of the femur length, followed by a full femur segment analyses. Trabecular bone was analysed at the

femoral distal metaphysis and vertebral body of Lumbar-1 (VBL-1) as described in **Chapter 2, Section 2.6.2**. Bone measurements and quantification were performed in accordance to the micro-CT settings described in **Chapter 2, Section 2.6.4.**

5.2.4. Dynamic Histomorphometry

Femora were cut with a slow speed saw to reveal the metaphyseal area followed by graded-ethanol dehydration and embedding in methylmetacrylate as described in **Chapter 2, Section 2.7.2.** Sagittal sections, 5 μm thick, were cut using a motorized microtome (Leica 2255, Germany) and stained for Tartrate Resistant Acid-phosphatase (TRAP) analysis of the TRAP+ cells and Toluidine Blue (TolB) for osteocytes analyses in the cortical region of distal metaphysis as described in **Chapter 2, Section 2.7.4 and 2.7.5**. Double label fluorochrome measures were measured on an unstained section as described in **Chapter 2, Section 2.7.3** using Olympus Microscope (Olympus DP73 and Olympus BX 53) and OsteoMeasure^{TM} morphometry system version 3.3.O.2 (Osteometrics, Atlanta, GA, USA).

5.2.5. Statistical Analysis

Two-way analysis of variance (ANOVA) was used to determine the contribution of diet and genotype on each of the variables. Least Significant Difference (LSD) post-hoc analyses were used to identify group/s which achieved significant differences at the level of $p < 0.05$.

5.3. RESULTS

Body weights of $VDR^{fl/fl}$ and ObVDR-KO fed NormCaP for 17w were not significantly different **(Figure 5.1. A and B).** The LowCaP fed ObVDR-KO mice were lighter than $VDR^{fl/fl}$ at 20w of age, an effect which was apparent from 6w of age

When fed NormCaP diet, serum calcium, phosphate, CrossLaps, or 1,25D were not different between $VDR^{fl/fl}$ and ObVDR-KO while ALP was significantly lower in ObVDR-KO mice. The ObVDR-KO has higher levels of PTH (mean increase of 60%) but this difference did not reach statistical significance. LowCaP diet for 17w increased serum ALP, PTH, 1,25D, and CrossLaps levels with decreased serum phosphate and FGF-23 levels in $VDR^{fl/fl}$ and/or ObVDR-KO mice. 1,25D and PTH levels are significantly higher (3-fold and 2-fold, respectively) in ObVDR-KO mice compared to $VDR^{fl/fl}$ mice fed LowCaP diet while serum calcium, phosphate, ALP, FGF-23 and CrossLaps levels were not different between the mouse genotypes (**Table 5.1**).

Bone structures (**Figure 5.2. A and B)** reveal marked changes in both flat and long bones after 17w of LowCaP diet with ObVDR-KO revealing a greater level of disruption than $VDR^{fl/fl}$ mice. Significant bulging, thinning and bending of the scapula and femora were observed in the ObVDR-KO mice. Marked growth plate disruption is a common feature of ObVDR-KO mice when fed LowCaP diet accompanied by increased cortical porosity in the region of distal metaphysis and mid-shaft (**Figure 5.2. C,D and F**). Trabecular bone volume reduction and thinning of the femoral cortices (**Figure 5.2. E and F**) were also observed in the $VDR^{fl/fl}$ group. Interestingly, amongst the $VDR^{fl/fl}$ mice fed LowCaP diet, I observed a greater interindividual variation of the above features ranging from no effects in some animals to clearly observable effects amongst other mice.

A.

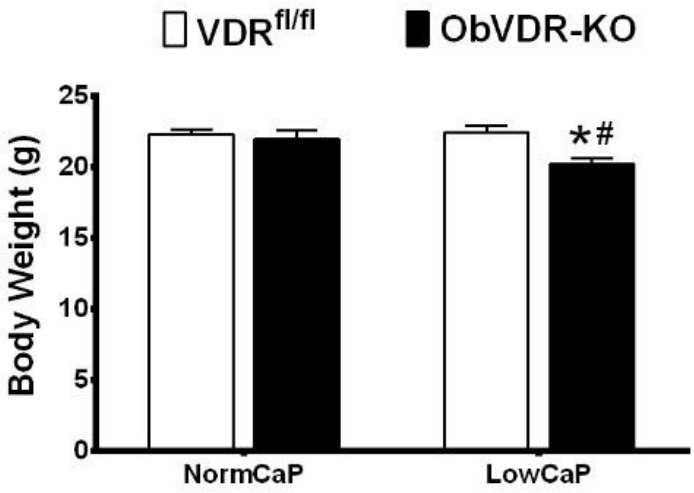

B.

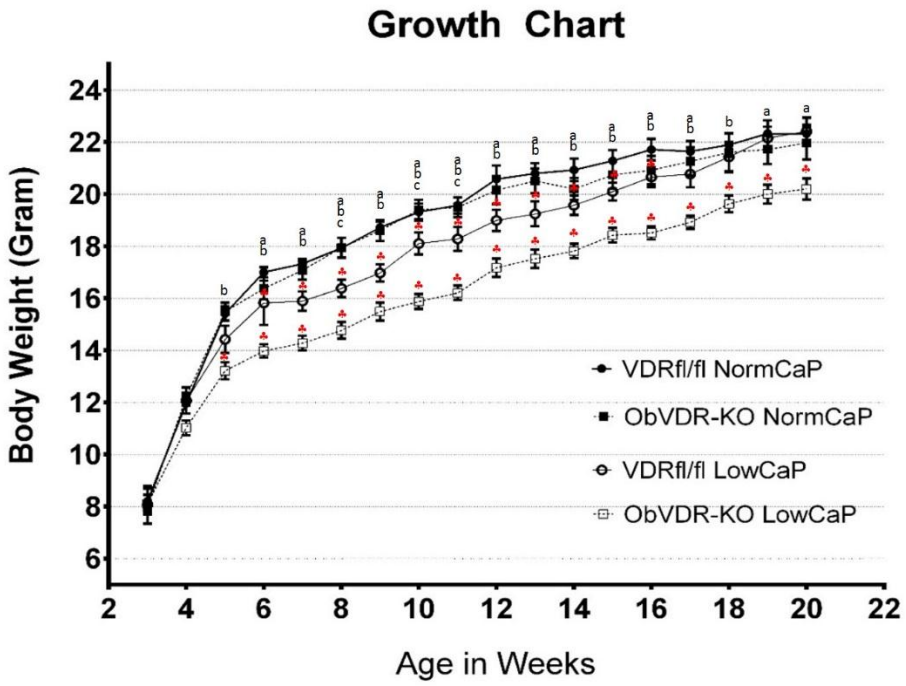

Figure 5.1. Body Weight at 20w (A) and Growth Chart (B) of the ObVDR-KO Mouse Model during Calcium/Phosphorus Restriction Study

Values are mean ± SEM, Two-way ANOVA significant at $p < 0.05$ for Genotype (a), dietary (b), and interaction (c). ♣ Post Hoc LSD $p < 0.05$ vs. NormCaP within the same genotype.

Table 5.1. Blood Biochemistry of $VDR^{fl/fl}$ and ObVDR –KO Mice

	NormCaP		LowCaP	
	$VDR^{fl/fl}$	**ObVDR-KO**	**$VDR^{fl/fl}$**	**ObVDR-KO**
(n)	***(8)***	***(10)***	***(7)***	***(13)***
Calcium (mmol/L)	2.47 ± 0.09	2.45 ± 0.08	2.34 ± 0.07	2.33 ± 0.13
Phosphate (mmol/L)[(b)]	1.69 ± 0.11	1.56 ± 0.13	1.22 ± 0.17♣	1.25 ± 0.12
ALP (mmol/L) [(a,b)]	187.56 ± 21.24	134.75 ± 7.65*	376.58 ± 123.39	504.74 ± 77.29♣
1,25D (pmol/L)[(a,b,c)]	289.0 ± 118.2	236.6 ± 48.0	1070.8 ± 158.2♣	2936.9 ± 291.5*♣
FGF-23 (pg/mL) [(b)]	334.2 ± 40.2	389.8 ± 16.4	177.4 ± 35.3♣	122.2 ± 23.4♣
PTH (pg/mL) [(b,c)]	201.34 ± 40.7	325.20 ± 40.7	709.63 ± 486.5♣	1351.74 ± 375.1*♣
CrossLaps (ng/mL) [(a,b)]	26.70 ± 1.70	27.65 ± 1.46	44.31 ± 4.22♣	51.66 ± 3.82♣

Values are mean ± SEM, Two-way ANOVA significant at $p < 0.05$ for Genotype (a), dietary (b), and interaction (c). Post Hoc LSD * $p < 0.05$ vs. $VDR^{fl/fl}$, ♣ $p < 0.05$ vs. NormCaP within the same genotype.

NormCaP		LowCaP	
VDR$^{fl/fl}$	**ObVDR –KO**	**VDR$^{fl/fl}$**	**ObVDR –KO**
A. X-Ray Images of Flat Bone (Scapula)			
	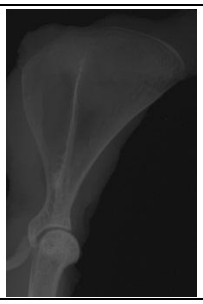		
B. X-Ray Images of Long Bone (Femur)			
			
C. 3D Reconstruction of Growth Plate Region			
	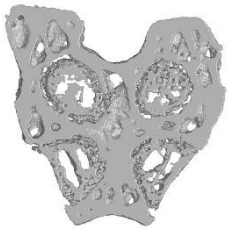	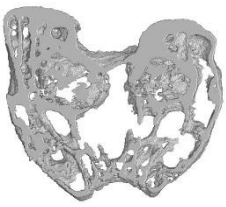	
D. 3D Reconstruction of Distal Metaphysis Region			
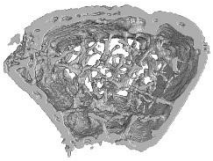	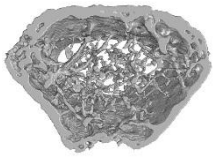	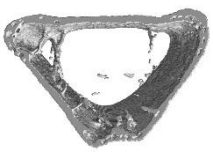	

E. 3D Reconstruction of Trabecular Bone at Distal Metaphysis

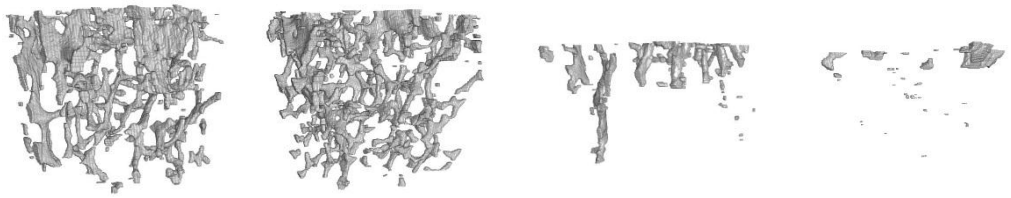

F. 3D Reconstruction of Trabecular Bone at VBL1

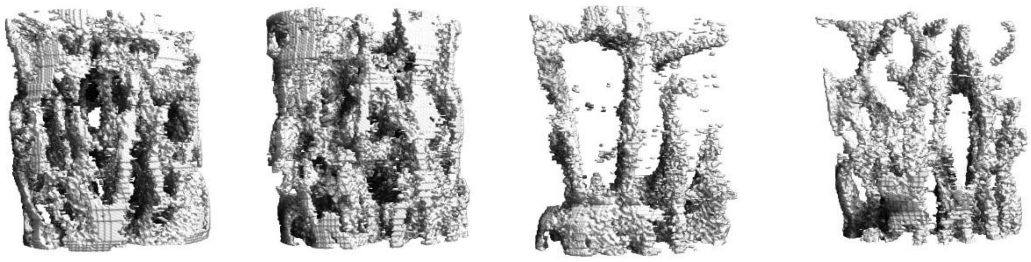

G. Transverse section at Mid-Point

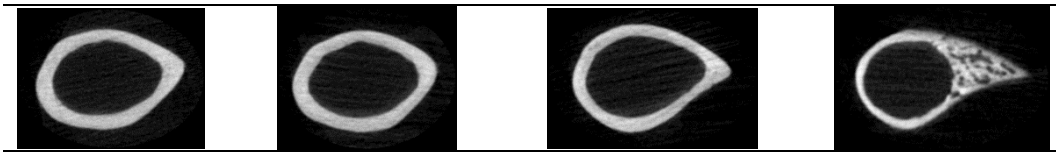

H. Transverse section of Vertebral Body L-1 (VBL1) at Caudal region

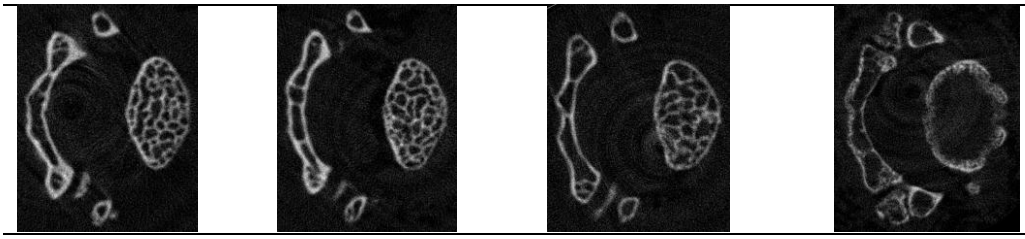

I. Transverse section of Vertebral Body L-1 (VBL1)

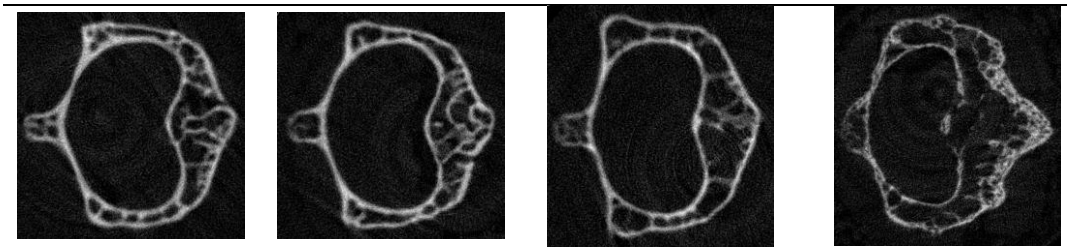

Figure 5.2. X-Ray Images of Flat Bone (Scapula) (A), and Long Bone (Femur) (B), 3D Reconstruction of femoral Growth Plate (C), Distal Metaphysis (D), Trabecular Region at Distal Metaphysis (E) and VBL-1 (D), and Micro-CT Images of Transaxial Section of Femur at Mid-Point (F), Caudal (G) and Mid Region (H) of VBL1 Following Dietary Treatments in $VDR^{fl/fl}$ and ObVDR-KO mice.

Femur length and total mineral content are not significantly different between $VDR^{fl/fl}$ and ObVDR-KO mice when fed the NormCaP diet (**Figure 5.3. A and B**). When fed LowCaP diet, femur length is significantly decreased in both $VDR^{fl/fl}$ and ObVDR-KO compared to NormCaP fed mice within the same genotype and is further decreased in ObVDR-KO mice compared to the $VDR^{fl/fl}$ mice. Femoral segmental analyses showed no significant changes between $VDR^{fl/fl}$ and ObVDR-KO fed NormCaP diet (**Figure 5.3. C**). However, when fed LowCaP diet, significant increases of bone volume in the distal metaphysis, third trochanter and femoral head regions were evident in ObVDR-KO mice compared to $VDR^{fl/fl}$ mice (**Figure 5.3. D**) associated with an apparent increase of total mineral content (**Figure 5.3. B**).

Measurement of total mineral content is dependent on total volume of the bone, therefore, the reduced femur length of OBVDR-KO mice influences this measurement. Comparison of bone mineral content with data presented in Chapter 4 indicate that, with NormCaP diet, WT and $VDR^{fl/fl}$ have similar structural features (**Figure 5.3. E**). However, when fed LowCaP, $VDR^{fl/fl}$ demonstrate minor but statistically significant structural changes in the distal metaphysis compared to WT mice (**Figure 5.3. F**). While the ObVDR-B6 mouse line has higher mineral content in every segment compared to the ObVDR-KO fed NormCaP (**Figure 5.3. G**), the LowCaP fed ObVDR-KO mice demonstrated pronounced structural changes in metaphyseal, third trochanter and femoral head regions compared to the ObVDR-B6 mice (**Figure 5.3. H**).

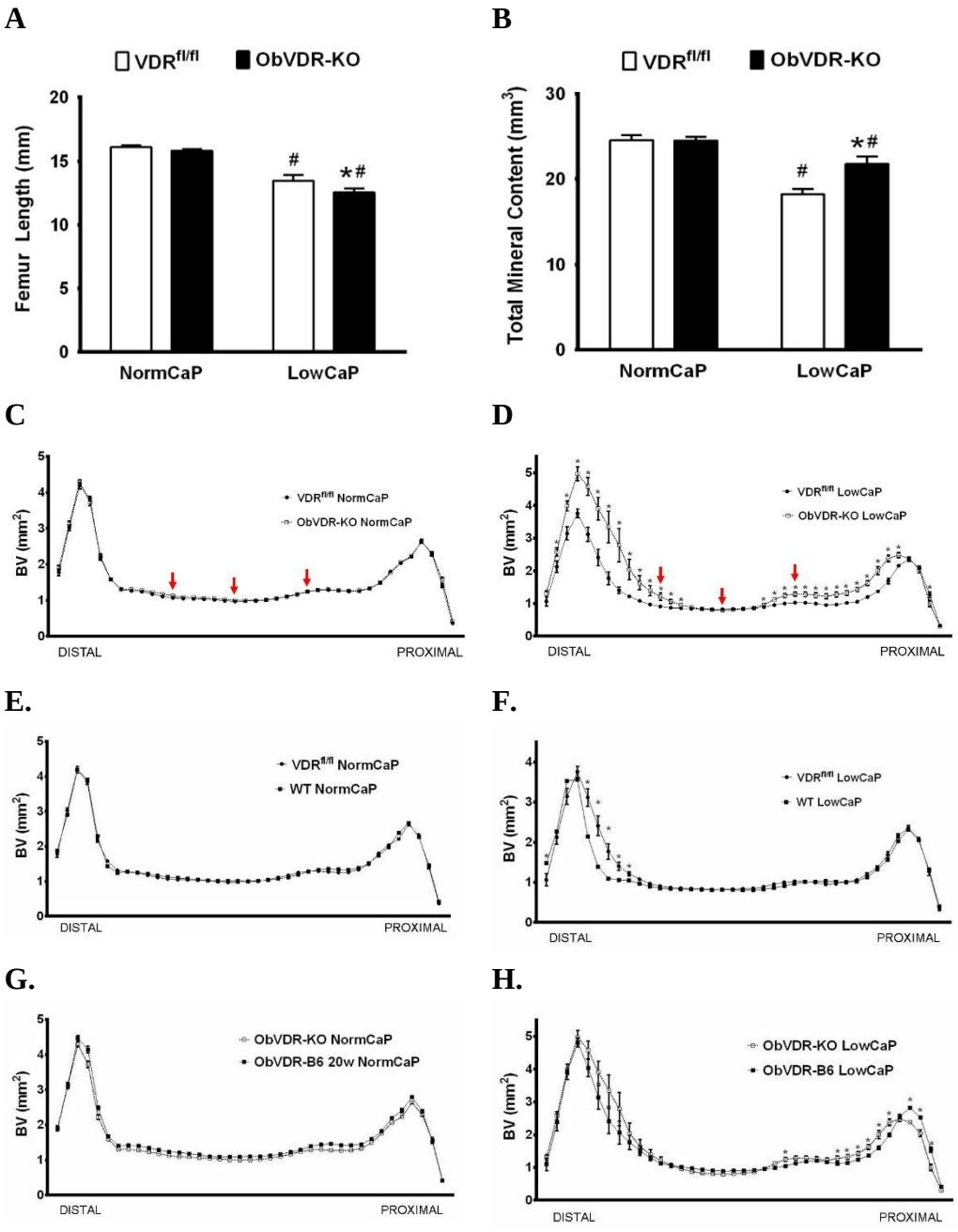

Figure 5.3. Femur length (A), Total Mineral Content (B) and Segmental Analyses Adjusted for Femur Length of VDR$^{fl/fl}$ and ObVDR –KO mice on NormCaP (C) and LowCaP (D) and Comparison Between WT and VDR$^{fl/fl}$ (E & F) and ObVDR-B6 and ObVDR-KO (G & H) on NormCaP and LowCaP diet.

Values are mean ± SEM, * $p < 0.05$ for VDR$^{fl/fl}$ vs. ObVDR-KO within same diet. # $p < 0.05$ for NormCaP vs. LowCaP within the same genotype. Red arrows indicates segment analysed in **figure 5.4**.

Mid-shaft cortical bone volumes are not different amongst the two mouse genotypes on either diet but there is a significant reduction with LowCaP diet (**Table 5.2**). Cortical thickness was unaffected in ObVDR-KO mice fed NormCaP diet, however the cortical quality might be reduced due to the presence of cortical porosity. When fed LowCaP diet, the $VDR^{fl/fl}$ mice experienced a significant reduction in cortical thickness due to changes in endosteal perimeter. The cortical thickness of the ObVDR-KO mice were unchanged due to maintenance of periosteal perimeter with decrease of endosteal perimeter suggesting that endosteal bone resorption was reduced in this mice on this diet. Increased cortical porosity is observed in ObVDR-KO mice when fed LowCaP diet compared to the NormCaP fed mice (**Table 5.2**), and this contributes to the changes in cortical thickness of the ObVDR-KO mice on Micro-CT analyses.

Table 5.2 Femoral Mid-shaft Region Cortical Analyses of $VDR^{fl/fl}$ and ObVDR-KO Mice

	NormCaP		LowCaP	
	$VDR^{fl/fl}$	**ObVDR-KO**	**$VDR^{fl/fl}$**	**ObVDR-KO**
(n)	***(8)***	***(10)***	***(7)***	***(13)***
Cor.BV (mm^3)[(b)]	1.51 ± 0.04	1.51 ± 0.04	1.11 ± 0.08♣	1.00 ± 0.03♣
Cor.Th (μm)[(a)]	224.39 ± 4.64	233.43 ± 3.25	192.84 ± 3.87♣	230.98 ± 12.29*
Ps.Pm (mm)	5.55 ± 0.06	5.48 ± 0.05	5.55 ± 0.05	5.61 ± 0.09
Es.Pm (mm)[(a,b,c)]	4.09 ± 0.06	3.98 ± 0.03	4.13 ± 0.07	3.70 ± 0.06*♣
Porosity (%)	None detected	0.14 ± 0.14	0.05 ± 0.05	23.04 ± 10.36*♣

Values are mean ± SEM, Two-way ANOVA significant at $p < 0.05$ for Genotype (a), dietary (b), and interaction (c). Post Hoc LSD * $p < 0.05$ for $VDR^{fl/fl}$ vs. ObVDR –KO within the same diet, ♣ $p < 0.05$ for NormCaP vs. LowCaP within the same genotype.

Detailed analyses on three segments of femoral cortical bone were conducted to identify effects of genotype and diet on the following regions; 1) the proximal end of the distal metaphysis (segment 12), 2) the diaphyseal mid-shaft (segment 18) and 3) the distal section of third trochanter (segment 25). Images in **figure 5.4** show distinct structural changes on these mice. When fed NormCaP diets, the cortical bone area, thickness and periosteal and endosteal perimeters are unaffected by ablation of the VDR gene in mature osteoblasts in all 3 analysed segments. However, when fed LowCaP diet, the ObVDR-KO mice exhibited massive cortical trabecularization at the distal metaphysis region as observed in segment 12, formation of the 'bone fin' as observed in segment 18 and structural changes with trabecularization of the third trochanter as observed in segment 25 (**Figure 5.4)**. These changes contribute to the differences in cortical bone volume, thickness, and perimeters of each analysed segments.

Distal femoral metaphyseal and vertebral trabecular bone volumes (**Table 5.3**) were comparable between $VDR^{fl/fl}$ and ObVDR-KO mice when fed the same diet with a marked reduction in both genotypes with LowCaP diet feeding. Trabecular bone loss occurred as a result of decreased trabecular number and connectivity with increased trabecular spacing concomitant with an increase in SMI, indicating a change from plate to rod-like structure. Each of these changes is consistent with features of increased bone resorption. There was an increase in trabecular thickness within the femoral metaphysis on LowCaP diet with significantly greater increase in the $VDR^{fl/fl}$ compared to the ObVDR-KO mice. In the L1-vertebrae analyses, trabecular thickness was decreased with LowCaP diet independent of the genotype.

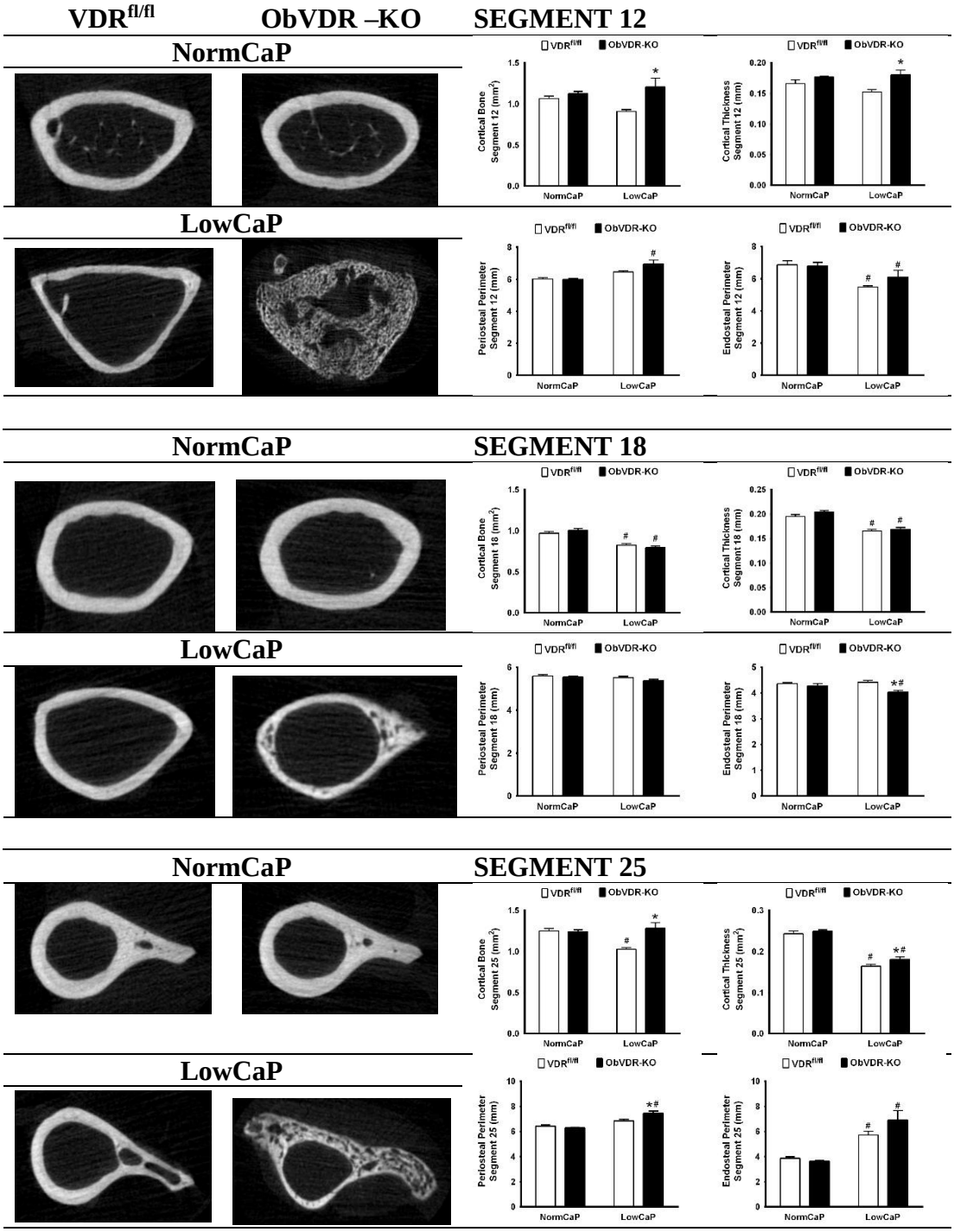

Figure 5.4. Micro-CT Transaxial Images of VDR$^{fl/fl}$ and ObVDR-KO Mice on Femoral Diaphyseal Region of Segment 12, 18 and 25 (left side) and Quantification of Cortical Bone Volume, Cortical Thickness, Periosteal Perimeter and Endosteal Perimeter of Each Segments (right side) Respectively.

Values are mean $\pm$ SEM, * $p < 0.05$ for VDR$^{fl/fl}$ vs. ObVDR-KO within same diet. # $p < 0.05$ for NormCaP vs. LowCaP within the same genotype

Table 5.3. Trabecular Analyses of $VDR^{fl/fl}$ and ObVDR-KO Mice

	NormCaP		LowCaP	
	$VDR^{fl/fl}$	**ObVDR-KO**	**$VDR^{fl/fl}$**	**ObVDR-KO**
(n)	***(8)***	***(10)***	***(7)***	***(13)***
DISTAL METAPHYSIS				
BV/TV (%)(b)	5.25 ±0.57	4.96 ±0.24	1.81 ±0.27♣	1.77 ±0.32♣
Tb.Th (µm)(b)	49.08 ±1.01	49.58 ±0.68	60.63 ±3.51♣	54.72 ±1.03*♣
Tb.Sp (µm) (b)	318.81 ±11.74	308.59 ±5.08	823.37 ±79.04♣	942.88 ±44.08♣
Tb.N (#/mm) (b)	1.07 ±0.12	0.999 ±0.04	0.30 ±0.05♣	0.32 ±0.06♣
SMI(b)	2.53 ±0.04	2.56 ±0.02	2.60 ±0.11♣	2.62 ±0.11♣
Conn.D (#/mm^3)(b)	20.47 ±6.12	16.92 ±2.48	3.81 ±1.11♣	7.93 ±1.82♣
VERTEBRAL BODY of L-1				
Height (mm)	2.98 ±0.04	2.88 ±0.03	2.92 ±0.06	2.92 ±0.04
BV/TV (%)(b)	30.28 ±1.71	28.45 ±1.00	12.15 ±1.55♣	14.48 ±1.45♣
Tb.Th (µm)(b)	49.76 ±0.21	47.75 ±0.53	43.14 ±1.22♣	42.38 ±0.99♣
Tb.Sp (µm)(b)	141.77 ±11.20	154.41 ±7.20	259.27 ±26.46♣	236.84 ±15.32♣
Tb.N (#/mm)(b)	6.08 ±0.33	5.97 ±0.23	2.81 ±0.32♣	3.43 ±0.34♣
SMI(b)	1.00 ±0.08	1.00 ±0.08	1.66 ±0.05♣	1.67 ±0.10♣
Conn.D (#/mm^3)(b)	945.78 ±58.53	1066.79 ±105.72	442.12 ±64.17♣	684.57 ±155.73♣

Values are mean ± SEM, Two-way ANOVA significant at $p < 0.05$ for Genotype (a), dietary (b), and interaction (c). Post Hoc LSD * $p < 0.05$, **$p < 0.001$ for $VDR^{fl/fl}$ and ObVDR –KO, ♣ $p < 0.05$ for NormCaP vs. LowCaP within the same genotype.

Histology sections of the distal femora are presented in **figure 5.4** and **figure 5.5.** Images of the cortical bones using fluorescence microscope show distinct double fluorochrome labels in all NormCaP fed mice (**Figure 5.4. B)**. Dynamic histomorphometry analyses in the trabecular region of distal metaphysis showed no significant changes in bone formation parameters between $VDR^{fl/fl}$ and ObVDR-KO fed NormCaP diet (**Table 5.4**).

The LowCaP fed $VDR^{fl/fl}$ mice demonstrated variation between distinct (3 of 7) and indistinct (4 of 7) double labels amongst individual mice indicating a possible variation in the degree of mineralisation defect amongst these mice. The fluorochrome labels in the ObVDR-KO mice fed LowCaP diet were extensive and all mice demonstrated indistinct and very blurred first label (calcein) with little or no evidence of the second label (xylenol orange) in the cortical region (**Figure 5.4. B and C**).

Mice fed LowCaP diet show very little trabecular bone (**Table 5.3).** Histological images of TRAP stain demonstrated no significant changes in any osteoclast variables between $VDR^{fl/fl}$ and ObVDR-KO on NormCaP diet (**Table 5.4)**. Average osteoclast size was increased in ObVDR-KO mice fed LowCaP diet and on observation from TRAP stain slides, TRAP(+) cells were found on the surface of cortices and inside the cortical pores (**Figure 5.5. C**)

Interestingly, I observed a difference in bone marrow cellularity of the femoral distal metaphysis between $VDR^{fl/fl}$ and ObVDR-KO mice when fed LowCaP diet. In the bone marrow area of the $VDR^{fl/fl}$ mice, there were less cells (lower cellular density) with more adipocytes compared to the ObVDR-KO mice (**Figure 5.6. C and D**).

Future studies could utilise staining with sudan-3 or oil red-O which stain adipocytes to investigate this difference between the mouse lines.

Analyses of the cortical region of the distal metaphysis showed no effect of genotype or dietary treatment on osteocyte density (**Figure 5.7**). Increased cortical porosity and possible increase in vascularisation of the cortices in the ObVDR-KO mice fed LowCaP diet were observed. This is shown by the segregation of cortical bones with structures that were different from the usual bone porosity appearance on histological view as depicted in **figure 5.7**.

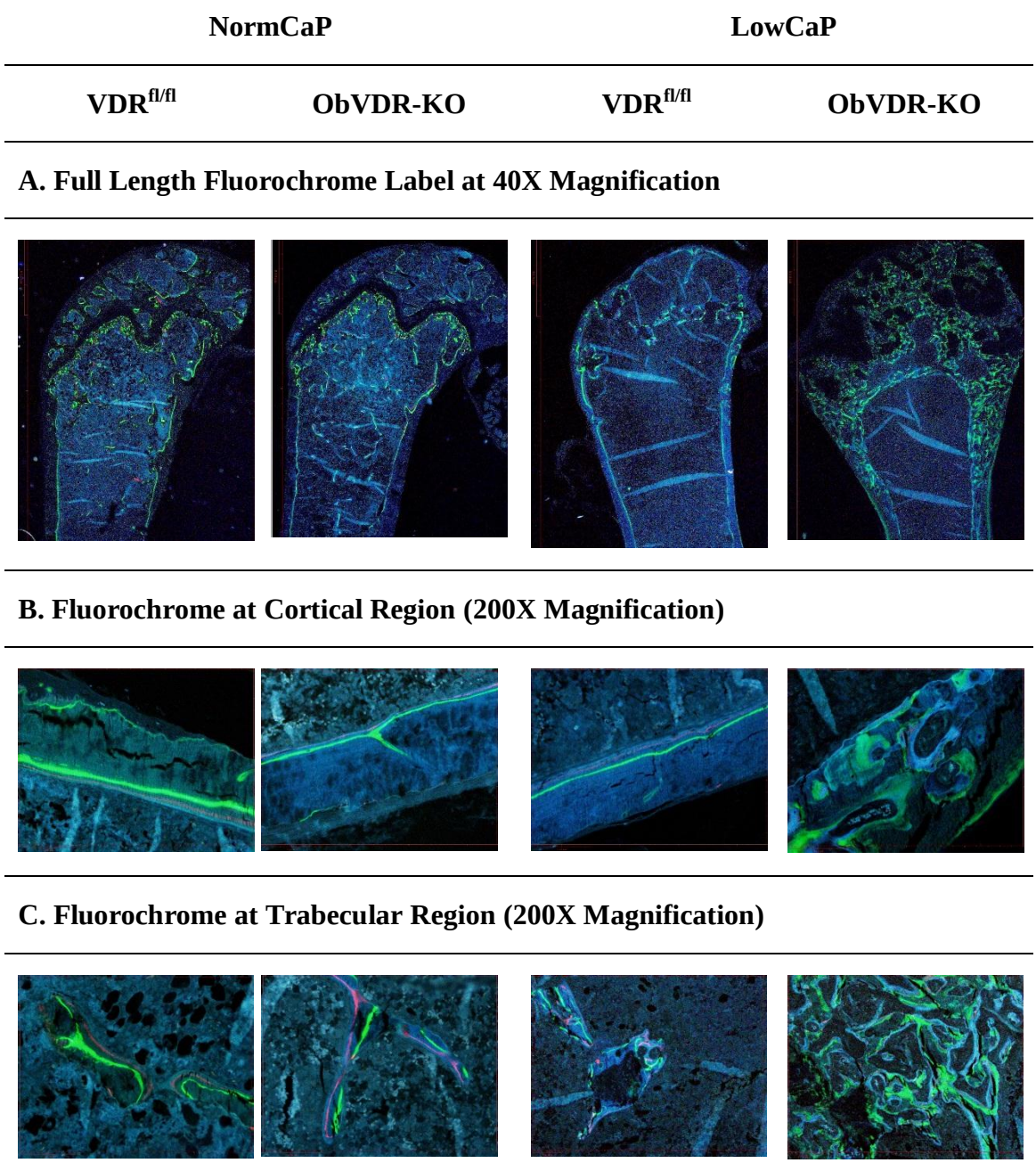

Figure 5.5. Images of Double Fluorochrome Labels of $VDR^{fl/fl}$ and ObVDR-KO mice Fed NormCaP and LowCaP diet on a Full Section (A), Cortical Region (B) and Trabecular Distal Metaphysis near Growth Plate Region (C).

NormCaP		LowCaP	
VDR$^{fl/fl}$	ObVDR-KO	VDR$^{fl/fl}$	ObVDR-KO
A. Full Sagittal Section of Distal Metaphysis at 40X Magnification			
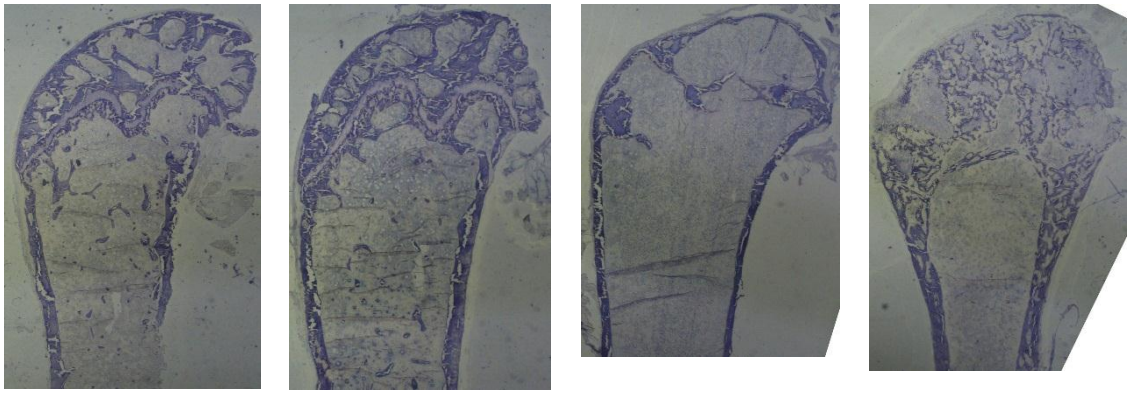			
B. TRAP stain Images at Growth Plate Region (100X Magnification)			
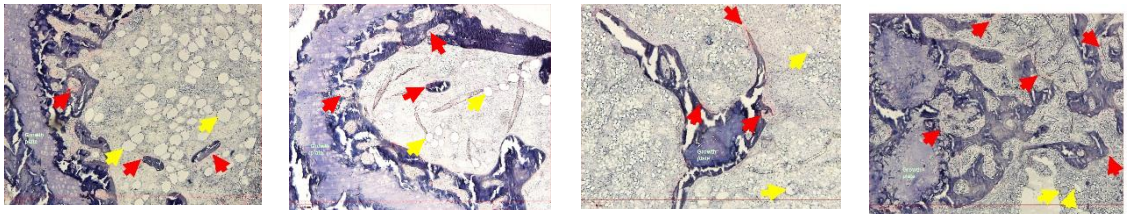			
C. TRAP Stain Images at Trabecular Region (200X Magnification)			
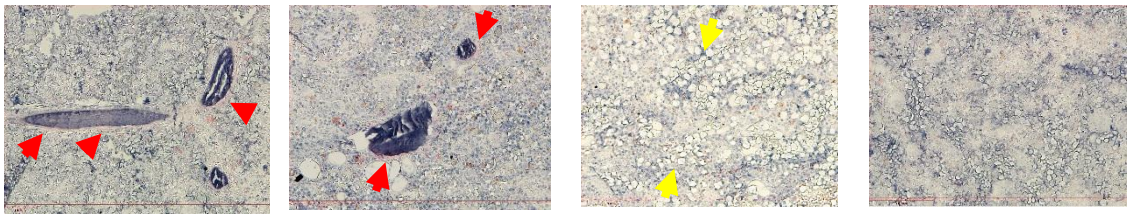			
D. TRAP Stain Images at Cortical Region (200X Magnification)			
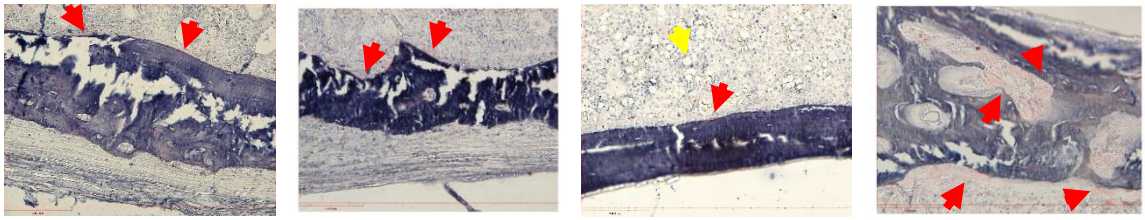			

Figure 5.6. Images of TRAP Staining in VDR$^{fl/fl}$ and ObVDR-KO Dietary Study at Full Sagittal Section (A), Growth Plate Region (B), Trabecular (C) and Cortical Region of Distal Metaphysis (D).

Table 5.4 Dynamic Histomorphometry Analyses of $VDR^{fl/fl}$ and ObVDR–KO Mice

	NormCaP		LowCaP	
	$VDR^{fl/fl}$	**ObVDR-KO**	**$VDR^{fl/fl}$**	**ObVDR-KO**
Double Label (n)	***(8)***	***(10)***	***(3/7 distinct; 4/7indistinct)***	***(0)***
MS/BS (%)	34.56 ±1.17	34.47 ±1.86	32.33±5.86	Indistinct label
MAR (µm/day)	1.75 ±0.05	1.82 ±0.09	1.93 ±0.16	Indistinct label
BFR/BV (%/t)	3.18 ±0.16	3.37 ±0.33	4.02 ±0.53	Indistinct label
TRAP +ve cells (n)	***(8)***	***(10)***	***(7)***	***(13)***
AveOc.Ar(mm^2)	0.00021 ±0.00001	0.00019 ±0.00001	0.00020 ±0.00003	0.00024 ±0.00001♣
Oc.S/BS (%)	23.86 ±2.96	28.01 ±1.61	23.95 ±4.88	28.0 ±5.48
N.Oc/B.Pm (#/mm)	8.33 ±1.05	10.23 ±0.73	9.18 ±1.92	10.48 ±2.09

Values are mean ± SEM, Two-way ANOVA significant at $p < 0.05$ for Genotype (a), dietary (b), and interaction (c). Post Hoc LSD * $p < 0.05$, ** $p < 0.001$ for $VDR^{fl/fl}$ and ObVDR –KO, ♣ $p < 0.05$ for NormCaP vs. LowCaP within the same genotype. Total Osteoclast Area (Oc.Ar), Average osteoclast size (AveOc.Ar), Osteoclast attachment surface or osteoclast surface per bone surface (Oc.S/BS)

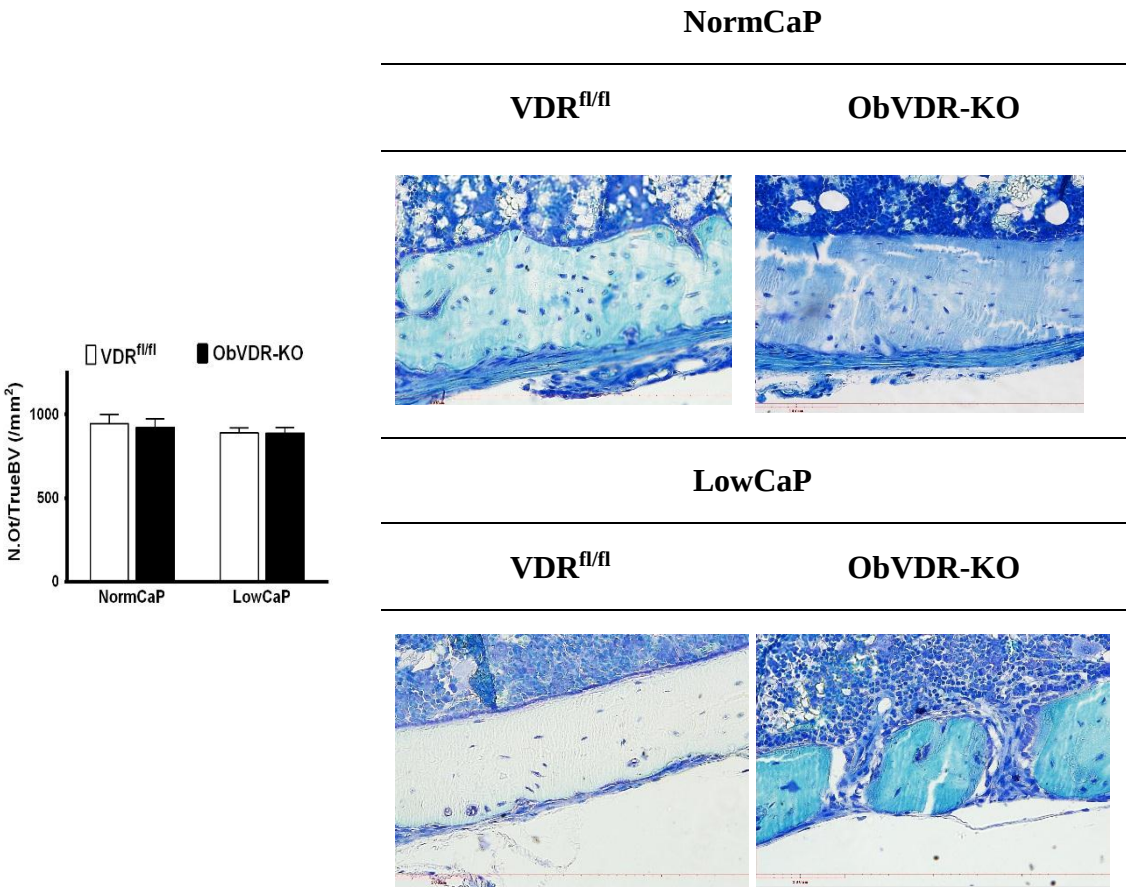

Figure 5.7. Osteocyte Density and Images of Toluidine Blue Staining at the Cortical Distal Metaphysis Region in VDR$^{fl/fl}$ and ObVDR –KO Mice.

Marked cortical porosity is observed in distal metaphysis of ObVDR-KO fed LowCaP. Osteocyte arrangement of the LowCaP fed animals on observation look smaller with thin processes assessed at 200x magnification

5.4. DISCUSSION

Inactivation of VDR in the mature osteoblastic lineage (ObVDR-KO) at 6w of age produced a marked increase in both femoral trabecular and cortical bone volumes compared to the control littermates, which by 12w and 26w of age was lost (194). As presented in this chapter, at 20w of age, ObVDR-KO and control mice fed the NormCaP diet demonstrated similar growth, femur length, femur cortical bone and trabecular bone volumes in femoral distal metaphysis and the vertebrae. There were no significant differences in the bone formation or bone resorption variables on dynamic histomorphometry analyses suggesting that deletion of VDR does not exert major effects on bone remodelling with adequate dietary calcium and phosphate.

Serum analyses demonstrated no significant differences between $VDR^{fl/fl}$ and ObVDR-KO mice fed NormCaP diet except for the mean serum ALP levels which was significantly lower in ObVDR-KO mice. This result can be considered consistent with an effect of decreased bone formation in the young, growing mice remaning detectable at 20w of age because of the longer time frame for formation compared to resorption. The major finding at 6w ObVDR-KO mice was impaired RANKL-mediated bone resorption coupled with decrease bone formation (194). Specific VDR deletion in osteoblasts using the *Col1a1-cre* recombinase mouse line produced an increase in male bone volume at 16w of age associated with decreased RANKL expression and osteoclast numbers suggesting impaired bone resorption (167) in osteoblast specific VDR ablated mice.

The above findings are in contrast to those reported in chapters 3 and 4 for mice overexpressing the gene for VDR in mature osteoblasts (ObVDR-B6 mice), which

have stronger and bigger bones when fed a NormCaP diet throughout the ages. The ObVDR-B6 phenotype is the result of decreased bone resorption in trabecular bone and effects on cortical bone perimeters suggesting both reduction of bone resorption and increased bone formation.

Under extreme dietary calcium/phosphate restriction for 17w, a very different phenotype is observed with a significant decreases in body weight, poorer weight accrual and reduction in growth rate for both LowCaP $VDR^{fl/fl}$ and greater decreases for ObVDR-KO mice compared with the NormCaP fed mice. Both $VDR^{fl/fl}$ and the ObVDR-KO mice fed LowCaP diet demonstrated reduced femur length, splayed metaphysis, abnormalities of the scapulae and changes to the 3rd trochanter structure with macroscopic features visible in 4 of 7 $VDR^{fl/fl}$ animals and all ObVDR-KO animals.

Increased ALP, PTH, 1,25D, and CrossLaps with decreased phosphate and FGF-23 serum levels were observed in all mice fed LowCaP diet. Significant increases of serum 1,25D and PTH levels in ObVDR-KO mice compared to $VDR^{fl/fl}$ on the LowCaP diet were also found. These findings suggest a major role for osteoblast VDR activity in contributing to the regulation of calciotropic hormone serum levels when dietary calcium and phosphate are limited. Normocalcaemia was maintained by both mouse genotypes on the LowCa/P diet but serum phosphate levels were decreased. Low serum phosphate is likely to reduce serum FGF-23 levels (96) which would contribute to increased serum 1,25D levels.

The most interesting changes are the increased serum 1,25D and PTH levels which were 3-fold and 2-fold higher respectively in ObVDR-KO mice fed LowCaP diet. These findings indicate that when the *Vdr* gene is deleted in mature osteoblasts, plasma calcium/PTH/1,25D homeostasis is significantly impaired with some contribution from the plasma phosphate/FGF-23/1,25D axis. The data suggest a primary effect of raised serum PTH levels and a secondary effect of both the increased serum PTH levels and reduced serum FGF-23 levels to raise serum 1,25D levels. Therefore, the VDR activity in mature osteoblast is the key regulator for calciotropic hormones to maintain plasma calcium homeostasis under severe dietary calcium and phosphate restrictions.

Under the LowCaP dietary conditions, ObVDR-KO mice demonstrated marked macroscopic and microscopic skeletal changes over and above those seen in $VDR^{fl/fl}$ controls (**Figure 5.2**) with significant changes in bone volume at 3 distinct femoral regions, the distal metaphysis, the third trochanter and the femoral head (**Figure 5.3D**). Microscopic analyses of these three regions indicate considerable cortical trabecularization. Thus, while cortical thickness in these regions was apparently increased due to a decrease of endosteal perimeter, the cortical bone mineral content remained constant due to the increase of cortical porosity in the ObVDR-KO mice. Micro-CT measurements are likely to be confounded because of the inability of the computer software to deal with immense pores occurring in the cortical bone; therefore results from these region must be interpreted with caution.

Clearly the LowCaP diet markedly increases the calciotropic hormone levels and the osteoblast alkaline phosphatase indicating high bone turnover driven by high PTH levels in the ObVDR-KO mice. The high level of fluorochrome labels particularly

surrounding the cortical pores (**Figure 5.5. B**) and osteoclasts visible within the cortical pores (**Figure 5.6. D**) clearly illustrate the high bone turnover. The nature of the fluorochrome labels is intriguing. In the mice fed the NormCaP diet and in 3 of 7 $VDR^{fl/fl}$ mice fed LowCaP diet, the labels are distinct and sharp indicating a healthy mineralization process. Indistinct labels were present in all ObVDR-KO and 4 of 7 $VDR^{fl/fl}$ mice fed LowCaP diet indicating a mineralization defect over the duration of the label injections (8 days).

The variation in phenotype amongst the LowCaP $VDR^{fl/fl}$ mice is intriguing. Genotype analyses were conducted several times using several different methods and primers to assure that these findings were not due to misclassification of mice (data not shown). It has been shown that a floxed allele can be converted into a knockout in the absence of a *Cre* transgene such as in Vasa-*cre* strains which expressed *Cre* mRNA/protein in the absence of *Cre* transgene in the oocytes (195). Furthermore, a study on EIIa-*cre*, B6.FVB-Tg(EIIa-*cre*)C5379Lmgd/J mouse line indicated that maternal or paternal inheritance of the *Cre* transgene may affect *Cre* expression and activity (163). Although most of the *Cre* mouse lines do not have differences in the phenotypes when transferred maternally or paternally (196), to investigate this phenomena amongst the ObVDR-KO mice is worthwhile. I observed that although most of the LowCaP fed mice had maternal *Cre* transmission (10 out of 13), there was no obvious pattern to signify maternal *Cre* inheritance produces inferior bone structure than that of the paternal inheritance. Since sites of *Cre* activity can be unexpected such as excision within non-intended cells or exerting an unpredictable deletion efficiencies (197), analyses of the *Cre* activity in this model during LowCaP diet are needed.

Quantification of VDR protein level in various tissues would be a future study to evaluate this *Cre* activity on LowCaP fed diet.

It is likely that the macroscopic changes to skeletal structures are arisen from the effects of mechanical forces exerted by the muscles during growth on poorly mineralised bone which is clearly undergoing a very high turnover. It is interesting that the major difference between the ObVDR-B6 mice (reported in Chapter 4) and the ObVDR-KO mice fed the LowCaP diet is the nature of the fluorochrome labels. In the ObVDR-B6 mice the double labels were distinct whereas in the ObVDR-KO mice the first label was clearly apparent but its edges were indistinct and the second label was not detected. However the effects on structure were very similar. Therefore while these observations suggest that the presence of VDR in mature osteoblasts allows for adequate mineralisation even under severe dietary calcium and phosphate restriction, the absence of VDR in mature osteoblasts curtailed the mineralization process under these conditions. Further evidence for a limitation of bone formation in the ObVDR-KO mice is the inability of the metaphyseal trabeculae to increase thickness under conditions of marked reduction in number of trabeculae unlike the $VDR^{fl/fl}$ mice (**Table 5.3**). The mechanism by which the compromised bone mineralisation process occurred are not fully understood and warrant further evaluation and studies.

5.5. CONCLUSION

This study further confirmed that VDR in mature osteoblasts modulates bone cell activity and/or plasma calcium/phosphate homeostasis. During adequate dietary calcium and phosphate intake, VDR deletion in mature osteoblasts did not affect bone structures at 20w of age although there was a decrease of ALP consistent with reduced

osteoblast number arising from reduced RANKL and stimulation of bone turnover in young, growing mice. This effect is markedly reduced with maturation of the animals and then the bone phenotype is lost.

In this study, prolonged severe dietary calcium/phosphate restriction was used to exert considerable stress on plasma calcium/phosphate homeostasis. VDR deletion in mature osteoblasts greatly affects bone structure, disrupts bone growth and growth plate, increases bone turnover and possibly reduced bone resorption and inhibits mineralisation. The markedly elevated PTH levels appear to stimulate high bone turnover and trabecularization of the cortical bone particularly in regions adjacent to the growth plates. Such high bone turnover provides sufficient calcium from the bone compartment to maintain calcium levels within the plasma compartment although the plasma phosphate levels declined significantly compared to the NormCaP fed animals irrespective of their osteoblast VDR status. The reduction of cortical endosteal perimeter is consistent with reduced bone resorption and the indistinct double fluorochrome labels are consistent with a limitation on bone formation.

Further data on bone VDR protein levels in the $VDR^{fl/fl}$ mice fed LowCaP would be useful since the *Cre/loxP* model has some limitations which may arise under extreme physiological conditions and may have confounded the phenotype of the control mice in this study.

CHAPTER 6: SUMMARY AND CONCLUSION

6.1. SUMMARY

6.1.1. Influence of Genetic Background on Activities of Osteoblast VDR

The genetic background of mice significantly effects skeletal structure and bone mineral homeostasis (198). Therefore, confirmation of the anabolic physiological role of overexpression of the *Vdr*-gene in mature osteoblasts in mice on a genetic background distinct from the original report was necessary. Backcrossing of the transgenic mouse line over-expressing the human *Vdr*-gene in mature osteoblasts (OSVDR) from *FVB/N* genetic background to *C57Bl6/J* (ObVDR-B6) was conducted. Overexpression of the human *Vdr* gene in mature osteoblasts plays a significant role on bone mineral accrual at cortical and trabecular sites of the *C57Bl6/J* transgenic mice similar to that reported for the OSVDR mice on the *FVB/N* background. A consistent increased in cortical bone volume and strength for both female and male ObVDR-B6 mice through the increased cortical thickness indicates the importance of VDR in cortical bone remodelling, possibly through enhancing VDR-mediated activities in osteocytes as well as osteoblasts. Most interestingly is the apparent sexual dimorphism of osteoblast VDR activities in adult mice (20w of age) where the female mice increased cortical bone volume largely due to increased periosteal expansion while the male mice have increased cortical bone volume due to the decrease in endosteal perimeter. These data suggest that in female mice VDR activity is stimulating periosteal bone formation while in male mice VDR activity is reducing bone resorption.

6.1.2. Effects of Normal Dietary Calcium/Phosphate on Vitamin D Activities within Mature Osteoblasts

When dietary calcium/phosphate was adequate, the ObVDR-B6 mice demonstrated increased bone mass and strength at 9 and 20w of age. This phenotype arose largely due to the decrease in bone resorption, on both trabecular and cortical bone, with a contribution of periosteal expansion suggesting an increase of bone formation. The decrease in bone resorption arose from decreased RANKL expression which reduces osteoclastogenesis. The mechanism by which periosteal expansion was achieved requires further study although Gardiner et al (36) reported increased periosteal bone formation rate with OSVDR mice on a similar diet.

In the ObVDR-KO mouse model fed normal dietary calcium/phosphate diet, deletion of VDR in mature osteoblasts did not alter bone structure or dynamic bone histomorphometry at 20w of age. As published elsewhere, ObVDR-KO mice exhibit increased trabecular bone phenotype at 6w of age which was markedly reduced at 12w (194). In this instance, the bone phenotype arose from decreased induction of RANKL and decreased osteoclastic bone resorption. Further investigation on the mechanism by which this phenotype is lost with maturity when growth and bone turnover reduces is warranted.

The only plasma calcium or phosphate regulating hormone modulated by the variation of VDR expression in mature osteoblasts when dietary calcium and phosphate are adequate is the lower serum FGF-23 levels in ObVDR-B6 mice. This effect is consistent with its synthesis being increased by increasing serum 1,25D levels and indicates that raising mature osteoblast and osteocyte VDR levels is equivalent to

increasing the VDR activity in these cells. No significant effects of ablation of the VDR gene in mature osteoblasts on circulating levels of 1,25D, PTH or FGF-23 during adequate calcium/phosphate diet were detected although PTH did increase by about 60 % but it did not achieve statistical significance. The effects of mature osteoblast/osteocyte VDR on PTH and FGF-23 serum levels require further investigation to elucidate the process and mechanisms involved in VDR activities of mature osteoblasts.

These data confirm that increased VDR activity in mature osteoblasts/osteocytes has the capacity to improve bone mineral status through both inhibition of osteoclastogenesis and stimulation of periosteal bone formation. However the phenotype of the ObVDR-KO mouse indicates that such activity is not necessary in adult animals when the calcium and phosphate nutrition are adequate.

6.1.3. Effects of Low Dietary Calcium/Phosphate on Vitamin D Activities within Mature Osteoblasts

An extremely low dietary calcium/phosphate diet to induce secondary hyperparathyroidism and supra-physiological levels of serum 1,25D was used to investigate the interaction between these calciotropic hormones and mature osteoblast VDR activities on bone mineral content and plasma calcium and phosphate homeostasis. Under these conditions, increased serum PTH and 1,25D levels and reduced serum FGF-23 levels were observed without hypocalcaemia or marked hypophosphatemia, although the serum phosphate levels were reduced when compared to adequate calcium/phosphate diet fed animals. These changes are likely to arise from the primary effect of the low dietary calcium stimulating PTH synthesis and

secretion and low dietary phosphate reducing FGF-23 synthesis and secretion, both of which can act to increase renal 1,25D synthesis and raised plasma 1,25D levels.

Femur length, femur total mineral content, femoral mid-shaft cortical bone volume, trabecular bone volume, and trabecular number in distal metaphysis and vertebrae were all significantly reduced in these mouse models. However, some features differed amongst the mouse models as depicted in the **table 6.1.** Differences between effects on appendicular and axial bone are also evident for VDR-mediated activity within the mature osteoblast. However, with regard to the ObVDR-KO model, such differences must be carefully examined and interpreted since conditional *Cre/loxP* models have limitations which may become evident under such supra-physiological or extreme conditions.

The effects of increasing osteoblast VDR level are consistent with the current understanding of 1,25D as a calciotropic hormone to maintain plasma calcium homeostasis. When dietary calcium is adequate the osteoblast VDR enhances the flux of calcium from the plasma compartment into the skeletal compartment. When dietary calcium is deficient, osteoblast VDR contributes to high bone turnover to the extent of macro-skeletal disruption to enhance the flux of calcium from the skeleton into the plasma compartment.

Table 6.1. Effects of Reducing Dietary Calcium/Phosphate from Normal to Extremely Low within the Same Genotype

Variable	WT	ObVDR-B6	$VDR^{fl/fl}$	ObVDR-KO
Body Weight	~	~	~	↓
Serum 1,25D	↑	↑↑	↑↑	↑↑↑
Serum PTH	N/A	N/A	↑	↑↑
Serum FGF-23	↓	↓↓	↓	↓
Femur length	↓	↓↓	↓↓	↓↓
Periosteal perimeter	~	↑	~	~
Endosteal perimeter	↑	↑	~	↓
Cortical porosity	Undetected	Observed (↑)	Observed (↑)	Observed (↑↑)
Tb. Th. Femur	~	~	↑↑	↑
SMI of Femur	~	~	↑	↑
Vertebral height	~	~	~	~
Tb. Th. Vertebrae	↓	↓	↓	↓
SMI of Vertebrae	~	~	↑	↑
Fluorochrome labels	Distinct double label	Distinct double label	Distinct first label, less distinct second label	Blurred first label, undetectable second label

~ comparable, ↑ increase, ↓ decrease,

It is interesting that these two mouse lines, ObVDR-B6 with overexpression of the *Vdr* gene in mature osteoblasts and ObVDR-KO with ablation of the *Vdr* gene in mature osteoblasts, demonstrate largely the same skeletal phenotype on extremely low calcium/phosphate diet with marked disruption of the growth plate and macro- and micro-architectural disruption of the skeleton to a greater extent than that found in control mice on this diet. Such an outcome clearly demonstrates the critical role of mature osteoblast VDR activity on bone growth. The overall evidence suggests that these models achieved this phenotype by different mechanisms. Both mouse lines maintained normocalcemia and only a minor decrease in serum phosphate levels by stimulating PTH and 1,25D secretion and decreasing FGF-23 levels. Unfortunately PTH levels are not available from ObVDR-B6 mice due to technical difficulties and therefore it is unknown whether these mice were similar to the ObVDR-KO mice with higher PTH levels than the controls; however the 1,25D levels were clearly increased over controls in both models. Therefore, high bone turnover phenotypes arise from the elevated levels of (probably) PTH and 1,25D in the ObVDR-B6 mice and PTH (and possibly 1,25D acting on immature osteoblasts) in the ObVDR-KO mice.

The skeletal architecture demonstrated that even when dietary calcium and phosphate are very low, ObVDR-B6 mice maintained increased periosteal circumference compared to WT mice suggesting that the ability to increase periosteal bone formation is preserved even under these extreme conditions. It would be expected that if increasing mature osteoblast/osteocyte VDR activity stimulated periosteal bone formation then ablation of mature osteoblast/osteocyte activity would reduce or limit periosteal bone formation. As stated above there is no evidence for reduced periosteal bone formation with ObVDR-KO mice on either diet. However, it is interesting to note

that femoral metaphyseal trabecular thickness apparently increased in the control $VDR^{fl/fl}$ mice fed the LowCaP diet. This is presumably as a result of increased mechanical forces on each surviving trabeculum following the marked reduction of trabecular number with this diet. While trabecular thickness in ObVDR-KO mice fed similar diet was increased, it did not progress to the extent of the control mice. These data, as they stand, provide some evidence that bone formation may be limited in the ObVDR-KO mice. However the data may be confounded by the marked reduction of trabecular bone in this region and the difficulty to distinguish between true trabecular bone and bone arising from the trabecularization of the cortices, which is very extensive in these mice. Clearly further work is required to investigate any such effects in more detail.

The dynamic histology data provide evidence to suggest that the marked disruption of skeletal structure between the mouse lines demonstrate different osteoclast and osteoblast activities. ObVDR-B6 mice demonstrated increased osteoclast number associated with increased *Rankl* expression suggestive of the effects of increased 1,25D and possibly PTH on osteoblast/osteocyte cells above the level of the control mice. Bone formation appeared to be adequate as indicated by extensive, distinct fluorochrome double labels, not different to the control mice. ObVDR-B6 mice appear to have demonstrated maintenance of the coupling between osteoclasts and osteoblasts even with the high bone turnover producing the marked reduction of bone volume similar to that observed with estrogen deficiency.

In ObVDR-KO mice, the osteoclast numbers were not different to the control mice although given the marked reduction in trabecular bone surface, the total number of

osteoclasts available for assessment is small and therefore the data are not robust. Furthermore, the ObVDR-KO mice demonstrated markedly disturbed fluorochrome labels with a wide, blurry first label and undetectable second label indicating a mineralization defect. The difficulty in interpreting these data is the appearance of the control mice, the $VDR^{fl/fl}$ mice, in which as discussed previously, 3 mice demonstrated relatively distinct double labels and 4 mice demonstrated labels similar to the appearance of the ObVDR-KO mice with some variation on the extent of the disturbance of the labels. Therefore, the mineralisation defect could be simply due to the floxed *Vdr* gene was not properly expressed or there was unexplained ablation of the *Vdr* gene in these mice. The fact that all the labels in ObVDR-KO mice were consistent and those in the $VDR^{fl/fl}$ mice were variable suggest that this mineralisation defect arises from the ablation of osteoblast VDR and not just the floxed *Vdr* gene. Therefore the suggestion from these data is that the phenotype of the ObVDR-KO mice when fed extremely low calcium and phosphate diet arises from high bone turnover from the markedly increased PTH and a limitation on bone formation.

6.2. LIMITATIONS

The studies described in this thesis have some design and research limitations which can be improved in future studies. The limited or absence of data from young growing ObVDR-B6 and ObVDR-KO mice fed both diets limits the interpretation of the effects of VDR activities in mature osteoblasts during the period of bone modelling including the dynamic histomorphometry analyses and gene expressions of the short term dietary study. The WT mice used in some of the studies were not littermates which may influence some of the findings although, our measurements made on ObVDR-B6 and non-littermates control WT mice did not indicate any detectable differences with those

observed using littermate controls. As well, some data are missing from the study including mRNA and protein analyses as well as some serum measurements. All of these omissions were due to resource and time limitations for this project.

There is also the issue of the status of the *Vdr*-floxed mice used as controls under the extreme condition of the low dietary calcium and phosphate which induced supra-physiological levels of calciotropic hormones. As discussed, I did not directly measure *Vdr* gene expression or VDR protein levels, which limits the interpretation of the ObVDR-KO mice under these conditions. Assessment of the *Cre* expression, activity and potential for gene deletion in the $VDR^{fl/fl}$ mice would be most helpful.

Although vertebral microCT analyses shown some significant differences in and between the mouse models, the omission of vertebral histomorphometry in the studies hampers the interpretation of these models especially the absence of double fluorescent label images to provide rate of bone formation analyses. Furthermore, the studies were conducted only on female mice, although preliminary studies have shown gender related differences in the activities of the VDR in mature osteoblasts.

6.3.FUTURE DIRECTIONS

The results in this thesis indicate that mature osteoblast VDR activities effect bone size, shape and structure as well as microarchitecture. They provide a rich source for generating new hypotheses regarding the cellular and molecular mechanisms involved. Further investigations of these mechanisms by which osteoblast VDR exerts these activities would be most useful. In particular further investigation of the periosteal bone formation rate, including any variation with age, is required to improve the

sensitivity of assessment as to whether such bone formation is reduced in the ObVDR-KO mouse line. As well, the apparent sexual dimorphism of mature osteoblast/osteocyte VDR requires further investigation to identify the cellular and molecular mechanisms contributing to these outcomes possibly through the interactions between either the estrogen and androgen receptors in female and male mice respectively.

On the extremely low calcium and phosphate diet, ObVDR-B6 have shown changes in growth plate width and area. Further investigation on the proliferative and hypertrophic zone of these mice and studies using 1,25D treatment could also uncover the role of mature osteoblasts VDR activities in chondrocytes activity and maturation. Further analyses using immunohistochemistry for osteocyte markers, nanoindentation, tissue mineral density, and mechanical strength analyses could be conducted to attest whether bone mineral accrual and changes of skeletal structure improves bone quality and strength especially in the LowCaP diet and or in 1,25D treated ObVDR-B6 for future studies. Similar studies and approaches can also be used in the ObVDR-KO mouse model to further strengthen the evidence of VDR in mature osteoblasts to modulate skeletal structure and mineral content.

The ObVDR-KO mice demonstrated bone marrow changes including adiposity and bone marrow cellularity possibly indicating an altered bone marrow niche. These observations suggest a role for VDR in mature osteoblasts in contributing to the maintenance of bone marrow integrity. Future studies could carefully examine this notion to further understand the effects of VDR on bone marrow health and whether

these changes also affect haematopoietic stem cells (HSC) and/or blood cell populations.

6.4. CONCLUSION

The findings of this thesis demonstrate that mature osteoblast VDR exerts critical activities contributing to maintaining plasma calcium and phosphate homeostasis, skeletal growth particularly in the long bones, and bone cell activities. The effects on maintaining plasma calcium and phosphate homeostasis include effects on plasma levels of calciotropic hormones such as 1,25D, PTH, and FGF-23 as well as bone cell activities. The outcomes from feeding extremely low calcium and phosphate diet have demonstrated a markedly disrupted skeleton with critical input from osteoblast VDR to achieve adequate plasma calcium levels. Therefore, osteoblast VDR activities markedly respond to calcium and phosphate nutrition consistent with the overriding outcome to maintain plasma calcium homeostasis at the expense of bone structure and integrity. These findings add to the knowledge that a direct role of vitamin D receptor in skeletal health do persist and that the VDR in mature osteoblasts do able to change bone structure, modulate mineral homeostasis and the maintenance of skeletal health.

REFERENCE LIST

1. Masi L 2008 Epidemiology of Osteoporosis. Clin Cases Miner Bone Metab **5**(1)**:**11-13.
2. WHO Study Group on assesment of fracture risk and its application to screening for postmenopausal osteoporosis 1994 Assessment of Fracture Risk and its Application to Screening for Post Menopausal Osteoporosis: Report of a WHO Study Group. World Health Organization.
3. Sennang AN, Mutmainnah, Pakasi RDN, Hardjoeno 2006 Analisis Kadar Osteokalsin Serum Osteopenia Dan Osteoporosis (The Analysis of Serum Osteocalcin Level on Osteopenic and Osteoporotic Subjects). Indonesian J Clin Path Med Lab **12**(2)**:**49 - 52.
4. AIHW 2008 A Picture of Osteoporosis in Australia. In: Welfare AIoHa (ed.) Arthritis. AIHW, Canberra.
5. Wilkins CH 2007 Osteoporosis Screening and Risk Management. Clin Interv Aging **2**(3)**:**389–394.
6. van Schoor NM, Lips P 2011 Worldwide Vitamin D Status. Best Pract Res Clin Endocrinol Metab **25**(4)**:**671-680.
7. Sahota O 2000 Osteoporosis and the Role of Vitamin D and Calcium-Vitamin D Deficiency, Vitamin D Insufficiency and Vitamin D Sufficiency. Age Ageing **29**(4)**:**301-4.
8. Bischoff-Ferrari HA 2010 Vitamin D and fracture prevention. Endocrinol Metab Clin N Am **39**(2)**:**347-353.

9. WHO Scientific Group 2007 WHO Scientific Group on the Assessment of Osteoporosis at Primary Health Care Level. World Health Organization Geneva, Switzerland.

10. Peters BS, Martini LA 2010 Nutritional Aspects of the Prevention and Treatment of Osteoporosis. Arq Bras Endocrinol Metabol **54**(2)**:**179-85.

11. Bryant RJ, Cadogan J, Weaver CM 1999 The New Dietary Reference Intakes for Calcium: Implications for Osteoporosis. J Am Coll Nutr **18**(5 Suppl)**:**406S-412S.

12. Lee CJ, Lawler GS, Johnson GH 1981 Effects of Supplementation of the Diets with Calcium and Calcium-rich Foods on Bone Density of Elderly Females with Osteoporosis. Am J Clin Nutr **34**(5)**:**819-23.

13. Dawson-Hughes B, Dallal GE, Krall EA, Sadowski L, Sahyoun N, Tannenbaum S 1990 A Controlled Trial of the Effect of Calcium Supplementation on Bone Density in Postmenopausal Women. N Engl J Med **323**(13)**:**878-83.

14. Teegarden D, Weaver CM 1994 Calcium Supplementation Increases Bone Density in Adolescent Girls. Nutr Rev **52**(5)**:**171-3.

15. Feskanich D, Willett WC, Colditz GA 2003 Calcium, Vitamin D, Milk Consumption, and Hip Fractures: a Prospective Study among Postmenopausal Women. Am J Clin Nutr **77**(2)**:**504-11.

16. Larsen ER, Mosekilde L, Foldspang A 2004 Vitamin D and Calcium Supplementation Prevents Osteoporotic Fractures in Elderly Community Dwelling Residents: A Pragmatic Population-Based 3-Year Intervention Study. J Bone Miner Res **19:**370 –378.

17. Hofer AM, Lefkimmiatis K 2007 Extracellular Calcium and cAMP: Second Messengers as "Third Messengers"? Physiology **22**(5)**:**320-327.

18. O'Toole JF 2011 Disorders of Calcium Metabolism. Nephron Physiol **118**(1)**:**p22-p27.

19. Allgrove J 2003 Disorders of Calcium Metabolism. Current Paediatrics **13**(7)**:**529-535.

20. Rajakumar K, Thomas SB 2005 Reemerging Nutritional Rickets: A Historical Perspective. Arch Pediatr Adolesc Med **159:**335-341.

21. Hochberg Z 2003 Introduction, Rickets – Past and Present In: Hochberg Z (ed.) Vitamin D and rickets S. Karger AG, Basel, Switzerland, pp 1 - 13.

22. Li YC, Amling M, Pirro AE, Priemel M, Meuse J, Baron R, Delling G, Demay MB 1998 Normalization of Mineral Ion Homeostasis by Dietary Means Prevents Hyperparathyroidism, Rickets, and Osteomalacia, But Not Alopecia in Vitamin D Receptor-Ablated Mice. Endocrinology **139**(10)**:**4391-4396.

23. Amling M, Priemel M, Holzmann T, Chapin K, Rueger JM, Baron R, Demay MB 1999 Rescue of the Skeletal Phenotype of Vitamin D Receptor-Ablated Mice in the Setting of Normal Mineral Ion Homeostasis: Formal Histomorphometric and Biomechanical Analyses. Endocrinology **140**(11)**:**4982-4987.

24. Ruohola JP, Laaksi I, Ylikomi T, Haataja R, Mattila VM, Sahi T, Tuohimaa P, Pihlajamaki H 2006 Association between Serum 25(OH)D Concentrations and Bone Stress Fractures in Finnish Young Men. J Bone Miner Res **21**(9)**:**1483-8.

25. Lips P, Graafmans WC, Ooms ME, Bezemer PD, Bouter LM 1996 Vitamin D Supplementation and Fracture Incidence in Elderly Persons. A Randomized, Placebo-controlled Clinical Trial. Ann Intern Med **124**(4)**:**400-6.

26. Meyer HE, Smedshaug GB, Kvaavik E, Falch JA, Tverdal A, Pedersen JI 2002 Can Vitamin D Supplementation Reduce the Risk of Fracture in the Elderly? A Randomized Controlled Trial. J Bone Miner Res **17**(4)**:**709-15.

27. Trivedi DP, Doll R, Khaw KT 2003 Effect of Four Monthly Oral Vitamin D3 (Cholecalciferol) Supplementation on Fractures and Mortality in Men and Women Living in the Community: Randomised Double Blind Controlled Trial. BMJ **326**(7387)**:**469-472.

28. Bischoff HA, Stähelin HB, Dick W, Akos R, Knecht M, Salis C, Nebiker M, Theiler R, Pfeifer M, Begerow B, Lew RA, Conzelmann M 2003 Effects of Vitamin D and Calcium Supplementation on Falls: A Randomized Controlled Trial. J Bone Miner Res **18**(2)**:**343-351.

29. Nordin BEC 1997 Calcium and Osteoporosis. Nutrition **13**(7–8)**:**664-686.

30. Bronner F 1994 Calcium and Osteoporosis. Am J Clin Nutr **60**(6)**:**831-6.

31. Anderson PH, Atkins GJ 2008 The Skeleton as an Intracrine Organ for Vitamin D Metabolism. Molec Asp Med **29**(6)**:**397-406.

32. Morris HA, Anderson PH 2010 Autocrine and Paracrine Actions of Vitamin D. Clin Biochem Rev **31** 129 - 138.

33. Atkins GJ, Anderson PH, Findlay DM, Welldon KJ, Vincent C, Zannettino ACW, O'Loughlin PD, Morris HA 2007 Metabolism of Vitamin D3 in Human Osteoblasts: Evidence for Autocrine and Paracrine Activities of 1α,25-Dihydroxyvitamin D3. Bone **40**(6)**:**1517-1528.

34. van Driel M, Koedam M, Buurman CJ, Hewison M, Chiba H, Uitterlinden AG, Pols HA, van Leeuwen JP 2006 Evidence for Auto/paracrine Actions of Vitamin D in Bone: 1alpha-Hydroxylase Expression and Activity in Human Bone Cells. FASEB J **20**(13)**:**2417-2419.

35. Kogawa M, Findlay DM, Anderson PH, Ormsby R, Vincent C, Morris HA, Atkins GJ 2010 Osteoclastic Metabolism of 25(OH)-Vitamin D3: a Potential Mechanism for Optimization of Bone Resorption. Endocrinology **151**(10)**:**4613-25.

36. Gardiner EM, Baldock PA, Thomas GP, Sims NA, Henderson NK, Hollis B, White CP, Sunn KL, Morrison NA, Walsh WR, Eisman JA 2000 Increased Formation and Decreased Resorption of Bone in Mice with Elevated Vitamin D Receptor in Mature Cells of the Osteoblastic Lineage. FASEB J **14**(13)**:**1908-16.

37. Baldock PA, Thomas GP, Hodge JM, Baker SUK, Dressel U, O'Loughlin PD, Nicholson GC, Briffa KH, Eisman JA, Gardiner EM 2006 Vitamin D Action and Regulation of Bone Remodeling: Suppression of Osteoclastogenesis by the Mature Osteoblast. J Bone Miner Res **21**(10)**:**1618-1626.

38. Clarke B 2008 Normal Bone Anatomy and Physiology. Clin J Am Soc Nephrol **3 Suppl 3:**S131-139.

39. Kini U, Nandeesh BN 2012 Physiology of Bone Formation, Remodeling, and Metabolism. In: Fogelman I, Gnanasegaran G, van der Wall H (eds.) Radionuclide and Hybrid Bone Imaging, 1 ed. Springer-Verlag Berlin Heidelberg, Berlin, Germany, pp 29-57.

40. Ilich JZ, Kerstetter JE 2000 Nutrition in Bone Health Revisited: A Story Beyond Calcium. J Am Coll Nutr **19**(6)**:**715-737.

41. Nalla RK, Kruzic JJ, Kinney JH, Balooch M, Ager Iii JW, Ritchie RO 2006 Role of Microstructure in the Aging-related Deterioration of the Toughness of Human Cortical Bone. Mater Sci Eng **26**(8)**:**1251-1260.

42. Parfitt AM 2005 Modeling and Remodeling:How Bone Cells Work Together. In: Feldman D, Pike JW, Glorieux FH (eds.) Vitamin D, 2nd Ed. ed., vol. 1. Elsevier, Inc., New York, pp 497-513.

43. Bonjour JP, Chevalley T, Ferrari S, Rizzoli R 2009 The Importance and Relevance of Peak Bone Mass in the Prevalence of Osteoporosis. SciELO **51 Suppl 1:**S5-17.

44. Parfitt AM 1984 Age-related Structural Changes in Trabecular and Cortical Bone: Cellular Mechanisms and Biomechanical Consequences. Calcif Tissue Int **36 Suppl 1:**S123-8.

45. Demontiero O, Vidal C, Duque G 2012 Aging and Bone Loss: New Insights for the Clinician. Ther Adv Musculoskelet Dis **4**(2)**:**61-76.

46. Xu LL, Yang NL 2008 Differentiation of Human Bone Marrow Mesenchymal Stem Cells into Osteoblasts In-vitro. CRTER **12**(38)**:**7483-7486.

47. Fuller K, Chambers TJ 1987 Generation of Osteoclasts in Cultures of Rabbit Bone Marrow and Spleen Cells. J Cell Physiol **132**(3)**:**441-52.

48. Marie PJ, Kassem M 2011 Osteoblasts in Osteoporosis: Past, Emerging, and Future Anabolic Targets. Eur J Endocrinol **165**(1)**:**1-10.

49. Bonewald LF 2010 The Osteocyte Network as a Source and Reservoir of Signaling Factors. Endocrinol Metab **25(3):**161-165.

50. Díaz-Flores L, Gutiérrez R, Madrid JF, Varela H, Valladares F, Acosta E, Martín-Vasallo P, Díaz-Flores L 2009 Pericytes Morphofunction, Interactions and Pathology in a Quiescent and Activated Mesenchymal Cell Niche. Histol Histopathol **24**(7)**:**909-969.

51. Paredes R, Arriagada G, Cruzat F, Villagra A, Olate J, Zaidi K, van Wijnen A, Lian JB, Stein GS, Stein JL, Montecino M 2004 Bone-Specific Transcription Factor Runx2 Interacts with the 1α,25-Dihydroxyvitamin D3 Receptor To Up-Regulate Rat Osteocalcin Gene Expression in Osteoblastic Cells. Mol Cell Biol **24**(20)**:**8847-8861.

52. Hidalgo-Bastida LA, Cartmell SH 2010 Mesenchymal Stem Cells, Osteoblasts and Extracellular Matrix Proteins: Enhancing Cell Adhesion and Differentiation for Bone Tissue Engineering. Tissue Eng Part B Rev **16**(4)**:**405-12.

53. Lemaire V, Tobin FL, Greller LD, Cho CR, Suva LJ 2004 Modeling the Interactions between Osteoblast and Osteoclast Activities in Bone Remodeling. J Theor Biol **229**(3)**:**293-309.

54. Bonewald LF, Johnson ML 2008 Osteocytes, Mechanosensing and Wnt Signaling. Bone **42**(4)**:**606-15.

55. Xiao Z, Camalier CE, Nagashima K, Chan KC, Lucas DA, De La Cruz MJ, Gignac M, Lockett S, Issaq HJ, Veenstra TD, Conrads TP, Beck Jr GR 2007 Analysis of the Extracellular Matrix Vesicle Proteome in Mineralizing Osteoblasts. J Cell Physiol **210**(2)**:**325-335.

56. Betts F, Blumenthal NC, Posner AS 1981 Bone Mineralization. J Cryst Growth **53**(1)**:**63-73.

57. Crockett JC, Rogers MJ, Coxon FP, Hocking LJ, Helfrich MH 2011 Bone Remodelling at a Glance. J Cell Sci **124**(7)**:**991-998.

58. Tu X, Delgado-Calle J, Condon KW, Maycas M, Zhang H, Carlesso N, Taketo MM, Burr DB, Plotkin LI, Bellido T 2015 Osteocytes Mediate the Anabolic Actions of Canonical Wnt/beta-catenin Signaling in Bone. Proc Natl Acad Sci U S A **112**(5)**:**E478-86.

59. Franz-Odendaal TA, Hall BK, Witten PE 2006 Buried Alive: How Osteoblasts Become Osteocytes. Dev Dyn **235**(1)**:**176-90.

60. Atkins GJ, Findlay DM 2012 Osteocyte Regulation of Bone mineral: a Little Give and Take. Osteoporos Int **23**(8)**:**2067-2079.

61. Burger EH, Klein-Nulend J, van der Plas A, Nijweide PJ 1995 Function of Osteocytes in Bone--their Role in Mechanotransduction. J Nutr **125**(7 Suppl)**:**2020S-2023S.

62. Teti A, Zallone A 2009 Do osteocytes contribute to bone mineral homeostasis? Osteocytic osteolysis revisited. Bone **44**(1)**:**11-16.

63. Wysolmerski JJ 2012 Osteocytic osteolysis: time for a second look? BoneKEy Reports **1:**229.

64. Sasaki T 2003 Differentiation and Functions of Osteoclasts and Odontoclasts in Mineralized Tissue Resorption. Microsc Res Techniq **61**(6)**:**483-495.

65. Udagawa N, Takahashi N, Jimi E, Matsuzaki K, Tsurukai T, Itoh K, Nakagawa N, Yasuda H, Goto M, Tsuda E, Higashio K, Gillespie MT, Martin TJ, Suda T 1999 Osteoblasts/Stromal Cells Stimulate Osteoclast Activation through Expression of Osteoclast Differentiation Factor/RANKL but not Macrophage Colony-Stimulating Factor: Receptor Activator of NF-kappa B Ligand. Bone **25**(5)**:**517-23.

66. Nakamura I, Takahashi N, Jimi E, Udagawa N, Suda T 2011 Regulation of Osteoclast Function. Mod Rheumatol**:**1-11.

67. Teitelbaum SL 2000 Bone Resorption by Osteoclasts. Science **289**(5484)**:**1504-1508.

68. Boyle WJ, Simonet WS, Lacey DL 2003 Osteoclast Differentiation and Activation. Nature **423**(6937)**:**337-342.

69. Nakamura K, Saito T, Yoshihara A, Ishikawa M, Tsuchiya Y, Oshiki R, Kobayashi R, Maruyama K, Hyodo K, Nashimoto M, Tsugawa N, Okano T, Oyama M, Yamamoto M 2009 Low Calcium Intake is Associated with Increased Bone Resorption in Postmenopausal Japanese Women: Yokogoshi Study. Public Health Nutr **12**(12)**:**2366-70.

70. Villereal ML, Palfrey HC 1989 Intracellular Calcium and Cell Function. Annu Rev Nutr **9:**347-76.

71. Horner J 2006 Basic Science of Disorders of Calcium Metabolism and Metabolic Diseases of Bone. Surgery **24**(6)**:**215-219.

72. Hoenderop JG, Nilius B, Bindels RJ 2005 Calcium Absorption Across Epithelia. Physiol Rev **85**(1)**:**373-422.

73. Blaine J, Chonchol M, Levi M 2014 Renal Control of Calcium, Phosphate, and Magnesium Homeostasis. Clin J Am Soc Nephrol.

74. Requirements JFWECoHVaM 2004 Vitamin and Mineral Requirements in Human Nutrition, 2nd Edition.

75. National Health and Medical Research Council 2006 Nutrient Reference Values for Australia and New Zealand; Including Recommended Dietary Intakes. In: Department of Health and Ageing (ed.). Commonwealth of Australia.

76. Ross AC, Manson JE, Abrams SA, Aloia JF, Brannon PM, Clinton SK, Durazo-Arvizu RA, Gallagher JC, Gallo RL, Jones G, Kovacs CS, Mayne ST, Rosen CJ, Shapses SA 2011 The 2011 Report on Dietary Reference Intakes for Calcium and Vitamin D from the Institute of Medicine: What Clinicians Need to Know. J Clin Endocrinol Metab **96**(1)**:**53-8.

77. Ma J, Johns RA, Stafford RS 2007 Americans are not Meeting Current Calcium Recommendations. Am J Clin Nutr **85**(5)**:**1361-6.

78. Bronner F 2003 Mechanisms of Intestinal Calcium Absorption. J Cell Biochem **88**(2)**:**387-393.

79. Pérez AV, Picotto G, Carpentieri AR, Rivoira MA, Peralta López ME, Tolosa De Talamoni NG 2008 Minireview on Regulation of Intestinal Calcium Absorption: Emphasis on Molecular Mechanisms of Transcellular Pathway. Digestion **77**(1)**:**22-34.

80. Fleet JC, Schoch RD 2010 Molecular Mechanisms for Regulation of Intestinal Calcium Absorption by Vitamin D and Other Factors. Crit Rev Clin Lab Sci **47**(4)**:**181-95.

81. Nijenhuis T, Hoenderop JJ, Bindels RM 2005 TRPV5 and TRPV6 in Ca2+ (re)absorption: Regulating Ca2+ Entry at the Gate. Pflugers Arch - Eur J Physiol **451**(1)**:**181-192.

82. Wasserman RH, Fullmer CS 1989 On the Molecular Mechanism of Intestinal Calcium Transport. Adv Exp Med Biol **249:**45-65.

83. Christakos S 2012 Recent Advances in our Understanding of 1,25-Dihydroxyvitamin D(3) Regulation of Intestinal Calcium Absorption. Arch Biochem Biophys **523**(1)**:**73-6.

84. Hoenderop JG, Nilius B, Bindels RJ 2002 Molecular Mechanism of Active Ca2+ Reabsorption in the Distal Nephron. Annu Rev Physiol **64:**529-49.

85. Friedman PA 2000 Mechanisms of Renal Calcium Transport. Exp Nephrol **8**(6)**:**343-350.

86. Boone M, Deen PMT 2008 Physiology and Pathophysiology of the Vasopressin-regulated Renal Water Reabsorption. Pflugers Arch - Eur J Physiol **456**(6)**:**1005-1024.

87. Bozic M, Valdivielso JM 2012 Calcium Signaling in Renal Tubular Cells. Adv Exp Med Biol **740:**933-44.

88. Kumar R 1990 Vitamin D Metabolism and Mechanisms of Calcium Transport. J Am Soc Nephrol **1**(1)**:**30-42.

89. Lieben L, Carmeliet G, Masuyama R 2011 Calcemic Actions of Vitamin D: Effects on the Intestine, Kidney and Bone. Best Pract Res Clin Endocrinol Metab **25**(4)**:**561-572.

90. Cannata-Andía JB, Gómez Alonso C 2002 Vitamin D Deficiency: A Neglected Aspect of Disturbed Calcium Metabolism in Renal Failure. Nephrol Dial Transplant **17**(11)**:**1875-1878.

91. Kerstetter JE, O'Brien KO, Insogna KL 2003 Dietary Protein, Calcium Metabolism, and Skeletal Homeostasis Revisited. Am J Clin Nutr **78**(3 Suppl)**:**584S-592S.

92. Peacock M 1991 Calcium Absorption Efficiency and Calcium Requirements in Children and Adolescents. Am J Clin Nutr **54(Suppl):**261S-265S.

93. Shu L, Ji J, Zhu Q, Cao G, Karaplis A, Pollak MR, Brown E, Goltzman D, Miao D 2010 The Calcium Sensing Receptor Mediates Bone Turnover

Induced by Dietary Calcium and Parathyroid Hormone in Neonates. J Bone Miner Res.

94. Marks J, Debnam ES, Unwin RJ 2010 Phosphate Homeostasis and the Renal-gastrointestinal Axis. Am J Physiol Renal Physiol **299**(2)**:**F285-F296.

95. Lien YH 2013 Phosphorus: Another Devil in our Diet? Am J Med **126**(4)**:**280-1.

96. Lederer E 2014 Regulation of Serum Phosphate. J Physiol **592**(Pt 18)**:**3985-95.

97. Kumar R 2009 Phosphate Sensing. Curr Opin Nephrol Hypertens **18**(4)**:**281-284.

98. Gattineni J, Baum M 2012 Genetic Disorders of Phosphate Regulation. Pediatr Nephrol **27**(9)**:**1477-87.

99. Bacchetta J, Salusky IB 2012 Evaluation of Hypophosphatemia: Lessons from Patients with Genetic Disorders. Am J Kidney Dis **59**(1)**:**152-9.

100. Lehmann B, Meurer M 2010 Vitamin D Metabolism. Dermatol Ther **23**(1)**:**2-12.

101. Morris HA 2005 Vitamin D: a Hormone for All Seasons - How Much is Enough? Clin Biochem Rev **26** 21 - 32.

102. Diamond TH, Eisman JA, Mason RS, Nowson CA, Pasco JA, Sambrook PN, Wark JD 2005 Vitamin D and Adult Bone Health in Australia and New Zealand: A Position Statement. Med J Australia **182**(6)**:**281-285.

103. Zittermann A 2003 Vitamin D in Preventive Medicine: Are We Ignoring the Evidence? Br J Nutr **89**(5)**:**552-72.

104. Christakos S, DeLuca HF 2011 Vitamin D: Is There a Role in Extraskeletal Health? Endocrinology **152**(8)**:**2930-2936.

105. Pittas AG, Dawson-Hughes B 2010 Vitamin D and Diabetes. J Steroid Biochem Mol Biol **121**(1-2)**:**425-9.

106. Touvier M, Chan DS, Lau R, Aune D, Vieira R, Greenwood DC, Kampman E, Riboli E, Hercberg S, Norat T 2011 Meta-analyses of Vitamin D Intake, 25-Hydroxyvitamin D Status, Vitamin D Receptor Polymorphisms, and Colorectal Cancer Risk. Cancer Epidemiol Biomarkers Prev **20**(5)**:**1003-16.

107. Holick MF 2005 Vitamin D: Important for Prevention of Osteoporosis, Cardiovascular Heart Disease, Type 1 Diabetes, Autoimmune Diseases, and Some Cancers. South Med J **98**(10)**:**1024-7.

108. Dijkstra SH, van Beek A, Janssen JW, de Vleeschouwer LHM, Huysman WA, van den Akker ELT 2007 High Prevalence of Vitamin D Deficiency in Newborn Infants of High-Risk Mothers. Arch Dis Child **92:**750–753.

109. Gordon CM, DePeter KC, Feldman HA, Grace E, Emans SJ 2004 Prevalence of Vitamin D Deficiency among Healthy Adolescents. Arch Pediatr Adolesc Med **158**(6)**:**531-537.

110. Bodnar LM, Simhan HN, Powers RW, Frank MP, Cooperstein E, Roberts JM 2007 High Prevalence of Vitamin D Insufficiency in Black and White Pregnant Women Residing in the Northern United States and Their Neonates. J Nutr **137:**447–452.

111. Van Der Meer IM, Karamali NS, Boeke AJP, Lips P, Middelkoop BJC, Verhoeven I, Wuister JD 2006 High Prevalence of Vitamin D Deficiency in Pregnant Non-Western Women in the Hague, Netherlands. Am J Clin Nutr **84**(2)**:**350-353.

112. van der Mei IA, Ponsonby AL, Engelsen O, Pasco JA, McGrath JJ, Eyles DW, Blizzard L, Dwyer T, Lucas R, Jones G 2007 The High Prevalence of

Vitamin D Insufficiency Across Australian Populations is only Partly Explained by Season and Latitude. Environ Health Perspect **115**(8)**:**1132-9.

113. Holick MF, Chen TC 2008 Vitamin D Deficiency: A Worldwide Problem with Health Consequences. Am J Clin Nutr **87**(4)**:**1080S-1086S.

114. Romagnoli E, Pepe J, Piemonte S, Cipriani C, Minisola S 2013 Value and Limitations of Assessing Vitamin D Nutritional Status and Advised Levels of Vitamin D Supplementation. Eur J Endocrinol **169**(4)**:**R59-R69.

115. Jones G, Prosser DE, Kaufmann M 2014 Cytochrome P450-mediated Metabolism of Vitamin D. J Lipid Res **55**(1)**:**13-31.

116. Bland R, Zehnder D, Hewison M 2000 Expression of 25-Hydroxyvitamin D3-1α-Hydroxylase along the Nephron: New Insights into Renal Vitamin D Metabolism. Curr Opin Nephrol Hypertens **9**(1)**:**17-22.

117. Henry HL 2011 Regulation of Vitamin D Metabolism. Best Pract Res Cl En **25**(4)**:**531-541.

118. Radermacher J, Diesel B, Seifert M, Tilgen W, Reichrath J, Fischer U, Meese E 2006 Expression Analysis of CYP27B1 in Tumor Biopsies and Cell Cultures. Anticancer Res **26**(4A)**:**2683-2686.

119. Anderson PH, O'Loughlin PD, May BK, Morris HA 2003 Quantification of mRNA for the Vitamin D Metabolizing Enzymes CYP27B1 and CYP24 and Vitamin D Receptor in Kidney using Real-Time Reverse Transcriptase-Polymerase Chain Reaction. J Mol Endocrinol **31**(1)**:**123-32.

120. Wang Y, Zhu J, DeLuca HF 2012 Where is the Vitamin D Receptor? Arch Biochem Biophys **523**(1)**:**123-133.

121. DeLuca HF 2014 History of the Discovery of Vitamin D and Its Active Metabolites. BoneKEy Rep **3**.

122. Bouillon R, Carmeliet G, Verlinden L, van Etten E, Verstuyf A, Luderer HF, Lieben L, Mathieu C, Demay M 2008 Vitamin D and Human Health: Lessons from Vitamin D Receptor Null Mice. Endocr Rev **29**(6)**:**726-76.

123. Dusso AS, Brown AJ, Slatopolsky E 2005 Vitamin D. Am J Physiol Renal Physiol **289**(1)**:**F8-28.

124. Haussler MR, Jurutka PW, Mizwicki M, Norman AW 2011 Vitamin D Receptor (VDR)-mediated Actions of 1α,25(OH)2 Vitamin D3: Genomic and Non-genomic Mechanisms. Best Pract Res Clin Endocrinol Metab **25**(4)**:**543-559.

125. Pike JW, Meyer MB, Bishop KA 2012 Regulation of Target Gene Expression by the Vitamin D Receptor - an Update on Mechanisms. Rev Endocr Metab Disord **13**(1)**:**45-55.

126. Nagpal S, Na S, Rathnachalam R 2005 Noncalcemic Actions of Vitamin D Receptor Ligands. Endocr Rev **26**(5)**:**662-687.

127. Idelevich A, Kerschnitzki M, Shahar R, Monsonego-Ornan E 2011 1,25(OH)2D3 Alters Growth Plate Maturation and Bone Architecture in Young Rats with Normal Renal Function. PLoS One **6**(6)**:**e20772.

128. Takeda S, Yoshizawa T, Nagai Y, Yamato H, Fukumoto S, Sekine K, Kato S, Matsumoto T, Fujita T 1999 Stimulation of Osteoclast Formation by 1,25-Dihydroxyvitamin D Requires its Binding to Vitamin D Receptor (VDR) in Osteoblastic Cells: Studies Using VDR Knockout Mice. Endocrinology **140**(2)**:**1005-8.

129. Kanzawa M, Sugimoto T, Kanatani M, Chihara K 2000 Involvement of Osteoprotegerin/Osteoclastogenesis Inhibitory Factor in the Stimulation of

Osteoclast Formation by Parathyroid Hormone in Mouse Bone Cells. Eur J Endocrinol **142**(6)**:**661-4.

130. Okada Y, Morimoto I, Ura K, Watanabe K, Eto S, Kumegawa M, Raisz L, Pilbeam C, Tanaka Y 2002 Cell-to-Cell Adhesion via Intercellular Adhesion Molecule-1 and Leukocyte Function-Associated Antigen-1 Pathway is Involved in 1α,25(OH)2D3, PTH and IL-1α-Induced Osteoclast Differentiation and Bone Resorption. Endocr J **49**(4)**:**483-95.

131. Rinotas V, Niti A, Dacquin R, Bonnet N, Stolina M, Han C-Y, Kostenuik P, Jurdic P, Ferrari S, Douni E 2014 Novel Genetic Models of Osteoporosis by Overexpression of Human RANKL in Transgenic Mice. J Bone Miner Res **29**(5)**:**1158-1169.

132. Bucay N, Sarosi I, Dunstan CR, Morony S, Tarpley J, Capparelli C, Scully S, Tan HL, Xu W, Lacey DL, Boyle WJ, Simonet WS 1998 Osteoprotegerin-deficient Mice Develop Early Onset Osteoporosis and Arterial Calcification. Gene Dev **12**(9)**:**1260-1268.

133. Suda T, Takahashi F, Takahashi N 2012 Bone Effects of Vitamin D - Discrepancies between In-vivo and In-vitro Studies. Arch Biochem Biophys **523**(1)**:**22-29.

134. Huang WH, Daniels LL, Wood DJ, Seydel U, Papadimitriou JM, Zheng MH 1999 Vitamin D Receptor mRNA is Expressed in Osteoclast-like Cells of Human Giant Cell Tumor of Bone (osteoclastoma). J Musculoskelet Res **03**(03)**:**201-207.

135. Wang Y, Zhu J, Deluca HF 2014 Identification of the Vitamin D Receptor in Osteoblasts and Chondrocytes but not Osteoclasts in Mouse Bone. J Bone Miner Res **29**(3)**:**685-692.

136. van de Peppel J, van Leeuwen JPTM 2014 Vitamin D and Gene Networks in Human Osteoblasts. Front Physiol **5 APR**.

137. Haussler MR, Whitfield GK, Kaneko I, Haussler CA, Hsieh D, Hsieh JC, Jurutka PW 2013 Molecular Mechanisms of Vitamin D Action. Calcif Tissue Int **92**(2)**:**77-98.

138. Turner AG, Dwivedi PP, Anderson PH, May BK, Morris HA 2009 Regulation of the 5′-Flanking Region of the Human CYP27B1 Gene in Osteoblast Cells. Mol Cell Endocrinol **311**(1-2)**:**55-61.

139. van Driel M, van Leeuwen JPTM 2014 Vitamin D Endocrine System and Osteoblasts. BoneKEy Rep **3**.

140. Yang D, Atkins GJ, Turner AG, Anderson PH, Morris HA 2013 Differential Effects of 1,25-Dihydroxyvitamin D on Mineralisation and Differentiation in Two Different Types of Osteoblast-like Cultures. J Steroid Biochem Mol Biol **136:**166-70.

141. Ikeda K, Ogata E 1999 The Effect of Vitamin D on Osteoblasts and Osteoclasts. Curr Opin Ortho **10**(5)**:**339-343.

142. Bergh JJ, Shao Y, Puente E, Duncan RL, Farach-Carson MC 2006 Osteoblast Ca2+ Permeability and Voltage-sensitive Ca2+ Channel Expression is Temporally Regulated by 1,25-Dihydroxyvitamin D3. Am J Physiol Cell Physiol **290**(3)**:**C822-C831.

143. Zhang X, Zanello LP 2008 Vitamin D Receptor-Dependent 1α,25(OH)2 Vitamin D 3-Induced Anti-apoptotic PI3K/AKT Signaling in Osteoblasts. J Bone Miner Res **23**(8)**:**1238-1248.

144. Martin A, Liu S, David V, Li H, Karydis A, Feng JQ, Quarles LD 2011 Bone Proteins PHEX and DMP1 Regulate Fibroblastic Growth Factor Fgf23

Expression in Osteocytes Through a Common Pathway Involving FGF Receptor (FGFR) Signaling. Faseb J **25**(8)**:**2551-62.

145. Geng S, Zhou S, Glowacki J 2011 Effects of 25-Hydroxyvitamin D(3) on Proliferation and Osteoblast Differentiation of Human Marrow Stromal Cells Require CYP27B1/1α-Hydroxylase. J Bone Miner Res **26**(5)**:**1145-53.

146. Quarles LD 2012 Skeletal Secretion of FGF-23 Regulates Phosphate and Vitamin D Metabolism. Nat Rev Endocrinol **8**(5)**:**276-86.

147. Jüppner H 2011 Phosphate and FGF-23. Kidney Int **79**(SUPPL. 121)**:**S24-S27.

148. David V, Dai B, Martin A, Huang J, Han X, Quarles LD 2013 Calcium Regulates FGF-23 Expression in Bone. Endocrinology **154**(12)**:**4469-4482.

149. Haussler MR, Haussler CA, Bartik L, Whitfield GK, Hsieh JC, Slater S, Jurutka PW 2008 Vitamin D Receptor: Molecular Signaling and Actions of Nutritional Ligands in Disease Prevention. Nutr Rev **66**(10 Suppl 2)**:**S98-112.

150. Thompson B, Towler DA 2012 Arterial Calcification and Bone Physiology: Role of the Bone-Vascular Axis. Nat Rev Endocrinol **8**(9)**:**529-43.

151. Eisman JA 2001 Pharmacogenetics of the Vitamin D Receptor and Osteoporosis. Drug Metab Dispos **29**(4 Pt 2)**:**505-12.

152. Yang D, Turner AG, Wijenayaka AR, Anderson PH, Morris HA, Atkins GJ 2015 1,25-Dihydroxyvitamin D3 and Extracellular Calcium Promote Mineral Deposition via NPP1 activity in a Mature Osteoblast Cell Line MLO-A5. Molec Cell Endocrinol**:**(accepted for publication).

153. Yang D 2015 The Interaction between Vitamin D and Extracellular Calcium on Osteogenic Differentiation Medicine, vol. Doctor of Philosophy. The University of Adelaide, Adelaide.

154. Anderson PH, Sawyer RK, Moore AJ, May BK, O'Loughlin PD, Morris HA 2008 Vitamin D Depletion Induces RANKL-mediated Osteoclastogenesis and Bone Loss in a Rodent Model. J Bone Miner Res **23:**1789–1797.

155. Mailhot G, Petit JL, Dion N, Deschenes C, Ste-Marie LG, Gascon-Barre M 2007 Endocrine and Bone Consequences of Cyclic Nutritional Changes in the Calcium, Phosphate and Vitamin D Status in the Rat: an In-vivo Depletion-Repletion-Redepletion Study. Bone **41**(3)**:**422-36.

156. Moyer-Mileur LJ, Xie B, Ball SD, Pratt T 2003 Bone Mass and Density Response to a 12-month Trial of Calcium and Vitamin D Supplement in Preadolescent Girls. J Musculoskelet Neuronal Interact **3**(1)**:**63-70.

157. Zhu K, Devine A, Dick IM, Wilson SG, Prince RL 2008 Effects of Calcium and Vitamin D Supplementation on Hip Bone Mineral Density and Calcium-related Analytes in Elderly Ambulatory Australian Women: a Five-year Randomized Controlled Trial. J Clin Endocrinol Metab **93**(3)**:**743-9.

158. Iwamoto J, Yeh JK, Takeda T, Sato Y 2004 Effects of Vitamin D Supplementation on Calcium Balance and Bone Growth in Young Rats Fed Normal or Low Calcium Diet. Horm Res **61**(6)**:**293-9.

159. Campbell JR, Douglas TA 1965 The Effect of Low Calcium Intake and Vitamin D Supplements on Bone Structure in Young Growing Dogs. Br J Nutr **19**(3)**:**339-51.

160. Vervloet MG, van Ittersum FJ, Buttler RM, Heijboer AC, Blankenstein MA, ter Wee PM 2011 Effects of Dietary Phosphate and Calcium Intake on Fibroblast Growth Factor-23. Clin J Am Soc Nephrol **6**(2)**:**383-9.

161. Eisman JA, Bouillon R 2014 Vitamin D: direct effects of vitamin D metabolites on bone: lessons from genetically modified mice. Bonekey Rep **3:**499.

162. Panda DK, Miao D, Bolivar I, Li J, Huo R, Hendy GN, Goltzman D 2004 Inactivation of the 25-Hydroxyvitamin D 1α-Hydroxylase and Vitamin D Receptor Demonstrates Independent and Interdependent Effects of Calcium and Vitamin D on Skeletal and Mineral Homeostasis. J Biol Chem **279**(16)**:**16754-16766.

163. Heffner CS, Pratt CH, Babiuk RP, Sharma Y, Rockwood SF, Donahue LR, Eppig JT, Murray SA 2012 Supporting Conditional Mouse Mutagenesis with a Comprehensive Cre Characterization Resources. Nature Communications **3**(1218)**:**1-9.

164. Friedel RH, Wurst, W., Wefers B, Kühn R 2011 Generating Conditional Knockout Mice. In: Hofker MH, van Deursen JM (eds.) Transgenic Mouse Methods and Protocols, Methods in Molecular Biology, Second ed., vol. 693. Springer Science+Business Media, London.

165. Sauer B 1998 Inducible Gene Targeting in Mice Using the Cre/lox System. Methods: A Companion to Methods in Enzymology **14:**381–392

166. Masuyama R, Stockmans I, Torrekens S, Van Looveren R, Maes C, Carmeliet P, Bouillon R, Carmeliet G 2006 Vitamin D Receptor in Chondrocytes Promotes Osteoclastogenesis and Regulates FGF23 Production in Osteoblasts. J Clin Invest **116**(12)**:**3150-9.

167. Yamamoto Y, Yoshizawa T, Fukuda T, Shirode-Fukuda Y, Yu T, Sekine K, Sato T, Kawano H, Aihara K, Nakamichi Y, Watanabe T, Shindo M, Inoue K, Inoue E, Tsuji N, Hoshino M, Karsenty G, Metzger D, Chambon P, Kato

S, Imai Y 2013 Vitamin D Receptor in Osteoblasts is a Negative Regulator of Bone Mass Control. Endocrinology **154**(3)**:**1008-20.

168. Lieben L, Masuyama R, Torrekens S, Van Looveren R, Schrooten J, Baatsen P, Lafage-Proust MH, Dresselaers T, Feng JQ, Bonewald LF, Meyer MB, Pike JW, Bouillon R, Carmeliet G 2012 Normocalcemia is Maintained in Mice under Conditions of Calcium Malabsorption by Vitamin D-induced Inhibition of Bone Mineralization. J Clin Invest **122**(5)**:**1803-1815.

169. Misof BM, Roschger P, Tesch W, Baldock PA, Valenta A, Messmer P, Eisman JA, Boskey AL, Gardiner EM, Fratzl P, Klaushofer K 2003 Targeted Overexpression of Vitamin D Receptor in Osteoblasts Increases Calcium Concentration without Affecting Structural Properties of Bone Mineral Crystals. Calcif Tissue Int **73**(3)**:**251-7.

170. Lam NN, Triliana R, Sawyer RK, Atkins GJ, Morris HA, O'Loughlin PD, Anderson PH 2014 Vitamin D Receptor Overexpression in Osteoblasts and Osteocytes Prevents Bone Loss during Vitamin D-Deficiency. J Steroid Biochem Mol Biol.

171. Jehan F, DeLuca HF 1997 Cloning and Characterization of the Mouse Vitamin D Receptor Promoter. Proc Natl Acad Sci U S A **94**(19)**:**10138-10143.

172. Clemens TL, Tang H, Maeda S, Kesterson RA, Demayo F, Pike JW, Gundberg CM 1997 Analysis of Osteocalcin Expression in Transgenic Mice Reveals a Species Difference in Vitamin D Regulation of Mouse and Human Osteocalcin Genes. J Bone Miner Res **12**(10)**:**1570–1576.

173. Bouxsein ML, Boyd SK, Christiansen BA, Guldberg RE, Jepsen KJ, Müller R 2010 Guidelines for Assessment of Bone Microstructure in Rodents using Micro-Computed Tomography. J Bone Miner Res **25**(7)**:**1468-1486.

174. Lee Y, Ha J, Kim HJ, Kim Y-S, Chang E-J, Song W-J, Kim H-H 2009 Negative Feedback Inhibition of NFATc1 by DYRK1A Regulates Bone Homeostasis. J Biol Chem **284**(48)**:**33343-33351.

175. Parfitt AM, Drezner MK, Glorieux FH, Kanis JA, Malluche H, Meunier PJ, Ott SM, Recker RR 1987 Bone Histomorphometry: Standardization of Nomenclature, Symbols, and Units. Report of the ASBMR Histomorphometry Nomenclature Committee. J Bone Miner Res **2**(6)**:**595-610.

176. Pawley N, Bishop NJ 2004 Prenatal and Infant Predictors of Bone Health: the Influence of Vitamin D. Am J Clin Nutr **80**(6)**:**1748S-1751S.

177. Boyce BF, Xing L 2008 Functions of RANKL/RANK/OPG in Bone Modeling and Remodeling. Arch Biochem Biophys **473**(2)**:**139-146.

178. Rauch F 2007 Bone Accrual in Children: Adding Substance to Surfaces. Pediatrics **119**(Supplement 2)**:**S137-S140.

179. Seeman E, Delmas PD 2006 Bone Quality — The Material and Structural Basis of Bone Strength and Fragility. N Engl J Med **354**(21)**:**2250-2261.

180. Xiong J, Onal M, Jilka RL, Weinstein RS, Manolagas SC, O'Brien CA 2011 Matrix-embedded Cells Control Osteoclast Formation. Nat Med **17**(10)**:**1235-41.

181. Schapira D, Linn S, Sarid M, Mokadi S, Kabala A, Silbermann M 1995 Calcium and Vitamin D Enriched Diets Increase and Preserve Vertebral Mineral Content in Aging Laboratory Rats. Bone **16**(5)**:**575-82.

182. Feng Y, Zhou M, Zhang Q, Liu H, Xu Y, Shu L, Zhang J, Miao D, Ren Y 2015 Synergistic Effects of High Dietary Calcium and Exogenous Parathyroid Hormone in Promoting Osteoblastic Bone Formation in Mice. Br J Nutr **113**(6)**:**909-22.

183. Sapir-Koren R, Livshits G 2011 Bone Mineralization and Regulation of Phosphate Homeostasis. IBMS BoneKEy **8**(6)**:**286-300.

184. Zhou X, Cui Y, Zhou X, Han J 2012 Phosphate/pyrophosphate and MV-related Proteins in Mineralisation: Discoveries from Mouse Models. Int J Biol Sci **8**(6)**:**778-90.

185. Perwad F, Azam N, Zhang MY, Yamashita T, Tenenhouse HS, Portale AA 2005 Dietary and Serum Phosphorus Regulate Fibroblast Growth Factor 23 Expression and 1,25-Dihydroxyvitamin D Metabolism in Mice. Endocrinology **146**(12)**:**5358-64.

186. Washbourne CJ, Tang JCY, Fraser DR 2012 The Effects of Storage Temperature and Repeat Freeze-Thaw Cycles on Stability of PTH (1-34) as Determined by the IDS-iSYS Automated Analyser ASBMR, vol. 27 (Suppl 1). J Bone Miner Res Minneapolis, Minnesota, USA.

187. Xiong J, Piemontese M, Thostenson JD, Weinstein RS, Manolagas SC, O'Brien CA 2014 Osteocyte-derived RANKL is a Critical Mediator of the Increased Bone Resorption Caused by Dietary Calcium Deficiency. Bone **66:**146-54.

188. Narayanan K, Ramachandran A, Hao J, He G, Park KW, Cho M, George A 2003 Dual Functional Roles of Dentin Matrix Protein 1: Implications In Biomineralization And Gene Transcription By Activation Of Intracellular Ca2+ Store. J Biol Chem **278**(19)**:**17500-17508.

189. Eapen A, Sundivakkam P, Song Y, Ravindran S, Ramachandran A, Tiruppathi C, George A 2010 Calcium-mediated Stress Kinase Activation by DMP1 Promotes Osteoblast Differentiation. J Biol Chem **285**(47)**:**36339-36351.

190. Nociti FH, Foster BL, Tran AB, Dunn D, Presland RB, Wang L, Bhattacharyya N, Collins MT, Somerman MJ 2014 Vitamin D Represses Dentin Matrix Protein 1 in Cementoblasts and Osteocytes. J Dent Res **93**(2)**:**148-154.

191. Siyam A, Wang S, Qin C, Mues G, Stevens R, D'Souza RN, Lu Y 2012 Nuclear Localization of DMP1 Proteins Suggests a Role in Intracellular Signaling. Biochem Biophys Res Commun **424**(3)**:**641-646.

192. Li H, Jiang X, Delaney J, Franceschetti T, Bilic-Curcic I, Kalinovsky J, Lorenzo JA, Grcevic D, Rowe DW, Kalajzic I 2010 Immature osteoblast lineage cells increase osteoclastogenesis in osteogenesis imperfecta murine. Am J Pathol **176**(5)**:**2405-13.

193. Ryan J 2016 Understanding the Role of the Vitamin D Receptor in Maintenance of Skeletal Health School of Pharmacy and Medical Sciences, vol. PhD. University of South Australia, Adelaide, pp 192.

194. Tsangari H, Russel T, Clarke M, Turner AG, Ryan JW, Straczak Y, Barratt K, Sawyer RK, Morris HA, Atkins GJ, Davey RA, Anderson PH 2013 Vitamin D Receptor in Mature Osteoblasts and Osteocytes is Required for Normal Bone Formation and Resorption ANZBMS 23rd Annual Scientific Meeting, Melbourne, Victoria, Australia.

195. Gallardo T, Shirley L, John GB, Castrillon DH 2007 Generation of a Germ Cell-specific Mouse Transgenic Cre-line, Vasa-Cre. Genesis **45**(6)**:**413-417.

196. Anonymous 2013 12 Things You Don't Know about Cre-Lox Jax Blog, vol. 2016, The Jackson Laboratory.

197. Garcia-Arocena D 2013 Cre-Lox Myths Busted Jax Blog, vol. 2016, The Jackson Laboratory

198. Wergedal JE, Sheng MH, Ackert-Bicknell CL, Beamer WG, Baylink DJ 2005 Genetic variation in femur extrinsic strength in 29 different inbred strains of mice is dependent on variations in femur cross-sectional geometry and bone density. Bone **36**(1)**:**111-22.

APPENDIX

Specialty Feeds

3150 Great Eastern Hwy
Glen Forrest
Western Australia 6071
p: +61 8 9298 8111
F: +61 8 9298 8700
Email: info@specialtyfeeds.com

Diet

Meat Free Rat and Mouse Diet

A fixed formulation diet for Laboratory Rats and Mice fortified with vitamins and minerals to meet the requirements of breeding animals after the diet is autoclaved or irradiated.

- Minor modifications were made to this fixed formulation on 27 Jan 2009. Please contact us for details.
- All nutritional parameters of this diet meet or exceed the NRC guidelines for Rats and Mice.
- The diet has been designed as a general ration for breeding and early growth in all rat and mouse strains. The total fat content has been deliberately kept low at around 5%, to maximise the long term breeding performance of most strains.
- The formulation is designed to be fed ad-lib to rodents of all ages. There is some indication that growth performance in a minority of strains can be improved by increasing dietary energy (fat content). BalbC mice, DA rats and some of the modified strains appear to be most susceptible to this problem. Please contact us if you are concerned about this issue.
- Mammalian meals have been excluded from the diet, however the diet does contain fish meal. We have formulated totally vegetarian diets, and maintained colonies for some time on these diets. Please contact us if you require such a diet.
- The feed is manufactured in a cylindrical form with a diameter of around 12 mm, length is variable from 10 mm to 30 mm. We have found that this form is ideal for overhead hopper feeding, maximising the ease of handling whilst minimising fines formation and the risk of bridging in the feed hopper. Pellet strength has been kept lower than conventional pelletised diets. While this leads to a slight increase in transit and storage damage to the diet (fines generation), we have found that juvenile mice often have a lower feed intake on harder pellets.
- The diet is packed in permeable bags suitable for direct loading into an autoclave. It is recommended that the diet be autoclaved at 120^{O} C for 20 minutes with a post autoclaving vacuum drying cycle. Some clumping of the diet can be expected, but the diet clumps can usually be easily broken. Modifying the drying time to leave some residual moisture in the diet can minimise the clumping. Do not autoclave at 135^{0} C as this will result in significant clumping that will be difficult to break.

Calculated Nutritional Parameters

Protein	20.00%
Total Fat	4.80%
Crude Fibre	4.80%
Acid Detergent Fibre	7.60%
Neutral Detergent Fibre	16.40%
Total Carbohydrate	59.40%
Digestible Energy	14.0 MJ / Kg
% Total Calculated Energy From Protein	23.00%
% Total Calculated Energy From Lipids	12.00%

Ingredients

A Fixed formula ration using the following ingredients:
Wheat, barley, Lupins, Soya meal, Fish meal, Mixed vegetable oils, Canola oil, Salt, Calcium carbonate, Dicalcium phosphate, Magnesium oxide, and a Vitamin and trace mineral premix.

Added Vitamins

Vitamin A (Retinol)	10 000 IU/Kg
Vitamin D (Cholecalciferol)	2 000 IU/Kg
Vitamin E (a Tocopherol acetate)	100 mg/Kg
Vitamin K (Menadione)	20 mg/Kg
Vitamin B1 (Thiamine)	80 mg/Kg
Vitamin B2 (Riboflavin)	30 mg/Kg
Niacin (Nicotinic acid)	100 mg/Kg
Vitamin B6 (Pryridoxine)	25 mg/Kg
Calcium Pantothenate	50 mg/Kg
Biotin	300 ug/Kg
Folic Acid	5.0 mg/Kg
Vitamin B12 (Cyancobalamin)	150 ug/Kg

Diet Form and Features

- Cereal grain base diet. 12 mm diameter pellets.
- Pack size 10 and 20 Kg Bags.
- Diet suitable for irradiation, also suitable for autoclave.
- Lead time 2 weeks

Added Trace Minerals

Magnesium	100 mg/Kg
Iron	70 mg/Kg
Copper	16 mg/Kg
Iodine	0.5 mg/Kg
Manganese	70 mg/Kg
Zinc	60 mg/Kg
Molybdenum	0.5 mg/Kg
Selenium	0.1 mg/Kg

Calculated Amino Acids

Valine	0.87%
Leucine	1.40%
Isoleucine	0.80%
Threonine	0.70%
Methionine	0.30%
Cystine	0.30%
Lysine	0.90%
Phenylanine	0.90%
Tyrosine	0.50%
Tryptophan	0.20%
Histidine	0.53%

Calculated Total Minerals	
Calcium	0.80%
Phosphorous	0.70%
Magnesium	0.20%
Sodium	0.18%
Potassium	0.82%
Sulphur	0.20%
Iron	200 mg/Kg
Copper	23 mg/Kg
Iodine	0.5 mg/Kg
Manganese	104 mg/Kg
Cobalt	0.7 mg/Kg
Zinc	90 mg/Kg
Molybdenum	1.2 mg/Kg
Selenium	0.4 mg/Kg
Cadmium	0.05 mg/Kg

Calculated Total Vitamins	
Vitamin A (Retinol)	10 950 IU/Kg
Vitamin D (Cholecalciferol)	2 000 IU/Kg
Vitamin E (a Tocopherol acetate)	110 mg/Kg
Vitamin K (Menadione)	20 mg/Kg
Vitamin C (Ascorbic acid)	No data
Vitamin B1 (Thiamine)	80 mg/Kg
Vitamin B2 (Riboflavin)	30 mg/Kg
Niacin (Nicotinic acid)	145 mg/Kg
Vitamin B6 (Pryridoxine)	28 mg/Kg
Pantothenic Acid	60 mg/Kg
Biotin	410 ug/Kg
Folic Acid	5 mg/Kg
Inositol	No data
Vitamin B12 (Cyancobalamin)	150 ug/Kg
Choline	1 640 mg/Kg

Calculated Fatty Acid Composition	
Myristic Acid 14:0	0.03%
Palmitic Acid 16:0	0.50%
Stearic Acid 18:0	0.14%
Palmitoleic Acid 16:1	0.01%
Oleic Acid 18:1	1.90%
Gadoleic Acid 20:1	0.03%
Linoleic Acid 18:2 n6	1.30%
a Linolenic Acid 18:3 n3	0.30%
Arachadonic Acid 20:4 n6	0.01%
EPA 20:5 n3	0.02%
DHA 22:6 n3	0.05%
Total n3	0.37%
Total n6	1.31%
Total Mono Unsaturated Fats	2.00%
Total Polyunsaturated Fats	1.77%
Total Saturated Fats	0.74%

Calculated data uses information from typical raw material composition. It could be expected that individual batches of diet will vary from this figure. **Diet post treatment by irradiation or auto clave could change these parameters**.

We are happy to provide full calculated nutritional information for all of our products, however we would like to emphasise that these diets have been specifically designed for manufacture by Specialty Feeds.

Specialty Feeds
3150 Great Eastern Hwy
Glen Forrest
Western Australia 6071
p: +61 8 9298 8111
F: +61 8 9298 8700
Email: info@specialtyfeeds.com

Diet
SF12-076

1% Calcium 0.625% Phosphorous Whey Protein Isolate Modification of SF04-053 VDRKO Rescue Diet

A VDRKO semi-pure rodent diet designed based on Harlan Teklads TD96348 (SF04-053).

- Casein has been replaced with Whey Protein Isolate
- Calcium has been reduced from 2.1 to 1%
- Phosphorous has been reduced from 1.26 to 0.625%
- Sodium and potassium levels have been kept constant against SF04-053
- Diet designed to be isoenergetic with SF12-075, SF12-077 and SF12-078

Calculated Nutritional Parameters

Protein	18.00%
Total Fat	5.00%
Crude Fibre	4.70%
AD Fibre	4.70%
Digestible Energy	14.7 MJ / Kg
% Total calculated digestible energy from lipids	12.70%
% Total calculated digestible energy from protein	22.30%

Diet Form and Features

- Semi pure diet. 12 mm diameter pellets.
- Pack size 5 Kg, vacuum packed in oxygen impermeable plastic bags, under nitrogen. Bags are packed into cardboard cartons to protect them during transit. Smaller pack quantity on request.
- Diet suitable for irradiation but not suitable for autoclave.
- Lead time 2 weeks for non-irradiation or 4 weeks for irradiation.

Ingredients

Whey Protein Isolate	199 g/Kg
Sucrose	237 g/Kg
Lactose	200 g/Kg
Maize Oil	50 g/Kg
Cellulose	98 g/Kg
Maize Starch	150 g/Kg
DL Methionine	3.0 g/Kg
Calcium Carbonate	17.2 g/Kg
Sodium Chloride	2.3 g/Kg
AIN93 Trace Minerals	1.4 g/Kg
Potassium Dihydrogen Phosphate	3.5 g/Kg
Potassium Sulphate	1.2 g/Kg
MonoCalcium Phosphate	23.8 g/Kg
Magnesium Oxide	0.7 g/Kg
Choline Chloride (75%)	2.5 g/Kg
AIN93 Vitamins	10 g/Kg
Vitamin D Supplement (28 500 IU/g)	0.04 g/Kg

Calculated Amino Acids	
Valine	1.16%
Leucine	2.11%
Isoleucine	1.31%
Threonine	1.41%
Methionine	0.80%
Cystine	0.59%
Lysine	1.86%
Phenylanine	0.59%
Tyrosine	0.61%
Tryptophan	0.36%

Calculated Total Minerals	
Calcium	1.00%
Phosphorous	0.63%
Magnesium	0.12%
Sodium	0.12%
Chloride	0.16%
Potassium	0.35%
Sulphur	0.30%
Iron	74 mg/Kg
Copper	7 mg/Kg
Iodine	0.2 mg/Kg
Manganese	22 mg/Kg
Cobalt	No data
Zinc	39 mg/Kg
Molybdenum	0.15 mg/Kg
Selenium	0.3 mg/Kg
Cadmium	No data
Chromium	1.0 mg/Kg
Fluoride	1.0 mg/Kg
Lithium	0.1 mg/Kg
Boron	0.9 mg/Kg
Nickel	0.5 mg/Kg
Vanadium	0.1 mg/Kg

Calculated Total Vitamins	
Vitamin A (Retinol)	4 000 IU/Kg
Vitamin D (Cholecalciferol)	2 140 IU/Kg
Vitamin E (a Tocopherol acetate)	76 mg/Kg
Vitamin K (Menadione)	1 mg/Kg
Vitamin C (Ascorbic acid)	None added
Vitamin B1 (Thiamine)	6 mg/Kg
Vitamin B2 (Riboflavin)	6 mg/Kg
Niacin (Nicotinic acid)	30 mg/Kg
Vitamin B6 (Pryridoxine)	7 mg/Kg
Pantothenic Acid	16 mg/Kg
Biotin	200 ug/Kg
Folic Acid	2 mg/Kg
Inositol	None added
Vitamin B12 (Cyancobalamin)	100 ug/Kg
Choline	1 410 mg/Kg

Calculated Fatty Acid Composition	
Myristic Acid 14:0	No data
Palmitic Acid 16:0	0.55%
Stearic Acid 18:0	0.10%
Palmitoleic Acid 16:1	No data
Oleic Acid 18:1	1.21%
Gadoleic Acid 20:1	No data
Linoleic Acid 18:2 n6	2.90%
a Linolenic Acid 18:3 n3	0.04%
Arachadonic Acid 20:4 n6	No data
EPA 20:5 n3	No data
DHA 22:6 n3	No data
Total n3	0.04%
Total n6	2.90%
Total Mono Unsaturated Fats	1.21%
Total Polyunsaturated Fats	2.94%
Total Saturated Fats	0.64%

Calculated data uses information from typical raw material composition. It could be expected that individual batches of diet will vary from this figure. **Diet post treatment by irradiation or auto clave could change these parameters**. We are happy to provide full calculated nutritional information for all of our products, however we would like to emphasise that these diets have been specifically designed for manufacture by Specialty Feeds.

Specialty Feeds

3150 Great Eastern Hwy
Glen Forrest
Western Australia 6071
p: +61 8 9298 8111
F: +61 8 9298 8700
Email: info@specialtyfeeds.com

Diet
SF12-077

0.03% Calcium 0.08% Phosphorous Whey Protein Isolate Modification of SF04-053 VDRKO Rescue Diet

A VDRKO semi-pure rodent diet designed based on Harlan Teklads TD96348 (SF04-053).

- Casein has been replaced with Whey Protein Isolate
- Calcium has been reduced from 2.1 to 0.03%
- Phosphorous has been reduced from 1.26 to 0.08%
- Sodium and potassium levels have been kept constant against SF04-053
- Diet designed to be isoenergetic with SF12-075, SF12-076 and SF12-078

Calculated Nutritional Parameters

Protein	18.00%
Total Fat	5.00%
Crude Fibre	4.70%
AD Fibre	4.70%
Digestible Energy	14.7 MJ / Kg
% Total calculated digestible energy from lipids	12.70%
% Total calculated digestible energy from protein	22.30%

Diet Form and Features

- Semi pure diet. 12 mm diameter pellets.
- Pack size 5 Kg, vacuum packed in oxygen impermeable plastic bags, under nitrogen. Bags are packed into cardboard cartons to protect them during transit. Smaller pack quantity on request.
- Diet suitable for irradiation but not suitable for autoclave.
- Lead time 2 weeks for non-irradiation or 4 weeks for irradiation.

Ingredients

Whey Protein Isolate	199 g/Kg
Sucrose	231 g/Kg
Lactose	200 g/Kg
Maize Oil	50 g/Kg
Cellulose	145 g/Kg
Maize Starch	150 g/Kg
DL Methionine	3.0 g/Kg
Calcium Carbonate	0.2 g/Kg
Sodium Chloride	2.3 g/Kg
AIN93 Trace Minerals	1.4 g/Kg
Potassium Citrate	1.5 g/Kg
Potassium Dihydrogen Phosphate	1.5 g/Kg
Potassium Sulphate	1.2 g/Kg
Magnesium Oxide	1.7 g/Kg
Choline Chloride (75%)	2.5 g/Kg
AIN93 Vitamins	10 g/Kg
Vitamin D Supplement (28 500 IU/g)	0.04 g/Kg

Calculated Amino Acids	
Valine	1.16%
Leucine	2.11%
Isoleucine	1.31%
Threonine	1.41%
Methionine	0.80%
Cystine	0.59%
Lysine	1.86%
Phenylanine	0.59%
Tyrosine	0.61%
Tryptophan	0.36%

Calculated Total Minerals	
Calcium	0.03%
Phosphorous	0.08%
Magnesium	0.12%
Sodium	0.12%
Chloride	0.16%
Potassium	0.35%
Sulphur	0.30%
Iron	48 mg/Kg
Copper	7 mg/Kg
Iodine	0.2 mg/Kg
Manganese	17 mg/Kg
Cobalt	No data
Zinc	39 mg/Kg
Molybdenum	0.15 mg/Kg
Selenium	0.3 mg/Kg
Cadmium	No data
Chromium	1.0 mg/Kg
Fluoride	1.0 mg/Kg
Lithium	0.1 mg/Kg
Boron	0.9 mg/Kg
Nickel	0.5 mg/Kg
Vanadium	0.1 mg/Kg

Calculated Total Vitamins	
Vitamin A (Retinol)	4 000 IU/Kg
Vitamin D (Cholecalciferol)	2 140 IU/Kg
Vitamin E (a Tocopherol acetate)	76 mg/Kg
Vitamin K (Menadione)	1 mg/Kg
Vitamin C (Ascorbic acid)	None added
Vitamin B1 (Thiamine)	6 mg/Kg
Vitamin B2 (Riboflavin)	6 mg/Kg
Niacin (Nicotinic acid)	30 mg/Kg
Vitamin B6 (Pryridoxine)	7 mg/Kg
Pantothenic Acid	16 mg/Kg
Biotin	200 ug/Kg
Folic Acid	2 mg/Kg
Inositol	None added
Vitamin B12 (Cyancobalamin)	100 ug/Kg
Choline	1 410 mg/Kg

Calculated Fatty Acid Composition	
Myristic Acid 14:0	No data
Palmitic Acid 16:0	0.55%
Stearic Acid 18:0	0.10%
Palmitoleic Acid 16:1	No data
Oleic Acid 18:1	1.21%
Gadoleic Acid 20:1	No data
Linoleic Acid 18:2 n6	2.90%
a Linolenic Acid 18:3 n3	0.04%
Arachadonic Acid 20:4 n6	No data
EPA 20:5 n3	No data
DHA 22:6 n3	No data
Total n3	0.04%
Total n6	2.90%
Total Mono Unsaturated Fats	1.21%
Total Polyunsaturated Fats	2.94%
Total Saturated Fats	0.64%

Calculated data uses information from typical raw material composition. It could be expected that individual batches of diet will vary from this figure. **Diet post treatment by irradiation or auto clave could change these parameters**. We are happy to provide full calculated nutritional information for all of our products, however we would like to emphasise that these diets have been specifically designed for manufacture by Specialty Feeds.

THE UNIVERSITY of ADELAIDE

RESEARCH BRANCH
Research Ethics and Compliance Unit

KIM GRAHAM
SECRETARY, ANIMAL ETHICS COMMITTEE MEDICAL
THE UNIVERSITY OF ADELAIDE
SA 5005
AUSTRALIA

TELEPHONE +61 8 8303 6310
FACSIMILE +61 8 8303 7325
email: kim.graham@adelaide.edu.au
CRICOS Provider Number 00123M

APPLICANT: Dr P Anderson
School of Medical Sciences Office

PROJECT TITLE: ***Vitamin D and Calcium interactions on Bone Metabolism***

PROJECT NUMBER: **M-2012-092** RM No: 0000013478

APPROVED BY THE UNIVERSITY OF ADELAIDE ANIMAL ETHICS COMMITTEE MEDICAL

FOR THE PERIOD 31 MAY 2012 to 31 MAY 2015

INVOLVING:

Mouse (C57black6 WT Female)	120
Mouse (CYP27B1 (-/+) Female)	80
Mouse (CYP27B1 (-/-) Female)	80
Mouse (CYP27B1-loxP (+/+) Female)	120
Mouse (OSCYP27B1(+/-) Female)	120
Mouse (OSVDRVDR(+/-) Female)	120
Mouse (ObCYP27B1KO (-/+) Female)	120
Mouse (ObCYP27B1KO (-/-) Female)	120
Mouse (ObVDRKO (-/+) Female)	120
Mouse (ObVDRKO (-/-) Female)	120
Mouse (VDR-loxP (+/+) Female)	120
Mouse (VDRKO (-/+) Female)	80
Mouse (VDRKO (-/-) Female)	80

This application is approved subject to 1) adjustment of the 16 hours fasting to be during daylight hours as much as possible (this is requested to reduce the impact of the fast given that 16 hours is a long period, and mice feed at night), 2) animals are to be monitored daily (minimum), 3) intervention or a cut-off points requiring euthanasia should be provided on CRS, 4) inclusion of treatment specific observations on the CRS, 5) phenotype reports are required, and 6) clarification that the student involved is a University of Adelaide student.

This approval is subject to notification of project commencement. Please send an email to the AEC Medical Secretary kim.graham@adelaide.edu.au giving the date when animal work actually begins.
Refer also to the accompanying letter setting out requirements applying to approval of this project.

....

PROFESSOR R RUSSELL, Convenor Date: 1.6.12

THE UNIVERSITY of ADELAIDE

RESEARCH BRANCH
Research Ethics and Compliance Unit

KIM GRAHAM
SECRETARY, ANIMAL ETHICS COMMITTEE MEDICAL
THE UNIVERSITY OF ADELAIDE
SA 5005
AUSTRALIA

TELEPHONE +61 8 8303 6310
FACSIMILE +61 8 8303 7325
email: kim.graham@adelaide.edu.au
CRICOS Provider Number 00123M

31 May 2012

Dr P Anderson
School of Medical Science, The University of Adelaide

Dear Dr P Anderson

Ref: ANIMAL ETHICS COMMITTEE PROJECT NO: M-2012-092

Vitamin D and Calcium interactions on Bone Metabolism

I write to advise you that the Animal Ethics Committee has approved the above project for the period from 31 May 2012 to 31 May 2015. Please refer to the enclosed endorsement sheet which gives further details and may include particular conditions applying to this approval. Your attention is drawn to the following requirements of the Australian code of practice for the care and use of animals for scientific purposes, 7th Edition 2004:

You have personal responsibility for all matters related to the welfare of the animals you use and you must act in accordance with all requirements of the Code.

Any adverse or unexpected effects that impact on animal wellbeing which occur during the period of the approved project must be reported promptly to the AEC.

You must ensure that records of the use and monitoring of animals used in this project are maintained. Records should include the origin and fate of issued animals, how animal welfare was assessed, any unexpected negative impact on animal wellbeing and notation of procedures.

You must provide an annual report to the AEC - the continuation of all projects is subject to receipt of written annual reports that should advise on: (i) what progress has been achieved; (ii) any problems that may have interfered with progress of the project; (iii) how many animals have been used; (iv) whether the wellbeing of the animals is consistent with that anticipated in the proposal; (v) whether any changes are envisaged; and (vi) whether the project is meeting its aims. You must inform the Committee when an approved project is completed or discontinued.

The above project number and approval expiry date must be included on the animal cage/pen label. All animals housed on University premises and subject to multiple ethics approvals must be identified by the display of the relevant approval numbers from all approving AECs.

Statistics regarding the use of animals in this project must be provided to the AEC annually for collation and report to the Minister responsible for animal welfare. It is necessary to apply to the AEC for approval if the project is to continue for a longer period of time, if additional animals are required or if any change to procedure is proposed. Please refer to the AEC website for further information on reporting and other matters including the AEC Animal User's Handbook: information about your responsibility to use animals humanely and ethically: http://www.adelaide.edu.au/ethics/animal/.

Yours sincerely

RICHARD RUSSELL
Convenor, Animal Ethics Committee Medical